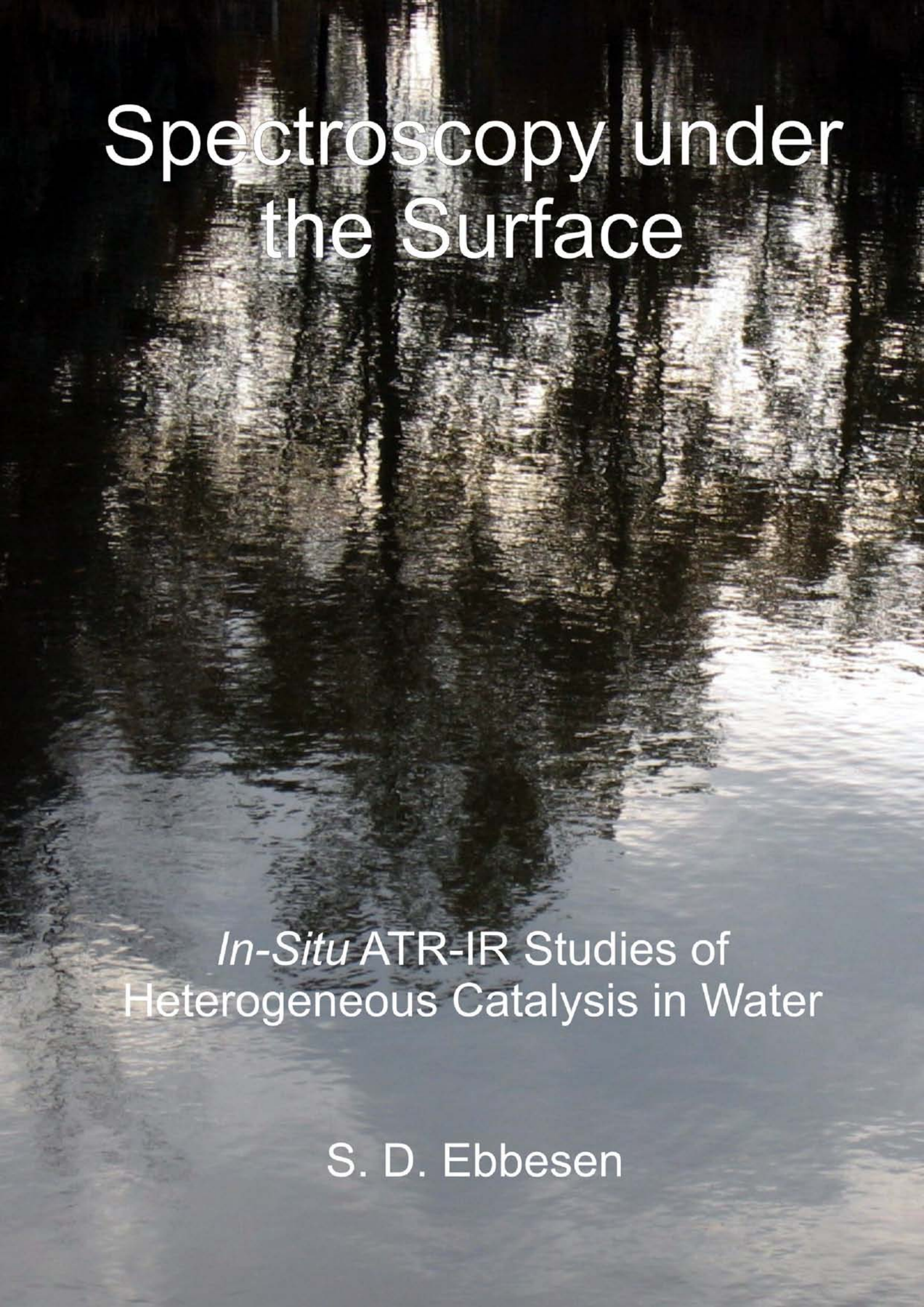
Spectroscopy under the Surface
In-Situ ATR-IR Studies of Heterogeneous Catalysis in Water
S. D. Ebbesen

Promotion Committee

Prof.dr.ir A. Bliek, Chairman	Universiteit Twente
Prof.dr.ir L. Lefferts, Promotor	Universiteit Twente
Dr. B. L. Mojet, Assistent promotor	Universiteit Twente
Prof. T. Bürgi	Université de Neuchâtel
Prof.dr.ir J.G.E. Gardeniers	Universiteit Twente
Prof.dr.ir M.T.M. Koper	Universiteit Leiden
Prof.dr.ir F.G. Mugele	Universiteit Twente
Dr. G. Mul	Technische Universiteit Delft
Dr. H. Oevering	DSM Research B.V., Geleen
Prof.dr.ir B.M. Weckhuysen	Universiteit Utrecht

The research described in this thesis was performed under the auspices of the NIOK, Netherlands Institute for Catalysis Research.

The research described was financially supported by DSM Research B.V., Geleen, The Netherlands.

ISBN: 978-90-365-2467-4

Printed by Gildeprint B.V., Enschede

SPECTROSCOPY UNDER THE SURFACE

IN-SITU ATR-IR STUDIES OF HETEROGENEOUS CATALYSIS IN WATER

DISSERTATION

to obtain
the doctor's degree at University of Twente,
on the authority of the rector magnificus,
prof.dr. W.H.M. Zijm,
on account of the decision of the graduation committee
to be publicly defended
on Thursday, 8th March, 2007 at 13.15

by

Sune Dalgaard Ebbesen

born on 27 August, 1977

in København, Danmark

This dissertation has been approved by the promoter

Prof.dr.ir. L. Lefferts

And the assistant promoter

Dr. B. L. Mojet

Contents

Summary

The chemical industry is always searching for more cost- and performance-efficient processes and the trend is therefore to use water as a solvent. The selection of water as a solvent offers many benefits; beside low cost, the advantages are the fact that it is environmentally benign, its availability and safety. The chemical industry is a major contributor to environmental pollution, largely due to the use of hazardous solvents. These solvents often end up in wastewater and can be removed by for example wet-air oxidation over several catalysts. At the same time, nitrite and nitrate levels in groundwater have increased over the last few decades. Denitrification (nitrite and nitrate removal) is therefore one of the most investigated hydrogenation reactions in ground-water treatment.

So far, detailed mechanistic studies of reactions carried out in water are lacking because it is difficult to study heterogeneous catalysis *in-situ* when the reaction is carried out in water. Vibrational spectroscopy is a versatile tool to study adsorption and reaction on catalytic surfaces in gas phase. Because liquids and water in particular, are strong absorbers of infrared radiation, normal transmission infrared spectroscopy is not applicable unless the pathlength of the light is very short, i.e. in the order of a few microns. Attenuated Total Reflection Infrared Spectroscopy (ATR-IR), however, is ideally suited for studying molecular vibrations at the solid-liquid interface since the evanescent wave is restricted to the region near the interface, thereby minimising the contribution from the liquid.

The work described in this thesis demonstrates the application of ATR-IR infrared spectroscopy to study adsorption and catalytic reactions on metal surfaces during heterogeneous catalytic reactions in aqueous phase. By coating an Internal Reflection Element (IRE) with a stable, thin (in the order of a few microns) catalyst layer, adsorption and reaction at the solid-aqueous interface was studied successfully. Properties of the technique and the influence of water on the supported metal catalysts were demonstrated using two reactions (i) CO oxidation and (ii) nitrite hydrogenation.

CO is a widely applied molecule to characterise supported noble metal catalysts and CO oxidation is a very simple reaction. Therefore CO adsorption and oxidation was used to demonstrate the technique and to give insight in the behaviour of supported catalysts in water. Denitrification, nitrite hydrogenation, is becoming more important due to the high nitrite and nitrate levels found in ground-water in Europe and the increasingly strict regulations for drinking water quality. The hydrogenation can be performed over single noble metal catalysts such as platinum and palladium catalysts. The heterogeneous hydrogenation of nitrite was investigated by ATR-IR, in order to resolve the hydrogenation mechanism.

Adsorption and oxidation of carbon monoxide

Adsorption and oxidation of carbon monoxide was performed in both gas and aqueous phase over Pt/ZnSe, Pt/Al_2O_3 and Pd/Al_2O_3, investigating the influence of water on both CO and the noble metal. Adsorption of CO from gas and aqueous phase on the supported catalysts revealed significant differences. (i) CO adsorption from aqueous phase results in a clear red shift of the CO stretch frequency compared to adsorption from dry gas. This red shift is caused by the influence of water on adsorbed CO, possibly *via* a direct interaction between the water molecules and adsorbed CO, most likely *via* hydrogen bonding. Moreover, (ii) the ratio of integrated intensities for linear and bridged CO (L/B ratio) decreased from gas phase to aqueous phase. In the field of catalyst characterisation it is well-known that upon increasing support alkalinity the red shift of linear and bridged CO is accompanied by a lower L/B ratio as a result of the increased back-donation from the noble metal particles. (iii) The infrared absorbance increased when adsorbing CO in aqueous phase, compared to in gas phase adsorption.

Based on the red shift and changed L/B ratio, it is not possible to decide whether the red shift is caused by the direct effect of water on the CO molecule, the indirect effect *via* modification of the metal particle potential, inducing an increased π-back-donation from the metal to CO, or a combination of both phenomena. Remarkably, the CO intensity increased drastically when adsorbed from aqueous phase compared to from gas phase. This can be caused by a polarisation of the CO molecule, for example *via* hydrogen bonding, which directly influences its extinction coefficient because of an increased transition dipole moment, thereby increasing the observed infrared intensity.

In aqueous phase, the stretch frequency of adsorbed CO was found to shift down with increasing pH. From electrochemistry it is known that a change in electrode

potential causes a shift in peak position of adsorbed CO. In gas phase chemistry the stretch frequency of adsorbed CO is regarded as a sensitive probe of metal-support interactions, which are known to influence the electronic properties of the supported metal and thus its catalytic activity. The observed red shift with increasing pH can be attributed to increasing π-back-donation from the supported metal to adsorbed CO, caused by decreasing potential of the supported metal particles.

The oxidation rate of pre-adsorbed CO increased in aqueous phase compared to in gas phase. In addition, an increase in pH significantly enhances the CO oxidation rate. Over Pt/Al_2O_3, the stretch frequency of adsorbed CO is linearly related to the CO oxidation rate, which suggests an effect of the metal particle potential on the rate-determining step of CO oxidation in aqueous phase. The increased π-back donation weakens the CO bond by supplying electrons in the anti-bonding orbital, therefore CO will be more reactive towards the p-electrons of adsorbed oxygen atoms. As a result, the CO molecule is more easily oxidised in aqueous phase and with increasing pH. Moreover oxidation of pre adsorbed CO on Pd/Al_2O_3 showed that the palladium particles are more easily oxidised in water and with increasing pH, further increasing the oxidation rate of adsorbed carbon monoxide. Scheme 1 summarises the influence of water and pH on both the CO stretch frequency and the CO oxidation rate. The presence of co-adsorbed and bulk water affect the metal particle potential and the CO transition dipole moment respectively, most likely via complex formation between CO and H_2O. This interaction alters the reaction mechanism and rate of CO oxidation. In addition, pH mainly affects the CO molecule *via* a potential change of the metal particle, which in turn is directly related to the observed rate of oxidation of CO. Moreover, on Pd/Al_2O_3, increased pH enhances the oxidation of the supported palladium particles, increasing the oxidation rate of adsorbed carbon monoxide further.

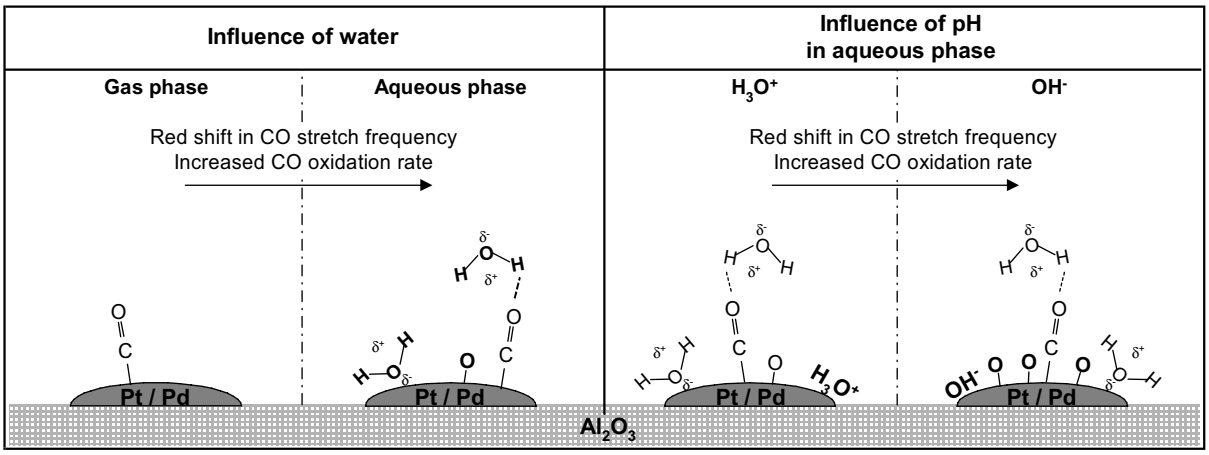

Scheme 1. Schematic presentation of the influence of water and pH on the CO stretch frequency and CO oxidation rate.

Nitrite hydrogenation

Catalytic hydrogenation is a relatively new method for the removal of nitrate and nitrite from water. Nevertheless, many groups have worked on developing active and selective catalysts or systems. It has been suggested that the reaction pathways for nitrite hydrogenation and electroreduction of NO adlayers are similar for both platinum and palladium catalysts. However in the present study we have clearly shown that there are significant differences in the heterogeneous hydrogenation of nitrite over Pt/Al_2O_3 and Pd/Al_2O_3. The adsorption of $NO_2^-{}_{(aq)}$ and $NH_4^+{}_{(aq)}$ show similar adsorption characteristics on both Pd/Al_2O_3 and Pt/Al_2O_3. The vibrational spectrum of the NO_2^- ion changed substantially upon adsorption, clearly indicating that NO_2^- chemisorbs onto the noble metal catalysts. Contrary, adsorption of NH_4^+ does not lead to significant changes of the vibrational spectrum of the ion, indicating that NH_4^+ does not chemisorb on the noble metal, but is stabilised via an electrostatic interaction. When comparing adsorption of hydroxylamine ($NH_2OH_{(aq)}$) on Pd/Al_2O_3 and Pt/Al_2O_3 significant differences were observed. On Pd/Al_2O_3, hydroxylamine is converted into a stable $NH_{2(ads)}$ fragment, whereas on Pt/Al_2O_3 hydroxylamine is converted into NO, possibly via $HNO_{(ads)}$ as an intermediate.

During hydrogenation of nitrite similar species to during adsorption and decomposition of NH_2OH were formed on the catalyst surface. Adsorption of NO_2^- on $H\text{-}Pd/Al_2O_3$ (where $NO_2^-{}_{(aq)}$ can react with adsorbed hydrogen) showed that nitrite hydrogenates to adsorbed NO, NH_2, and NH_4^+. Moreover, subsequent hydrogenation showed that $NO_{(ads)}$ is most likely converted to N_2, while the hydrogenation of $NH_{2(ads)}$ produces solely NH_4^+. Interestingly, NH_4^+ is only produced after almost all $NO_{(ads)}$ has

disappeared, showing that $NO_{(ads)}$ is more reactive toward hydrogen than $NH_{2(ads)}$ and that $NO_{(ads)}$ is not converted to NH_4^+. On platinum, nitrite hydrogenates to $NO_{(ads)}$ and NH_4^+ as well. However, in contrast to hydrogenation of NO adsorbed on Pd/Al_2O_3, hydrogenation of NO on Pt/Al_2O_3 produces both N_2O and ammonia, *via* "HNO"$_{(ads)}$ as an intermediate.

To a small extent N_2O was observed during all hydrogenation experiments over Pt/Al_2O_3. Nitrogen is believed to be formed from reduction of N_2O over platinum, thus indicating the formation of small amounts of nitrogen. On Pd/Al_2O_3, on the other hand, nitrogen is formed via hydrogenation of NO, which was formed at relatively high amounts compared to NH_2 and NH_4^+. The main species on Pt/Al_2O_3 are, NO and "HNO"$_{(ads)}$, which hydrogenate to both N_2O and NH_4^+. The "HNO"$_{(ads)}$ intermediate is observed during the continuous hydrogenation of nitrite over Pt/Al_2O_3. On Pd/Al_2O_3, on the other hand, $NO_{(ads)}$ and $NH_{2(ads)}$ are observed during the continuous hydrogenation, of which $NO_{(ads)}$ is more reactive to hydrogen, and hydrogenates to nitrogen, whereas $NH_{2(ads)}$ hydrogenates to ammonia. These findings indicate that, different steps in the formation of ammonia are rate limiting over platinum and palladium; hydrogenation of "HNO"$_{(ads)}$ is rate limiting for Pt/Al_2O_3, whereas the hydrogenation of $NH_{2(ads)}$ is rate limiting over Pd/Al_2O_3.

This study is the first to show the surface intermediates during heterogeneous hydrogenation of nitrite over supported palladium and platinum catalysts. In literature, it was suggested that the reaction pathways for heterogeneous catalytic hydrogenation of nitrite and for electroreduction of NO adlayers are the same for both platinum and palladium catalysts. However, it is clearly shown that nitric oxide adsorbed on Pt/Al_2O_3 hydrogenates to ammonia, with "HNO"$_{(ads)}$ as an intermediate. On Pd/Al_2O_3, the other hand, nitric oxide does not produce ammonia, since ammonia is formed *via* hydrogenation of $NH_{2(ads)}$ only.

The main difference between the mechanism for hydrogenation of nitrite on Pt/Al_2O_3 and Pd/Al_2O_3 proposed here and the mechanism previously suggested in literature involves identification of the key adsorbed intermediate. The same surface intermediates are involved on both metals as shown in Scheme 2, but the species observed which are involved in the rate determining step(s) are quite different: $NO_{(ads)}$ and $NH_{2(ads)}$ on palladium versus "HNO"$_{(ads)}$ on platinum. It was previously suggested that nitric oxide, formed on both noble metal catalysts, hydrogenates to ammonia and nitrogen. Our spectroscopic evidence clearly shows that on palladium adsorbed nitric oxide does not hydrogenate to ammonia, whereas on platinum, it is found as a product from hydrogenation of nitric oxide.

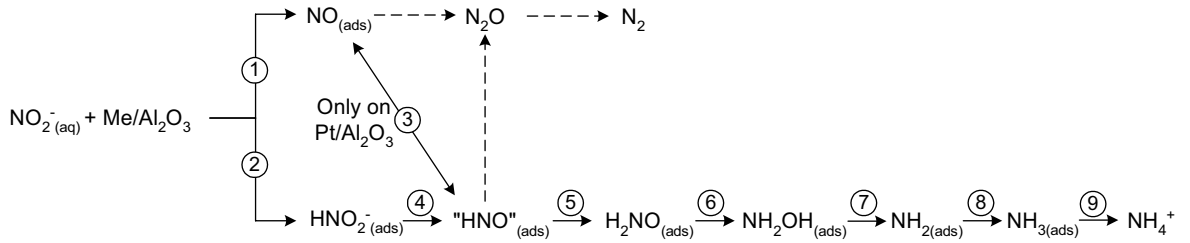

Scheme 2. Reaction scheme of the catalytic hydrogenation of nitrite over Pd/Al_2O_3 and Pt/Al_2O_3. The dotted lines represent possible reaction pathways for N_2O and N_2 formation, although at present there is no evidence for these pathways. Step ③ applies for Pt/Al_2O_3 only. All other steps apply for both catalysts.

This study convincingly shows that ATR-IR spectroscopy can be applied to study adsorption and reaction on supported catalysts in dry gas, wet gas as well as aqueous phase. As such, ATR-IR spectroscopy allows direct comparison between adsorption and reactions in gas and liquid phase. To improve the understanding of heterogeneous catalysis in aqueous phase in detail, theoretical calculations are necessary. Furthermore, combination of ATR-IR spectroscopy with other techniques offers more opportunities; e.g. a system to detect dissolved gases, can gain more insight in reactions where gaseous products are formed.

Samenvatting

De chemische industrie is altijd op zoek naar efficiëntere processen. De trend is daarbij om water te gebruiken als oplosmiddel. De keuze voor water biedt veel voordelen; naast de lage kosten is het gebruik van water milieuvriendelijk, is het overal verkrijgbaar en is het veilig in gebruik. De chemische industrie levert een grote bijdrage aan milieuvervuiling, voor een groot deel veroorzaakt door schadelijke oplosmiddelen. Deze oplosmiddelen eindigen vaak in afvalwater, waaruit ze verwijderd kunnen worden met behulp van bijvoorbeeld wet-air oxidatie over verschillende katalysatoren. Bovendien zijn de laatste decennia de nitriet en nitraat concentraties in grondwater aanzienlijk gestegen. Denitrificatie (nitriet en nitraat verwijdering) is daarom een van de meest bestudeerde hydrogeneringsreacties in de behandeling van grondwater.

Tot nu toe ontbreken gedetailleerde mechanistische studies van reacties uitgevoerd in water, omdat het moeilijk is heterogene katalysatoren *in-situ* te bestuderen als de reactie in water uitgevoerd wordt. Infrarood vibratiespectroscopie is een veelzijdige methode die gebruikt wordt om gasfase adsorptie en reactie op katalysatoroppervlakken te bestuderen. Vloeistoffen, in het bijzonder water, adsorberen infraroodstraling in sterke mate. Daarom is normale transmissie infrarood spectroscopie alleen toepasbaar als de weglengte van het licht erg kort is; in de ordegrootte van een paar micron. *Attenuated Total Reflection Infrared Spectroscopy* (ATR-IR) is echter zeer geschikt voor het bestuderen van moleculaire vibraties op het vast-vloeistof oppervlak omdat het infrarood licht beperkt is tot vlakbij het katalysatoroppervlak, waardoor de invloed van de vloeistof minimaal is.

Het werk beschreven in dit proefschrift toont de toepassing van ATR-IR spectroscopie om adsorptie en katalytische reacties op metaalkatalysatoren tijdens heterogeen katalytische reacties in water te bestuderen. Door een Intern Reflectie Element (IRE) te bedekken met een stabiele, dunne (ordegrootte van enkele microns) katalysatorlaag, zijn de adsorptie en reactie op het grensvlak succesvol bestudeerd. Eigenschappen van de techniek en de invloed van water op de

gedragen metaal katalysatoren zijn aangetoond door gebruik te maken van twee voorbeeldreacties: (i) CO oxidatie en (ii) nitriet hydrogenering.

CO is een veel toegepast molecuul om gedragen edelmetaal katalysatoren te karakteriseren, bovendien is CO oxidatie een relatief eenvoudige reactie. Om deze redenen is CO adsorptie en oxidatie gebruikt om de toepassing van ATR-IR spectroscopie te tonen en om inzicht te geven in het gedrag van gedragen katalysatoren in water. Stikstofverwijdering wordt steeds belangrijker door het hoge nitriet en nitraat gehalte in grondwater in Europa en de steeds strengere regelgeving voor drinkwaterkwaliteit. Hydrogenering kan worden uitgevoerd met edelmetaal katalysatoren zoals platina en palladium katalysatoren. De heterogene hydrogenering van nitriet is bestudeerd met behulp van ATR-IR spectroscopie, om het mechanisme van de hydrogeneringsreactie vast te stellen.

Adsorptie en oxidatie van koolmonoxide

Adsorptie en oxidatie van koolmonoxide is uitgevoerd in gasfase en in water over Pt/ZnSe, Pt/Al_2O_3 en Pd/Al_2O_3, waarbij de invloed van water op zowel CO als het edelmetaal is bestudeerd. Adsorptie van CO uit gas en water op de gedragen katalysatoren levert significante verschillen. In vergelijking met adsorptie uit de gasfase levert CO adsorptie uit water (i) een duidelijke roodverschuiving van de CO strekfrequentie op. Deze roodverschuiving wordt veroorzaakt door de invloed van water op geadsorbeerd CO, mogelijk via een directe interactie tussen de water moleculen en geadsorbeerd CO, waarschijnlijk via de vorming van waterstofbruggen. Bovendien is (ii) de verhouding tussen de geïntegreerde intensiteiten voor lineair en gebrugd geadsorbeerd CO (L/G verhouding) lager in water dan in de gasfase. In het werkveld van katalysatorkarakterisering is het algemeen bekend dat als de drager meer basisch wordt, de roodverschuiving van lineair en gebrugd CO vergezeld gaat met een lagere L/G verhouding. Dit is als gevolg van de *π-back-donation* van het edelmetaal naar het CO molecuul. (iii) Bij CO adsorptie uit water steeg de infrarood adsorptie in vergelijking met adsorptie uit de gasfase.

Gebaseerd op de roodverschuiving en verandering in L/G verhouding is het niet mogelijk om te bepalen of de roodverschuiving veroorzaakt wordt door het directe effect van water op het CO molecuul, het indirecte effect via aanpassing van de potentiaal van het metaal, dat een hogere *π-back-donation* veroorzaakt, of een combinatie van beide. Het is opmerkelijk dat bij adsorptie uit water in vergelijking met uit de gasfase de CO intensiteit dramatisch stijgt. Dit kan veroorzaakt worden door polarisatie van het CO molecuul, bijvoorbeeld door de vorming van waterstofbruggen,

die een directe invloed uitoefent op de absorptiecoëfficiënt door een groter dipool moment. Hierdoor stijgt de geobserveerde intensiteit.

In water schuift de strekvibratie van geadsorbeerd CO naar lagere frequentie bij het verhogen van de pH. Uit de elektrochemie is bekend dat een verandering van de elektrodepotentiaal een verschuiving veroorzaakt in de positie van de piek van geadsorbeerd CO. In gasfasechemie wordt de strekfrequentie van CO beschouwd als een indicatie voor metaal-drager interacties, die de elektronische eigenschappen van het gedragen metaal en daarmee op de katalytische activiteit beïnvloeden. De geobserveerde roodverschuiving bij het verhogen van de pH kan worden toegeschreven aan een verhoogde π-*back-donation* van het gedragen metaal naar het geadsorbeerde CO, veroorzaakt door een afnemende potentiaal van de gedragen metaaldeeltjes.

De oxidatiesnelheid van vooraf geadsorbeerd CO steeg in water ten opzichte van in gasfase. Daarnaast levert een verhoging van de pH tevens een significante verhoging van de CO oxidatiesnelheid. Over Pt/Al_2O_3 is de strekfrequentie van geadsorbeerd CO lineair gerelateerd aan de CO oxidatiesnelheid, wat een effect van de potentiaal van het metaal op de snelheidsbepalende stap van CO oxidatie in water suggereert. De verhoogde π-*back-donation* verzwakt de CO binding doordat elektronen in de antibindende orbitaal terechtkomen. Daardoor wordt CO reactiever voor de p-elektronen van geadsorbeerde zuurstofatomen, met als gevolg dat het CO molecuul makkelijker oxideert in water en bij verhoogde pH. Bovendien, laat oxidatie van vooraf geadsorbeerd CO op Pd/Al_2O_3 zien dat ook de palladium deeltjes makkelijker oxideren in water en bij verhoogde pH, wat de oxidatiesnelheid van geadsobeerd koolmonoxide verder verhoogt. Schema 1 vat de invloed van water en pH op de CO strekfrequentie en de CO oxidatiesnelheid samen. De aanwezigheid van gecoadsorbeerd en bulk water beïnvloeden respectievelijk de potentiaal van het metaal en het CO overgangsdipoolmoment, hoogstwaarschijnlijk door de vorming van een $CO\text{-}H_2O$ complex. Deze interactie tussen CO en H_2O verandert het reactiemechanisme en de CO oxidatiesnelheid. De pH beïnvloedt het CO molecuul via een verandering van de potentiaal van het metaal, wat direct gerelateerd is aan de waargenomen oxidatiesnelheid van CO. Over Pd/Al_2O_3, verbetert bovendien een stijgende pH de oxidatie van de gedragen palladium deeltjes. Dit levert een verdere stijging van de oxidatiesnelheid van geadsorbeerd koolmonoxide op.

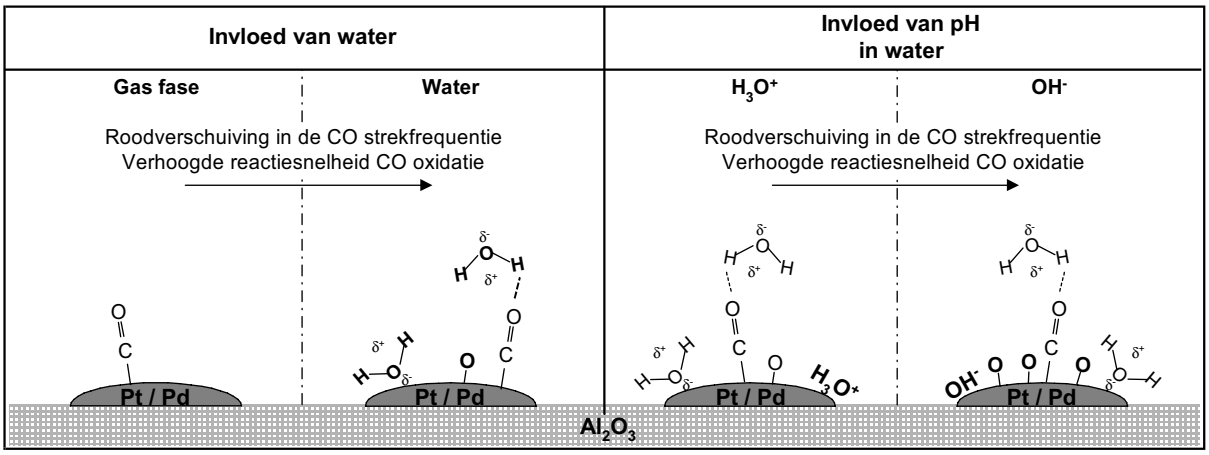

Schema 1. Schematische weergave van de invloed van water en pH op de CO strekfrequentie en de oxidatiesnelheid van CO.

Nitriet hydrogenering

Katalytische hydrogenering is een relatief nieuwe methode om nitraat en nitriet uit water te verwijderen. Veel groepen werken aan de ontwikkeling van actieve en selectieve katalysatoren en systemen. Er is voorgesteld dat de reactiemechanismen over zowel platina en palladium voor nitriet hydrogenering en elektroreductie van NO adsorptielagen vergelijkbaar zijn. In de huidige studie wordt duidelijk aangetoond dat er significante verschillen zijn voor de heterogene hydrogenering van nitriet over Pt/Al_2O_3 en Pd/Al_2O_3. $NO_2^-{}_{(aq)}$ en $NH_4^+{}_{(aq)}$ hebben vergelijkbare adsorptie karakteristieken op zowel Pt/Al_2O_3 en Pd/Al_2O_3. Het vibratiespectrum van het NO_2^- ion veranderde substantieel tijdens adsorptie op beide metalen, wat wijst op NO_2^- chemisorptie op de edelmetaalkatalysatoren. In tegenstelling tot NO_2^- leidt de adsorptie van NH_4^+ niet tot significante veranderingen in het vibratiespectrum van het ion, wat suggereert dat NH_4^+ niet chemisorbeert op het edelmetaal, maar gestabiliseerd wordt via elektrostatische interactie. Bij het vergelijken van adsorptie van hydroxylamine ($NH_2OH_{(aq)}$) op Pd/Al_2O_3 en Pt/Al_2O_3 zijn significante verschillen waargenomen. Op Pd/Al_2O_3 wordt hydroxylamine omgezet tot een stabiel $NH_{2(ads)}$ fragment, terwijl het op Pt/Al_2O_3 wordt omgezet in NO, mogelijk via $HNO_{(ads)}$ als intermediair.

Tijdens de hydrogenering van nitriet zijn vergelijkbare adsorbaten op het katalytische oppervlak waargenomen als tijdens de adsorptie en ontleding van NH_2OH. Adsorptie van NO_2^- op $H\text{-}Pd/Al_2O_3$ (waar $NO_2^-{}_{(aq)}$ kan reageren met geadsorbeerd waterstof) laat zien dat nitriet hydrogeneert tot geadsorbeerd NO, NH_2, and NH_4^+. Daaropvolgende hydrogenering laat bovendien zien dat $NO_{(ads)}$ hoogstwaarschijnlijk

omgezet wordt naar N_2, terwijl de hydrogenering van $NH_{2(ads)}$ alleen NH_4^+ oplevert. Interessant genoeg wordt NH_4^+ pas geproduceerd als bijna al het $NO_{(ads)}$ is weggereageerd. Dat betekent dat $NO_{(ads)}$ makkelijker met waterstof reageert dan $NH_{2(ads)}$ en bovendien dat $NO_{(ads)}$ niet wordt omgezet tot NH_4^+. Over platina hydrogeneert nitriet ook tot $NO_{(ads)}$ and NH_4^+, maar in tegenstelling tot de hydrogenering van NO geadsorbeerd op Pd/Al_2O_3, levert de hydrogenering van NO geadsorbeerd op Pt/Al_2O_3 zowel N_2O als ammoniak, met "HNO"$_{(ads)}$ als intermediair.

Tijdens alle hydrogeneringsexperimenten over Pt/Al_2O_3 werd een kleine hoeveelheid N_2O waargenomen. Dit is een indicatie voor de vorming van kleine hoeveelheden stikstof, het meest waarschijnlijke hydrogeneringsproduct van N_2O. Over Pt/Al_2O_3 wordt stikstof gevormd via de hydrogenering van NO, dat in grote hoeveelheden gevormd wordt, in vergelijking met NH_2 en NH_4^+. De belangrijkste intermediaren op Pt/Al_2O_3 zijn NO en "HNO"$_{(ads)}$, die hydrogeneren naar N_2O en NH_4^+. "HNO"$_{(ads)}$ is waargenomen tijdens continue hydrogenering van nitriet over Pt/Al_2O_3. Op Pd/Al_2O_3 daarentegen, zijn $NO_{(ads)}$ en $NH_{2(ads)}$ waargenomen tijdens continue hydrogeneringsexperimenten. Hiervan is $NO_{(ads)}$ het meest reactieve adsorbaat in combinatie met waterstof en produceert stikstof, terwijl $NH_{2(ads)}$ hydrogeneert tot ammoniak. Bovenstaande bevindingen duiden erop dat voor de twee katalysatoren verschillende stappen in de vorming van ammoniak snelheidsbepalend zijn; over Pt/Al_2O_3 is de hydrogenering van "HNO"$_{(ads)}$ snelheidsbepalend, terwijl de hydrogenering van $NH_{2(ads)}$ snelheidsbepalend is over Pd/Al_2O_3.

Deze studie toont voor het eerst de oppervlakte-intermediaren tijdens heterogene hydrogenering van nitriet over gedragen palladium en platina katalysatoren. In de literatuur is gesuggereerd dat het reactiemechanisme voor zowel heterogeen katalytische hydrogenering van nitriet als voor elektroreductie van geadsorbeerd NO hetzelfde is over platina en palladium katalysatoren. Hier is echter aangetoond dat geadsorbeerd stikstofoxide op Pt/Al_2O_3 tot ammoniak hydrogeneert, met "HNO"$_{(ads)}$ als intermediair. Over Pd/Al_2O_3 produceert stikstofoxide geen ammoniak, maar wordt ammoniak alleen gevormd via hydrogenering van $NH_{2(ads)}$.

Het belangrijkste verschil tussen het hier voorgestelde mechanisme voor de hydrogenering van nitriet over Pt/Al_2O_3 en Pd/Al_2O_3 en het mechanisme voorgesteld in de literatuur betreft het vaststellen van de belangrijkste geadsorbeerde intermediair. Dezelfde oppervlakte-intermediairen zijn betrokken bij de hydrogenering over beide edelmetaal katalysatoren, maar de intermediairen betrokken in de snelheidsbepalende stap(pen) zijn verschillend: $NO_{(ads)}$ en $NH_{2(ads)}$ op palladium versus "HNO"$_{(ads)}$ op platina. Eerder is gesuggereerd dat stikstofoxide, gevormd op

beide edelmetaal katalysatoren, tot ammoniak en stikstof hydrogeneert. Onze resultaten bewijzen dat stikstofoxide geadsorbeerd op palladium niet tot ammoniak hydrogeneert, terwijl dit wel het geval is op platina.

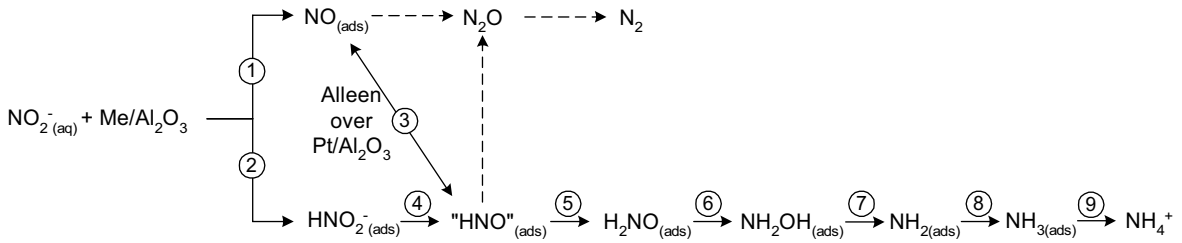

Schema 2. Reactieschema van de katalytische hydrogenering van nitriet over Pd/Al_2O_3 en Pt/Al_2O_3. De stippellijnen geven mogelijke reactiepaden voor N_2O en N_2 weer, hoewel er op dit moment geen bewijs is voor deze reactiepaden. Stap ③ is alleen van toepassing op Pt/Al_2O_3, alle andere stappen zijn geldig voor beide katalysatoren.

Deze studie toont duidelijk dat ATR-IR spectroscopie toegepast kan worden om adsorptie en reactie op gedragen katalysatoren, in droog en vochtig gas en in water te bestuderen. Als zodanig biedt ATR-IR spectroscopie de mogelijkheid een directe vergelijking te maken tussen adsorptie en reactie in gas en vloeistoffase. Voor het verder vergroten van het begrip van heterogene katalyse in water kunnen theoretische berekeningen behulpzaam zijn. Verder kan de combinatie van ATR-IR spectroscopie met andere technieken nog meer mogelijkheden bieden; bijvoorbeeld de combinatie met een systeem om opgeloste gassen in water te detecteren kan inzicht geven in reacties waarbij gasvormige producten ontstaan.

CHAPTER 1

General Introduction

Abstract

The majority of infrared studies on surface species in gas phase have been performed on thin discs of the catalyst, where transmittance is measured. Liquids, and especially water, are strong absorbers of infrared intensity so transmission infrared spectroscopy is not suitable to apply. Attenuated Total Reflection Infrared Spectroscopy however is ideally suited for studying molecular vibrations at the solid-liquid interface since the evanescent wave is restricted to the region near the interface. One of the most investigated and well characterised reactions in heterogeneous catalysis is the oxidation of carbon monoxide to carbon dioxide. Oxidation of carbon monoxide can be carried out both by molecular oxygen or by electrochemical oxidation. Hydrogenation of nitrate and nitrite is one of the most investigated reactions for water treatment applications. These two reactions will be studied in the present thesis and are therefore described in detail in this chapter.

The objective of the research described in this thesis is to gain general understanding of the reaction mechanism involved. Special emphasis will be on the influence of water and pH on these two reactions. Based in the surface intermediates and reaction mechanism, the influence of reaction conditions kinetics (activity and selectivity) can be understood better. Furthermore a general understanding of heterogeneous catalytic reactions in aqueous phase would close the gap between studies on electrochemical and heterogeneous catalytic reactions.

1.1 Introduction

Catalytic treatment of both waste- and groundwater treatment is receiving more and more attention over the past decades. The majority of the processes used in water purification are the oxidation of pollutants. To a lesser extent also hydrogenation processes are also studied for water treatment [1].

In the chemical industry it has become a trend to use water as a solvent. It offers many advantages over the use of organic solvents, i.e. low cost of water, its availability and the fact that it is safe to use and environmentally friendly. At present however the chemical industry is still a major contributor to environmental pollution, partly due to the use of hazardous solvents. Out of the top 10 chemicals released or disposed of by the chemical industry in the mid-1990s, five were solvents, namely, methanol, toluene, xylene, methyl ethyl ketone, and methylene chloride [2]. These solvents often end up in wastewater and can be removed by for example wet-air oxidation over several catalysts [1]. At the same time, nitrite and nitrate levels in groundwater have increased over the last few decades [3,4]. Denitrification (nitrite and nitrate removal) is therefore one of the most investigated hydrogenation reactions in ground-water treatment [5-16].

So far, detailed mechanistic studies of heterogeneous catalytic reactions are lacking because it is difficult to study reactions *in-situ* if the reaction is carried out in water. In gas phase, vibrational spectroscopy is a versatile tool to study adsorption and reaction on catalytic surfaces. However, in liquid phase reactions application of normal transmission infrared spectroscopy is not suitable unless the pathlength of the light is very short, i.e. in the order of a few microns, because liquids, water in particular, are strong absorbers of infrared radiation. Nevertheless Attenuated Total Reflection Infrared Spectroscopy (ATR-IR), is ideally suited to study molecular vibrations at the solid-liquid interface because the evanescent wave is restricted to the region near the interface, thereby minimising the contribution from the liquid [17].

In order to gain a general understanding of the factors influencing the activity and selectivity for reactions occurring in aqueous phase, the surface intermediates during adsorption and oxidation of carbon monoxide as well as adsorption and hydrogenation of nitrite hydrogenation will be investigated by ATR-IR spectroscopy in water. For this purpose characterisation of heterogeneous catalysts in liquid phase by ATR-IR will be described. In combination with vibrational spectroscopy carbon monoxide is widely applied as a probe molecule to characterise supported noble metal catalysts [18-29]. In addition, the relative simplicity of carbon monoxide

oxidation makes this reaction an ideal model of heterogeneous catalytic reactions, and allows for a detailed *in-situ* study. Furthermore hydrogenation of nitrite and nitrate over noble metal catalysts will be studied, since this reaction is well investigated, although no mechanistic evidence is provided. Additionally it is well known that pH of the solution greatly influences both the activity and selectivity of the noble metal catalysts in nitrate and nitrite hydrogenation.

1.2 *In-situ* characterisation of supported catalysts in liquid phase

Infrared spectroscopy has been used extensively to investigate the surface chemistry of heterogeneous catalysts in gas phase. The technique has made great contribution to the structural knowledge of adsorbed species during adsorption and catalytic reactions. The majority of infrared studies on surface species have been performed on thin wafers of the catalyst, where transmittance is measured, which was first described in 1956 [30]. However, many catalytic reactions take place at the solid liquid interface, where infrared spectroscopic studies have not received much attention so far. Liquids, and especially water, are strong absorbers of infrared intensity so transmission infrared spectroscopy is not suitable to apply unless the pathlength is very short; i.e. in the order of a few microns. Attenuated Total Reflection Infrared Spectroscopy (ATR-IR) however is ideally suited for studying molecular vibrations at the solid-liquid interface since the evanescent wave is restricted to the region near the interface, thereby minimising the contribution from the liquid. ATR-IR is often applied as an analytical tool to study the solution composition and protein structure in biochemistry [31] and to resolve reaction mechanisms of a variety of homogeneously catalysed processes [32-39]. On the other hand the use of ATR-IR to study liquid phase heterogeneous catalysis has only started to receive attention recently [40-47] as recently reviewed [48].

Application of the ATR-IR technique to study adsorption and reactions at the interface between solids and liquids was first reported in 1986 [46]. Herein the potential of ATR-IR spectroscopy was discovered due to aggregation of goethite on the Internal Reflection Element (IRE), although the signal was found to vary due to the aggregation. This finding encouraged the same authors to study the absorption of organic substrates on goethite [49-51]. More stable signals can be obtained by depositing a very thin layer of solid particles on the IRE [40,43,45,52-55]. It is essential that the thickness of the layer is in the same order as the penetration depth of the infrared radiation (i.e. a few microns). Coating the IRE was applied for model catalysts in organic solutions [40,56] and powder catalysts in both organic solutions [57-60] and in aqueous solutions [41,44]. Only a few studies on the application of

ATR-IR on the solid aqueous interface have been reported. The small number of studies is due to instability of the coated catalyst layer in aqueous phase.

ATR-IR is well suited for studying species involved in surface processes such as reactants, intermediates and products, and the catalytic surface itself [39]. In relation to the study presented in this thesis, reactions involving CO have been investigated before by ATR-IR spectroscopy, while nitrate/nitrite hydrogenation have never been studied using ATR-IR. Recently, adsorption of CO on Pt/Al_2O_3 from aqueous solution examined with ATR-IR was reported [41,44]. In one study the adsorption and oxidation of CO over Pt/Al_2O_3 was investigated in several solvents including water [44]. In another study CO adsorption on Pt/Al_2O_3 was investigated in relation to the water-gas shift reaction and methanol reforming [41].

1.2.1 Internal Reflection Spectroscopy

Unlike in transmission spectroscopy, where the infrared beam passes through the sample, in internal reflection spectroscopy, the infrared radiation is passed through an Internal Reflection Element (IRE), which is an infrared transparent crystal of high refractive index. Internal reflection spectroscopy was developed simultaneously and independently by Harrick [61] and Fahrenfort [62]. The sample is placed in close contact with the IRE. Incident infrared radiation is focussed onto the edge of the IRE, reflected through the IRE and directed to a detector as shown in Figure 1.1; a schematic diagram of a typical, commercially available horizontal accessory for internal reflection spectroscopy.

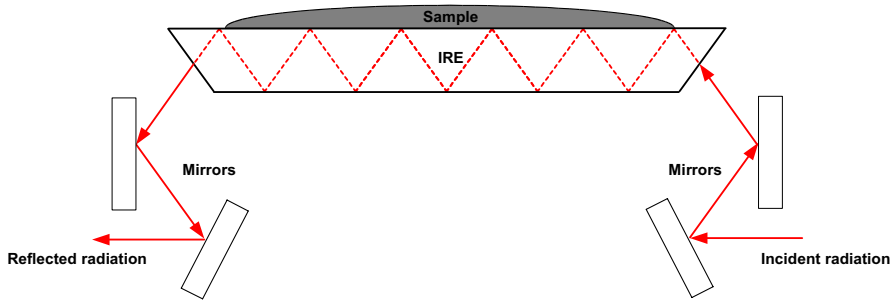

Figure 1.1. Schematic diagram of a typical, commercially available horizontal ATR accessory.

Light striking the interface between the two media (sample and IRE) of different refractive indices (n) will be partially reflected and partially transmitted; the beam is refracted according to Snell's law. If the angle of incidence is closer to the reflecting surface than the critical angle ($\theta > \theta_c$), the light will no longer cross the reflecting surface and will be totally reflected instead. The larger the angle to the normal, the smaller is the fraction of light transmitted, until the critical angle when total internal

reflection occurs (Figure 1.2A). This only occurs where light travels from a medium with a higher refractive index into one with a lower refractive index. At the critical angle ($\theta = \theta_c$), the light is refracted so it travels along the reflecting surface; the critical angle is given by:

$$\theta_c = \sin^{-1}(n_{21}) \tag{1.1}$$

If $\theta < \theta_c$, the beam will split. Some of the beam will reflect off the surface, and some will refract as it passes through; grey beam in Figure 1.2A (θ_1).

If $\theta > \theta_c$, total internal reflection occur and the entire beam reflects from the surface; black beam in Figure 1.2A (θ_2).

Although total reflection occurs at the interface when $\theta > \theta_c$, the electromagnetic field penetrates a fraction of a wavelength beyond the reflecting surface into the less dense medium. The penetration depth is defined as the distance required for the amplitude of the electric field to fall to e^{-1} of its original value at the interface and is given by equation (1.2) and illustrated in Figure 1.2B:

$$d_p = \frac{\lambda_1}{2 \cdot \pi \cdot (\sin^2\theta - n_{21}^{\,2})^{1/2}} \tag{1.2}$$

n_1 is the refractive index of the IRE and n_2 the refractive index of the medium on top of the IRE. λ_1 is the wavelength in the IRE and is given by $\lambda_1 = \lambda / n_1$.

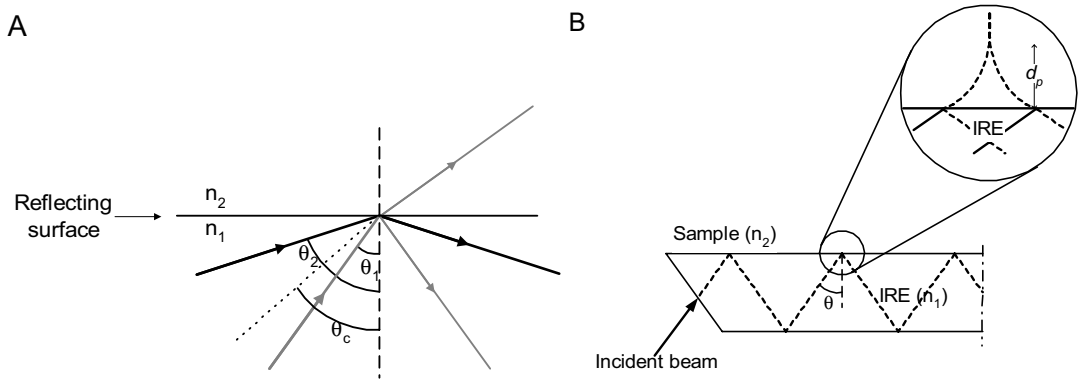

Figure 1.2. Schematic overview of the reflection at the surface (A) and the penetration depth into the sample (B).

When a sample is brought in close proximity to the surface of the IRE so it interacts with this penetrating field, total reflection is disrupted. If the sample absorbs the radiation, the wave becomes attenuated and an absorption spectrum of the sample can be obtained. This technique is known as Attenuated Total Reflection Spectroscopy, ATR Spectroscopy.

1.3 Adsorption and oxidation of carbon monoxide

Adsorption of carbon monoxide is a widely applied molecule to characterise supported noble metal catalysts [18-29]. Interactions between CO and the active metal are known to be affected by modifications of the metal particles, i.e. *via* metal support interactions and/or its surrounding medium. These changes are reflected in shifts of the CO absorption bands. Co-adsorption of CO with other molecules also affects the stretch frequency; the co-adsorption of water is known to influence the CO stretch frequency significantly [20,21,23,41,44,63-66]. Since CO vibrations are so sensitive, CO is an ideal model compound to characterise supported noble metal catalysts.

Scientifically, oxidation of carbon monoxide is one of the simplest catalytic reactions and thus is widely used as a model system to understand heterogeneous catalysis. This reaction over noble metal catalysts was first studied in 1922 [67] and it still remains worthy of investigation because of the unique possibility to characterise the adsorption / reaction *in-situ*. Before the 1970s the oxidation of CO was believed to proceed via an Eley–Rideal mechanism. Nowadays it is well-known that the CO oxidation over noble metal catalysts, where platinum and palladium catalysts are among the most active, proceeds via the three-step Langmuir-Hinshelwood reaction scheme shown by reaction 1.3 – 1.5 [68-75]:

$$CO_{(g)} \rightleftarrows CO_{(ads)} \tag{1.3}$$

$$O_{2(g)} \rightleftarrows 2\,O_{(ads)} \tag{1.4}$$

$$O_{(ads)} + CO_{(ads)} \rightarrow CO_{2(g)} \tag{1.5}$$

On both platinum and palladium catalysts CO adsorbs associatively and starts to desorb above approximately 350 K, whereas O_2 adsorbs dissociatively above approximately 100 K and desorbs associatively above 720 K [76]. $CO_{(ads)}$ diffuses rapidly over the surface and reacts with $O_{(ads)}$ to yield CO_2, which immediately desorbs into the gas phase. For gas phase CO oxidation it was reported that for

platinum catalysts higher CO activity was found for samples with CO bands at lower wavenumber, which was accompanied by a lower L/B ratio and attributed to increased electron density on the metal particles [29,77].

Even though the overall reaction, as shown by reaction 1.6, looks very simple the reaction kinetics are in fact rather complicated, and various phenomena have been associated with its occurrence on the noble metal surface, such as: rate dependencies varying from negative first order to positive first order for each reactant [68,71,78-80], surface diffusion of adsorbed CO [68,81-83], adsorbate island formation [71,84-86], rate oscillations [87-91], and metal surface restructuring under reaction conditions [92].

$$2\ CO + 2\ O_2 \rightarrow 2\ CO_2 \qquad (1.6)$$

Many studies have been addressed the oscillations in rate and CO coverage, and numerous explanations have been provided to explain this behavior. These include heat transfer effects [88], surface restructuring [93,94], redox of surface atoms [95,96], mass transfer limitations [90], and carbon deposition [97,98]. The intent of the present investigation is not to study the oscillatory behavior and, in fact, all CO oxidation experiments were performed transient, avoiding any oscillatory behavior.

1.3.1 Electrochemical adsorption and oxidation of carbon monoxide

Electrochemical adsorption and oxidation of CO on platinum is among the most extensively studied reactions in electrochemistry, since it is of great fundamental interest [65,99-103]. Electrochemical studies are confined to dense conducting electrodes, often single crystals, and adsorption behaviour is therefore often compared to studies on single crystals. From electrochemical studies it is well known that water influences the adsorbed state of CO on platinum catalysts considerably. Furthermore, single crystal studies also report on the influence of water on adsorbed CO [64-66]. A clear red shift was observed for both linear and bridged CO on platinum upon gradual addition of D_2O, which was explained by a combination of increased π-back-donation from Pt to CO and a change in CO dipole moment [64,65]. Beside the influence of water it is well-known that a change in electrode potential also causes a shift in peak position of adsorbed CO [99,104,105]. Moreover, a linear relation between pH of the solution and the observed metal potential was published [100], which was accompanied by a relation between the corrected potential and the observed frequency of adsorbed CO [99,106].

In the 1960s it was proposed that a reactant-pair of water and CO was involved in the reaction mechanism for the electrochemical oxidation of adsorbed CO [101]. Nowadays it is generally accepted that an activated complex of water and CO is involved in the reaction mechanism, although the exact nature of this specie is speculative [101,103]. The mechanism assumes a Langmuir-Hinshelwood type reaction between carbon monoxide and a oxygen containing surface specie, adsorbed on adjacent sites, to form CO_2. The oxygen containing specie for electro oxidation is thought to result from oxidation of water at the electrode surface and is usually supposed to be adsorbed OH. The activated complex involved in the reaction is either a direct complex between water and CO ($CO\text{-}H_2O$) [101] (reaction 1.7 – 1.10 below), which oxidises to give CO-OH, or a complex between CO and a specie originating from oxidation of water; a complex between CO and $OH_{(ads)}$ [103] (reaction 1.11 – 1.14).

$$CO_{(aq)} \rightleftarrows CO_{(ads)} \tag{1.7}$$

$$CO_{(ads)} + H_2O \rightarrow CO\text{-}H_2O_{(ads)} \tag{1.8}$$

$$CO\text{-}H_2O_{(ads)} \rightarrow CO\text{-}OH_{(ads)} + H^+ + e^- \tag{1.9}$$

$$CO\text{-}OH_{(ads)} \rightarrow CO_{2(aq)} + H^+ + e^- \tag{1.10}$$

Or

$$CO_{(aq)} \rightleftarrows CO_{(ads)} \tag{1.11}$$

$$H_2O \rightarrow OH_{(ads)} + H^+ + e^- \tag{1.12}$$

$$CO_{(ads)} + OH_{(ads)} \rightarrow CO\text{-}OH_{(ads)} \tag{1.13}$$

$$CO\text{-}OH_{(ads)} \rightarrow CO_{2(aq)} + H^+ + e^- \tag{1.14}$$

Electrochemical oxidation of CO over either platinum or gold, was reported to be fastest in alkaline solutions, where the CO stretch frequency was lowest [100,106]. It is well known that pH influences the activity of CO oxidation in aqueous phase significantly. Details on the influence of pH on heterogeneous catalytic reactions have on the other hand not been resolved.

Because of the applications of CO as a probe molecule in order to examine modifications of the metal particles and/or its surrounding medium, CO is an ideal model compound to characterise supported noble metal catalysts. Moreover because

of the simplicity of CO oxidation, CO adsorption and oxidation it is an ideal reaction to study the details of the influence of water and pH on oxidation reactions.

1.4 Water treatment

Industrial plants generate increasing amounts of waste water, which often contain toxic organic compounds. Furthermore inorganic compounds like nitrate and nitrites arising from agricultural fertilizers, septic tank systems and animal waste disposal are of increasing concern. Waste- and ground water treatments are therefore receiving more and more attention.

The wet-air oxidation (WAO) process has a great potential for the treatment of waste water containing high concentrations of organic matter. In the WAO processes, which can be performed over several oxidation catalysts, the organic contaminants are either partially degraded by means of an oxidizing agent into biodegradable intermediates or converted into inorganic compounds such as CO_2, H_2O and inorganic salts [107-110].

Denitrification; nitrite and nitrate hydrogenation, is retrieving increased attention due to the high nitrite and nitrate levels found in groundwater throughout Europe. In some cases these levels even exceed legal limits causing local wells to be closed down [3,4]. Nitrate and nitrite are potentially hazardous to humans, especially to infants, causing the condition methemoglobinemia, also known as blue baby syndrome [111]. Methemoglobinemia prevents blood cells from absorbing oxygen, leading to suffocation and possible death. Consumption of high levels of nitrate and nitrite is also under the suspicion of causing other health problems, for example gastric cancer [111]. Three techniques for nitrate and nitrite removal are proposed; biological denitrification, electrochemical reduction and catalytic hydrogenation over supported noble metal catalysts. The biological processes have a slow reaction rate, causing these processes to be insufficient for ground water treatment [112]. The most promising method for nitrate and nitrite removal is based on selective hydrogenation over noble metal catalysts, which was described for the first time in 1989 [6]. To date, the catalytic hydrogenation of nitrite and nitrate for use in water purification have been examined extensively in order to develop efficient catalysts [5-16]. Although kinetic experiments rarely provide enough evidence to decide on reaction mechanisms, since no *in-situ* studies of surface intermediates have been performed, a reaction mechanism for the hydrogenation mechanism was proposed based on kinetic measurements only [13-16]. Beside the heterogeneous catalytic hydrogenation of nitrates, more insight in the surface intermediates is provided from

electrochemical reduction of nitrite and nitrate, which has also been studied in order to remove nitrate from ground water [113].

1.4.1 Nitrate and nitrite hydrogenation by noble metal catalysts

Over noble metal catalysts nitrate was found to hydrogenate to nitrogen and ammonia with nitrite as an intermediate [6], as shown in reaction (1.15) to (1.17):

$$NO_3^- + 5\ H_2 \rightarrow NH_4^+ + 2\ OH^- + H_2O \quad (1.15)$$

$$2\ NO_3^- + 5\ H_2 \rightarrow N_2 + 2\ OH^- + 4\ H_2O \quad (1.16)$$

$$NO_3^- + 4\ H_2 \rightarrow NO_2^- + H_2O \quad (1.17)$$

The produced nitrite as shown in reaction (1.17) can undergo further hydrogenation to yield nitrogen and ammonia:

$$2\ NO_2^- + 3\ H_2 \rightarrow N_2 + 2\ OH^- + 2\ H_2O \quad (1.18)$$

$$NO_2^- + 3\ H_2 \rightarrow NH_4^+ + 2\ OH^- \quad (1.19)$$

Nitrite hydrogenation can be performed over single noble metal catalysts such as platinum and palladium catalysts, where palladium catalysts posses a higher selectivity to nitrogen. High selectivity towards nitrogen is essential, since ammonia is toxic and therefore an undesirable side product. Nitrate hydrogenation on the other hand requires promoted metal catalysts; bimetallic noble metal catalysts have shown high activity and selectivity to nitrogen [112]. It is reported that palladium catalysts promoted by copper are the most active and selective bimetallic catalysts for the reduction of nitrate to nitrogen [5-12]. Other suitable promoters are tin [114] and indium [9]. Although it is generally accepted that single noble metal catalysts do not show activity towards to nitrate hydrogenation, supported platinum and palladium catalysts were shown to be active, but with a very low activity [115,116]. Furthermore both pH and hydrogen concentration were found to influence the selectivity. At high hydrogen concentration, the main product is ammonia [5,117,118], whereas the highest selectivity to nitrogen is found at low pH [6,14,119-122]. Based on kinetic studies, adsorbed NO was suggested as an intermediate [12]. Several authors have proposed a reaction scheme including adsorbed NO as a key intermediate for the catalytic hydrogenation of nitrate / nitrite [13-16] over supported bimetallic catalysts as shown in Scheme 1.1.

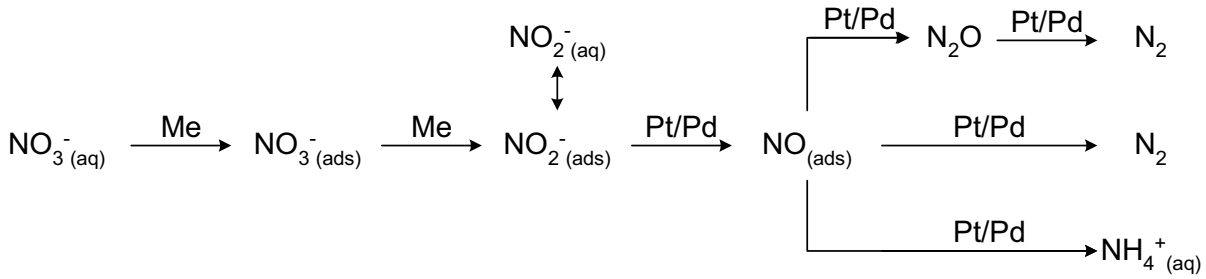

Scheme 1.1. Scheme of nitrate (and nitrite) hydrogenation over bimetallic platinum or palladium catalysts, after [13,14].

Of the reaction intermediates and products proposed in Scheme 1.1 only the formation of NO_2^-, N_2, N_2O and NH_4^+ were supported with experimental evidence [7,8,12-14]. Dissociative adsorption of hydrogen on the noble metal surface [123] is assumed to be the first step in the hydrogenation of nitrate, followed by reaction with nitrate to form nitrite as the rate limiting step. The formed nitrite partially desorbs from the surface and has been detected in the solution. Either adsorbed nitrite reacts with hydrogen, via a Langmuir-Hinselwood mechanism [13,117,124,125], or $NO_{2\,(aq)}^-$ reacts with adsorbed hydrogen via an Eley-Rideal mechanism on adsorbed hydrogen [12]. Nitrite is believed to hydrogenate to adsorbed nitric oxide although it has never been detected. Nitric oxide is believed to undergo further hydrogenation to nitrogen and ammonia, as shown in Scheme 1.1.

1.4.2 Electrochemical reduction of nitrate and nitrite

Electrochemical reduction is also investigated for removal of nitrite and nitrate from waste water. The electrochemical reduction of nitrate has been shown to be a more complex surface reaction than the heterogeneous catalytic hydrogenation proposed in Scheme 1.1. The electrochemical reduction was investigated on platinum electrodes mainly and involves a large number of intermediates such as NO_2, HNO_2, NO, N_2O, N_2, H_2NO, NH_2OH, NH_3 and NH_4^+ [126-135]. Formation of the reduction products is dependent on the applied potential, the electrolyte, the acidity and the nitrate concentration.

It was shown that the electro reduction of nitrate follows different mechanisms depending of the acidity of the nitrate solution, although in all cases nitric oxide was shown to be a stable intermediate during nitrate reduction over platinum [128,136]. Further it was shown that hydrogen inhibits the reduction, by blocking the adsorption sites for the nitrate ions. At low nitrate concentration, the rate-determining step is the reduction of nitrate to nitrite. Nitrite is subsequently reduced to adsorbed NO [126-

135]. NO adlayers are normally formed from nitrite or nitrate solutions where the electrode is held at a controlled potential according to reaction (1.20) [136], which shows that adsorbed NO is formed as an intermediate during electro reduction of nitrate and nitrite as well [126,133,137-140].

$$NO_2^- + 2\,H^+ + e^- \rightarrow NO_{(ads)} + H_2O \qquad (1.20)$$

The electrochemical reduction of adsorbed NO was shown to yield ammonia mainly on both polycrystalline platinum and single crystal platinum electrodes [135,140-143]. The electrochemical reduction of nitric oxide to ammonia was shown to proceed via a stepwise hydrogenation process involving the formation of HNO, HNOH, NH_2OH and NH_2 [126,134,135,138,142,144-149]:

$$NO_{(ads)} + H^+ + e^- \rightarrow NOH_{(ads)} \qquad (1.21)$$

$$NOH_{(ads)} + H^+ + e^- \rightarrow H_2NO_{(ads)} \qquad (1.22)$$

$$H_2NO_{(ads)} + H^+ + e^- \rightarrow H_2NOH_{(ads)} \qquad (1.23)$$

$$H_2NOH_{(ads)} + 3\,H^+ + 2\,e^- \rightarrow NH_4^+ + H_2O \qquad (1.24)$$

Beside ammonia also traces of N_2O were detected and shown to be an intermediate in the formation of nitrogen. Formation of N_2O was suggested to result from either dimerisation of HNO or NOH, resulting in a NO dimer as a precursor for N_2O formation [126,135,145,148,150-155], or via dissociation of NO on steps [143]. Infrared spectroscopy is widely used to identify the surface intermediates during electrochemical reactions, and adsorbed NO_2, HNO_2, NO, N_2O, H_2NO, NH_2OH and NH_3 was proven as intermediates during electrochemical reduction of nitrate/nitrie over platinum electrodes [126-135].

The experimental data currently available on hydrogenation/reduction of nitrate, nitrite and NO adlayers are insufficient to understand the mechanism of heterogeneous hydrogenation fully. Moreover there is little insight into the factors controlling the activity and selectivity of palladium and platinum catalysts for hydrogenation of nitrate and nitrite to nitrogen. Unfortunately, the knowledge gained from electrochemical studies using FT-IR spectroscopy cannot be compared to catalytic studies directly. First, FT-IR spectra can only be obtained using very thin liquid layers, inducing mass transfer problems during experiments. Second, electrochemical studies are confined to dense conducting electrodes, often single

crystals, which are very different from catalysts, which contain nano-particles on porous (non-conducting) support materials. Therefore identification of the reaction intermediates is the key step in clarifying any hydrogenation mechanism.

1.5 Scope and outline of this thesis

The objective of the research described in this thesis is to gain experimental proof for the presence of surface intermediates present during catalytic reactions in aqueous phase. Information on surface intermediates provides better understanding of the reaction mechanism involved. Based in the surface intermediates and reaction mechanism, the influence of reaction conditions kinetics (activity and selectivity) can be understood better. Furthermore a general understanding of heterogeneous catalytic reactions in aqueous phase would close the gap between studies on electrochemical and heterogeneous catalytic reactions. For this purpose adsorption and oxidation of carbon monoxide were investigated on platinum and palladium catalysts from both gas and aqueous phase. Furthermore nitrate and nitrite hydrogenation was investigated in aqueous phase. In order to examine both the influence of the presence of water and the influence of pH, carbon monoxide adsorption and oxidation were carried out in gas phase and at various pH in aqueous phase. For that purpose an infrared cell operating in ATR mode has been developed. The scientific output gained on the behaviour of the supported noble metal, during adsorption and oxidation of carbon monoxide, is used to describe the mechanistic aspects of the catalytic hydrogenation of nitrite and nitrate. Description of the ATR-IR cell as well as preparation of stable catalyst layers are described in Chapter 2.

Chapter 3 reports on the influence of water on carbon monoxide adsorption and oxidation on Pt/ZnSe. Chapter 4 and 5 describe the detailed study of the influence of water and pH on adsorption and oxidation of carbon monoxide on platinum and palladium supported on alumina. Furthermore, the results are compared to electrochemical oxidation of carbon monoxide.

In relation to the heterogeneous hydrogenation of nitrite, adsorption and decomposition of nitrite, ammonia and hydroxylamine from aqueous phase were examined on Pd/Al_2O_3, Pt/Al_2O_3 and Al_2O_3 and presented in Chapter 6. These results are used to describe the hydrogenation mechanism of nitrite over Pd/Al_2O_3 (Chapter 7) and Pt/Al_2O_3 (Chapter 8) at neutral pH. Furthermore, the influence of hydrogen concentration on the reaction mechanism for nitrite hydrogenation is investigated in Chapter 7. Finally, the results of the present research are summarised in Chapter 9.

1.6 References

[1] A. Pintar, Catal.Today 77 (2003) 451.
[2] P.T. Anastas, L.G. Heine, T.C. Williamson, Green Chemical Syntheses and Processes, American Chemical Society, Washington, D.C, 2000.
[3] World Health Organization, Water and health in Europe, WHO, Regional Office for Europe, Copenhagen, 2002.
[4] World Health Organization, Nitrate and nitrite in Drinking-water, WHO, Regional Office for Europe, Copenhagen, 2003.
[5] S. Hörold, K.D. Vorlop, T. Tacke, M. Sell, Catal.Today 17 (1993) 21.
[6] K.D. Vorlop, T. Tacke, Chem.Ing.Tech. 61 (1989) 836.
[7] S. Hörold, T. Tacke, K.D. Vorlop, Environ.Technol. 14 (1993) 931.
[8] K.D. Vorlop, U. Prusse, Environmental catalysis (1999) 195
[9] M. Hahnlein, U. Prusse, J. Daum, V. Morawsky, M. Koger, M. Schroder, M. Schnabel ,K.D. Vorlop, Preparation of catalysts VII (1998) 99
[10] U. Prüsse, J. Daum, C. Bock, K.D. Vorlop, Stud.Surf.Sci.Catal. 130 (2000) 2237.
[11] A. Pintar, J. Batista, J. Levec, Water.Sci.Technol. 37 (1998) 177.
[12] J. Wärnå, I. Turunen, T. Salmi, T. Maunula, Chem.Eng.Sci. 49 (1994) 5763.
[13] A. Pintar, J. Batista, J. Levec, T. Kijiuchi, Appl.Catal.B 11 (1996) 81.
[14] U. Prüsse, M. Hahnlein, J. Daum, K.D. Vorlop, Catal.Today 55 (2000) 79.
[15] K. Daub, G. Emig, M.J. Chollier, M. Callant, R. Dittmeyer, Chem.Eng.Sci. 54 (1999) 1577.
[16] J. Daum, K.D. Vorlop, Chem.Eng.Tech. 22 (1999) 199.
[17] N.J. Harrick, Internal Reflection Spectroscopy, Interscience Publishing, New York, 1967.
[18] M. Bartok, J. Sakany, A. Sitkei, J.Catal. 72 (1981) 236.
[19] S. Boujana, D. Demri, J. Cressely, A. Kiennemann, J.P. Hindermann, Catal.Lett. 7 (1990) 359.
[20] A. Bourane, O. Dulaurent, D. Bianchi, Langmuir 17 (2001) 5496.
[21] D.C. Koningsberger, D.E. Ramaker, J.T. Miller, J. de Graaf, B.L. Mojet, Top.Catal. 15 (2001) 35.
[22] G. Larsen, G.L. Haller, Catal.Lett. 3 (1989) 103.
[23] B.L. Mojet, J.T. Miller, D.E. Ramaker, D.C. Koningsberger, J.Catal. 186 (1999) 373.
[24] B.L. Mojet, D.C. Koningsberger, Catal.Lett. 39 (1996) 191.
[25] B.L. Mojet, J.T. Miller, D.C. Koningsberger, J.Phys.Chem.B. 103 (1999) 2724.
[26] V. Pitchon, M. Primet, H. Praliaud, Appl.Catal. 62 (1990) 317.

[27] M. Primet, J.Catal. 88 (1984) 273.
[28] F. Stoop, F.J.C.M. Toolenaar, V. Ponec, J.Catal. 73 (1982) 50.
[29] T. Visser, T.A. Nijhuis, A.M.J. van der Eerden, K. Jenken, Y. Ji, W. Bras, S. Nikitenko, Y. Ikeda, M. Lepage, B.M. Weckhuysen, J.Phys.Chem.B. 109 (2005) 3822.
[30] R.P. Eischens, S.A. Francis, W.A. Pliskin, J.Phys.Chem. 60 (1956) 194.
[31] S.A. Tatulian, Biochemestry 42 (2003) 11898.
[32] C.L. Schulman, M.G. Richmond, W.H. Watson, A. Nagl, J.Organomet.Chem. 368 (1989) 367.
[33] W.R. Moser, B.J. Marshik-Guerts, S.J. Okrasinski, J.Mol.Catal.A 143 (1999) 71.
[34] W.R.M. Oser, C.J. Papile, S.J. Weininger, J.Catal. 41 (1987) 293.
[35] W.R. Moser, J.E. Cnossen, A.W. Wang, S.A. Krouse, J.Catal. 95 (1985) 21.
[36] D.E. Leyden, R.S.S. Murthy, J.B. Atwater, J.P. Blitz, Anal.Chim.Acta 200 (1987) 459.
[37] M. Allmendinger, R. Eberhardt, G. Luinstra, B. Rieger, J.Am.Chem.Soc. 124 (2002) 5646.
[38] J.R. Zoeller, N.L. Buchanan, T.J. Dickson, K.K. Ramming, Catal.Today 49 (1999) 431.
[39] W.R. Moser, J.R. Berard, P.J. Melling, R.J. Burger, App.Spectrosc. 46 (1992) 1105.
[40] D. Ferri, T. Bürgi, A. Baiker, J.Phys.Chem.B. 105 (2001) 3187.
[41] R. He, R.R. Davda, J.A. Dumesic, J.Phys.Chem.B 109, (2005) 2810.
[42] B.A. Holmen, M.I. Tejedor-Tejedor, W.H. Casey, Langmuir 13 (1997) 2197.
[43] C. Keresszegi, T. Bürgi, T. Mallat, A. Baiker, J.Catal. 211 (2002) 244.
[44] I. Ortiz-Hernandez, C.T. Williams, Langmuir 19 (2003) 2956.
[45] R.P. Sperline, Y. Song, H. Freiser, Langmuir 8 (1992) 2183.
[46] M.I. Tejedor-Tejedor, M.A. Anderson, Langmuir 2 (1986) 203.
[47] C. Keresszegi, D. Ferri, T. Mallat, A. Baiker, J.Phys.Chem.B. 109 (2005) 958.
[48] T. Bürgi, A. Baiker, Adv.Catal. 50 (2006) 227.
[49] E.C. Yost, M.I. Tejedor-Tejedor, M.A. Anderson, Environ,Sci.Technol. 24 (1990) 822.
[50] M.I. Tejedortejedor, E.C. Yost, M.A. Anderson, Langmuir 8 (1992) 525.
[51] M.I. Tejedortejedor, E.C. Yost, M.A. Anderson, Langmuir 6 (1990) 979.
[52] S.J. Huo, B. Sulzberger, Langmuir 10 (1994) 3587.
[53] P.A. Connor, K.D. Dobson, A.J. McQuillan, Langmuir 11 (1995) 4193.
[54] K.D. Dobson, P.A. Connor, A.J. McQuillan, Langmuir 13 (1997) 2614.
[55] J.M. Kesselman-Truttmann, S.J. Hug, Environ,Sci.Technol. 33 (1999) 3171.
[56] D. Ferri, T. Bürgi, A. Baiker, J.Catal. 210 (2002) 160.

[57] D. Ferri, S. Frauchiger, T. Burgi, A. Baiker, J.Catal. 219 (2003) 425.
[58] A. Gisler, T. Bürgi, A. Baiker, J.Catal. 222 (2004) 461.
[59] T. Bürgi, A. Baiker, J.Phys.Chem.B. 106 (2002) 10649.
[60] T. Bürgi, R. Wirz, A. Baiker, J.Phys.Chem.B. 107 (2003) 6774.
[61] N.J. Harrick, J.Phys.Chem. 64 (1960) 1110.
[62] J. Fahrenfort, Spectrochimica Acta 17 (1961) 698.
[63] M.A. Henderson, Surf.Sci.Reports 46 (2002) 5.
[64] N.C. Yee, G.S. Chottiner, D.A. Scherson, J.Phys.Chem.B. 109 (2005) 7610.
[65] N. Kizhakevariam, X. Jiang, M.J. Weaver, J.Chem.Phys. 100 (1994) 6750.
[66] G. Rupprechter, T. Dellwig, H. Unterhalt, H.J. Freund, J.Phys.Chem.B. 105 (2001) 3797.
[67] I. Langmuir, Trans.Faraday.Soc. 17 (1922) 672.
[68] G. Ertl, T. Engel, Adv.Catal. 28 (1979) 1.
[69] G. Ertl, Adv.Catal. 37 (1990) 213.
[70] T. Engel, G. Ertl, Chem.Phys.Lett. 54 (1978) 95.
[71] T. Engel, G. Ertl, J.Chem.Phys. 69 (1978) 1267.
[72] C.T. Campbell, G. Ertl, H. Kuipers, J. Segner, J.Chem.Phys. 73 (1980) 5862.
[73] A. Alavi, P.J. Hu, T. Deutsch, P.L. Silvestrelli, J. Hutter, Phys.Rev.Lett. 80 (1998) 3650.
[74] T.E. Madey, H.A. Engelhardt, D. Menzel, Surf.Sci. 48 (1975) 304.
[75] G. Ertl, Surf.Sci. 299-300 (1994) 742.
[76] A.N. Artsyukhovich, V.A. Ukraintsev, I. Harrison, Surf.Sci. 347 (1996) 303.
[77] F.J. Gracia, S. Guerrero, E.E. Wolf, J.T. Miller, A.J. Kropf, J.Catal. 233 (2005) 372.
[78] P.J. Berlowitz, C.H.F. Peden, D.W. Goodman, J.Phys.Chem. 92 (1988) 5213.
[79] S. Ladas, H. Poppa, M. Boudart, Surf.Sci. 102 (1981) 151.
[80] N.W. Cant, P.C. Hicks, B.S. Lennon, J.Catal. 54 (1978) 372.
[81] E. Gillet, S. Channakhone, V. Matolin, M. Gillet, Surf.Sci. 152 (1985) 603.
[82] W.H. Weinberg, C.M. Comrie, R.M. Lambert, J.Catal. 41 (1976) 489.
[83] V. Matolin, E. Gillet, Surf.Sci. 166 (1986) L115.
[84] D. Mukesh, W. Morton, C.N. Kenney, M.B. Cutlip, Surf.Sci. 138 (1984) 237.
[85] H. Conrad, G. Ertl, J. Kuppers, Surf.Sci. 76 (1978) 323.
[86] E.M. Stuve, R.J. Madix, C.R. Brundle, Surf.Sci. 146 (1984) 155.
[87] M. Ehsasi, C. Scidel, H. Ruppender, W. Drachsel, J.H. Block, K. Christmann, Surf.Sci. 210 (1989) L198.
[88] D.J. Kaul, E.E. Wolf, J.Catal. 93 (1985) 321.
[89] D.T. Lynch, S.E. Wanke, J.Catal. 88 (1984) 333.
[90] P.J. Plath, K. Moller, N.I. Jaeger, J.Chem.Soc.Faraday Trans. 84 (1988) 1751.

[91] L.F. Razon, R.A. Schmitz, Catal.Rev.-Sci.Eng. 28 (1986) 89.
[92] I. Kevrekidis, L.D. Schmidt, R. Aris, Surf.Sci. 137 (1984) 151.
[93] S. Ladas, R. Imbihl, G. Ertl, Surf.Sci. 198 (1988) 42.
[94] F. Schuth, E. Wicke, Ber.Bunsenges.Phys.Chem. 93 (1989) 491.
[95] B.C. Sales, J.E. Turner, M.B. Maple, Surf.Sci. 114 (1982) 381.
[96] J.E. Turner, M.B. Maple, Surf.Sci. 147 (1984) 647.
[97] V.A. Burrows, S. Sundaresan, Y.J. Chabal, S.B. Christman, Surf.Sci. 180 (1987) 110.
[98] N.A. Collins, S. Sundaresan, Y.J. Chabal, Surf.Sci. 180 (1987) 136.
[99] S.-C. Chang, M.J. Weaver, J.Chem.Phys. 92 (1990) 4582.
[100] A. Couto, A. Rincón, M.C. Pérez, C. Gutiérrez, Electrochim.Acta 46 (2001) 1285.
[101] S. Gilman, J.Phys.Chem. 68 (1964) 70.
[102] H.L. Lam-Wing, A. Wieckowski, M.J. Weaver, J.Phys.Chem. 92 (1988) 6985.
[103] N.P. Lebedeva, A. Rodes, J.M. Feliu, M.T.M. Koper, R.A. van Santen, J.Phys.Chem.B. 106 (2002) 9863.
[104] S.A. Wasileski, M.T.M. Koper, M.J. Weaver, J.Phys.Chem.B. 105 (2001) 3518.
[105] J. Xu, J.T. Yates, Surf.Sci. 327 (1995) 193.
[106] K. Kunimatsu, A. Aramata, H. Nakajima, H. Kita, J.Electroanal.Chem. 207 (1986) 293.
[107] V.S. Mishra, V.V. Mahajani, J.B. Joshi, Ind.Eng.Chem.Res. 34 (1995) 2.
[108] F. Luck, Catal.Today 53 (1999) 81.
[109] J. Levec, A. Pintar, Catal.Today 24 (1995) 51.
[110] S. Imamura, Ind.Eng.Chem.Res. 38 (1999) 1743.
[111] C.S.Bruningfann, J.B.Kaneene, Vet.Hum.Toxicol 35, (1993) 521.
[112] A. Kapoor, T. Viraraghavan, J.Environ.Eng. 123 (1997) 371.
[113] L. Szpyrkowicz, S. Daniele, M. Radaelli, S. Specchia, Appl.Catal.B 66 (2006) 40.
[114] U. Prüsse, S. Hörold, K.-D. Vorlop, Chem.Ing.Tech. 69 (1997) 93.
[115] N. Barrabes, J. Just, A. Dafinov, F. Medina, J.L.G. Fierro, J.E. Sueiras, P. Salagre, Y. Cesteros, Appl.Catal.B 62 (2006) 77.
[116] K.J. Reddy, J.P. Lin, Wat.Res. 34 (2000) 995.
[117] Y. Matatov-Meytal, V. Barelko, I. Yuranov, M. Sheintuch, Appl.Catal.B 27 (2000) 127.
[118] Y. Matatov-Meytal, Y. Shindler, M. Sheintuch, Appl.Catal.B 45 (2003) 127.
[119] F. Deganello, L.F. Liotta, A. Macaluso, A.M. Menezia, G. Deganello, Appl.Catal.B 24 (2000) 265.

[120] Y. Matatov-Meytal, V. Barelko, I. Yuranov, L. Kiwi-Minsker, A. Renken, M. Sheintuch, Appl.Catal.B 31 (2001) 233.
[121] A. Pintar, M. Setinc, J. Levec, J.Catal. 174 (1998) 72.
[122] W. Gao, J. Chen, X. Guan, R. Jin, F. Zhang, N. Guan, Catal.Today 93-95 (2004) 333.
[123] C.A.L.Y. Leon, M.A. Vannice, Appl.Catal. 69 (1991) 269.
[124] K. Daub, V.K. Wunder, R. Dittmeyer, Catal.Today 67 (2001) 257.
[125] A. Pintar, M. Setinc, J. Levec, J.Catal. 174 (1998) 72.
[126] M.C.P.M. da Cunha, J.P.I. De Souza, F.C. Nart, Langmuir 16 (2000) 771.
[127] M.T. de Groot, M.T.M. Koper, J.Electroanal.Chem. 562 (2004) 81.
[128] G.E. Dima, A.C.A. de Vooys, Koper M.T.M., J.Electroanal.Chem. 554-555 (2003) 15.
[129] H.N. Heckner, J.Electroanal.Chem. 44 (1973) 9.
[130] J.F. van der Plas, E. Barendrecht, Electrochim.Acta 25 (1980) 1463.
[131] S. Silva, M.J. Sottomayor, A. Martins, Electrochim.Acta 39 (1994) 491.
[132] O.A. Petrii, T.A. Safonova, J.Electroanal.Chem. 331 (1992) 897.
[133] M.C.P.M. da Cunha, M. Weber, F.C. Nart, J.Electroanal.Chem. 414 (1996) 163.
[134] K. Nishimura, K. Machida, M. Enyo, Electrochim.Acta 36 (1991) 877.
[135] A.C.A. de Vooys, Koper M.T.M., R.A. van Santen, J.A.R. van Veen, Electrochim.Acta 46 (2001) 923.
[136] A. Rodes, R. Gomez, J.M. Orts, J.M. Feliu, A. Aldaz, J.Electroanal.Chem. 359 (1993) 315.
[137] Weaver M.J., S.Z. Zou, C. Tang, J.Chem.Phys. 111 (1999) 368.
[138] V. Rosca, M.T.M. Koper, J.Phys.Chem.B. 109 (2005) 16750.
[139] V. Rosca, G.L. Beltramo, M.T.M. Koper, Langmuir 21 (2005) 1448.
[140] R. Gomez, A. Rodes, J.M. Orts, J.M. Feliu, J.M. Perez, Surf.Sci. 342 (1995) L1104.
[141] A. Rodes, V. Climent, J.M. Orts, J.M. Pérez, A. Aldaz, Electrochim.Acta 44 (1998) 1077.
[142] G.L. Beltramo, M.T.M. Koper, Langmuir 19 (2003) 8907.
[143] J.F.E. Gootzen, R.M. van Hardeveld, W. Visscher, R.A. van Santen, J.A.R. van Veen, Recl.Trav.Chim.Pays-Bas 115 (1996) 480.
[144] L.J.J. Janssen, M.M.J. Pieterse, E. Barendrecht, Electrochim.Acta 22 (1977) 27.
[145] J.A. Colucci, M.J. Foral, S.H. Langer, Electrochim.Acta 30 (1985) 521.
[146] G.E. Dima, G.L. Beltramo, M.T.M. Koper, Electrochim.Acta 50 (2005) 4318.
[147] F. Balbaud, G. Sanchez, G. Santarini, G. Picard, Eur.J.Inorg.Chem. 4 (2000) 665.

[148] A.C.A. de Vooys, Koper M.T.M., R.A. van Santen, J.A.R. van Veen, J.Catal. 202 (2001) 387.
[149] V. Rosca, Koper M.T.M., Surf.Sci. 584 (2005) 258.
[150] I. Paseka, J. Vonkova, Electrochim.Acta 25 (1980) 1251.
[151] I. Paseka, A. Hodinar, Electrochim.Acta 27 (1982) 1461.
[152] A.C.A. de Vooys, G.L. Beltramo, B. van Riet, J.A.R. van Veen, M.T.M. Koper, Electrochim.Acta 49 (2004) 1307.
[153] J.H. MacNeil, P.A. Berseth, G. Westwood, W.C. Trogler, Environ,Sci.Technol. 32 (1998) 876.
[154] S. Kuwabata, S. Uezumi, K. Tanaka, T. Tanaka, Inorg.Chem. 25 (1986) 3018.
[155] V. Rosca, G.L. Beltramo, M.T.M. Koper, J.Electroanal.Chem. 566 (2004) 53.

CHAPTER 2

Experimental

Abstract

Attenuated Total Reflection Infrared Spectroscopy is a powerful tool for investigation of heterogeneous catalysts during reactions in strongly absorbing solvents. Correct design of the ATR-IR-cell allows for a good mimic of a normal liquid phase heterogeneous catalytic experiment. The home built *In-Situ* ATR-IR flow-through-cell used for the studies in the present thesis will be presented. For studies of the catalyst surface, it is essential that the catalyst layer is immobilized on the IRE. Preparation methods are described for both supported and unsupported catalysts that result in strongly attached layers which are stable for many days in a water flow. For experiments carried out in aqueous phase, it is necessary to subtract the signals from the liquid water spectrum. Moreover, the presence of dissolved gasses influences the intensity of the water spectrum. A detailed description for subtracting the water spectrum is given. Moreover, detailed description of the experimental procedures is included.

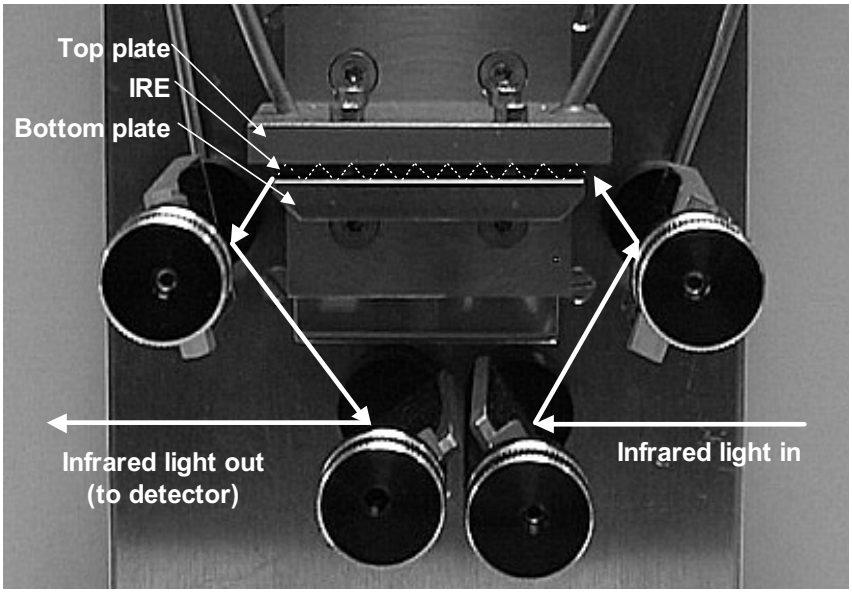

Home built in-situ ATR-IR flow-through-cell, presented in Figure 2.1

2.1 *In-situ* ATR-IR Spectroscopy

All *in-situ* ATR-IR spectra were recorded using a home-built stainless steel flow-through-cell as shown in Figure 2.1. The H-ATR accessory as shown in Figure 1.1 of chapter 1 was used as a model for construction of the cell, which was used for the catalytic experiments. The flow-through chamber was created by a spacer placed between the Internal Reflection Element (IRE) and the polished steel top plate. The thickness of the spacer was 0.3 mm, the length and width of the exposed area of the IRE were 40 and 10 mm, respectively. This creates a total volume of the cell of 120 μL. The flow in and out of the cell takes place via connections in the top plate, as shown in Figure 2.1. Aqueous flow was regulated by a belt pump (Watson Marlow 503s) mounted downstream of the ATR-IR cell (Figure 2.2) and if not mentioned otherwise, aqueous flow rates were 1 mL min^{-1}, resulting in a residence time in the cell of 7.2 seconds. The cell was mounted within the sample compartment of an infrared spectrometer (Bruker Tensor 27) equipped with a MCT detector. All ATR-IR spectra were recorded at room temperature (294 K) in an air-conditioned room. Infrared spectra were recorded by averaging of 128 scans with a resolution of 4 cm^{-1}. The *in-situ* ATR-IR cell was a part of the apparatus, schematically shown in Figure 2.2.

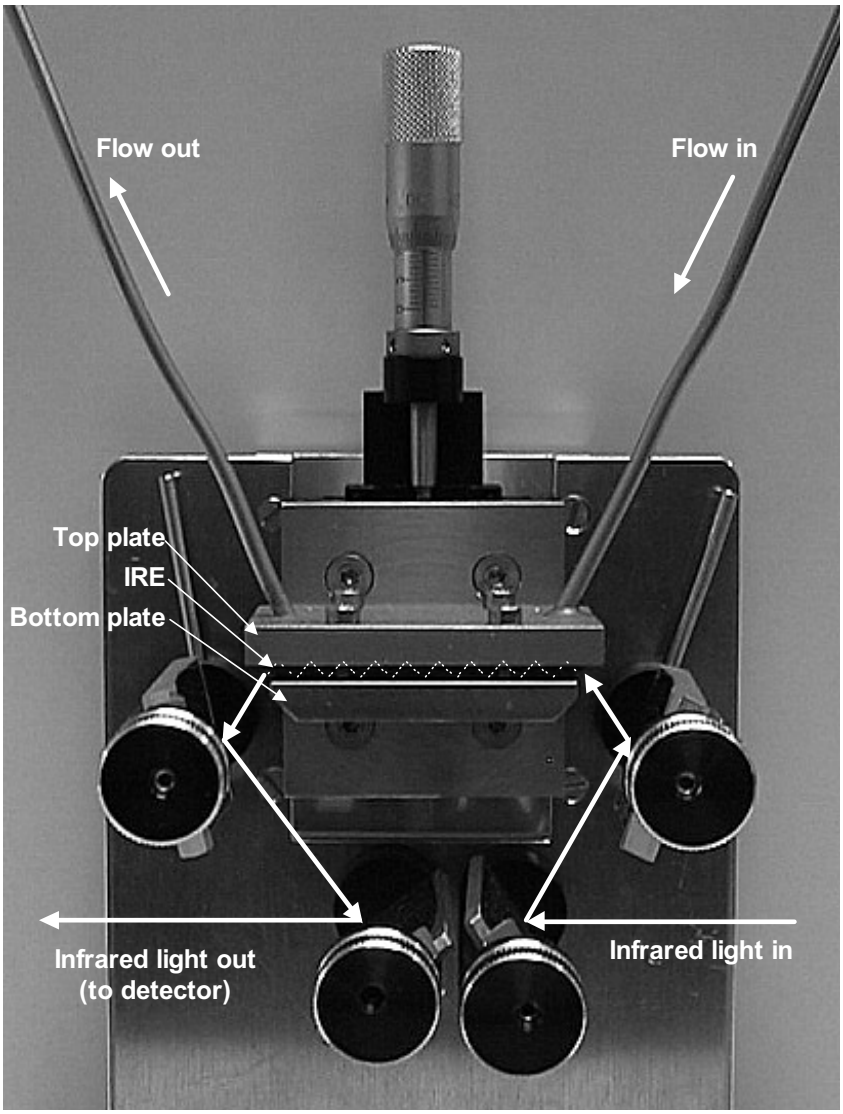

Figure 2.1. Home built in-situ ATR-IR flow-through-cell.

In the present thesis, oxidation and hydrogenation reactions are examined. Therefore the aqueous phase has to be saturated with either oxygen, hydrogen or an inert gas (for blank experiments). Bubble tanks (Figure 2.2) were used to ensure fast and complete saturation of the aqueous phase.

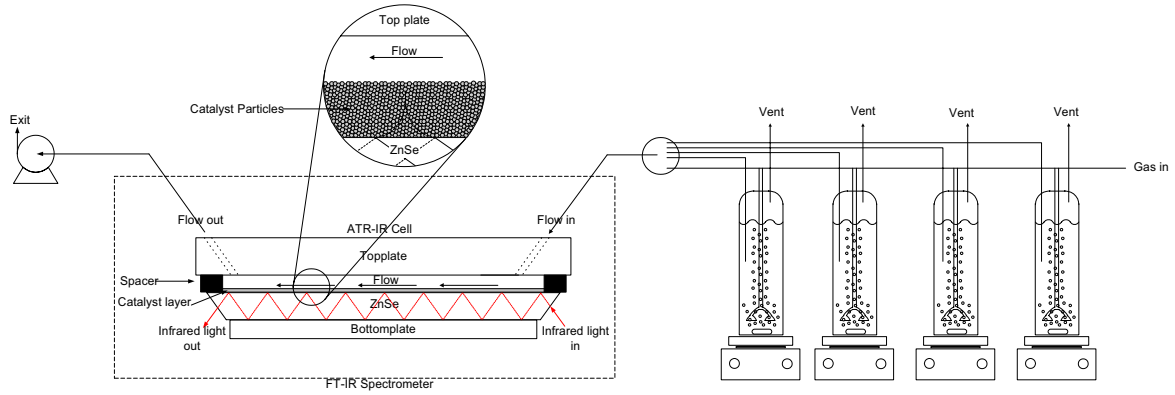

Figure 2.2. Schematic presentation of experimental setup with saturators and the FTIR spectrometer equipped with the home-built flow-through ATR-IR cell

A wide variety of materials are commercially available for use as IRE's. The most common among those include germanium, silicon, zinc selenide and zinc sulphide. A summary of their properties are given in Table 2.1. . The choice for a specific IRE material depends upon a number of factors. These include the spectral range of interest, the adsorbent/adsorbate system under investigation, the nature of the solvent, the pH range and the physical and chemical properties of the different IRE materials.

Table 2.1. Physical and chemical properties of IRE materials [1].

Material	Refractive index at 1000 cm^{-1}	Maximum useful temperature	Usable wavelength range in ATR	Remarks
Germanium (Ge)	4.02	125 ºC	5.500-830 cm^{-1}	Hard and brittle, temperature sensitive; chemically inert.
Silicon (Si)	3.42	300 ºC	8.300-1.500 cm^{-1}	Hard and brittle. Withstands thermal shock; chemically inert.
Zinc Selenide (ZnSe)	2.49	300 ºC (oxidises above 300°C)	20.000-650 cm^{-1}	Withstands limited mechanical and thermal shock. Soluble in acids and strong base.
Zinc Sulphide (ZnS)	2.27	300 ºC	17.000-950 cm^{-1}	Comparable to ZnSe, but slightly harder; chemically inert

For the investigation of powder catalysts, zinc selenide IRE's have the advantage of possessing a low refractive index, which results in a large penetration depth and

consequently stronger signals. Furthermore, zinc selenide IRE's have a better mechanical and thermal resistance than i.e. germanium IRE's. The transparent window for zinc selenide is between 20.000 – 650 cm^{-1}, making it a suitable material for studying both CO adsorption/oxidation and nitrate/nitrite hydrogenation. For these reasons a commercial trapezoidal 45º, 50×20×2 mm zinc selenide IRE, giving 25 reflections of which 13 is at the catalyst interface, was used for all ATR-IR experiments (International Crystal Laboratories).

After preparation of the thin catalyst layer in the IRE (see section 2.3.3) the coated IRE was mounted within the cell. The cell was then purged with either gaseous argon or argon saturated Q2-water for gaseous and aqueous phase experiments respectively (argon saturated Q2-water was flushed until a stable background spectrum was obtained, after approximately 12 hours).

2.1.1 Materials

For all experiments Q2-water was used (prepared by use of Millipore Milli-Q water treatment system from Amphotech Ltd). First air/oxygen was removed from the water by saturation with argon for several days. Afterwards, the water was saturated with CO, Ar, O_2 or H_2 at room temperature (294 K) using gas flow rates of 40 mL min^{-1}. All concentrations of gases in water are calculated based on saturation at room temperature and 1 atm. pressure. Q2-Water saturated with CO, Ar, O_2 or H_2 is denoted CO/H_2O, Ar/H_2O, O_2/H_2O and H_2/H_2O respectively. The pH of the solutions were adjusted with either H_2SO_4 (95-97%, Merck), H_3PO_4 (85%, Merck), HCl (37%, Merck) or NaOH (Merck) and measured by a pH meter (744 pH meter, Metrohm).

For pH adjustment of the solutions used for the examination of nitrite and nitrate hydrogenation, HCl (37%, Merck) or NaOH (Merck) was used. It is known that chlorine slightly decreases the reaction rate for nitrite and nitrate hydrogenation [2]. Still HCl is used for pH adjustment, since it is not infrared active, unlike H_2SO_4 and H_3PO_4 as can be seen from Figure 2.3. H_2SO_4 and H_3PO_4 are characterised by infrared peaks in the region between 1300 and 1000 cm^{-1}, which would interfere with the adsorption peaks for $NO_2^-{}_{(aq)}$ and adsorbed NO_2^- on noble metal catalysts, as will be described in detail in the chapters on nitrite hydrogenation (Chapter 6 – 8). Solutions of $NH_4^+{}_{(aq)}$, $NH_2OH_{(aq)}$ $NO_2^-{}_{(aq)}$ and $NO_3^-{}_{(aq)}$ were prepared from Ar/H_2O with NH_4Cl (99.999%, Alfa Aesar), $NH_2OH{\cdot}HCl$ (99%, Alfa Aesar), $NaNO_2$ (Merck) and $NaNO_3$ (Aldrich) respectively.

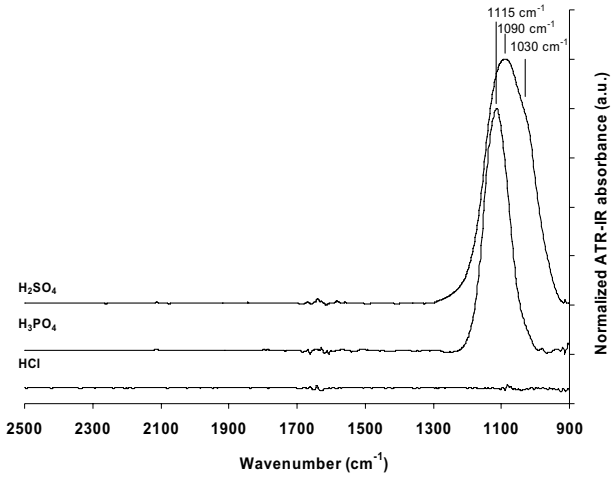

Figure 2.3. Water corrected ATR-IR spectra of H_2SO_4, H_3PO_4 and HCl at pH 5.

2.2 ATR-IR data treatment

For experiments carried out in aqueous phase, signals from the liquid water spectrum have been subtracted. Figure 2.4A shows the ATR-IR spectrum of water. Both liquid water and water vapour are characterised by two strong peaks, a broad peak at 3260 cm^{-1} corresponding to O–H stretching and a peak at 1635 cm^{-1} from the scissor bending were detected. However, in the case of liquid water additionally weaker near-infrared peaks (300-900 cm^{-1}) have been reported, which have no corresponding peaks in water vapour spectra [3]. An effect of these peaks can be found in the mid-infrared region, where a combination of the scissor bending at 1635 cm^{-1} and the very broad libration band in the near-infrared region is detected as a broad, weak peak at around 2120 cm^{-1} (Figure 2.4A). Clearly, the scissor bending (1635 cm^{-1}) and the broad combination band (2120 cm^{-1}) are located in the same infrared region as the adsorption peaks for nitric oxide and carbon monoxide adsorbed on noble metal catalysts.

Figure 2.4B shows the ATR-IR spectra of water saturated with respectively H_2, O_2 or CO in the region of the combination band. It is seen the intensity of the peaks changed due to the type of dissolved gas. Compared to H_2 saturated water, the combination band broadened and decreased in intensity when saturated with CO and O_2.

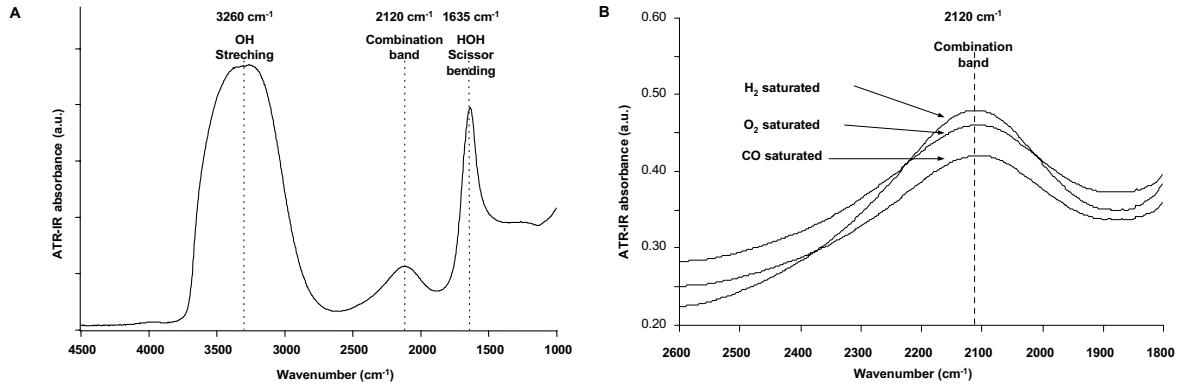

Figure 2.4. ATR-IR spectra of pure water on a clean ZnSe IRE (A) and water saturated with different gasses in the region of the combination peak (B).

Since during the experiments water is saturated with different gases it is necessary to include the change in peak intensity of the combination band, in the data analysis. The effect of dissolved gases can be treated by subtraction of a scaled background chosen by a fit to the spectrum of the sample to obtain a corresponding water spectrum.

2.2.1 Curve fitting

After subtraction of the water spectra, the residual spectra showed a complexity of peaks. For this reason, curve fitting was applied, using a Lorentzian function. The applied Lorentzian line-shape function centered at the frequency ω_0 is given by:

$$I(\omega)=A \cdot \frac{2}{\pi} \cdot \frac{w}{4 \cdot (\omega-\omega_0) + w^2} \qquad (2.1)$$

With:

$I(\omega)$: the intensity at a given frequency ω.

A: the integrated area.

w: the full width at half of the maximum intensity.

The squared difference between the sample spectra and the calculated spectra is calculated and minimised. As initial values for the peak position (ω_0), the maximum intensity was used and the peak width calculated from the spectra f the pure specie was employed.

2.3 Preparation of powder catalysts and catalyst layers on the IRE

For investigation of adsorption and reaction on the supported catalysts, platinum and palladium powder catalysts were first prepared and characterised. Investigation of the powder catalysts requires that they are immobilised on the IRE. Several methods can be used for the immobilisation. Preparation of stable layers of supported catalyst for ATR-IR was reported previously by evaporation of an aqueous suspension of the catalyst powder on the IRE without further treatment [4-6]. However, replication of this treatment in our laboratory did not result in stable layers when water was flushed. In the following a method to immobilize the catalyst layer by application of colloidal alumina followed by calcination and reduction will be described. This method did result in a smooth and stable catalyst layer, without influencing the properties of the catalyst.

2.3.1 Pt/Al_2O_3

Pt/Al_2O_3 was prepared by wet impregnation according to the following procedure. Al_2O_3 (Aluminum oxide C, Degussa, primary particle size 13 nm) was pre-calcined for 5 h at 823 K (heating/cooling rate 5 K/min) in stagnant air. The powder was then impregnated with a solution of $H_2PtCl_6 \cdot 6H_2O$ (Alfa Aesar) to yield a catalyst with 5 wt% metal loading. The catalyst solution was mixed for 2 h followed by drying at 335 K for 2 h in a rotating evaporator. The impregnated Pt/Al_2O_3 powder was calcined at 673 K for 3 h (heating rate 5 K/min) in flowing synthetic air (30 ml/min). Subsequently, the calcined catalyst was reduced at 673 K for 3 h (heating rate 5 K/min) in flowing hydrogen (30 ml/min).

2.3.2 Pd/Al_2O_3

The Pd/Al_2O_3 powder catalyst was prepared by adsorption. Al_2O_3 (Aluminum oxide C, Degussa) was pre-calcined for 5 h at 823 K (heating rate 5 K/min) in stagnant air. In order to obtain highly dispersed palladium particles, the Al_2O_3 powder was impregnated with a solution of palladium acetylacetonate ($Pd(acac)_2$) (Alfa Aesar) in toluene to yield a catalyst with a 5 wt% palladium loading. An excess of 30% of $Pd(acac)_2$ was dissolved in 400 mL toluene and 10 gram of Al_2O_3 was added to the solution, which was subsequently stirred for 24 h. The mixture was filtered and dried at 323 K for 15 h and calcined at 573 K (heating/cooling rate 1 K/min) in flowing synthetic air (30 ml/min). After each adsorption of $Pd(acac)_2$, the metal loading was measured using X-ray fluorescence spectroscopy (XRF) (Phillips PW 1480

spectrometer) and the metal dispersion was measured by CO chemisorption. To obtain a palladium loading of 5 wt%, the procedure was repeated (sing the remaining filtrate from the previous adsorption). The final catalyst was reduced at 223 K for 2 h (heating/cooling rate 1 K/min) in flowing hydrogen (30 ml/min), followed by flushing at 600 K for 1 h (heating/cooling rate 1 K/min) in flowing argon (30 ml/min), to avoid formation of palladium hydride.

2.3.3 Preparation of thin catalyst layers on the IRE

A suspension of Al_2O_3, Pt/Al_2O_3 or Pd/Al_2O_3 was prepared from the catalyst powders (0.10 g Al_2O_3, 0.30 g Pt/Al_2O_3 or 0.15 g Pd/Al_2O_3) in 50 mL water. The pH was adjusted to 3.5 using nitric acid to stabilise the small alumina particles. Different amounts of the powders were used because that was necessary to prevent cracking of the final layer. The suspension was milled for one hour in a ball-mill (Fritsch Pulverisette) to obtain Al_2O_3 particles of a few nanometer in size. Colloidal alumina (aluminum oxide, 20% in H_2O colloidal suspension, Alfa Aesar, particle size 5 nm) was added, which is the general methodology for preparing wash coats in monolithic catalysts [7]. For preparation of the Al_2O_3, Pt/Al_2O_3 and Pd/Al_2O_3 layer 0.025 mL, 0.075 mL and 0.0375 mL colloidal alumina were added respectively (corresponding to 5 wt% of the catalyst).

The catalyst layers were prepared on a ZnSe IRE by adding 1 mL of the catalyst/water suspension on one side of the IRE. The suspension was allowed to evaporate over night at room temperature. Subsequently, the catalyst layer/IRE was heated to 573 K for 2 h (heating rate 1 K/min) in flowing argon to ensure removal of all NO_x species on the catalyst surface. The procedure was repeated twice for the Al_2O_3 layer and once for the Pd/Al_2O_3 layer, in order to limit the formation of cracks in the final catalyst layer. About 6 mg of catalyst was deposited on the IRE in all cases. An additional reduction treatment was necessary for Pt/Al_2O_3 to remove all NO_x species (heating to 673 K in hydrogen, heating/cooling rate 10 K/min).

The γ-Al_2O_3 support used for the preparation of the supported catalysts (see below) was also immobilised on an ATR crystal to perform reference experiments of adsorbed species. Alumina was pre-treated by mimicking the calcination step in the preparation of the palladium and platinum catalysts, to obtain a stable thin layer of alumina. A suspension of 10 g of pre-calcined Al_2O_3 in 200 mL water was made and stirred for 2 h at room temperature, followed by drying at 335 K for 2 h in a rotating evaporator. Subsequently the Al_2O_3 powder was calcined at 673 K for 2 h (heating rate 5 K/min) in synthetic air (30 ml/min).

2.4 Preparation of thin film catalyst

2.4.1 Pt/ZnSe

The thin platinum catalyst layer was prepared by evaporating a solution containing 0.05 mg platinum prepared from dihydrogen hexachloroplatinate (0.088 mg $H_2PtCl_6 \cdot 6H_2O$ / mL H_2O) (Alfa Aesar) on a ZnSe IRE. The solution was left to evaporate overnight at 273 K in air followed by drying at 398 K for 2 hours in flowing synthetic air and subsequent reduction in 50% H_2/N_2 at 498 K for another 2 hours (flow rate 30 mL min^{-1}, heating and cooling ramp 1 K min^{-1}).

The catalyst is denoted Pt/ZnSe and to ensure identical conditions for intensity comparison the same layer was used throughout all experiments presented in Chapter 3; CO adsorption and oxidation over Pt/ZnSe.

2.5 Catalyst characterisation

The elemental composition of the powder catalysts was determined with X-ray fluorescence spectroscopy (XRF) (Phillips PW 1480 spectrometer).

Platinum dispersion was determined with H_2 chemisorption using 0.2 g of catalyst in a home-built volumetric system. The sample was reduced at 473 K in H_2 for 1 h. After reduction the sample was degassed at 473 K in vacuum (10^{-6} mbar). The sample was cooled to room temperature (293 K) in vacuum and the H_2 adsorption isotherm was measured. After the first isotherm the sample was degassed at room temperature, followed by a second H_2 adsorption isotherm. The hydrogen chemisorption capacity (H/Pt) was calculated by extrapolation of the hydrogen uptake to zero pressure, which corresponds to the difference between the first and second isotherm [8].

Palladium dispersion was determined with CO chemisorption of 0.15 g of catalyst in a dynamic system (ChemiSorb 2750, Micromeritics). The sample was reduced at 323 K in H_2 for 1 h (heating rate 1 K/min). After reduction the sample was purged with argon at 323 K and cooled to room temperature. Subsequently, pulses of 0.1 ml CO were introduced to the sample, until zero uptake was observed (around 10 pulses). The CO uptake was monitored by a Thermal Conductivity Detector (TCD). The dispersion and palladium surface area were calculated assuming stoichiometric adsorption of one CO molecule per Pd surface atom.

BET specific surface area of the powders was measured with N_2 adsorption-desorption at 77 K in a ASAP 2400 (Micromiretics) instrument.

The structure of the layers deposited on the IRE was studied with Scanning Electron Microscopy (SEM) (LEO 1550 FEG SEM). Since the ATR-crystals could not be broken to be examined, the preparation of the sample layers was mimicked on a glass plate. The glass plate was cut through from the back side using a diamond cutter and the sample layer was carefully broken and studied by SEM. In the case of Pt/ZnSe, Atomic Force Microscope (AFM) was used to characterise the platinum catalyst film.

Temperature Programmed Desorption (TPD) of N_xO_y-species was carried out to determine the required temperature for total removal of nitric acid during calcination and reduction of the catalyst layer on the IRE. A suspension of 5 wt% colloidal alumina - 5 wt% Pt/Al_2O_3 (or Pd/Al_2O_3) was prepared in water with nitric acid at pH 3.5. The suspension was dried and 2 gram of 5 wt% Pt/Al_2O_3 or Pd/Al_2O_3 powder was loaded into a glass tube reactor. TPD was performed in either synthetic air (calcination) or hydrogen (reduction) and a combination of synthetic air followed by hydrogen. N_xO_y-species were detected with an on-line mass spectrometer (Omnistar GSD 300, Balzers Instruments). It is crucial that all N_xO_y species are removed during the pre-treatment of the catalyst, to ensure that the observed adsorbed species during the reaction originate from the reaction investigated and not from the pre-treatment.

2.6 Results

2.6.1 Catalyst characterisation

2.6.1.1 Pt/ZnSe

Atomic Force Microscope was used to characterise the platinum catalyst layer on the ZnSe IRE. The catalyst layer consisted of platinum clusters up to 30 nm as shown in Figure 2.5. From an average particle size of 30 nm, the dispersion of the platinum was calculated to be 3% to 4%, resulting in a surface area of 0.015 m^2. The catalyst layer prepared by evaporation was found to adhere to the IRE in such way that no loss of IR signal was observed when water was flown over the layer for over three days. The film was sufficiently transparent for ATR-IR experiments, as it shows transmission of 15% approximately.

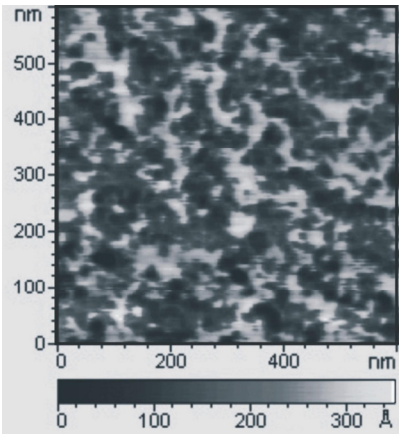

Figure 2.5. AFM image of prepared platinum film on the ZnSe IRE.

2.6.1.2 Al_2O_3/ZnSe

The specific surface area after calcination at 823 K, as determined by N_2 fysisorption of the Al_2O_3 support powder, was 125 m^2/g. After pre-treatment (suspension and drying) the surface area of the Al_2O_3 powder was 120 m^2/g. For measurement of the thickness of the alumina layer deposited on the IRE, a layer prepared on a glass plate was studied by SEM. Figure 2.6 shows typical SEM micrographs of the Al_2O_3 layer on a glass plate. The thickness of the catalyst layer was measured to be 6.50 ± 0.5 μm over the full length of the plate. Even though the layer was cracked, as can be seen in the top view of Figure 2.6, it remained stable during aqueous flow for several days. Based on the layer thickness and the catalyst amount the void fraction including pore volume is calculated to be 75%.

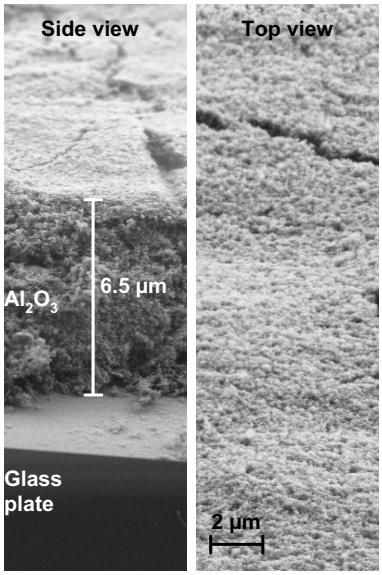

Figure 2.6. SEM micrographs of a Al_2O_3 layer on a glass plate with identical dimensions as the ZnSe IRE (Left: side view; right: top view).

2.6.1.3 Pt/Al_2O_3 and Pt/Al_2O_3/ZnSe

After impregnation, calcination and reduction, the 5 wt% Pt/Al_2O_3 powder sample had a surface area of 115 m^2/g. Hydrogen chemisorption capacity (H/Pt) was 0.75, resulting in $1.92 \cdot 10^{-4}$ mol surface platinum atoms per gram catalyst. Figure 2.7 shows typical SEM micrographs of the Pt/Al_2O_3 catalyst layer on a glass plate. The layer was smooth on the nanometer length scale and consisted of small particles of approximately 20-30 nm in size. No distinction between alumina and platinum particles can be made because of the high platinum dispersion. The thickness of the catalyst layer was measured to be 3.50 ± 0.25 μm over the full length of the plate. Based on the layer thickness and the catalyst amount the void fraction including pore volume was calculated to be 50%.

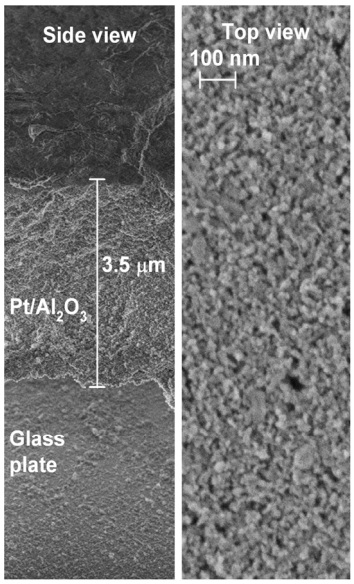

Figure 2.7. SEM micrographs of a Pt/Al_2O_3 layer on a glass plate with identical dimensions as the ZnSe IRE (Left: side view; right: top view).

After preparing a suspension of 5 wt% colloidal alumina - 5 wt% Pt/Al_2O_3 in water with pH adjusted to 3.5 with nitric acid, the suspension was dried and TPD was performed. Figure 2.8A and B shows the TPD of nitric acid performed on 5 wt% Pt/Al_2O_3 – 5 wt% colloidal alumina performed in synthetic air (Figure 2.8A) and hydrogen (Figure 2.8B).

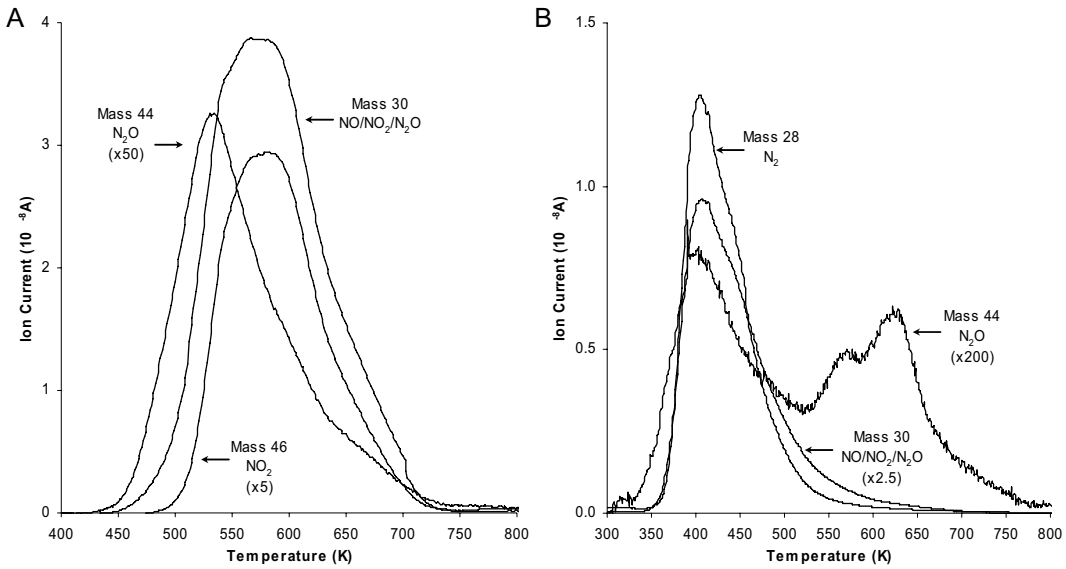

Figure 2.8. TPD of nitric acid performed on 5wt% Pt/Al_2O_3. (A) in synthetic air, (B) in hydrogen.

During calcination (Figure 2.8A) mass 30, 44 and 46 (NO, N_2O and NO_2) were detected and removal of N_xO_y-species in air occur up to 750 K. The IRE (ZnSe) can only withstand temperatures up to 573 K in air, since it oxidises at higher temperatures. It is therefore necessary to reduce the catalyst/IRE at high temperature to remove the remaining N_xO_y-species, since it is known that the ZnSe IRE is stable in H_2 at higher temperatures. During reduction (Figure 2.8B) mass 28, 30 and 44 (N_2, NO, N_2O and NO_2) were detected and all N_xO_y-species were removed at 750 K.

2.6.1.4 Pd/Al_2O_3 and Pd/Al_2O_3/ZnSe

The Pd/Al_2O_3 catalyst was prepared by repeated adsorption of $Pd(acac)_2$ as described in section 2.3.2. After adsorption the palladium loading and dispersion were determined by XRF and CO chemisorption, as shown in Figure 2.9.

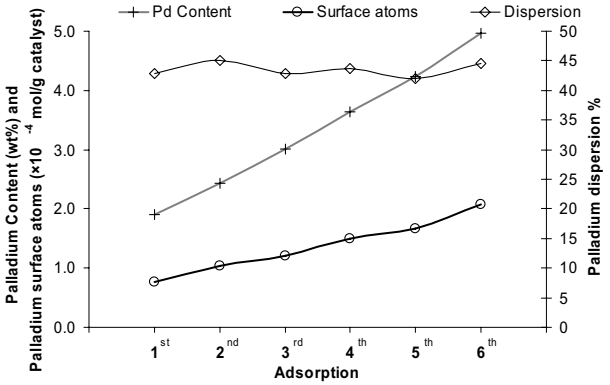

Figure 2.9. Palladium loading, surface atoms and dispersion after each adsorption of $Pd(acac)_2$ on Al_2O_3.

After the first adsorption of $Pd(acac)_2$ the palladium loading was 1.9 wt%, with palladium dispersion of 43%. After the final, the palladium loading increased to 5.0 wt%, while the palladium dispersion remained constant (45% after the 6th adsorption). The results shown in Figure 2.9 clearly show that by repeated adsorption of $Pd(acac)_2$ on Al_2O_3 it is possible to prepare highly dispersed Pd/Al_2O_3 catalysts with high palladium loading. The palladium loading of the final catalyst was 5.0 wt% with a dispersion of 45%, resulting in $2.06 \cdot 10^{-4}$ mol surface palladium atoms per gram catalyst. TPD of nitric acid was performed on the palladium catalyst, where all N_xO_y-species was removed during inert flow at 600 K.

For measurement of the thickness of the Pd/Al_2O_3 catalyst layer deposited on the IRE, a catalyst layer was prepared on a glass plate. Figure 2.10 shows typical SEM micrographs of the prepared 5 wt% Pd/Al_2O_3 catalyst layer on the glass plate. The prepared layer consisted of small particles of a few nanometer size and the layer was cracked as was the case for the Al_2O_3 layer. The thickness of the Pd/Al_2O_3 layer was 5.0 ± 0.5 μm, resulting in a void fraction including pore volume of 70%.

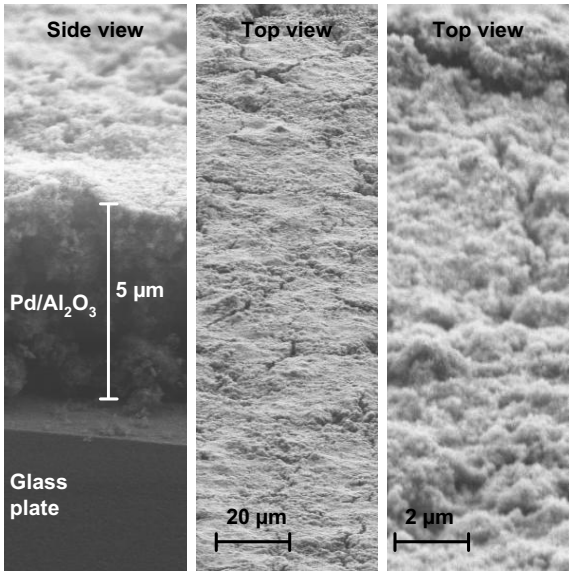

Figure 2.10. SEM micrograph of the 5 wt% Pd/Al_2O_3 layer on glass plate.

Table 2.2 summarises the characterisation data of the Al_2O_3, Pd/Al_2O_3 and Pt/Al_2O_3 catalyst layers.

Table 2.2. Characterization of the Al_2O_3, Pd/Al_2O_3 and Pt/Al_2O_3 catalyst layers.

	Metal content	Metal dispersion	Accessible metal/g catalyst	Layer thickness	BET surface area	Void fraction + pore volume
Al_2O_3	—	—	—	6.5 ± 0.5 μm	125 $m^2.g^{-1}$	75%
Pt/Al_2O_3	5.0 wt% Pt	0.75[b]	0.192 mmol	3.5 ± 0.25 μm	115 $m^2.g^{-1}$	50%
Pd/Al_2O_3	5.0 wt% Pd	0.45[a]	0.206 mmol	5.0 ± 0.5 μm	115 $m^2.g^{-1}$	70%

a - Pd dispersion was determined by CO chemisorption assuming CO:Pd = 1.

b - Pt dispersion was determined by H_2 chemisorption assuming H:Pt = 1.

In order to investigate whether the preparation method influences the catalytically active noble metal particles CO adsorption on Pt/Al_2O_3 was performed on a thin layer of Pt/Al_2O_3 on an ZnSe IRE and as a self-supporting wafer. Figure 2.11 shows the normalised ATR-IR and transmission FTIR spectra after CO adsorption on respectively a thin layer of Pt/Al_2O_3 on an ZnSe IRE and a self-supporting wafer, both prepared from the same 5 wt% Pt/Al_2O_3 powder catalyst. It can clearly be seen that both spectra are identical, so any change of the catalytically active platinum particles due to the preparation method can be excluded.

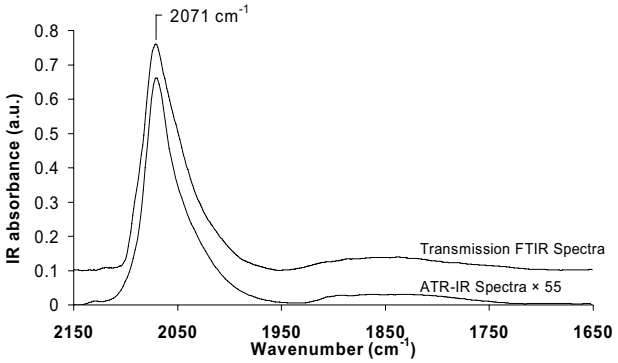

Figure 2.11. Normalised ATR-IR and transmission FTIR spectra after CO adsorption on respectively a Pt/Al_2O_3 layer on the IRE and a self-supporting wafer.

2.6.2 Penetration depth for ZnSe in gas and aqueous phase

To compare the intensities in gas and aqueous phase, the penetration depth is calculated for both situations. The penetration depth (d_p) can be calculated according to $d_p = \lambda_1 / 2\cdot\pi\left(\sin^2\theta - n_{21}^2\right)^{1/2}$ as described in equation (1.25) in the Introduction (Chapter 1). n_2 for air and water are 1.00 and 1.33 respectively [9] and n_1-ZnSe is 2.43. Therefore the penetration depths in gas and aqueous phase are:

d_{p-Air}: 0.55 μm
$d_{p-Water}$: 0.69 μm

2.6.3 Penetration depth for Pt/Al_2O_3 and Pd/Al_2O_3 in gas and aqueous phase

The IRE-catalyst-reactant system consists of several phases of which the exact reflective indices are unknown. Therefore the calculation of the exact penetration depth when a porous catalyst layer is deposited on the IRE is complicated. Although both dense Al_2O_3, palladium and platinum have high reflective indices, it has been published that porosity significantly decreases the index of reflection [10].

It has recently been shown that the reflective index of a porous material can be calculated with:

$$n_{eff} = \sqrt{(1-\phi)n_c^2 + \phi n_d^2} \qquad (2.2)$$

Where n being the respective refractive index and ϕ the porosity [10]. The refractive index n_2 can be calculated from the respective indices for Al_2O_3, platinum, palladium, air and water [9]:

n_2 - Al_2O_3:	1.67
n_2 - Pt:	4.70
n_2 - Pd:	3.10
n_2 - Air/vacuum:	1.00
n_2 - Water:	1.33

First, the refractive index n_{eff} of the present Pt/Al_2O_3 (or Pd/Al_2O_3) catalyst was calculated. Assuming a mixture of 99.07 vol% Al_2O_3 and 0.93 vol% of Pt (calculated from 5 wt% Pt/Al_2O_3 and the density of respectively Al_2O_3 and Pt):

$n_{eff,\ Pt/Al_2O_3} = \sqrt{0.9907(1.67)^2 + 0.0093(4.7)^2} = 1.72$. Subsequently, the porosity was taken into account. The Pt/Al_2O_3 layer has a void fraction including pore volume of 50% as calculated from the layer thickness and deposited amount on the IRE. This result in the following refractive indices for pores filled with either air or water:

$$n_{Pt/Al_2O_3,\ \text{pores filled with air}} = \sqrt{0.5(1.72)^2 + 0.5(1.00)^2} = 1.41$$

$$n_{Pt/Al_2O_3,\ \text{pores filled with water}} = \sqrt{0.5(1.72)^2 + 0.5(1.33)^2} = 1.54$$

When calculating the respective penetration depth according to the above formula (1.25), the penetration depths when the pores are filled with either air or water are:

$d_{p\ -\ Pt/Al_2O_3,\ \text{pores filled with air}}$: 0.81 μm

$d_{p\ -\ Pt/Al_2O_3,\ \text{pores filled with water}}$: 1.06 μm

Calculation of the penetration depth for Pd/Al_2O_3 was performed as described for Pt/Al_2O_3, assuming a mixture of 99.46 vol% Al_2O_3 and 0.54 vol% palladium for the 5 wt% Pd/Al_2O_3 and a void fraction including pore volume of 70%. Table 2.3 summarises the calculated refractive indices (n_{eff}) and penetration depths of the various catalyst layers in both gas and aqueous phase.

Accordingly the penetration depth for the Pt/Al_2O_3 catalyst layer in aqueous phase is 1.06 times the penetration depth for the Pd/Al_2O_3 catalyst layer.

Table 2.3. Calculated refractive index (n) and penetration depth (d_p) of the various catalyst layers in gas and aqueous phase.

	$n_{2\ –\ Gas\ phase}$	$n_{2\ –\ Aqueous\ phase}$	$d_{p\ –\ Gas\ phase}$	$d_{p\ –\ Aqueous\ phase}$	$d_{p\ -\ Aqueous} / d_{p\ -\ Gas}$
ZnSe	1.00	1.33	0.55 μm	0.69 μm	1.25
Pt/Al_2O_3/ZnSe	1.41	1.54	0.81 μm	1.06 μm	1.29
Pd/Al_2O_3/ZnSe	1.24	1.44	0.79 μm	1.00 μm	1.27

2.7 Estimation of the amount of probed metal sites for Pt/Al_2O_3 and Pd/Al_2O_3

For both Pt/Al_2O_3 and Pd/Al_2O_3, 6 mg is deposited on the IRE. For Pt/Al_2O_3 the thickness of the layer is 3.5 μm and assuming an equal distribution of the catalyst particles, this result in an amount of catalyst in the first micrometer (equal to the penetration depth) of 1.7 mg. In 1.7 mg of catalyst there are $0.33 \cdot 10^{-6}$ mol accessible platinum sites (0.192 mmol / g catalyst).

For Pd/Al_2O_3, the thickness was 5.0 μm resulting in 0.9 mg of catalyst in the first micrometer, resulting in $0.19 \cdot 10^{-6}$ mol accessible palladium sites (0.206 mmol / g catalyst).

As a consequence of the denser Pt/Al_2O_3 catalyst layer approximately 1.75 times more metal sites will be probed for Pt/Al_2O_3 than for Pd/Al_2O_3.

2.8 References

[1] UV-VIS-IR Optical Materials: http://www.harrricksci.com/H_optics.cfm

[2] C.G.M.van de Moesdijk, The Catalytic Reduction of Nitrate and Nitric Oxide to Hydroxylamine: Kinetics and Mechanism, Doctoral Thesis, Technische Hogeschool, Eindhoven, 1979.

[3] D. Eisenberg, W. Kauzmann, The Structure and Properties of Water, Oxford, The Clarendon Press, Oxford University Press, New York, 1969.

[4] T. Bürgi, A. Baiker, J.Phys.Chem.B. 106 (2002) 10649.

[5] R. He, R.R. Davda, J.A. Dumesic, J.Phys.Chem.B. 109 (2005) 2810.

[6] I. Ortiz-Hernandez, C.T. Williams, Langmuir 19 (2003) 2956.

[7] T.A.Nijhuis, A.E.W.Beers, T.Vergunst, I.Hoek, F.Kapteijn, J.Moulijn, Catal.Rev.-Sci.Eng. 43 (2001) 345.

[8] J.E. Benson, H.S. Hwang, M. Boudart, J.Catal. 4 (1965) 704.

[9] R.C. Weast (Eds.), Handbook of Chemistry and Physics. 48th edition, The Chemical Rubber CO, Cleveland, Ohio, 1970.

[10] M.M. Braun, L. Pilon, Thin Solid Films 496 (2006) 505.

CHAPTER 3

CO adsorption and oxidation over Pt/ZnSe

Abstract

Adsorption of carbon monoxide and oxidation of pre-adsorbed carbon monoxide from gas and aqueous phase were studied on a platinum catalyst deposited on a ZnSe Internal Reflection Element (IRE) using Attenuated Total Reflection Infrared Spectroscopy (ATR-IR Spectroscopy). The results of this study convincingly show that it is possible to prepare platinum metal layers strongly attached to an IRE, which are stable for over three days in aqueous phase experiments. It is shown that ATR-IR spectroscopy is a suitable technique to study adsorption and catalytic reactions occurring at the interface of a solid catalyst in an aqueous reaction mixture, even with an extreme low surface area catalyst. Clearly, ATR-IR spectroscopy allows direct comparison of reactions on a catalytic surface in gas and liquid phase on the same sample. CO was found to adsorb both linearly and bridged on the platinum metal layer when adsorbed from gas phase, but only linear CO was detected in aqueous solution, though with five times higher intensity. Oxidation of pre-adsorbed CO on platinum occurs in both gas phase, wetted gas and in aqueous media, and was found to be two times faster in aqueous phase compared to gas phase oxidation due to a promoting effect of water. Moreover, during oxidation at room temperature CO_2 adsorbed on Pt/ZnSe was detected in both gas and aqueous phase.

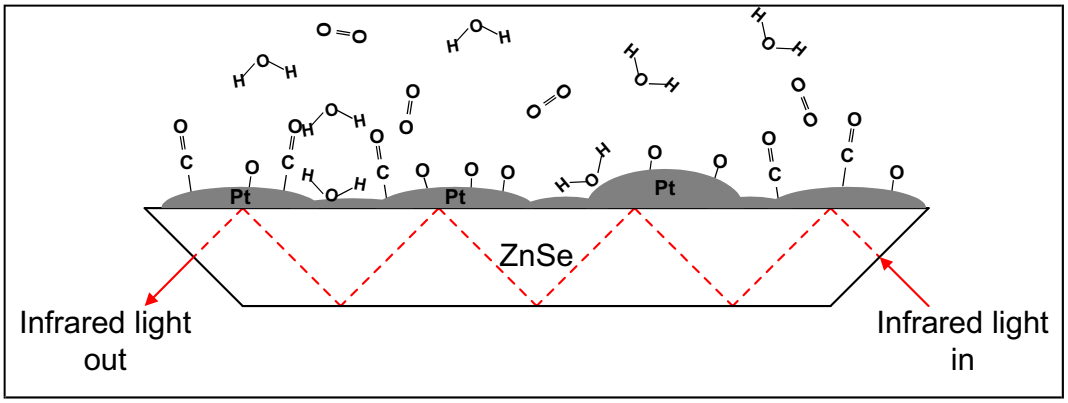

3.1 Introduction

Vibrational spectroscopy plays a key role in studies of adsorption and catalytic reactions at metal surfaces. Infrared spectroscopy has long been used as a sensitive technique for detection of adsorbed species at the metal-gas interface. However, also many catalytic reactions take place at a metal-liquid-interface e.g. the catalytic removal of nitrate from drinking water. It is important to be able to examine the interface by infrared spectroscopy to gain insight in adsorption and reaction mechanism. However infrared spectroscopic studies at the metal-liquid-interface have not yet received much attention, although recently some papers have shown the clear difference between adsorption in gas phase and liquid phase as will be reviewed below [1-4].

Normally, liquids are strong absorbers of infrared radiation so transmission infrared spectroscopy is not suitable to apply unless the pathlength is very short, i.e. in the order of a few microns. Attenuated Total Reflection Infrared Spectroscopy (ATR-IR), however, is ideally suited for studying molecular vibrations at the solid-liquid interface because the evanescent wave is restricted to the region near the interface, thereby minimizing the contribution from the liquid [5]. The restriction of the infrared radiation to the interface is especially important when water is used as solvent, since water is a very strong absorber in the mid-infrared region. ATR-IR have for long been used as a analytical tool to study the solution composition and to study protein structure in biochemistry [6]. On the other hand application of ATR-IR to study adsorption and reactions at the solid-liquid-interface has only recently started [1,2,7-11].

In the earlier applications of ATR-IR to study the solid-liquid-interface, the technique was used to study the goethite-aqueous-interface where the oxide particles were suspended in water [11]. The signal intensity varied due to aggregation of the suspension [8].

More stable signals can be obtained by depositing a very thin solid layer on an internal reflection element (IRE). In that case, it is essential that the thickness of the layer does not exceed the penetration depth of the infrared radiation (i.e. less than one micron). This approach was first introduced by depositing an Al_2O_3 film on the IRE by sputtering, to study adsorbed species at the Al_2O_3/water interface [10]. However, it was not possible to examine adsorption for longer periods than three hours since the Al_2O_3 layer became continuously thinner during water exposure [10].

In addition, in the field of heterogeneous catalysis, ATR-IR was applied to study reactions with supported catalysts in organic solvents (cyclohexane or dichloromethane) [7,9] Supported and unsupported model catalysts were prepared by physical vapor deposition [7]. Recently, adsorption of CO on Pt/Al_2O_3 from aqueous solution examined with ATR-IR was reported [1,2]. In one study the adsorption and oxidation of CO over Pt/Al_2O_3 was investigated in several solvents including water [2]. In another study CO adsorption on Pt/Al_2O_3 was investigated in relation to water-gas shift reaction and methanol reforming [1]. Clear spectral differences were observed between adsorption from gas and liquid phase [1,2] and the reaction order for the water-gas shift reaction and methanol reforming was reported to be influenced by the presence of water [1].

In addition to supported catalysts, ATR-IR was used to compare CO adsorption from gas and aqueous phase on thin platinum and palladium films [12]. Adsorption was performed from aqueous solution and subsequently infrared spectra were collected after removing the liquid by flushing. Comparison was only possible for the palladium film because the platinum film was unstable in contact with water, whereas palladium films were more resistant [13]. The stability of thin metal layers used as catalyst films for ATR-IR is generally a problem in aqueous phase, especially in the case of platinum [12-14]. The interaction of monolayers of water (D_2O) and CO was examined on single crystal platinum (Pt(100) and Pt(111)) by Infrared Reflection Absorption Spectroscopy [3,4]. In both cases the electronic properties of adsorbed CO were found to be altered by the presence of water.

On the other hand, in electrochemistry the use of thin metal layers combined with infrared spectroscopy has been applied. Electrochemical studies combined with infrared spectroscopy at the solid-liquid-interface are mainly done by RAIRS (Reflection Absorption Infrared Spectroscopy) and not ATR-IR. In electrochemistry several studies reported the use of RAIRS to study the electro oxidation of CO on platinum [15,16]. However, in RAIRS the catalyst (e.g. a platinum film or electrode) is placed in close contact with the prism, thereby displacing the liquid during IR measurements, to ensure a short pathlength through the liquid and having the catalyst film in the infrared beam; during reaction the catalyst is pulled back from the prism and exposed to the solution [15,16]. Although in electrochemistry many publications appeared on RAIRS, the main disadvantage of this technique is that the sample has to be put very close to the IR-window, which does not allow rapid transport of adsorbing/reacting molecules in the liquid. In contrast, with ATR-IR it is possible to follow the reaction *in-situ* without the need to displace the solution since the catalyst film is in contact with the IRE. Nevertheless, the combination of

electrochemistry and ATR-IR has only been applied by one group to study the electro oxidation of CO over platinum, but only very poor spectra for adsorbed CO were reported [17].

In conclusion, application of ATR-IR allows for mimicking operating conditions of liquid phase catalytic reactions, without introducing additional mass-transfer limitations. Moreover, experiments can be performed in both gas and liquid phase on the same sample, offering the possibility to clarify the effect of solvent, and water in particularly, on the spectral properties and reactivity of adsorbed species on metal surfaces. It is the objective of this work to prepare and investigate a stable thin platinum layer at an IRE and show the possibilities for *in-situ* ATR-IR examination of adsorption and reactions occurring on a stable platinum layer in both gas and aqueous solution. As a first step towards examination of catalytic reactions on unsupported catalysts in aqueous phase, adsorption and oxidation of pre-adsorbed carbon monoxide on a platinum layer is examined in dry and wetted gas as well as in aqueous solution.

3.2 Experimental

The experimental procedure, materials and catalyst preparation are described in detail in the Experimental Section (Chapter 2).

The characteristics of the Pt/ZnSe catalyst film examined in this chapter are also described in detail experimental section. The catalyst layer consisted of platinum clusters up to 30 nm. Dispersion of the platinum was calculated to be between 3% and 4% assuming a particle size of 30 nm resulting in a surface area of 0.015 m^2.

3.2.1 *In-situ* ATR-IR Spectroscopy

Attenuated Total Reflection Infrared (ATR-IR) spectra were recorded at room temperature (294 K) with a Tensor 27 (Bruker) infrared spectrometer by averaging of 100 scans with a resolution of 4 cm^{-1}. Infrared spectra were recorded using a home built stainless steel flow through cell as described in the Experimental Section (Chapter 2).

For experiments performed in wetted atmosphere, gasses (Ar, CO and O_2) were moistened with 2.5 vol% water (calculated on saturation at room temperature and 1 atm. pressure) in the two glass saturators. A schematic presentation of the experimental setup is shown in the Experimental Section (Chapter 2).

After purging the sample compartment with dry nitrogen for 2 hours (during the reduction in 10% H_2/Ar, gas), the cell was flushed with argon while the background spectrum was recorded. When experiments were performed in aqueous solution, the cell was flushed with hydrogen-saturated water while a background spectrum was recorded. All flow rates used in the experiments were 5 mL min^{-1} for both gases and liquid.

3.3 Results

3.3.1 Adsorption of dry CO on Pt/ZnSe

After reduction (see experimental section) 1% CO/Ar was introduced into the cell. Figure 2.1 shows the ATR-IR spectra obtained during flow of carbon monoxide over Pt/ZnSe. During CO flow no gaseous CO was detected but only adsorbed CO was found with a distinct asymmetric infrared peak at 2030 cm^{-1} (width at half height of about 50 cm^{-1}), and a small broad peak at 1830 cm^{-1}. The intensity levelled off in time and a saturation value was reached after about 30 minutes. During adsorption the peak positions remained constant.

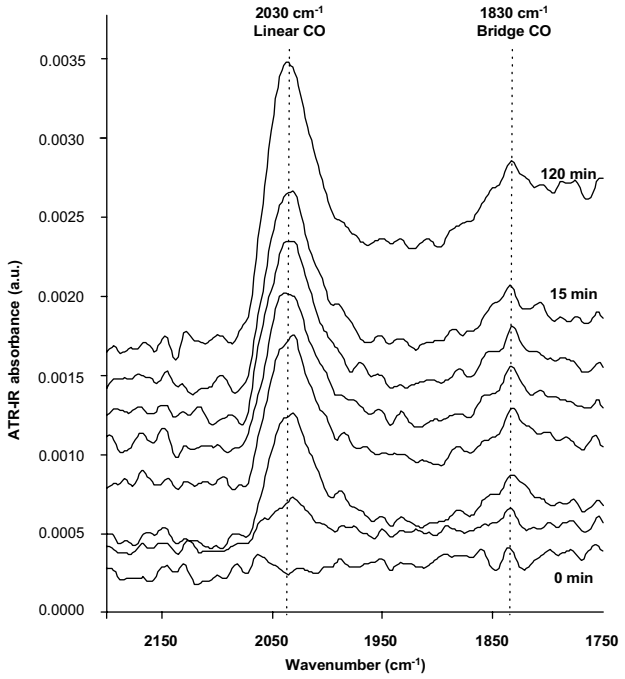

Figure 2.1. ATR-IR spectra as a function of time showing the region of CO adsorption on Pt/ZnSe while dry CO was flown (1% CO/Ar).

3.4 Adsorption of wetted CO on Pt/ZnSe

To examine whether water has an influence on the adsorption of carbon monoxide on the Pt/ZnSe catalyst, CO adsorption was performed in wetted atmosphere. After background measurement, argon moistered with water was flown over, and adsorbed water on Pt/ZnSe was observed (not shown).

Subsequently wetted 1% CO/Ar (2.5 % H_2O) was introduced into the cell. Again two bands developed at 2030 and 1830 cm^{-1} (not shown). When adsorbing CO from wetted gas the observed intensities were comparable to adsorption from dry gas as shown in Figure 2.5. Peak positions and widths for adsorbed CO remained constant during adsorption.

3.5 Adsorption of carbon monoxide on Pt/ZnSe from aqueous phase

Subtraction of the scaled background from the spectra of adsorbed CO on Pt/ZnSe resulted in the spectra shown in Figure 2.2. An asymmetric infrared peak at 2030 cm^{-1}, developed in time when an aqueous solution saturated with CO was flown over the sample. With increasing coverage the peak position shifted from around 2020 cm^{-1} to 2030 cm^{-1} at saturation level. The width at half height was found to be between 50 and 55 cm^{-1} similar to gas phase experiments. However, no bridged adsorbed CO could be detected at 1830 cm^{-1}, which can be either due to the lower signal to noise ratio or to the absence of bridged CO. When adsorbed from aqueous solution it took approximately one hour to approach saturation level, the intensity kept increasing slightly as for adsorption in wet atmosphere (Figure 2.5). Moreover the intensity was around 5 times higher for adsorption from aqueous phase compared to adsorption from dry or wetted gas. After oxidation of CO (vide infra) and drying of the sample, adsorption of CO from dry gas resulted again in a five times lower intensity compared to adsorption from aqueous solution, illustrating the stability of the sample.

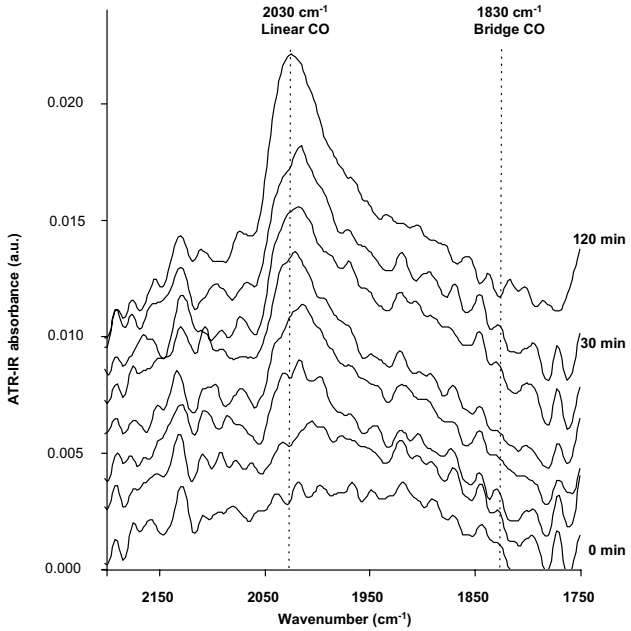

Figure 2.2. ATR-IR spectra as a function of time showing adsorbed CO on Pt/ZnSe while water saturated with CO was flown (0.035 % CO/H_2O).

3.5.1 Oxidation of pre-adsorbed carbon monoxide on Pt/ZnSe

Figure 2.3 shows the ATR-IR spectra collected during oxidation of pre-adsorbed CO on Pt/ZnSe by flowing dry 10% O_2/Ar. Both linear and bridge adsorbed CO peaks decreased during oxidation, while simultaneous a sharp peak developed at 2340 cm^{-1} (close to the gas phase signal for CO_2 at 2340-2360 cm^{-1}).

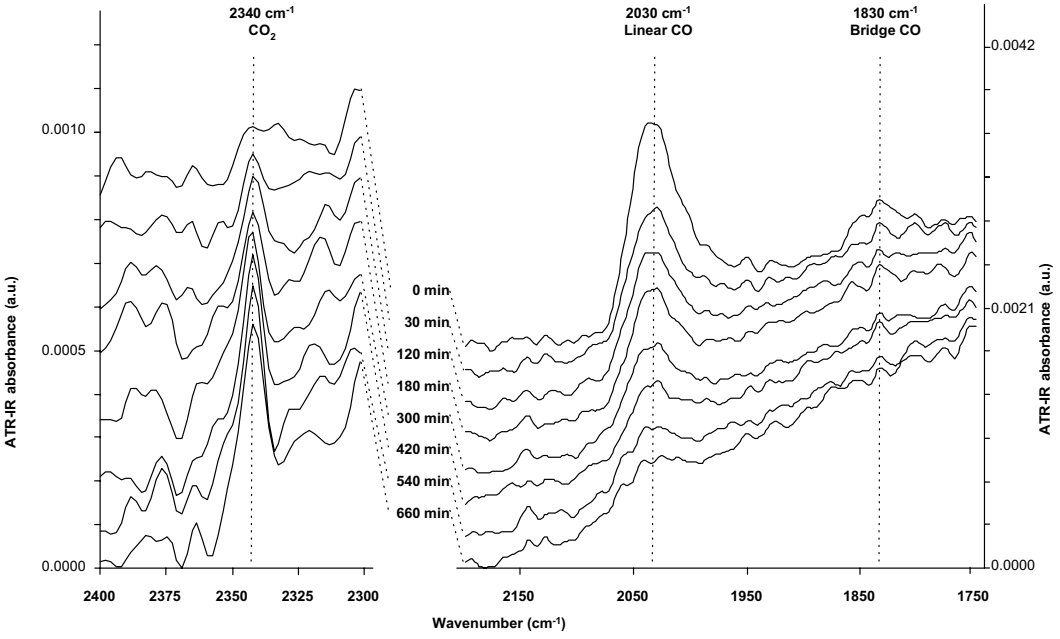

Figure 2.3. ATR-IR spectra as a function of time while flowing dry gas phase oxygen (10% O_2/Ar) over Pt/ZnSe with pre-adsorbed CO.

Oxidation of pre-adsorbed CO from wetted gas was performed in wetted 10% O_2/Ar over Pt/ZnSe (not shown). Again both peaks for linear and bridge adsorbed CO decreased, while a peak developed at 2340 cm^{-1}.

Figure 2.4 shows the ATR-IR spectra collected during oxidation of pre-adsorbed CO in aqueous solution. When oxygen saturated water (0.5 % O_2/H_2O) was flown over the Pt/ZnSe catalyst, first a shift in peak position of linear adsorbed CO on platinum, from 2030 cm^{-1} to 2035 cm^{-1} occurred within five minutes, while the intensity remained constant. After the shift in peak position, adsorbed CO disappeared and a peak at 2340 cm^{-1} evolved.

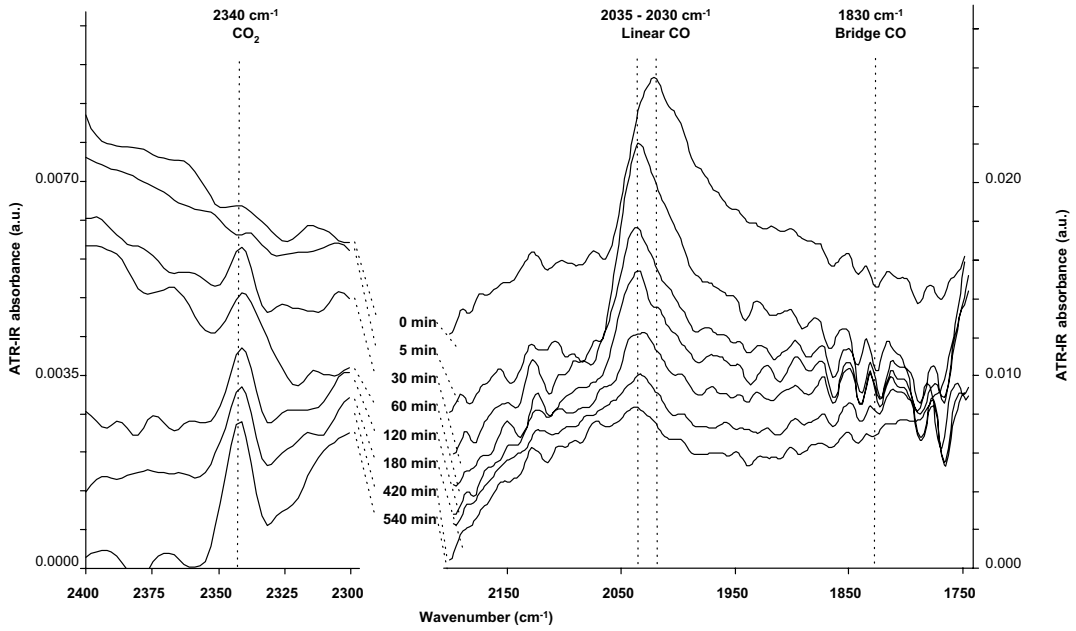

Figure 2.4. ATR-IR spectra showing adsorbed CO and CO_2 on Pt/ZnSe while oxygen saturated water was flown (0.5 % O_2/H_2O).

3.6 Discussion

This study convincingly shows that it is possible to prepare platinum metal layers strongly attached to an IRE, which are stable for many hours in aqueous phase experiments. Especially in water, the stability of metal layers was reported to be a major problem [12-14]. In previous studies the metal layer was prepared by sputtering, while in the present study a chemical route was chosen. Deposition of the layer by evaporation of a solution containing a platinum precursor, followed by calcination and reduction treatments obviously leads to a stable metal layer.

3.6.1 CO adsorption

When Pt/ZnSe was exposed to CO, in dry gas, wetted gas or water, distinct peaks developed in all cases around 2030 cm^{-1}, which can be assigned to linearly adsorbed CO on platinum metal particles. In addition, small bands developed at 1830 cm^{-1} when adsorbed from either dry or wet gas, which can be assigned to bridged CO. In general, CO stretch frequencies vary between 2000 and 2100 cm^{-1} when adsorbed in linear geometry onto platinum metal surfaces, though mostly between 2050 cm^{-1} and 2090 cm^{-1} [18-21]. Stretch frequencies for CO adsorbed in bridged geometry are normally found between 1750 cm^{-1} and 2000 cm^{-1} [20-23]. The high linear to bridge ratio as observed for Pt/ZnSe sample indicates the presence of large metal particle [24] in agreement with the AFM picture (Shown in the experimental section, Chapter 2). However, normally large platinum metal particles show CO absorption frequencies above 2065 cm^{-1} [24], while in this study, a much lower peak position is found (2030 cm^{-1}). A possible explanation for this could be that he platinum electronic properties are affected via a metal-support interaction [25]. Since the AFM picture, and the linear to bridge ratio indicate the presence of large particles, this metal-support interaction must be extensive, otherwise such a large shift cannot be explained. Consequently, these results might be explained by an alloying of Pt with ZnSe from the IRE as a result of the preparation method of the sample that includes calcination at 398K and reduction at 498K. This alloying could alter the platinum electronic properties in such a way that a unique adsorption is created, which is different from pure platinum layers or single crystals. Unfortunately, no techniques are available to investigate this hypothesis. Characterization techniques, such as XPS, LEIS, SEM-EDX will not be able to distinguish Se signals of the crystal from Pt-Se alloys.

Interestingly, the observed integrated intensity of the linear CO band increased with higher water content on the sample (Figure 2.5), while no shift in peak position was detected. The intensity change was found to be reproducible on the same sample by alternating dry and wet experiments, indicating sample stability under the applied experimental conditions. A slight increase in intensity was found from dry to wet gas, but a five-times higher intensity was observed when CO adsorbed from aqueous phase compared to gas phase.

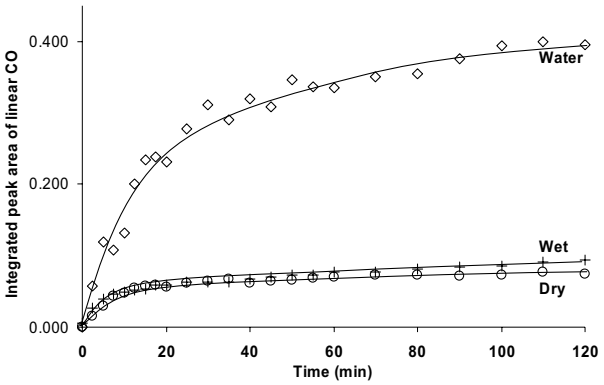

Figure 2.5. Integrated peak areas of linear CO adsorbed on Pt/ZnSe when CO was adsorbed from either dry (○) or wetted (+) gas or CO-saturated water (◊).

Comparison of CO adsorption on Pt/Al_2O_3 from gas and aqueous phase showed a clear red shift of up to 35 cm^{-1}, both in our laboratory (to be published) and in literature [1,9]. The shift in infrared frequency is a complex matter and involves several factors such as the dipole moment, adsorption geometry, metal – CO bond length and strength [4]. The interaction of monolayers of heavy water (D_2O) and CO has been examined on single crystal platinum (Pt(100) and Pt(111)) by IRAS [3,4]. In both cases the spectral properties of adsorbed CO were found to be altered by the presence of water. A clear red shift was observed for the frequency of both linear and bridge CO adsorbed on platinum, which was explained a combination of increased π-backdonation from Pt to CO and a change in CO dipole moment [3,4]. Changes in intensity of the infrared peaks have, however, not been discussed in literature to the best of our knowledge. Possible causes for this higher intensity could be (1) increase of number of adsorption sites, (2) higher coverage, (3) change in penetration depth, (4) larger extinction coefficient.

An increased number of adsorption sites, due to disintegration of platinum particles when exposed to water, can be excluded as an explanation for the increased intensity, since the experiments showed that the results are reproducible in both gas and liquid phase when performing repeating dry and wet experiments on the same sample, Further, the intensities levelled off in time in all cases (Figure 2.5). CO is well known to adsorb strongly on platinum, and full coverage is easily reached in gas phase at 1 atmosphere. For this reason CO is often used for determination of metal dispersion [26]. It seems therefore impossible that adsorption of CO from aqueous solution would lead to a five times higher monolayer coverage on the platinum particles compared to gas phase adsorption.

According to the calculations of the penetration depth shown in the experimental section (Chapter 2) an increase of more than 1.25 times due to the difference in refractive index of water and air, can not be explained by a change in penetration depth [27]. This increase in penetration depth is much less than the factor five observed in the intensity of the CO band. Secondly, the platinum layer was probed by AFM to be around 30 nm thick, which is much smaller than the penetration depth of the light in either gas or water phase. As a result, the change in penetration depth cannot change the number of sites that is being probed in these samples and thus cannot account for the increase in intensity when CO is adsorbed from aqueous solution.

Finally, it was reported that addition of water does not change the extinction coefficient of adsorbed CO when water vapor was added to adsorbed CO on Pt/Al_2O_3 [28]. This is in agreement with our present results, since hardly any change in intensity was observed between CO adsorption from dry or wet gas. An increased intensity of the infrared peaks when adsorbed from aqueous media was previously reported for CO adsorption on palladium supported on a germanium IRE, but no explanation for this phenomenon was given [12]. Based on the results of this study, we suggest that the observed intensity change can be attributed to a higher extinction coefficient of the CO stretch vibration caused by the presence of water in liquid phase. In this situation the adsorbed CO molecules are fully surrounded by polar water molecules which will affect the dipole moment of the CO molecule, which in turn is reflected in the larger extinction coefficient. It would be expected that a change in dipole moment of the adsorbed CO molecule would also result in a shift of the peak position. However, since the overall shift is a complex matter involving both dipole moment and back donation, as discussed above, it might be speculated that these factors cancel out in this specific case of Pt/ZnSe.

3.6.2 CO oxidation

When oxygen was flown over Pt/ZnSe containing pre-adsorbed CO, a decrease in intensity of adsorbed CO was observed in dry gas, wet gas and aqueous phase, accompanied by the development of a peak with increasing intensity at 2340 cm^{-1} (Figure 2.3 and 5), which is about 9 cm^{-1} lower than gas phase CO_2. Moreover, the ATR-IR technique is very sensitive to adsorbed species while free reactants and products are very difficult to observe. For example, in our experiments gas phase CO could not be observed in any experiment. In electrochemistry the peak at 2340 cm^{-1} is normally assigned to trapped CO_2 at the interface between platinum and water, formed by oxidation of adlayer CO during a potential sweep [16,29]. In gas phase

however, CO_2 was reported to desorb from Pt(111) at temperatures above 95 K [30]. In our experiments nevertheless, a flow of CO_2 at room temperature over reduced Pt/ZnSe yielded the exact same peak at 2340 cm^{-1}, which could not be removed by flushing with inert gas. Moreover, nothing was detected when CO_2 was flown over a clean ZnSe IRE. It is clearly surprising to find CO_2 adsorbed on platinum at room temperature. Based on literature and our experiments it seems reasonable to assign the peak at 2340 cm^{-1} to adsorbed CO_2. However, it also seems that the Pt/ZnSe sample does not contain pure platinum metal particles, since then no adsorption of CO_2 in gas phase should have been found at room temperature. In addition, Pt/ZnSe also showed extremely low linear CO stretch frequencies for CO adsorption on large pure Pt particles *(vide ante)*. Both observations suggest a chemical modification of the platinum particles by interaction with the ZnSe IRE, for example via alloy formation or strong SMSI effects. This could alter the platinum electronic properties in such a way that a unique adsorption and reaction behavior is created, which is different from pure platinum layers or single crystals. Unfortunately, as said above, at present no techniques are available to investigate this hypothesis. Nevertheless, this result immediately illustrates the extreme sensitivity of ATR-IR for adsorbed species and enables the detection of adsorbed CO_2 on low surface area Pt/ZnSe at room temperature, which was not reported before.

The normalized integrated peak areas for linear CO during the oxidation of carbon monoxide in the three different media are shown in Figure 2.6. Remarkably, the initial rate of oxidation, defined as Δ (normalized integrated peak area for linear CO) per minute, was found to increase from dry gas ($9.7\ 10^{-3}$), to wetted gas ($12.5\ 10^{-3}$), to aqueous solution ($20.8\ 10^{-3}$) (Figure 2.6B). The larger observed oxidation rate cannot be attributed to the increased extinction coefficient, since the data were normalized. Consequently, the data show an enhancement of the CO oxidation rate induced by the presence of water.

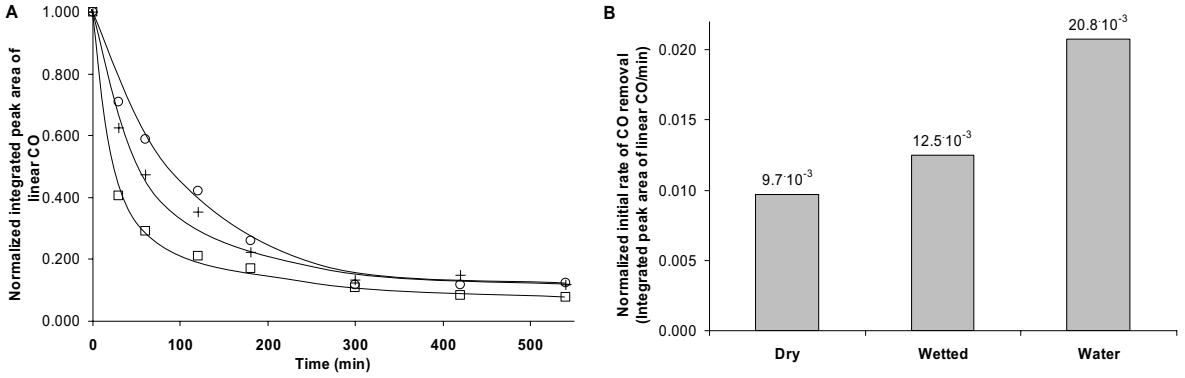

Figure 2.6. A: Normalized integrated peak areas of linear CO on Pt/ZnSe during oxidation from either dry (○) or wetted (+) gas or CO-saturated water (◊); B: normalized initial oxidation rate in the three media.

Further, when oxidation was performed in aqueous solution, the peak for linear CO first shifted to a higher wavenumber (from 2030 to 2035 cm^{-1}) before it started to loose intensity. Similar shifts in peak position have been reported for gas phase oxidation of CO on Pt/Al_2O_3 [31]. In that study, the authors attributed the blue shift to an electronic effect of adsorbed oxygen atoms close to the adsorbed CO molecules. In the present study, the blue shift is not observed in dry or wet gas phase experiments, but only in solution. In addition, the CO oxidation rate also remarkably enhanced in excess of water, while wet gas only had a moderate influence. Interestingly, in literature DFT calculations have been published indicating that during CO oxidation in water over Pt(111) and PtRu(111) surfaces, the dissociation of water is favored over PtRu(111) surfaces while it is found to be more difficult on Pt(111) [32]. The increased water dissociation contributes to the bifunctional mechanism proposed for CO oxidation in solution [33,34]. Since in the present study the spectral phenomena of both adsorbed CO and CO_2 on Pt/ZnSe suggest a chemical modification of the platinum particles *via* for example alloying with the ZnSe IRE, it could be speculated that the increased oxidation rate is also caused by an enhanced water dissociation due to this alloy formation. Nevertheless, in the absence of oxygen no CO oxidation is observed, indicating that the observed increased oxidation rate must be the overall result of a complex interaction between water, CO and oxygen on the Pt/ZnSe surface.

3.7 Conclusion

This study convincingly shows that ATR-IR spectroscopy can be applied to study CO adsorption and reaction on extremely low surface area Pt/ZnSe samples in dry gas, wet gas as well as aqueous solution. As such, ATR-IR spectroscopy allows direct

comparison between adsorption and reactions in gas and liquid phase. For the first time it is shown to be possible to prepare a catalyst film that is stable in aqueous solution for over three days. The layer was found to adhere strongly to the IRE during aqueous flow, and consequently, the catalyst layer could be used repeatedly.

Even that no change in infrared frequency for adsorbed CO was detected comparing adsorption in gas and aqueous phase the properties of CO considerably changed. The integrated peak area of linearly adsorbed CO on Pt/ZnSe was found to increase drastically in aqueous phase compared to adsorption from gas phase. Moreover, the presence of water promoted CO oxidation, most likely by a complex interaction of water, CO and oxygen and the Pt/ZnSe surface. Finally, the oxidation product CO_2 was found to be adsorbed on the Pt/ZnSe surface at room temperature in dry, wetted and aqueous phase, giving rise to an infrared peak at 2340 cm^{-1}. All observations suggest a chemical modification of the platinum particles by interaction with the ZnSe IRE, for example *via* alloy formation or strong SMSI effects.

3.8 References

[1] R. He, R.R. Davda, J.A. Dumesic, J.Phys.Chem.B 109, (2005) 2810.

[2] I. Ortiz-Hernandez, C.T. Williams, Langmuir 19 (2003) 2956.

[3] N.C. Yee, G.S. Chottiner, D.A. Scherson, J.Phys.Chem.B. 109 (2005) 7610.

[4] N. Kizhakevariam, X. Jiang, M.J. Weaver, J.Chem.Phys. 100 (1994) 6750.

[5] N.J.Harrick, Internal Reflection Spectroscopy, 1967.

[6] S.A. Tatulian, Biochemestry 42 (2003) 11898.

[7] D. Ferri, T. Bürgi, A. Baiker, J.Phys.Chem.B. 105 (2001) 3187.

[8] B.A. Holmen, M.I. Tejedor-Tejedor, W.H. Casey, Langmuir 13 (1997) 2197.

[9] C. Keresszegi, T. Bürgi, T. Mallat, A. Baiker, J.Catal. 211 (2002) 244.

[10] R.P. Sperline, Y. Song, H. Freiser, Langmuir 8 (1992) 2183.

[11] M.I. Tejedor-Tejedor, M.A. Anderson, Langmuir 2 (1986) 203.

[12] E. Zippel, M.W. Breiter, R. Kellner, J.Chem.Soc.Faraday Trans. 87 (1991) 637.

[13] Y. Zhu, H. Uchida, T. Yajima, M. Watanabe, Langmuir 17 (2001) 146.

[14] E. Zippel, R. Kellner, J.Electroanal.Chem. 289 (1990) 297.

[15] H.L. Lam-Wing, A. Wieckowski, M.J. Weaver, J.Phys.Chem. 92 (1988) 6985.

[16] N.P. Lebedeva, A. Rodes, J.M. Feliu, M.T.M. Koper, R.A. van Santen, J.Phys.Chem.B. 106 (2002) 9863.

[17] Y. Zhu, H. Uchida, M. Watanabe, Langmuir 15 (1999) 8757.

[18] S.D. Jackson, S.D. Ackson, B.M. Glanville, J. Willis, G.D. Mclellan, G. Webb, R.B. Moyes, S. Simpson, P.B. Wells, R. Whyman, J.Catal 139, (1993) 207.

[19] W.K. Kuhn, J. Szanyi, D.W. Goodman, Surf.Sci.Lett 274, (1992) L611.

[20] J. Xu, J.T. Yates, Surf.Sci. 327 (1995) 193.

[21] P.C. Welch, P.S.W. Mills, C. Mason, P. Hollins, J.Elect.Spectr and Rel.Phenom. 64-65 (1993) 151.

[22] S.D. Jackson, S.D. Ackson, B.M. Glanville, J. Willis, G.D. Mclellan, G. Webb, R.B. Moyes, S. Simpson, P.B. Wells, R. Whyman, J.Catal 139, (1993) 207.

[23] W.K. Kuhn, J. Szanyi, D.W. Goodman, Surf.Sci.Lett 274, (1992) L611.

[24] M.J. Kappers, J.H. Vandermaas, Catal.Lett. 10 (1991) 365.

[25] B.L. Mojet, J.T. Miller, D.E. Ramaker, D.C. Koningsberger, J.Catal. 186 (1999) 373.

[26] M. Primet, M. El Azhar, R. Frety, M. Guenin, Appl.Catal. 59 (1990) 153.

[27] S.D. Ebbesen, B.L. Mojet, L. Lefferts, J.Catal. Submitted (2006)

[28] A. Bourane, O. Dulaurent, D. Bianchi, Langmuir 17 (2001) 5496.

[29] M. Watanabe, Y. Zhu, H. Uchida, J.Phys.Chem.B. 104 (2000) 1762.

[30] C.L. Kao, A. Carlsson, R.J. Madix, Surf.Sci 497, (2002) 356.
[31] M. Primet, J.Catal 88, (1984) 273.
[32] S. Desai, M. Neurock, Electrochim.Acta 48 (2003) 3759.
[33] H.A. Gasteiger, N. Markovic, P.N. Ross, E.J. Cairns, J.Phys.Chem. 98 (1994) 617.
[34] S. Wasmus, A. Kuver, J.Electroanal.Chem. 461 (1999) 14.

CHAPTER 4

CO adsorption and oxidation over Pt/Al_2O_3 Promotion effects by water and pH

Abstract

The adsorption and oxidation of carbon monoxide over a Pt/Al_2O_3 catalyst layer deposited on a ZnSe Internal Reflection Element was investigated both in gas phase and water using Attenuated Total Reflection Infrared Spectroscopy. A preparation method is described which results in a strongly attached layer that is stable for many days in a water flow. Both adsorption and oxidation of CO are largely affected by the presence of liquid water. It influences the metal particle potential as well as the CO molecule directly, which is reflected in large red shifts (45 cm^{-1}) and a fourfold higher intensity when the experiments are carried out in water. Furthermore, the rate of CO oxidation changes significantly when carried out in water as compared to gas phase. Finally, with increasing pH, CO stretching frequencies shift to lower wave numbers accompanied by a large increase in CO oxidation rate.

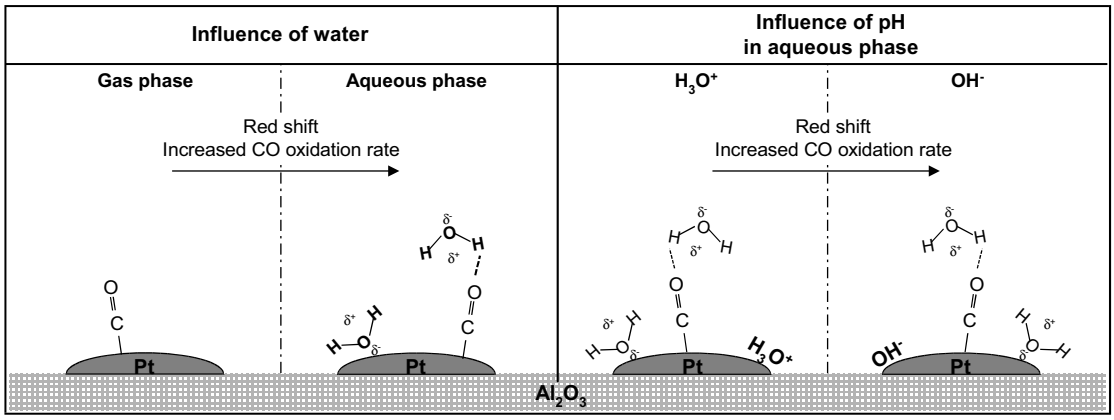

The influence of water and pH on the CO stretch frequency and CO oxidation rate, presented in Figure 4.8.

4.1 Introduction

Detailed mechanistic studies of heterogeneous catalytic reactions in aqueous phase are lacking because it is difficult to study heterogeneous catalysts *in-situ* if the reaction is carried out in water. Only recently, ATR-IR spectroscopic studies at the metal-liquid-interface have started to receive attention [1-7]. For example, the adsorption and oxidation of CO, and dissociation of small molecules such as formaldehyde over Pt/Al_2O_3 catalysts was reported [6]. In addition, ATR-spectroscopic studies of the water-gas shift reaction and methanol reforming over Pt/Al_2O_3 was combined with kinetic studies [4]. In our lab, we showed the large effect of water on the oxidation rate of CO compared to gas phase CO oxidation over Pt/ZnSe [2]. CO is a widely applied molecule to characterize supported noble metal catalysts [8-19]. Interactions between CO and the active metal are reflected in shifts of the CO absorption bands, which in turn are know to be affected by metal support interactions. Since the vibrations are so sensitive for modifications of the metal particles and/or its surrounding medium, CO is an ideal model compound to characterize supported noble metal catalysts. In addition, CO oxidation is a very simple reaction which allows for a detailed *in-situ* study of reaction parameters, such as the effect of solvent or pH.

Especially the details of the influence of pH on heterogeneous catalytic reactions in water have not been resolved completely. For this reason, the objective of this study is to unravel the details of the influence of water and the pH on the CO adsorption and oxidation on Pt/Al_2O_3 using *in-situ* ATR-IR spectroscopy

4.2 Experimental

The experimental procedure, materials and catalyst preparation are described in details in the experimental section (Chapter 2). All spectra presented in the following section are corrected for the water background as published by our group.

The characteristics of the 5 wt% Pt/Al_2O_3 catalyst (dispersion 75%) examined in the present study are described in detail in the experimental section. 6 mg. of catalyst was deposited on the Internal Reflection Element (IRE), resulting in 1.16 10^{-6} mol surface platinum atoms. The thickness of the catalyst layer was measured to be 3.50 ± 0.25 μm.

After assembling the cell in the IR spectrometer the cell was purged with gaseous argon followed by a reducing gas flow for 2 hours (10% H_2/Ar) to remove surface

oxygen, hereafter adsorption experiments were performed. For experiments in aqueous phase, the catalyst was reduced in hydrogen saturated Q2-water (denoted H_2/H_2O) (7.8 10^{-5} mol H_2/L) prior to adsorption experiments.

4.3 Results

4.3.1 Adsorption of CO from gas and aqueous phase

After assembling the ATR-IR cell and reducing the catalyst layer (see experimental section), dry gas phase CO was introduced into the cell. Figure 4.1 shows the ATR-IR spectra obtained during flow of CO over Pt/Al_2O_3.

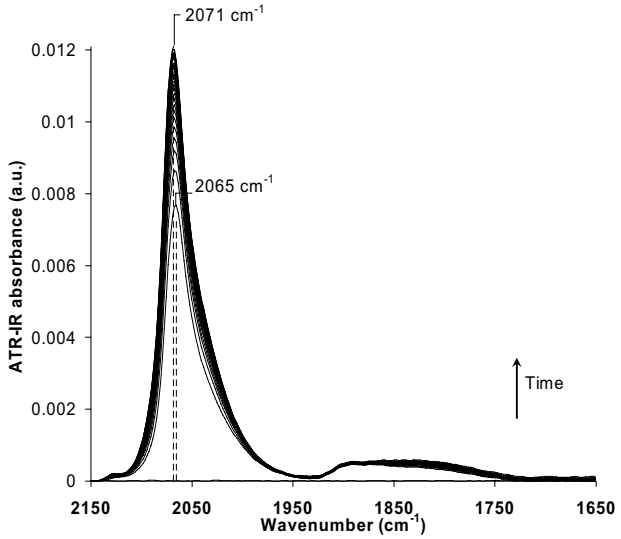

Figure 4.1. ATR-IR spectra as a function of time (time interval: 1.5 minutes) showing the region of CO adsorption on Pt/Al_2O_3 while dry CO was flown (1% CO/Ar).

During CO flow no gaseous CO was detected whereas linearly adsorbed CO on platinum was initially detected with a distinct asymmetric infrared peak appearing at 2065 cm^{-1}, which shifted to 2071 cm^{-1}, due to dipole-dipole coupling with increasing surface coverage [20,21] at saturation level after 5 minutes. Since the CO concentration was low, this time was needed to dose the stoichiometric amount of CO for the platinum particles to adsorb; it is not the result of diffusion limitations within the catalyst layer. Bridging CO on platinum was identified by a very broad peak with low intensity between 1750 and 1900 cm^{-1}. Peak positions for both linear and bridging CO on Pt/Al_2O_3 are similar to positions reported in literature [10,21-23]. After flowing dry CO, the cell was flushed with dry argon for 15 min and subsequently a dry oxygen rich stream (10 % O_2/Ar) was introduced to oxidize the adsorbed CO. CO was only partly removed during oxidation at room temperature (see also section:

Oxidation of pre-adsorbed CO). In order to be able to use the catalyst layer again, the IRE with catalyst was oxidized *ex-situ* at 523 K for 2 hours in flowing synthetic air (30 ml.min^{-1}, heating/cooling rate 1 K.min^{-1}) followed by reduction at 523 K for 2 hours in flowing hydrogen (30 ml/min, heating/cooling rate 1 K.min^{-1}), exposed to air and mounted in the ATR-IR cell. Subsequently, the cell was purged with gaseous argon (15 min.) and followed by reduction for 2 hours (10% H_2/Ar) to remove surface oxygen. Subsequently, hydrogen saturated Q2-water (7.8 10^{-5} mol H_2/L) was introduced (until a stable background was obtained, several hours) followed by a flow of Q2-water at pH 6.9 saturated with CO (1.4 10^{-6} mol CO/L) and ATR-IR spectra were collected (Figure 4.2).

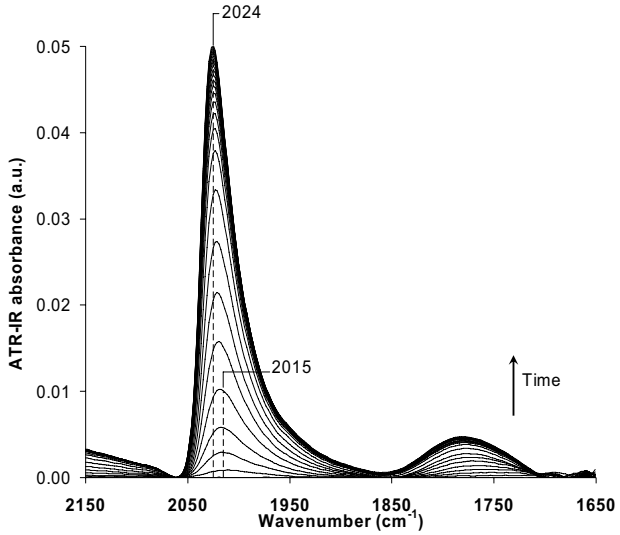

Figure 4.2. Water corrected ATR-IR spectra as a function of time (time interval of 1.5 minutes) showing the region of CO adsorption on Pt/Al_2O_3 while CO in water (1.4 10^{-6} mol CO/L) was flown at pH 6.9. Note the four times higher infrared intensity for adsorbed CO as compared to adsorption from gas phase (Figure 4.1).

When adsorbed from aqueous phase, linear CO was initially detected by a peak at 2015 cm^{-1} which shifted to 2024 cm^{-1} at increasing coverage, due to dipole-dipole coupling [20,21]. Bridging CO was detected by a very broad peak with its maximum around 1780 cm^{-1}. During subsequent flow of pure Q2-water the intensity of the bands for both linear and bridging CO remained constant, indicating that the layer with adsorbed CO was stable. After flowing water, the adsorbed CO was oxidized by oxygen in Q2-water (1.3 10^{-4} mol O_2/L) removing all CO (see also section: Oxidation of pre-adsorbed CO). Subsequently, the catalyst layer was reduced *in-situ* by hydrogen in water (7.8 10^{-5} mol H_2/L) for several hours in order to repeat experiments. Repetition of experiments showed that the oxidation/reduction treatment to clean the catalyst from CO had no influence on the observed CO

spectra. This was particularly important, since this allowed comparison of intensities of different experiments on the same Pt/Al_2O_3 sample.

Additionally, the effect of pH on CO adsorption in aqueous phase was examined. CO in Q2-water at pH 4.9, 5.0, 6.9 and 9.1 (pH adjusted with either H_2SO_4, H_3PO_4 or NaOH) was flown over the same Pt/Al_2O_3 catalyst layer as used for CO adsorption in gas and aqueous phase and ATR-IR spectra were recorded (Figure 4.3). After each adsorption experiment, adsorbed CO was oxidized by introducing oxygen in water ($1.3\ 10^{-4}$ mol O_2/L) at the same pH as during CO-adsorption; as a result CO was removed completely. After oxidation the catalyst layer was reduced *in-situ* by hydrogen in water as described above.

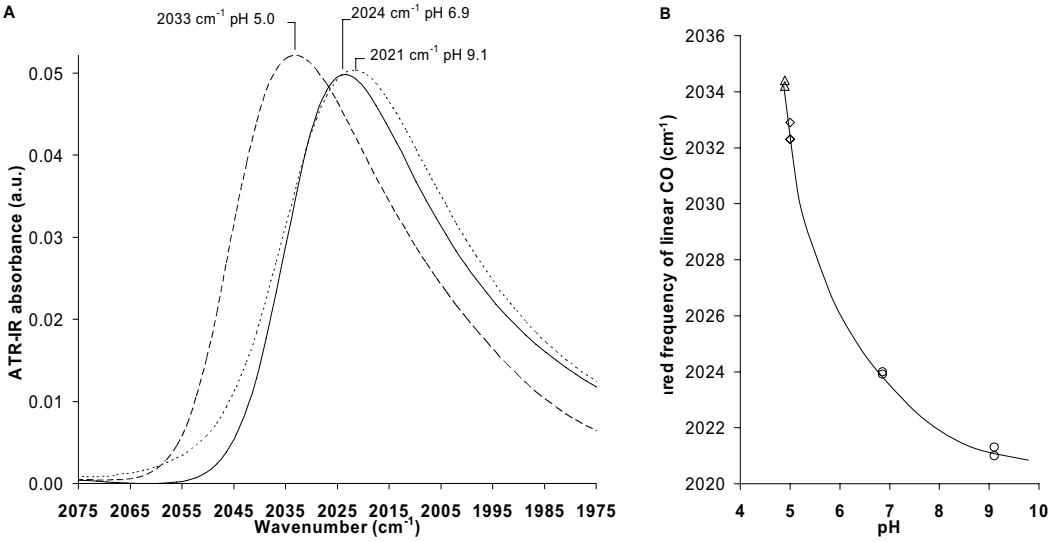

Figure 4.3. A: Water corrected ATR-IR spectra of linearly adsorbed CO on Pt/Al_2O_3 while CO in aqueous phase ($1.4\ 10^{-6}$ mol CO/L) at different pH was flown and B: ATR-IR frequency of linearly adsorbed CO on Pt/Al_2O_3 in aqueous phase as a function of pH (Δ: adjusted with H_3PO_4, ◊: adjusted with H_2SO_4, ○: adjusted with NaOH).

Figure 4.3A and B clearly shows a shift of 12 cm^{-1} to lower wave number with increasing pH from 5.0 to 9.1 for the band of linearly adsorbed CO. Likewise, shifts were found for bridging CO (not shown), but because of the very broad peaks the exact peak positions could not be reliably determined. At pH 5, we find no significant differences in peak position between H_3PO_4 and H_2SO_4 solutions, indicating that influence of the counter ion is insignificant as compared to the influence of pH. Although peaks clearly shifted with changing pH, only slight differences in linear to bridge ratio were observed, and no relation between pH and linear to bridge ratio could be determined.

4.3.2 Oxidation of pre-adsorbed CO

After CO adsorption on the Pt/Al_2O_3 layer, the adsorbed CO was oxidized by oxygen (either dry gas phase or in aqueous phase), during which ATR-IR spectra were recorded. The normalized integrated peak area of linearly adsorbed CO, during oxidation, is shown in Figure 4.4 as a function of time, for both gas and aqueous phase (pH 6.9). In both experiments, an immediate decrease in the peak intensity of linear and bridging CO was observed during oxidation of pre-adsorbed CO, but no CO_2 was detected. Chromatic effects are absent in this experiment, because of the high amount of oxygen in the feed compared to the amount of platinum present on the IRE.

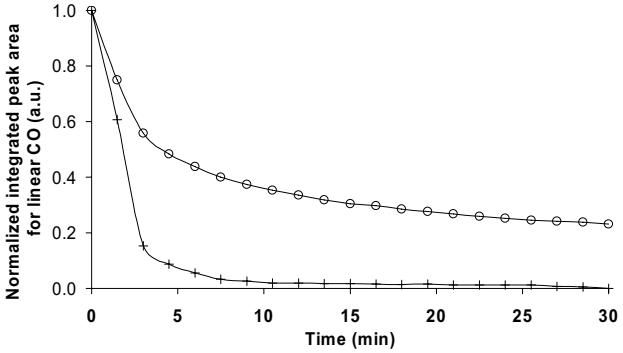

Figure 4.4. Normalized integrated peak area of linear CO adsorbed on Pt/Al_2O_3 versus time during oxidation from gas (○) and aqueous phase at pH 6.9 (+).

The initial rate of disappearance of adsorbed CO was the lowest in gas phase and approximately doubled in aqueous phase. After flowing oxygen in water for 10 min, 98% CO was oxidized whereas only 65% of the CO was oxidized in gas phase after 10 min. The initial rate of disappearance of adsorbed CO in aqueous phase was also investigated at different pH (Figure 4.5), each point indicates an individual experiment at a specific pH and the experiments were performed randomly. As a reference, the gas phase oxidation rate is indicated as a horizontal line.

Clearly, the initial rate of disappearance of adsorbed CO increased with increasing pH and the rates in aqueous phase were always higher than in gas phase.

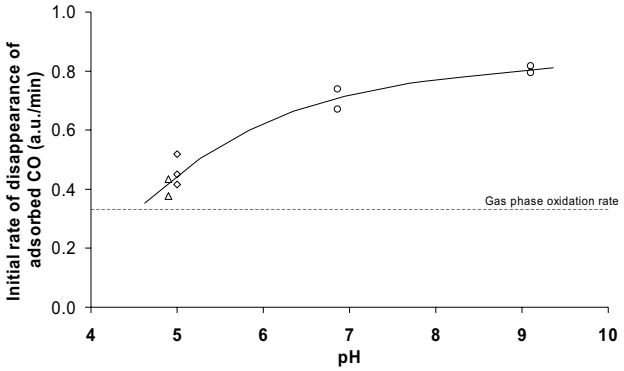

Figure 4.5. Initial rate of disappearance of pre-adsorbed CO in aqueous phase as a function of pH (integrated peak area for linear CO/min) (Δ: adjusted with H_3PO_4, ◊: adjusted with H_2SO_4, ○: adjusted with NaOH).

4.4 Discussion

4.4.1 Catalyst characterization

The applied method of catalyst immobilisation on an IRE resulted evidently in a stable catalyst layer when applied for days in flowing aqueous solutions. Although previously preparation of stable layers of supported catalyst for ATR-IR was reported by evaporation of a aqueous suspension of the catalyst powder on the IRE without further treatment [1,4,6], replication of this treatment in our laboratory did not result in stable layers when water was flushed. The modified method reported here by application of colloidal alumina followed by calcination and reduction to immobilize the catalyst layer did result in a very smooth and stable Pt/Al_2O_3 layer, without influencing the properties of the catalyst, which could be used repeatedly.

4.4.2 CO adsorption from gas and aqueous phase

Adsorption of CO from gas or aqueous phase on the same catalyst sample revealed clear differences, as can be seen from Figure 4.6. CO adsorption from aqueous phase results in a CO redshift of 47 cm^{-1} compared to dry gas phase adsorption. Moreover, the IR absorbance increased approximately four times. Third, the ratio of integrated intensities for linear and bridging CO (L/B ratio) decreased from 6.9 in gas phase to 4.1 in aqueous phase.

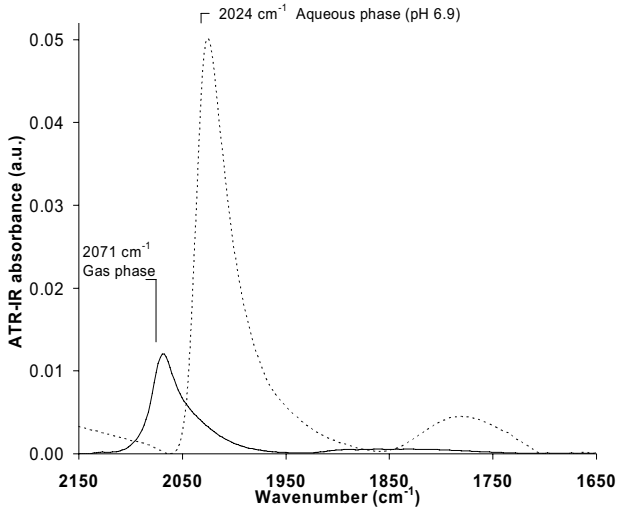

Figure 4.6. ATR-IR spectra showing the region of CO adsorption on Pt/Al_2O_3 from gas phase CO or CO in aqueous phase.

The observed red shift in the presence of water is in accordance with several other studies reporting shifts from 11 cm^{-1} to 34 cm^{-1} to lower wave number [4]. Also single crystal studies report on the influence of water on adsorbed CO [5,7,24]. The spectral properties of adsorbed CO were altered by the presence of heavy water for both Pt(100) and Pt(111) [5,7]. A clear red shift was observed for both linear and bridging CO on platinum upon gradual addition of D_2O, which was explained by a combination of increased π-back-donation from Pt to CO together with a change in CO dipole moment [5,7]. For a differently pretreated Pt – Al_2O_3 sample, CO was adsorbed from CH_2Cl_2, and linear adsorbed CO on Pt was found between 2030 and 2058 cm^{-1} , depending on the pre-treatment procedure [3]. Unfortunately, no gas phase spectra were shown in that paper, so the effect of the solvent could not be estimated for that particular sample. Nevertheless, the authors report large Pt particles (6 nm) for which it is generally accepted that gas phase CO adsorption leads to bands around 2070 – 2090 cm^{-1} [10,21,23,25]. As such it seems that also CH_2Cl_2 induced a shift of the CO stretch frequency. This suggests for both water and CH_2Cl_2 the possibility of a direct interaction between solvent molecules and adsorbed CO, most likely *via* hydrogen bonding. Preliminary calculations, however, show that the effect of co-adsorption of water has a more distinct effect on the CO peak position than the formation of hydrogen bonds [26].

In the field of catalyst characterization it is well-known that upon increasing support alkalinity the red shift of linearly and bridging CO is accompanied by a lower linear to bridge ratio as a result of the increased back-donation from the noble metal particles [15,19,27,28]. Also in the present study, the linear to bridge ratio shows a clear

decrease from 6.9 to 4.1 when the CO bands shifts to lower wave number. Based on the red shift and changed L/B ratio, no distinction can be made between a direct effect of water on the CO molecule or an indirect effect *via* modification of the metal particle potential, inducing an increased back-donation from the metal to CO, or a combination of both phenomena.

Remarkably, the CO intensity increased about 4 times when adsorbed from aqueous phase compared to gas phase adsorption. This observation is similar to previous results where we found a 5 times higher intensity for CO on Pt/ZnSe comparing CO adsorption from aqueous phase with gas phase [2]. Unfortunately, papers reporting on intensity changes upon addition of water are scarce.

At first instance, it seems likely that the increase in intensity could be caused by a larger penetration depth, which depends on the refractive index of the sample on top of the IRE [29]. In general, the refractive index of a porous material can be calculated from the individual refractive indices of the porous material and the surrounding medium [30]. Calculations showed that changing the medium from gas to water only increases the penetration depth 1.29 times (see supplementary information), which is significantly less than the factor of 4 increase in intensity.

A higher CO-coverage in aqueous phase can also be excluded as a reason for the higher IR intensity, since CO is well known to adsorb strongly on platinum, and full coverage is easily reached in gas phase at 1 atmosphere. For this reason CO chemisorption is often used to determine metal particle dispersion [31]. It is therefore not possible that adsorption of CO from aqueous phase leads to a four times higher coverage compared to gas phase adsorption.

A possible remaining explanation for the increase in intensity is a change in extinction coefficient upon addition of water. It was shown that adsorption of wetted CO (with water vapour) on Pt/Al_2O_3 did not change the extinction coefficient of adsorbed CO [10]. However, the addition of bulk water showed a dramatic effect on the intensity of adsorbed CO, similar to the present study [2]. For this reason, we propose that the surrounding of adsorbed CO by an excess of water molecules results in a polarisation of the CO molecule, for example *via* hydrogen bonding, which directly influences its extinction coefficient because of an increased transition dipole moment.

In addition, the stretch frequency of linearly CO adsorbed on Pt/Al_2O_3 was found to shift down with increasing pH as shown in Figure 4.3B. In electrochemistry it is well-known that a change in electrode potential causes a shift in peak position of

adsorbed CO [32-34]. Moreover, a linear relation between pH of the solution and the observed metal potential was published [35] which was accompanied by a relation between the corrected potential and the observed frequency of adsorbed CO [32,36]. Unfortunately, it is difficult to compare those results directly with the observations in the present study because of the applied potential in electrochemistry. In fact, to do so we would need IR spectra of adsorbed CO at open circuit potential of a reacting electrode, which are not available to the best of our knowledge because of severe mass transfer problems. In gas phase chemistry the stretch frequency of adsorbed CO is regarded as a sensitive probe of metal-support interactions [8-19], which are known to influence the electronic properties of the supported metal and thus its catalytic activity [13]. As a final point, a strong direct effect of pH on the CO stretch frequency, for example through the formation of a $CO\text{-}H^+$ adduct, can be excluded. Such adduct formation would result in a weakening of the CO bond, which would result in a shift to lower frequency with decreasing pH. However, exactly the opposite trend is observed.

In conclusion, we attribute all observed spectral changes when comparing gas phase and adsorption from aqueous phase with different pH, i.e. the red shifts, decreased L/B ratio and fourfold increased intensity, to a combination of increased back-donation from the supported metal and a direct effect of water on the transition dipole moment of adsorbed CO.

4.4.3 Oxidation of pre-adsorbed CO in gas and aqueous phase

Figure 4.4 clearly shows an increased rate of disappearance of adsorbed CO in aqueous phase compared to the gas phase oxidation experiment. In addition, increasing pH from 4.9 to 9.1 significantly enhances the CO oxidation rate. Similarly, we showed recently that the oxidation rate of pre-adsorbed CO on Pt/ZnSe was about twice as fast in aqueous phase at neutral pH compared to gas phase [2]. In electro-oxidation of CO over either platinum or gold in acidic and alkaline solutions, it was found that the electro oxidation was fastest in alkaline solutions where the CO stretch frequency was lowest [35,36], which is in agreement with this study. Moreover, the stretch frequency of adsorbed CO can be linearly related to the CO oxidation rate as depicted in Figure 4.7. This linear relationship points towards an effect of the metal particle potential on the rate-determining step of CO oxidation in aqueous phase.

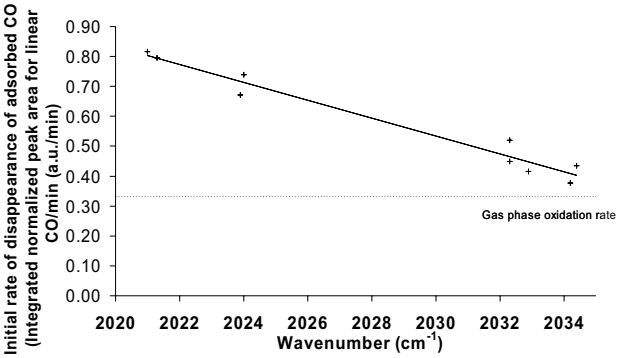

Figure 4.7. Initial rate of disappearance of pre-adsorbed CO in aqueous phase as a function of infrared frequency of linearly adsorbed CO on Pt/Al_2O_3; for comparison, gas phase oxidation rate is indicated with the dotted line.

For gas phase CO oxidation it was reported that for zeolite supported catalysts higher CO activity was found for samples with CO bands at lower wave number, which was accompanied by a lower L/B ratio [19]. Based on XAFS experiments, the authors attributed the increased oxidation activity to an increased electron density on the metal particles. The increased potential induces a higher π-back donation from the metal particle to CO, which results in a red shift of the CO stretch frequency and a lower L/B ratio. Similar trends were observed for sulphur poisoned Pt/SiO_2 catalysts [37]. For the first time we show here that the same relation holds for CO oxidation over Pt/Al_2O_3 in aqueous phase. In gas phase experiments the red shift is normally accompanied by a decreased L/B ratio, which is only observed when comparing the gas phase and aqueous phase experiments in the present study. With changing pH no significant difference in L/B ratio was found. However, in gas phase the reported shifts in band position are much larger (up to 100 cm^{-1}) than in our study (13 cm^{-1} from pH 4.9 to 9.1). The increased π-back donation weakens the C-O bond by supplying electrons in the anti-bonding orbital [38], that will be more reactive towards the p-electrons of adsorbed oxygen atoms. As a result, the CO molecule is more easily oxidized with increasing pH.

From this perspective it is also interesting to extrapolate the found linear relationship to the gas phase oxidation rate indicated in Figure 4.7. The two lines intercept at 2037 cm^{-1} which is significantly lower than the observed frequency for adsorbed CO in gas phase (2071 cm^{-1}). This observation demonstrates that the linear relation between peak position and oxidation rate can not be universally applied. The most likely explanation for this is a change of mechanism in the presence of water. For a given mechanism, the CO band position can be directly related to the oxidation

activity as shown in Figure 4.7 and published in literature for gas phase oxidation [19].

It is well accepted that the mechanism for CO oxidation in gas phase on platinum catalysts proceeds via a three step Langmuir-Hinselwood reaction mechanism, where adsorbed CO reacts with dissociatively adsorbed oxygen (Scheme 4.1) [39,40]. In addition, CO oxidation in aqueous phase has been examined extensively in electrochemistry [5,32,35,41-43]. The oxygen containing species for electro oxidation is thought to result from oxidation of water at the electrode surface and is usually supposed to be adsorbed OH [41,43]. Previously, also an activated complex was proposed, such as adsorbed CO-H_2O on platinum which forms CO-OH during oxidation [41]. Since in the present study the oxidation of CO on Pt/Al_2O_3 in aqueous phase did not take place in the absence of O_2 we can exclude the formation of OH^- from water on the platinum surface. This is in agreement with DFT calculations showing that during CO oxidation in water over Pt(111) water could not dissociate on uncharged Pt(111) [44]. Moreover, in heterogeneous catalysis it is well-known that water does not dissociate on platinum particles in water-gas-shift or steam reforming at high temperatures.

Obviously, the reaction mechanism of CO oxidation by O_2 over Pt/Al_2O_3 in aqueous phase is not only different from gas phase oxidation, but also from electro-chemical oxidation where water is generally accepted as the oxygen source, electrons are removed via the electrode and the reaction can be performed in the absence of dissolved molecular oxygen. Since the adsorption of CO from aqueous phase already revealed a direct effect of liquid water on the CO molecules *(reflected in a higher extinction coefficient, vide ante)* we propose an activated complex of CO molecules and water, $\left[(CO)\cdot(H_2O)_y\right]^*$ to be a reaction intermediate for CO oxidation by O_2 in aqueous phase (Scheme 4.1). Due to hydration of the adsorbed CO molecule, the CO bond is weakened to a large extent, as reflected in the large red shift and decreased L/B ratio, which facilitates its oxidation. The exact configuration of the CO-water complex remains unclear for the moment and is currently subject of theoretical calculations. Moreover, an effect of water on adsorbed dissociated oxygen cannot be excluded yet.

Scheme 4.1. Proposed reaction mechanism of CO and O_2 in gas phase and aqueous phase.

Gas phase [39,40]	Aqueous phase [this paper]
$CO + * \rightleftarrows CO^*$	$CO + * \rightleftarrows CO^*$
$O_2 + 2 * \rightleftarrows 2\ O^*$	$CO^* + y\ H_2O(l) \rightleftarrows \left[(CO)\times(H_2O)_y\right]^*$
$O^* + CO^* \rightarrow CO_2 + 2^*$	$O_2 + 2 * \rightleftarrows 2\ O^*$
	$O^* + \left[(CO)\times(H_2O)_y\right]^* \rightarrow CO_2 + y\ H_2O(l) + 2^*$

The asterisk signifies a platinum site, and X* an adsorbed specie on platinum.

Finally, Figure 4.8 summarizes the findings of this study. The presence of co-adsorbed and bulk water affect respectively the metal particle potential and the CO transition dipole moment, most likely via complex formation between CO and H_2O. This interaction alters the reaction mechanism and rate of CO oxidation. In addition, the pH mainly affects the CO molecule *via* a potential change of the metal particle, which in turn is directly related to the observed rate of oxidation.

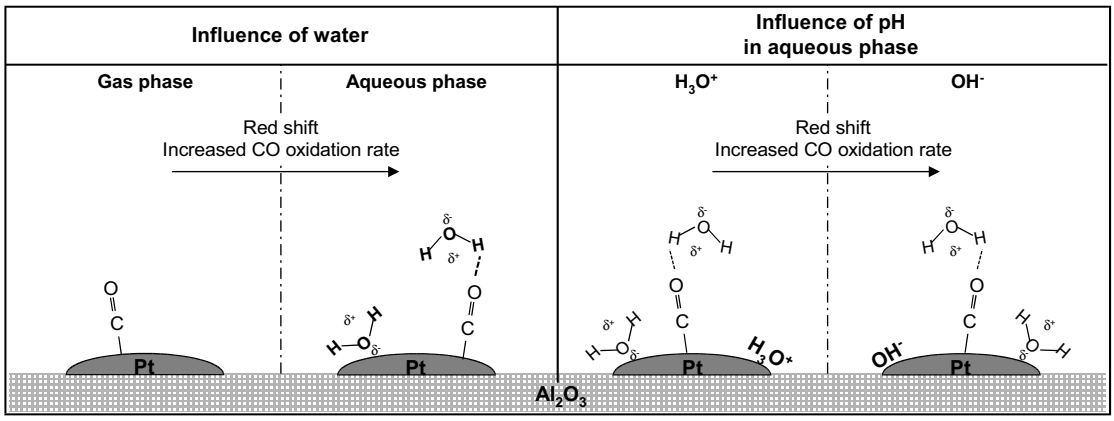

Figure 4.8. Schematic presentation of the influence of water and pH on the CO stretch frequency and CO oxidation rate (more details can be found in the text).

4.5 Conclusion

This study convincingly shows the benefit of ATR-IR spectroscopy to compare properties of adsorbed molecules on supported noble metal catalysts in gas phase and aqueous phase, since exactly the same catalyst can be used for both types of experiments. The aqueous solution influences the properties of CO adsorbed on

Pt/Al_2O_3 considerably. A large red shift, a decreased L/B ratio and a fourfold increased intensity are observed, resulting from a combination of increased back-donation from the metal and a direct effect of water on the transition dipole moment of adsorbed CO. As a result the reaction mechanism is altered by the presence of liquid water compared to gas phase or electro-chemical CO oxidation. The pH effect on the CO oxidation rate can be fully attributed to a potential change of the metal particles, which in turn affects the CO stretch frequency that is linearly related to the oxidation rate.

4.6 References

[1] T. Bürgi, A. Baiker, J.Phys.Chem.B. 106 (2002) 10649.

[2] S.D. Ebbesen, B.L. Mojet, L. Lefferts, (Chapter 3 in this thesis), Langmuir 22 (2006) 1079.

[3] D. Ferri, T. Bürgi, A. Baiker, J.Phys.Chem.B. 105 (2001) 3187.

[4] R. He, R.R. Davda, J.A. Dumesic, J.Phys.Chem.B. 109 (2005) 2810.

[5] N. Kizhakevariam, X. Jiang, M.J. Weaver, J.Chem.Phys. 100 (1994) 6750.

[6] I. Ortiz-Hernandez, C.T. Williams, Langmuir 19 (2003) 2956.

[7] N.C. Yee, G.S. Chottiner, D.A. Scherson, J.Phys.Chem.B. 109 (2005) 7610.

[8] M. Bartok, J. Sakany, A. Sitkei, J.Catal. 72 (1981) 236.

[9] S. Boujana, D. Demri, J. Cressely, A. Kiennemann, J.P. Hindermann, Catal.Lett. 7 (1990) 359.

[10] A. Bourane, O. Dulaurent, D. Bianchi, Langmuir 17 (2001) 5496.

[11] D.C. Koningsberger, D.E. Ramaker, J.T. Miller, J. de Graaf, B.L. Mojet, Top.Catal. 15 (2001) 35.

[12] G. Larsen, G.L. Haller, Catal.Lett. 3 (1989) 103.

[13] B.L. Mojet, J.T. Miller, D.E. Ramaker, D.C. Koningsberger, J.Catal. 186 (1999) 373.

[14] B.L. Mojet, D.C. Koningsberger, Catal.Lett. 39 (1996) 191.

[15] B.L. Mojet, J.T. Miller, D.C. Koningsberger, J.Phys.Chem.B. 103 (1999) 2724.

[16] V. Pitchon, M. Primet, H. Praliaud, Appl.Catal. 62 (1990) 317.

[17] M. Primet, J.Catal. 88 (1984) 273.

[18] F. Stoop, F.J.C.M. Toolenaar, V. Ponec, J.Catal. 73 (1982) 50.

[19] T. Visser, T.A. Nijhuis, A.M.J. van der Eerden, K. Jenken, Y. Ji, W. Bras, S. Nikitenko, Y. Ikeda, M. Lepage, B.M. Weckhuysen, J.Phys.Chem.B. 109 (2005) 3822.

[20] E.V. Benvenutti, L. Franken, C. Moro, Langmuir 15 (1999) 8140.

[21] A. Bourane, O. Dulaurent, D. Bianchi, J.Catal. 196 (2000) 115.

[22] R. Barth, R. Pitchai, R.L. Anderson, X. Verykios, J.Catal. 116 (1989) 61.

[23] A. Bourane, D. Bianchi, J.Catal. 220 (2003) 3.

[24] G. Rupprechter, T. Dellwig, H. Unterhalt, H.J. Freund, J.Phys.Chem.B. 105 (2001) 3797.

[25] R. Barth, R. Pitchai, R.L. Anderson, X. Verykios, J.Catal. 116 (1989) 61.

[26] M. Neurock, University of Virginia, Department of Chemical Engineering, Charlottesville, USA (May 2006) Personal communication, unpublished results.

[27] M.J. Kappers, M. Vaarkamp, J.T. Miller, F.S. Modica, M.K. Barr, J.H. Vandermaas, D.C. Koningsberger, Catal.Lett. 21 (1993) 235.
[28] D.E. Ramaker, J. de Graaf, J.A.R. van Veen, D.C. Koningsberger, J.Catal. 203 (2001) 7.
[29] N.J. Harrick, Internal Reflection Spectroscopy, Interscience Publishing, New York, 1967.
[30] M.M. Braun, L. Pilon, Thin Solid Films 496 (2006) 505.
[31] M. Primet, M. El Azhar, R. Frety, M. Guenin, Appl.Catal. 59 (1990) 153.
[32] S.-C. Chang, M.J. Weaver, J.Chem.Phys. 92 (1990) 4582.
[33] S.A. Wasileski, M.T.M. Koper, M.J. Weaver, J.Phys.Chem.B. 105 (2001) 3518.
[34] J. Xu, J.T. Yates, Surf.Sci. 327 (1995) 193.
[35] A. Couto, A. Rincón, M.C. Pérez, C. Gutiérrez, Electrochim.Acta 46 (2001) 1285.
[36] K. Kunimatsu, A. Aramata, H. Nakajima, H. Kita, J.Electroanal.Chem. 207 (1986) 293.
[37] F.J. Gracia, S. Guerrero, E.E. Wolf, J.T. Miller, A.J. Kropf, J.Catal. 233 (2005) 372.
[38] G. Blyholder, J.Phys.Chem. 68 (1964) 2772.
[39] G. Ertl, T. Engel, Adv.Catal. 28 (1979) 1.
[40] G. Ertl, Adv.Catal. 37 (1990) 213.
[41] S. Gilman, J.Phys.Chem. 68 (1964) 70.
[42] H.L. Lam-Wing, A. Wieckowski, M.J. Weaver, J.Phys.Chem. 92 (1988) 6985.
[43] N.P. Lebedeva, A. Rodes, J.M. Feliu, M.T.M. Koper, R.A. van Santen, J.Phys.Chem.B. 106 (2002) 9863.
[44] S. Desai, M. Neurock, Electrochim.Acta 48 (2003) 3759.

CHAPTER 5

CO adsorption and oxidation over Pd/Al_2O_3 Promotion effects by water and pH

Abstract

Adsorption and oxidation of carbon monoxide over a Pd/Al_2O_3 catalyst layer was investigated both in gas and aqueous phase. Both adsorption and oxidation of CO are significantly affected by the presence of liquid water. Water influences the potential of the metal particles as well as the dipole moment of the adsorbed CO molecule directly, which is both reflected in large red shifts and a threefold higher intensity when experiments are carried out in aqueous phase. Furthermore, the rate of CO oxidation increases significantly by both the presence of water and by increasing the pH. Enhancement of the oxidation rate is attributed to both weakening of the CO bond by increasing potential of the metal particle, similar to CO oxidation over Pt/Al_2O_3. However, palladium differs from platinum because the oxidation of palladium is promoted in water and with increasing pH, further enhancing the oxidation of CO over Pd/Al_2O_3.

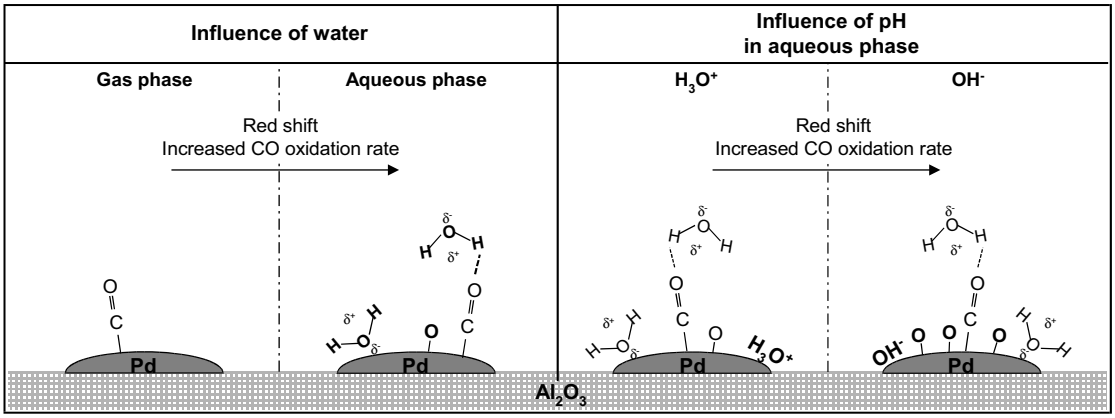

5.1 Introduction

The relative simplicity of CO oxidation makes the reaction an ideal model of a heterogeneous catalytic reaction and allows for a detailed *in-situ* study. Interactions between CO and the active metal are reflected in shifts of the CO absorption bands, which in turn are known to be affected by metal support interactions. Since the vibrations are so sensitive for modifications of the metal particles and/or its surrounding medium, adsorption of CO as a probe molecule in combination with vibrational spectroscopy is widely applied to characterise supported noble metal catalysts [1-18].

CO oxidation has been frequently studied over both single-crystal palladium surfaces and over well-dispersed, supported palladium catalysts [19-22]. In gas phase the addition of water vapour was shown to increase the oxidation activity over palladium catalysts, but no explanation was given for this increase [23]. Only a few studies have reported on reactions involving CO in aqueous phase. For example, the adsorption and oxidation of CO and the dissociation of small molecules such as formaldehyde over Pt/Al_2O_3 catalysts was reported [24]. In addition, ATR-spectroscopic studies of the water-gas shift reaction and methanol reforming over Pt/Al_2O_3 were combined with kinetic studies [25]. In our lab, we showed the large effect of water on the CO stretch frequency and observed an increase of the CO oxidation rate compared to gas phase CO oxidation over Pt/Al_2O_3 and Pt/ZnSe [1,26]

It is the objective of this study to examine the effect of water and pH on the palladium supported on alumina and on the oxidation of CO over Pd/Al_2O_3. CO adsorption and oxidation on Pd/Al_2O_3 is therefore investigated as a model reaction, using *in-situ* ATR-IR spectroscopy. Similarities and differences between adsorption and oxidation of CO over Pt/Al_2O_3 and Pd/Al_2O_3 will be discussed.

5.2 Experimental

The experimental procedure, materials and catalyst preparation are described in detail in the Experimental Section (Chapter 2). All spectra presented in the following section are corrected for the water background. The integrated peak areas are calculated using curve fitting of the spectra, following the procedure described in the Experimental Section (Chapter 2).

The characteristics of the 5 wt% Pd/Al_2O_3 (dispersion 45%) catalyst examined in the present study are also described in detail in the Experimental Section (Chapter 2).

6 mg of catalyst was deposited on the Internal Reflection Element (IRE), resulting in $1.3 \cdot 10^{-6}$ mol accessible surface palladium atoms deposited on the IRE. The thickness of the catalyst layer was 5.0 ± 0.5 μm.

After assembling the cell in the IR spectrometer the cell was purged with gaseous argon followed by a reducing gas flow for 2 hours at 294 K (10% H_2/Ar) to remove surface oxygen, before adsorption experiments were performed. For experiments in aqueous phase, the catalyst was reduced in hydrogen saturated Q2-water H_2/H_2O ($4.1 \cdot 10^{-4}$ mol/L H_2; saturation at 0.1 bar). In gas phase, formation of β-palladium-hydride occurs at hydrogen pressures above 0.025 bar [27]. Even though the concentration is lower in aqueous phase, the chemical potential of hydrogen is assumed to be equal in gas and aqueous phase, if the same concentration is used for saturation. Saturation of the aqueous phase with a hydrogen pressures above 0.025 bar will therefore result in formation of β-palladium-hydride during reduction in aqueous phase. The Pd/Al_2O_3 catalyst used in this study therefore consists of β-palladium-hydride after reduction in both gas and aqueous phase.

5.3 Results

5.3.1 Adsorption of CO from gas and aqueous phase

After assembling the ATR-IR cell and reduction of the catalyst layer, dry gas phase CO was introduced into the cell. Figure 5.1 shows the ATR-IR spectra obtained during flow of CO over the pre-reduced Pd/Al_2O_3 catalyst.

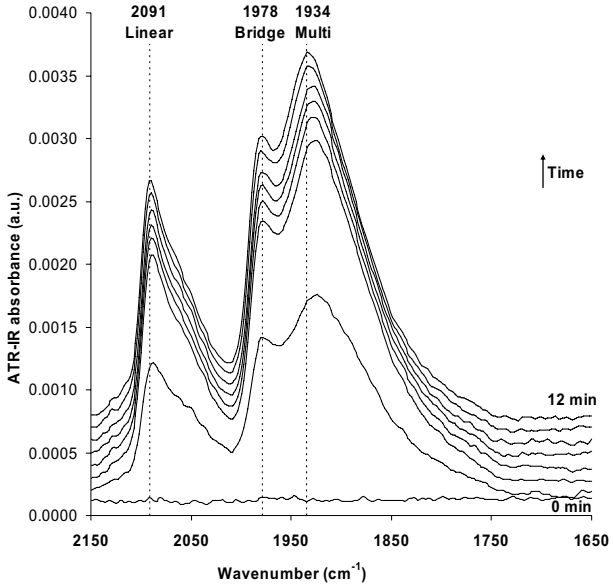

Figure 5.1. ATR-IR spectra as a function of time showing CO adsorption on Pd/Al_2O_3 while dry CO was flown over the catalyst layer (1% CO/Ar).

During CO flow no gaseous CO was detected whereas adsorbed CO on palladium was detected with a distinct asymmetric infrared peak, with a shoulder at the low frequency side, appearing at 2086 cm^{-1}, shifting to 2091 cm^{-1} with increasing time and two broad peaks; one at 1975 cm^{-1} shifting to 1978 cm^{-1} and one at 1928 cm^{-1} shifting to 1934 cm^{-1} with increasing time. These blue shifts are attributed to dipole-dipole coupling of adsorbed CO with increasing surface coverage [10,16]. Infrared bands in the range of 2060 – 2100 cm^{-1} are normally assigned to linear bound CO on palladium, while bands in the range between 1750 – 2000 cm^{-1} are assigned to bridged and multi bonded CO on palladium [28-34]. Therefore the peak at 2091 cm^{-1} is assigned to linear bonded CO. The other two overlapping peaks, can be assigned to bridged CO (1979 cm^{-1}) and multi bonded CO (1934 cm^{-1}) adsorbed on palladium. The ratio between the integrated peak intensities of the linear and bridged/multi bonded absorption band (L/B-M ratio) is 0.27. This ratio is significantly lower compared to CO adsorption on platinum (L/B ratio of 6.9), as shown in Chapter 4, and is a result of the difference in the electronic properties of platinum and palladium [10,17,28-36].

After flowing dry gaseous CO, the cell was first flushed with dry argon for 10 minutes. During flow of argon the intensity of the peaks for both linear and bridge CO remained constant. Subsequently a dry oxygen rich stream (10% O_2/Ar) was introduced into the cell to remove adsorbed CO (see section 5.3.3). After oxidation, the cell was flushed with argon and the catalyst layer was reduced *in-situ* for several hours by H_2 (gas) in order to repeat adsorption/oxidation experiments.

After finalising the gas phase experiments, Ar/H_2O was introduced into the cell, containing the same catalyst layer. Subsequently, the catalyst layer was reduced *in-situ* by H_2/H_2O ($8.2 \cdot 10^{-5}$ mol H_2/L; saturated at 0.1 bar) until a stable background spectrum was obtained, after approximately 12 hours. After reduction, CO/H_2O ($1.4 \cdot 10^{-6}$ mol CO/L; saturated at 0.01 bar) at pH 7.1 was introduced and ATR-IR spectra were collected, as shown in Figure 5.2.

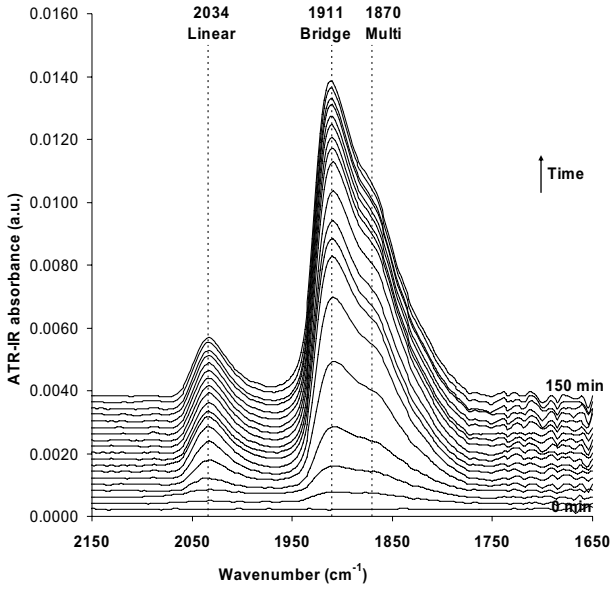

Figure 5.2. Water corrected ATR-IR spectra recorded while CO/H_2O ($1.4 \cdot 10^{-6}$ mol CO/L) was flown over Pd/Al_2O_3 at pH 7.1.

CO adsorbed on Pd/Al_2O_3 from aqueous phase at pH 7.1 was detected by a peak for linear CO at 2028 cm^{-1}, shifting to 2034 cm^{-1} with increasing time. Bridged and multi bonded CO was again detected by two peaks; bridged CO was observed at 1906 cm^{-1} shifting to 1911 cm^{-1} and multi bonded CO was detected at around 1870 cm^{-1}. Again the blue shifts are attributed to an increased dipole-dipole coupling of adsorbed CO with increasing surface coverage [10,16]. Compared to gas phase adsorption (Figure 5.1) linear, bridged and multi bonded CO show a significant red shift of 57 cm^{-1} for linear CO; 67 cm^{-1} for bridge CO and 67 cm^{-1} for multi bonded CO in the presence of water (Figure 5.1 and Figure 5.2). The shifts are in agreement with previous studies performed by our group on CO adsorption on Pt/Al_2O_3 [1].

After CO adsorption in aqueous phase, the cell was flushed with Ar/H_2O. The intensity of the peaks for linear, bridged and multi bonded CO remained constant, indicating that the layer with adsorbed CO was stable. Subsequent to Ar/H_2O flushing, adsorbed CO was oxidised/removed by flowing O_2/H_2O ($1.3 \cdot 10^{-4}$ mol O_2/L). Thereupon, the cell was flushed with Ar/H_2O and the catalyst layer was reduced

in-situ by H_2/H_2O ($7.8 \cdot 10^{-5}$ mol H_2/L) for several hours. After this treatment experiments could be repeated with reproducible results.

5.3.2 CO adsorption from pH 5.0 – 9.0 in aqueous phase

Beside the influence of water, the effect of pH on CO adsorption in aqueous phase was also examined. The ATR-IR cell, containing the same Pd/Al_2O_3 catalyst layer as used for CO adsorption in gas and aqueous phase, was flushed with Ar/H_2O first. Subsequently, the catalyst layer was reduced *In-Situ* by H_2/H_2O at respectively pH 5.0, 7.0, 7.1, 8.5 and 9.0 followed by inert flow (Ar/H_2O) at the according pH. CO/H_2O with the same pH was flown over the Pd/Al_2O_3 catalyst layer and ATR-IR spectra were recorded. Figure 5.3 shows the ATR-IR spectra of CO adsorbed on Pd/Al_2O_3 at pH 5.0, 7.1 and 9.0. The spectra for the intermediate pH values vary gradually between those shown in Figure 5.3. After each adsorption experiment, adsorbed CO was oxidised by O_2/H_2O ($1.3 \cdot 10^{-4}$ mol O_2/L) at the same pH value as used during CO adsorption. Subsequently, the cell was flushed with Ar/H_2O and the catalyst layer was reduced *in-situ* by H_2/H_2O ($7.8 \cdot 10^{-5}$ mol H_2/L) for several hours as a pre-treatment for the next adsorption/oxidation experiment.

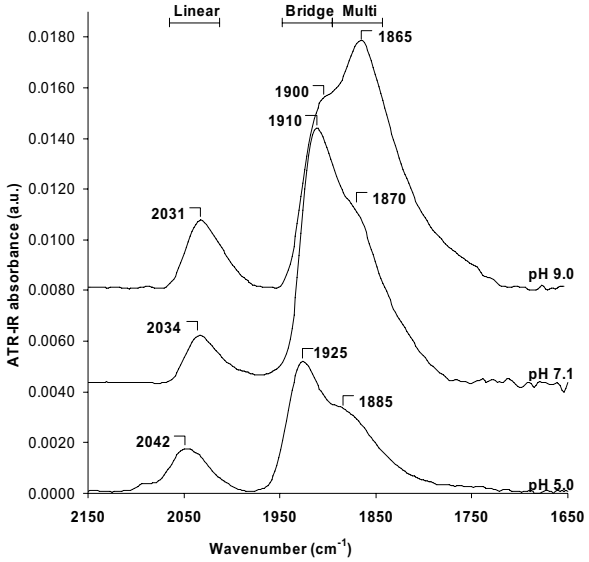

Figure 5.3. Water corrected ATR-IR spectra for CO adsorption on Pd/Al_2O_3 after CO in water ($1.4 \cdot 10^{-6}$ mol CO/L) at pH 5.0, 7.1 and 9.0 was flown for 150 minutes.

As described in the previous section (Figure 5.2), when CO was adsorbed at neutral pH (pH 7.1), linear CO was detected at 2034 cm^{-1}, bridged CO at 1912 cm^{-1} and multi bonded CO at 1870 cm^{-1} (Figure 5.3), By lowering the pH to 5.0 a blue shift of 8 cm^{-1} to 2042 cm^{-1} was observed for linear CO (Figure 5.3). Bridged and multi bonded CO also showed a blue shift to 1925 and 1885 cm^{-1}, respectively. Increasing the pH to

9.0, which is just above the isoelectric point of alumina ($IEP_{Al_2O_3}$ = 8.5 [37]), resulted in a small red shift for all adsorbed CO species. Linear adsorbed CO was detected at 2031 cm^{-1}, bridged bonded CO at 1909 cm^{-1} and multi bonded CO was observed at 1865 cm^{-1} (Figure 5.3).

Figure 5.3 clearly shows that the intensity of adsorbed CO varies with pH; the integrated area increased from 0.55 a.u. at pH 5.0 to 1.18 a.u. at pH 9.0. The integrated peak areas for at pH 7.0 (1.07) was similar to pH 9.0. Moreover, the ratio between the integrated peak intensities of the linear and bridged/multi bonded absorption band (L/B-M ratio) decreased with increasing pH; the L/B-M ratio decreased from 0.14 at pH 5.0 to 0.06 at pH 7.1 and 0.04 at pH 9.0. Furthermore, the ratio between bridged/multi bonded CO (B/M ratio) also decreased; from 0.63 at pH 5.0 to 0.56 at pH 7.1 and 0.39 at pH 9.0.

5.3.3 Oxidation of pre-adsorbed CO

5.3.3.1 Oxidation in gas phase

As described above, after adsorption of CO on the Pd/Al_2O_3 catalyst layer, adsorbed CO was oxidised by dry gas phase oxygen. Figure 5.4A shows ATR-IR spectra recorded during oxidation of pre-adsorbed CO on Pd/Al_2O_3 in gas phase. The integrated peak areas for adsorbed CO, shown in Figure 5.4B, are calculated by curve fitting of the spectra into the respective peaks following to the procedure described in the Experimental Section (Chapter 2).

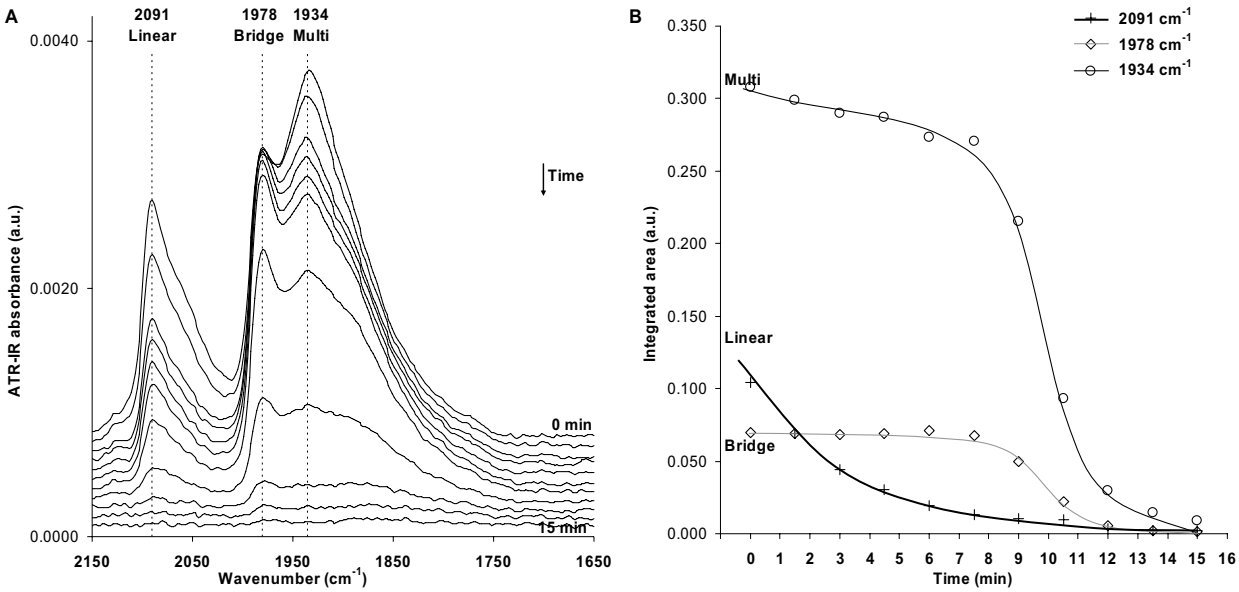

Figure 5.4. A: ATR-IR spectra obtained while oxygen (10% O_2/Ar) was flown over Pd/Al_2O_3, with pre-adsorbed CO; B: Integrated peak areas of observed species during oxidation.

During oxidation of pre-adsorbed CO a decrease in the peaks for linear and bridged CO was observed, but no CO_2 was detected. Initially the peak for linear CO decreases while shifting from 2091 to 2088 cm^{-1}, followed by a decrease of bridged and multi bonded adsorbed CO after 8 minutes, with a simultaneous red shift of approximately 3 cm^{-1} for both species. The red shifts are caused by decreased dipole-dipole coupling at lower coverage of adsorbed CO [10,16]. The observation that linear CO is more reactive to oxygen, and is oxidised before oxidation of bridged and multi bonded CO occurs, is in agreement with literature reporting on CO oxidation over Pd/Al_2O_3 [38].

5.3.3.2 Oxidation in aqueous phase

As described above, CO oxidation was also performed in aqueous phase. After adsorption of CO in aqueous phase the cell was flushed with Ar/H_2O, at the same pH as for CO adsorption. During flow of Ar/H_2O the intensity of the peaks for linear, bridged and multi bonded CO remained constant. Subsequently, O_2/H_2O ($1.3 \cdot 10^{-4}$ mol O_2/L) was flown over the same Pd/Al_2O_3 catalyst layer with pre adsorbed CO. The oxidation experiments were performed at respectively pH 5.0, 7.0, 7.1, 8.5 and 9.0 (same pH as for CO adsorption), but for clarity only the spectra at pH 5.0, 7.1 and 9.0 are shown in Figure 5.5A, C and E, respectively. The integrated peak areas for adsorbed CO during oxidation are shown in Figure 5.5B, D and F. On first sight, it seems like bridged CO is the main specie adsorbed on the palladium surface at pH 5.0 and 7.1 (Figure 5.5A and C). However, the integrated peak areas based on peak deconvolution (shown in Figure 5.5B and D) reveal multi bonded CO as the dominating specie. This is caused by the fact that the peak for multi bonded CO is approximately twice as broad as the peak for bridge bonded CO (as normally found for CO adsorbed on palladium catalysts).

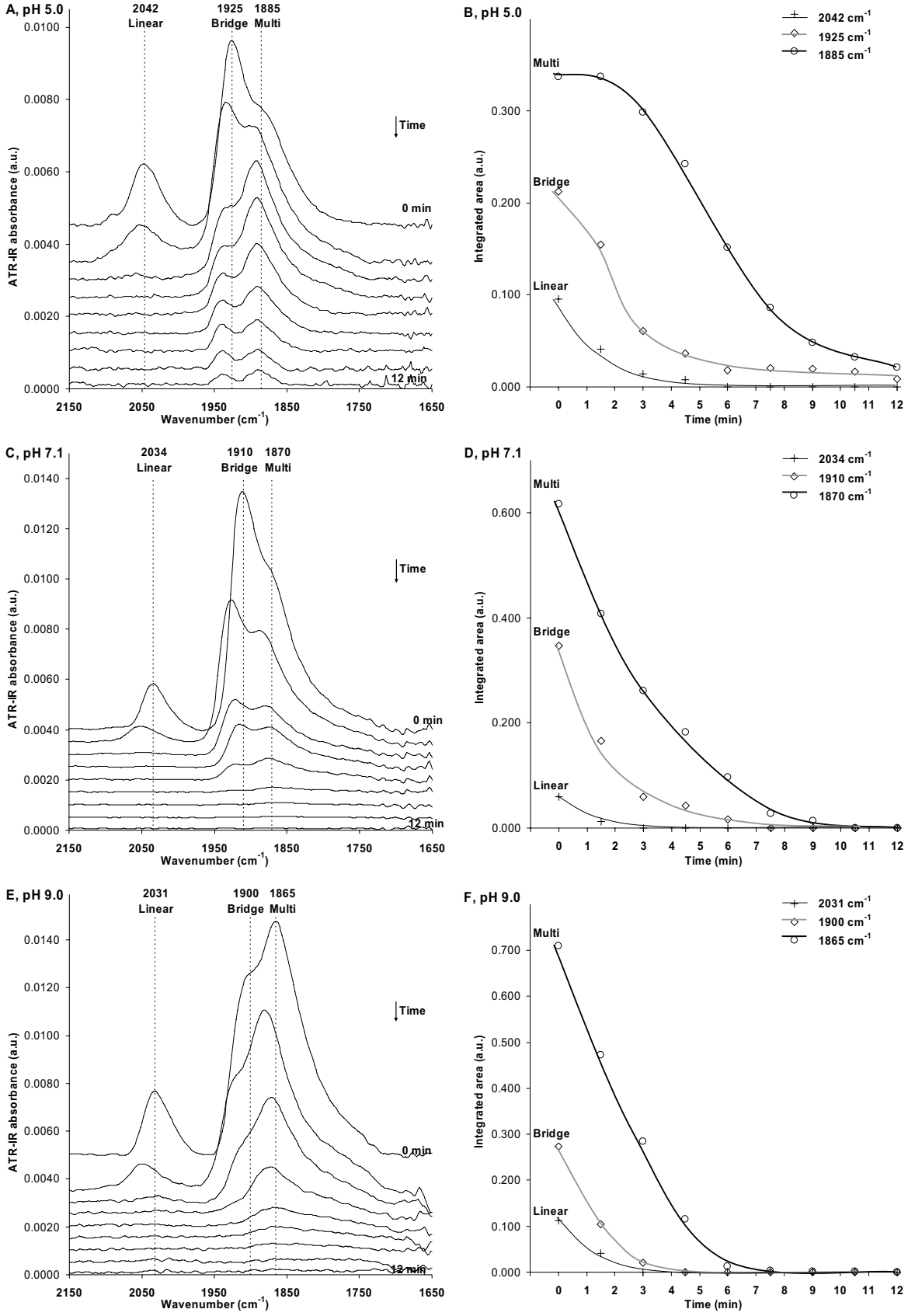

Figure 5.5. Water corrected ATR-IR spectra and integrated peak areas during oxidation of pre adsorbed CO on Pd/Al_2O_3 in aqueous phase at A, B: pH 5.0; C, D: pH 7.1 and E, F: pH 9.0.

As for gas phase, during oxidation of pre adsorbed CO a decrease in the peaks for linear and bridged CO was observed, but again no CO_2 was detected. During oxidation in water at pH values ranging from 7.0 – 9.0 the peaks for linear, bridged and multi bonded CO initially decreased. At lower pH (5.0), an initial period, where only linear and bridged CO were oxidised, was observed. This was also the case for gas phase oxidation, although for oxidation in aqueous phase at pH 5.0 this initial period was only 1.5 minutes (Figure 5.5A, B) compared to the 8 minutes during gas phase oxidation (Figure 5.4A, B). In addition, the peak positions for adsorbed CO in aqueous phase show a blue shift during oxidation. The blue shift is 9 – 10 cm^{-1} during oxidation at pH 5.0; 13 – 14 cm^{-1} at pH 7.1 and 16 – 17 cm^{-1} at pH 9.0. The oxidation rate of adsorbed CO increases with increasing pH, as shown in Figure 5.5. The oxidation rate is highest at pH 9.0, where CO was completely removed after 7.5 minutes, whereas it took 10.5 minutes to remove all CO at pH 7.1. The CO oxidation rate was lowest at pH 5.0, where 12 minutes were not sufficient for complete removal of CO, despite the fact that the initial CO coverage at pH 5.0 was low.

5.4 Discussion

5.4.1 CO adsorption from gas and aqueous phase

Comparison of the adsorption of CO from gas or aqueous phase revealed clear spectral differences. For comparison, Figure 5.6 shows the ATR-IR spectrum at saturation level for both situations. CO adsorption was performed on the exact same catalyst layer in both experiments, allowing for direct comparison between adsorption from gas and aqueous phase.

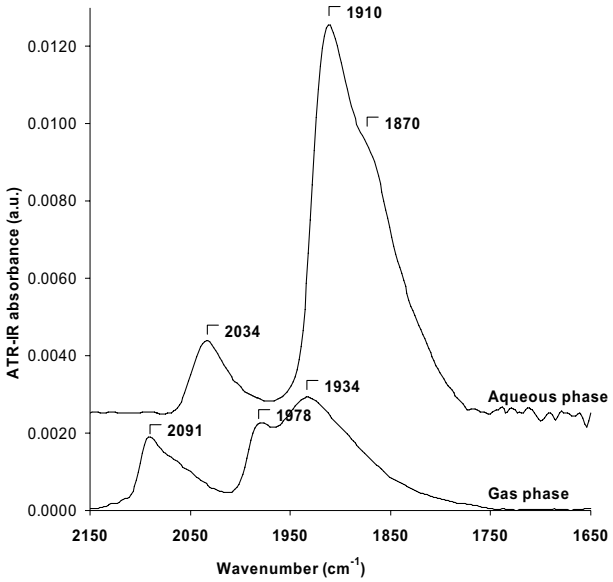

Figure 5.6. ATR-IR spectrum of CO adsorbed on Pd/Al_2O_3 from gas phase CO and water corrected ATR-IR spectrum of CO adsorbed on Pd/Al_2O_3 from aqueous phase at pH 7.1.

From Figure 5.6 it can clearly be seen that, when changing from gas to aqueous phase, a significant red shift for absorbed CO is observed. Linear CO shifted from 2091 to 2034 cm^{-1} (57 cm^{-1}), bridged adsorbed CO shifted from 2978 to 2011 cm^{-1} (67 cm^{-1}) and multi bonded CO shifted from 1934 to 1870 cm^{-1} (64 cm^{-1}). In addition, the integrated peak areas of adsorbed CO were three times higher when adsorbed from aqueous phase than from gas phase. Moreover, the ratio between the integrated peak intensities of the linear and bridged/multi bonded absorption band (L/B-M ratio) decreased from 0.27 in gas phase to 0.06 in aqueous phase, i.e. more CO is adsorbed in bridged and multi bonded configuration in aqueous phase.

The red shift of 57 – 67 cm^{-1} in peak position for adsorbed CO in the presence of water, is similar to results obtained on Pt/Al_2O_3, as recently published by us, where a red shift of around 50 cm^{-1} was observed for adsorbed CO [1]. In literature, CO has also been adsorbed on Pd/Al_2O_3 from dichloromethane and cyclohexane [11,39]. It was found that CO adsorbed from these solvents shows a lower frequency than found in gas phase adsorption. Using dichloromethane, linear CO was observed between 2054 and 2048 cm^{-1}, while multi bonded CO was detected between 1860 and 1820 cm^{-1} [11]. Adsorbed from cyclohexane, linear CO was detected at 2068 cm^{-1} and multi bonded CO was detected 1968 cm^{-1} [39]. CO adsorbed on palladium in presence of water has been investigated in a few studies only. CO adsorbed on Pd(100) was characterised by one peak at 1860 cm^{-1}, shifting to 1955 cm^{-1} with increasing coverage [40]. On Pd(111), adsorbed CO at low coverage was characterised by one peak (1840 – 1870 cm^{-1}), which split into two peaks with

increasing coverage. At saturation, one study reported that the two peaks were located at 1925 cm^{-1} and 1882 cm^{-1} [40], whereas another study reported the location to be 1956 cm^{-1} and 1917 cm^{-1} [41]. On Pd(poly), adsorbed CO in the presence of water was characterised by two peaks; one at 2064 cm^{-1} (linear CO) and one at 1959 cm^{-1} (either bridged or multi bonded CO) [42].

In all cases the peak frequencies of adsorbed CO were found to show a significant red shift in the presence of solution (water, cyclohexane or dichloromethane) compared to gas phase adsorption, in agreement with the present study.

In addition to the clear shift in peak position, Figure 5.6 also shows a threefold increase in intensity when CO is adsorbed from aqueous phase compared to gas phase adsorption. This increase in intensity is in good agreement with previous results of CO adsorption on both Pt/Al_2O_3 and Pt/ZnSe in gas and aqueous phase [1,26]. A higher CO-coverage in aqueous phase can be excluded as an explanation for the increased intensity, since CO is well known to adsorb strongly on palladium and full coverage is easily reached in gas phase at 1 atmosphere [43]. According to the calculations of the penetration depth shown in the Experimental Section (Chapter 2) the difference in refractive index of water and air, can cause a maximal increase in intensity of 1.27 times, because of the increased penetration depth. This increase is significantly lower than the observed increase in the intensity of the CO band.

It is well-known that a red shift of linear and bridged adsorbed CO is accompanied by a lower linear to bridged/multi bonded ratio as a result of the increased π-back-donation from the noble metal particles, *e.g.* upon increasing support alkalinity [12,14,44,45]. A significant decrease in the L/B-M ratio from 0.27 in gas phase to 0.06 in aqueous phase was indeed found in the present study (Figure 5.6).

On platinum, a clear red shift was observed for both linear and bridged CO upon gradual addition of D_2O, which was explained by a combination of increased π-back-donation from platinum to CO along with a change in CO dipole moment [15,46]. On Pt/Al_2O_3 we showed that the shift in peak position caused by water was accompanied by a decrease in the L/B ratio. We propose that the surrounding of adsorbed CO on Pd/Al_2O_3 by an excess of water molecules results in polarisation of the CO molecule, *via* hydrogen bonding, a modification of the metal particle potential or a combination of both phenomena. This explains the observed increased CO intensity, the red shift of the peak position and the decrease in the L/B ratio. Polarisation directly influences the extinction coefficient, because of an increased transition dipole moment. Modification of the metal particle potential shifts the peak position, inducing increased

π-back-donation from the metal to CO. This explanation is identical to the explanation offered previously for the influence of water on CO adsorbed on Pt/Al_2O_3 [1].

In conclusion, the red shift, increased infrared intensity and decreased L/B-M ratio can be explained by both a direct effect of water on the CO molecule as well as an indirect effect *via* modification of the metal particle potential, inducing an increased π-back-donation from the metal to CO.

5.4.1.1 CO adsorption in aqueous phase at pH 5.0 – 9.0

The stretch frequency of both linear, bridged and multi bonded CO on Pd/Al_2O_3 was found to shift down with increasing pH. The peak positions for linear adsorbed CO are correlated to pH, as shown in Figure 5.7. Because of the overlap of the broad peaks no correlation between peak position and pH can be claimed for bridged and multi bonded CO. The broad overlapping peaks for bridge and multi coordinated CO, did not allow for precise determination of the peak position, even though the peaks were fitted into two separate peaks, the uncertainty in the peak position was ± 3 cm^{-1}.

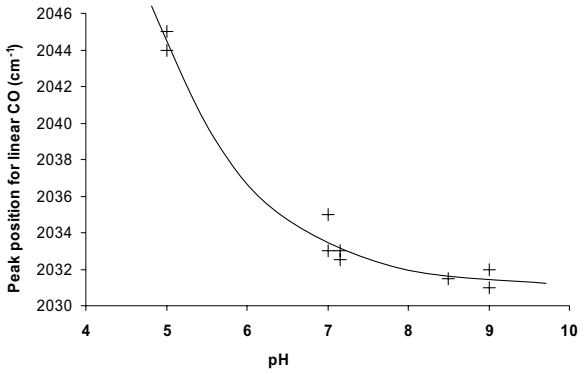

Figure 5.7. ATR-IR frequency of linearly adsorbed CO on Pd/Al_2O_3 in aqueous phase as a function of pH.

By increasing the pH from 5.0 to 9.0 a red shift of 13 cm^{-1} was detected and the L/B-M ratio decreased from 0.14 to 0.04. Remarkably the shift in peak position for CO adsorbed at pH 5.0 compared to pH 9.0 is exactly the same as we have recently published for CO adsorbed on Pt/Al_2O_3 in the same pH interval [1]. The red shift in CO stretch frequency with increasing pH can not be due to dipole-dipole coupling, as this would cause a blue shift with increasing coverage with increasing pH, opposite to the observation shown in Figure 5.7.

A direct effect of pH on the CO stretch frequency, for example through the formation of a $CO\text{-}H^+$ or $CO\text{-}OH^-$ adduct, can be excluded. The formation of a $CO\text{-}H^+$ adduct at low pH would result in a weakening of the CO bond, shifting the CO adsorption band

to lower frequency with decreasing pH. However, exactly the opposite trend is observed. At high pH the CO absorption band would shift to higher frequency if a $CO\text{-}OH^-$ adduct were formed; again, exactly the opposite trend is found.

In electrochemistry, it is well-known that a change in electrode potential causes a shift in peak position of adsorbed CO [47-49]. Moreover, a linear relation between pH of the solution and the observed metal potential was reported [50], which was accompanied by a relation between the corrected potential and the observed frequency of adsorbed CO [47,51]. Furthermore, the stretch frequency of adsorbed CO is regarded as a sensitive probe of metal-support interactions in gas phase chemistry [2-9,12,14,17,18]. Metal-support interactions are known to influence the electronic properties of the supported metal and consequently its catalytic activity [9]. These observations indicate that the pH of the solution influences the electrode potential, which can be observed by the change in the stretch frequency of adsorbed CO, comparable to metal-support interactions in gas phase.

The increased potential of the metal particles, suggested both in electro chemistry and gas phase chemistry, leads to an increased π-back-donation from the supported metal to CO. Hereby electrons are supplied to the anti-bonding orbital, consequently weakening the CO bond [52], leading to both a red shift of the CO adsorption band and a lower L/B-M ratio. Therefore we attribute the observed spectral changes when increasing pH to an increased potential of the supported metal particles, similar to over Pt/Al_2O_3.

From Figure 5.3, it is clear that the intensity of the CO bands vary with pH. As shown in Chapter 4, the pH of the solution does not influence the CO intensity of the CO peak over Pt/Al_2O_3; apparently both the extinction coefficient and the surface coverage remain unchanged with changing pH. A compensating effect is unlikely, because CO is known to adsorb strongly on platinum and full coverage is to be expected. The response of the extinction coefficient to pH is assumed to be the same over both palladium and platinum. Thus, the lower intensity for adsorbed CO at low pH, as shown in Figure 5.3, must be caused by a lower coverage. At present this effect of pH can not be explained, but it can be speculated that after reduction H/H^+ is more strongly adsorbed on the surface at low pH (*vide infra*). This will induce a competitive effect between CO and H/H^+ and as a consequence a lower CO coverage is observed at low pH.

5.4.2 Oxidation of pre-adsorbed CO

5.4.2.1 CO oxidation from gas and aqueous phase

From Figure 5.4 and Figure 5.5 it is clear that the oxidation rate of adsorbed CO in aqueous phase increased considerably compared to oxidation in gas phase, which is in good agreement with our recent publication of CO oxidation over Pt/Al_2O_3 [1] and Pt/ZnSe [26]. In addition, increasing pH from 5.0 to 9.0 significantly enhances the CO oxidation rate, again in good agreement with our recent publication of CO oxidation over Pt/Al_2O_3 [1]. Titration effects can be excluded, as sufficient oxygen is available to oxidise all adsorbed CO within 10 seconds, assuming stoichiometric adsorption of one CO molecule per palladium surface atom.

For gas phase CO oxidation it was reported that for zeolite supported catalysts higher CO activity was found for samples with CO bands at lower wave number, which was accompanied by a lower L/B ratio [14]. Based on XAFS experiments, the authors attributed the increased oxidation activity to an increased electron density on the metal particles. Oxidation of CO in aqueous phase has been examined extensively in electrochemistry, although mostly over platinum electrodes [46,47,50,53-55]. The oxygen containing species for electro oxidation is thought to result from electrochemical oxidation of water, resulting in an activated complex between CO and water [53,55]. Obviously, oxidation of CO on Pd/Al_2O_3 in aqueous phase did not take place in the absence of oxygen and chemical formation of OH^- from water on the palladium surface is excluded. Nevertheless, formation of an activated complex of CO and water, similar to an activated complex proposed in electrochemistry, as a reaction intermediate for CO oxidation by oxygen in aqueous phase is a reasonable proposition to explain the increased reaction rate in water, as suggested previously for Pt/Al_2O_3 [1]. The CO bond in the activated complex is weakened by a combination of increased π-back-donation from the supported metal and a direct effect of water on the transition dipole moment of adsorbed CO. The increased π-back donation weakens the CO bond by supplying electrons in the anti-bonding orbital [52]. The CO molecule will therefore be more reactive toward the p-electrons of adsorbed oxygen atoms. As a result, the CO molecule is more easily oxidised in aqueous phase.

During oxidation in aqueous phase, a clear blue shift in CO stretch frequency of adsorbed CO was observed (Figure 5.5). No such effect was observed during oxidation in gas phase (Figure 5.4) or during oxidation of CO in aqueous phase over Pt/Al_2O_3 (Chapter 4). The observed blue shifts are certainly not due to decreasing dipole-dipole coupling with decreasing coverage, since this would cause a red shift

[10,16]. On the other hand, it is well known that CO stretch frequencies shift to higher wave number on oxidised metal particles [32]. The observed blue shifts are therefore attributed to surface oxidation of the supported palladium particles, indicating that oxidation of palladium is facilitated in aqueous phase. We propose that the resulting increase in the surface coverage of oxygen is not only causing the observed blue shift, but also contributes to the increase in the oxidation rate (Figure 5.4 and Figure 5.5). Increased oxidation of noble metal catalysts in the presence of water was previously reported [56]. In short, the presence of water influences the adsorbed CO molecule as well as the oxidation of palladium, both phenomena leading to an increased CO oxidation rate.

5.4.2.2 CO oxidation in aqueous phase at pH 5.0 – 9.0

Besides lowering the CO stretch frequency, an increase in pH was also found to enhance the oxidation of adsorbed CO on palladium (Figure 5.5 and Figure 5.7). In addition, the blue shift observed during CO oxidation in aqueous phase increased with increasing pH (9 – 10 cm^{-1} at pH 5.0; 13 – 14 cm^{-1} at pH 7.1 and 16 – 17 cm^{-1} at pH 9.0), indicating an increased oxidation of the supported palladium particles with increasing pH. This leads to a higher surface coverage of oxygen, increasing the oxidation rate (Figure 5.5).

The larger blue shift observed during oxidation of pre adsorbed CO with increasing pH, indicates that palladium is oxidized faster at higher pH values, as shown in Figure 5.5. In our previous study on CO oxidation over Pt/Al_2O_3, no indications on oxidation of platinum was observed, in agreement with the slower oxidation found for CO on platinum and with the fact that pH only slightly increases the oxidation of platinum compared to palladium [57]. Beside the oxidation of palladium, the CO oxidation rate is also increased by the increased π-back donation weakening the CO bond and causing the CO molecule to be more easily oxidised with increasing pH. Consequently, the same mechanism applies for both the effect of water and the increase in pH; the negative charge and the oxidation rate of palladium particles are increased, both leading to a higher oxidation rate of adsorbed CO.

In electro oxidation of CO over both platinum and gold in acidic and alkaline solutions, it was found that the electro oxidation was fastest in alkaline solutions, where the CO stretch frequency was lowest [50,51], in agreement with this study. Moreover, an increased rate of oxidation of palladium with an increase in pH was reported [57,58]. The increased oxidation rate of adsorbed CO with increasing pH points toward an effect of the metal particle potential on the rate-determining step of

CO oxidation in aqueous phase. This is further supported by the decreasing L/B-M ratio with increasing pH.

As for Pt/Al_2O_3, both the presence of water and increased pH influence the potential of the supported palladium particles, reflected in the changed CO stretch frequency and altered L/B-M ratio. The change in potential influences the adsorbed CO molecule by weakening the CO bond. Contrary to CO adsorption / oxidation on Pt/Al_2O_3, the oxidation of palladium during CO oxidation is also influenced by both the presence of water and pH; water and increased pH increase the oxidation of palladium. The increased oxidation indicates a higher surface coverage of adsorbed oxygen on palladium, increasing the oxidation rate of adsorbed CO. Both the weakening of the CO bond and the increased oxidation of palladium result in a higher CO oxidation rate in aqueous phase and with increasing pH.

5.5 Conclusion

Both the presence of water and the pH of the aqueous solution influence the properties of CO adsorbed on Pd/Al_2O_3 considerably. A large red shift, a decreased L/B-M ratio and a threefold increased intensity are observed when CO adsorption is carried out in aqueous phase compared to in gas phase. These phenomena result from a combination of increased π-back-donation from the metal and a direct effect of water on the transition dipole moment of adsorbed CO. By increasing the pH the π-back-donation increases even further, causing a further red shift and decrease in L/B-M ratio.

The oxidation rate of pre-adsorbed CO is increased in the presence of water and by increasing pH. Both cause an increase in the potential of the supported metal particles, leading to a weakening of the CO bond and to increasing the CO oxidation rate. Furthermore, water and high pH facilitate the oxidation of the palladium particles, which contributes to a further increase of the CO oxidation rate.

5.6 References

[1] S.D. Ebbesen, B.L. Mojet, L. Lefferts, (Chapter 4 in this thesis), J.Catal 246 (2007) 66.

[2] V. Pitchon, M. Primet, H. Praliaud, Appl.Catal. 62 (1990) 317.

[3] G. Larsen, G.L. Haller, Catal.Lett. 3 (1989) 103.

[4] S. Boujana, D. Demri, J. Cressely, A. Kiennemann, J.P. Hindermann, Catal.Lett. 7 (1990) 359.

[5] B.L. Mojet, D.C. Koningsberger, Catal.Lett. 39 (1996) 191.

[6] M. Bartok, J. Sakany, A. Sitkei, J.Catal. 72 (1981) 236.

[7] F. Stoop, F.J.C.M. Toolenaar, V. Ponec, J.Catal. 73 (1982) 50.

[8] M. Primet, J.Catal. 88 (1984) 273.

[9] B.L. Mojet, J.T. Miller, D.E. Ramaker, D.C. Koningsberger, J.Catal. 186 (1999) 373.

[10] A. Bourane, O. Dulaurent, D. Bianchi, J.Catal. 196 (2000) 115.

[11] D. Ferri, T. Bürgi, A. Baiker, J.Catal. 210 (2002) 160.

[12] B.L. Mojet, J.T. Miller, D.C. Koningsberger, J.Phys.Chem.B. 103 (1999) 2724.

[13] D. Ferri, T. Bürgi, A. Baiker, J.Phys.Chem.B. 105 (2001) 3187.

[14] T. Visser, T.A. Nijhuis, A.M.J. van der Eerden, K. Jenken, Y. Ji, W. Bras, S. Nikitenko, Y. Ikeda, M. Lepage, B.M. Weckhuysen, J.Phys.Chem.B. 109 (2005) 3822.

[15] N.C. Yee, G.S. Chottiner, D.A. Scherson, J.Phys.Chem.B. 109 (2005) 7610.

[16] E.V. Benvenutti, L. Franken, C. Moro, Langmuir 15 (1999) 8140.

[17] A. Bourane, O. Dulaurent, D. Bianchi, Langmuir 17 (2001) 5496.

[18] D.C. Koningsberger, D.E. Ramaker, J.T. Miller, J. de Graaf, B.L. Mojet, Top.Catal. 15 (2001) 35.

[19] T. Engel, G. Ertl, Chem.Phys.Lett. 54 (1978) 95.

[20] T. Matsushima, J.M. White, J.Catal. 40 (1975) 334.

[21] T. Engel, G. Ertl, J.Chem.Phys. 69 (1978) 1267.

[22] H. Conrad, G. Ertl, J. Kuppers, Surf.Sci. 76 (1978) 323.

[23] M.N. Desai, J.B. Butt, J.S. Dranoff, J.Catal. 79 (1983) 95.

[24] I. Ortiz-Hernandez, C.T. Williams, Langmuir 19 (2003) 2956.

[25] R. He, R.R. Davda, J.A. Dumesic, J.Phys.Chem.B. 109 (2005) 2810.

[26] S.D. Ebbesen, B.L. Mojet, L. Lefferts, (Chapter 3 in this thesis), Langmuir 22 (2006) 1079.

[27] F.A. Lewis, The Palladium Hydrogen System, Academic Press, New York, 1967.

[28] J.L. Duplan, H. Praliaud, Appl.Cat. 67 (1990) 325.

[29] W.K. Kuhn, J. Szanyi, D.W. Goodman, Surf.Sci.Lett. 274 (1992) L611.
[30] R.S. Monteiro, L.C. Dieguez, M. Schmal, Catal.Today 65 (2001) 77.
[31] E. Ozensoy, D.C. Meier, D.W. Goodman, J.Phys.Chem.B. 106 (2002) 9367.
[32] A. Palazov, C.C. Chang, R.J. Kokes, J.Catal. 36 (1975) 338.
[33] G. Rupprechter, H. Unterhalt, M. Morkel, P. Galletto, L. Hu, H.J. Freund, Surf.Sci. 502-503 (2002) 109.
[34] M. Skotak, Z. Karpinski, W. Juszczyk, J. Pielaszek, L. Kepinski, D.V. Kazachkin, V.I. Kovalchuk, J.L. d'Itri, J.Catal. 227 (2004) 11.
[35] R. Barth, R. Pitchai, R.L. Anderson, X. Verykios, J.Catal. 116 (1989) 61.
[36] A. Bourane, D. Bianchi, J.Catal. 220 (2003) 3.
[37] P. Hollins, Surf.Sci.Reports 16 (1992) 53.
[38] K.I. Choi, M.A. Vannice, J.Catal. 131 (1991) 1.
[39] C. Keresszegi, D. Ferri, T. Mallat, A. Baiker, J.Catal. 234 (2005) 64.
[40] K. Yoshioka, F. Kitamura, M. Takeda, M. Takahashi, M. Ito, Surf.Sci. 227 (1990) 90.
[41] S. Zou, R. Gomez, Weaver M.J., J.Electroanal.Chem. 474 (1999) 155.
[42] Y.G. Yan, Q.X. Li, S.J. Huo, M. Ma, W.B. Cai, M. Osawa, J.Phys.Chem.B. 109 (2005) 7900.
[43] J.E. Benson, H.S. Hwang, M. Boudart, J.Catal. 30 (1973) 146.
[44] M.J. Kappers, M. Vaarkamp, J.T. Miller, F.S. Modica, M.K. Barr, J.H. Vandermaas, D.C. Koningsberger, Catal.Lett. 21 (1993) 235.
[45] D.E. Ramaker, J. de Graaf, J.A.R. van Veen, D.C. Koningsberger, J.Catal. 203 (2001) 7.
[46] N. Kizhakevariam, X. Jiang, M.J. Weaver, J.Chem.Phys. 100 (1994) 6750.
[47] S.-C. Chang, M.J. Weaver, J.Chem.Phys. 92 (1990) 4582.
[48] S.A. Wasileski, M.T.M. Koper, M.J. Weaver, J.Phys.Chem.B. 105 (2001) 3518.
[49] J. Xu, J.T. Yates, Surf.Sci. 327 (1995) 193.
[50] A. Couto, A. Rincón, M.C. Pérez, C. Gutiérrez, Electrochim.Acta 46 (2001) 1285.
[51] K. Kunimatsu, A. Aramata, H. Nakajima, H. Kita, J.Electroanal.Chem. 207 (1986) 293.
[52] G. Blyholder, J.Phys.Chem. 68 (1964) 2772.
[53] S. Gilman, J.Phys.Chem. 68 (1964) 70.
[54] H.L. Lam-Wing, A. Wieckowski, M.J. Weaver, J.Phys.Chem. 92 (1988) 6985.
[55] N.P. Lebedeva, A. Rodes, J.M. Feliu, M.T.M. Koper, R.A. van Santen, J.Phys.Chem.B. 106 (2002) 9863.

[56] J.A.A. van den Tillaart, Platinum Catalysis with Oxygen in Water - Catalyst characterization and kinetics of partial ethanol oxidation, Doctoral Thesis, Technische Universiteit , Eindhoven, 1994.

[57] L.D. Burke, M.M. McCarthy, M.B.C. Roche, J.Electroanal.Chem. 167 (1984) 291.

[58] L.D. Burke, M.B.C. Roche, J.Electroanal.Chem. 186 (1985) 139.

CHAPTER 6

Adsorption of NO_2^-, NH_4^+ and NH_2OH on Pd/Al_2O_3, Pt/Al_2O_3 and Al_2O_3

Abstract

In relation to the heterogeneous hydrogenation of nitrite, adsorption of NO_2^-, NH_4^+ and NH_2OH from aqueous phase was examined on Pd/Al_2O_3, Pt/Al_2O_3 and Al_2O_3. None of the investigated inorganic nitrogen compounds adsorb on alumina. $NO_{2\,(aq)}^-$ and $NH_{4\,(aq)}^+$ on the other hand show similar adsorption characteristics on both Pd/Al_2O_3 and Pt/Al_2O_3. The vibrational spectrum of the NO_2^- ion changed substantially upon adsorption, clearly indicating that NO_2^- chemisorbs onto the supported metal catalysts. Contrary, adsorption of NH_4^+ does not cause significant change in the vibrational spectrum of the ion, indicating that electrostatic interaction dominates the adsorption of ammonia ions instead of chemisorption. When comparing interaction of $NH_2OH_{(aq)}$ on Pd/Al_2O_3 and Pt/Al_2O_3 significant differences were observed. On Pd/Al_2O_3, NH_2OH is converted into a stable $NH_{2(ads)}$ fragment, whereas on Pt/Al_2O_3, NH_2OH is converted into NO, possible via $HNO_{(ads)}$ as an intermediate.

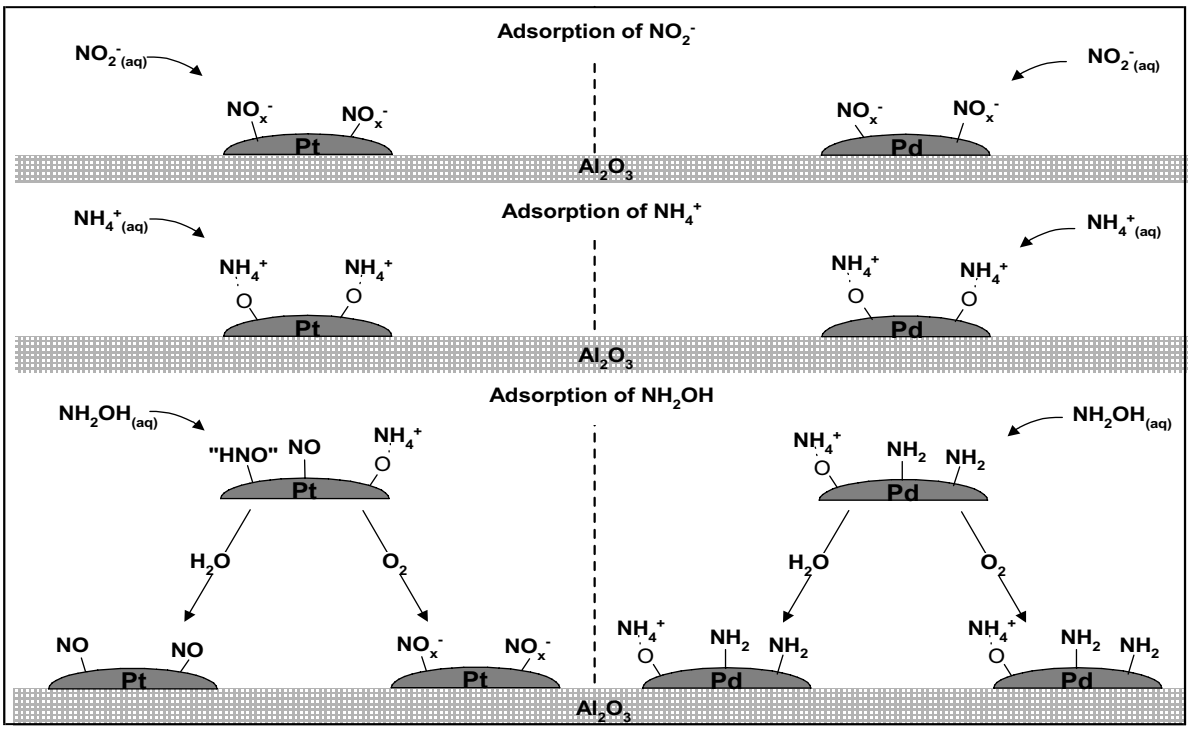

6.1 Introduction

Waste- and ground-water treatments are retrieving more and more attention because of increasing pollution of ground-water [1]. Water purification in general includes oxidative treatments next to hydrogenation processes [2]. Denitrification, like nitrite and nitrate hydrogenation, is becoming more important due to the high nitrite and nitrate levels found in ground-water in Europe, which in some cases exceeds legal limits, and local wells had to be closed [1,3].

Nitrate and nitrite are potential human health hazards, especially to infants, causing a condition known as methemoglobinemia, also called blue baby syndrome [4]. Methemoglobinemia prevents blood cells from absorbing oxygen, leading to suffocation and possible death. Consumption of high levels of nitrate and nitrite are also under the suspicion to cause other health problems, for example gastric cancer [4].

Denitrification is one of the mostly investigated hydrogenation reactions in ground-water treatment. Hydrogenation of nitrate and nitrite over noble metal catalysts was for the first time reported in 1989 [5]. Nitrate was reported to first hydrogenate to nitrite, which in turn converted into nitrogen and ammonia.

Nitrite hydrogenation can be performed over single noble metal catalysts such as platinum and palladium catalysts, of which palladium shows higher selectivity to nitrogen. On the other hand, single noble metal catalysts hardly show any activity towards nitrate [6,7]. To obtain high activity the noble metal catalysts have to be promoted by a transition-group metal [8]. In this way also high selectivity towards nitrogen is achieved, which is important because ammonia is toxic as well. It was reported that palladium promoted with copper is the most active and selective bimetallic catalyst for nitrate reduction to nitrogen [5,9-15] .

Based on kinetic studies, adsorbed NO wad suggested as an intermediate [9], and several authors have proposed a reaction scheme including adsorbed NO as the key intermediate for the catalytic hydrogenation of nitrate and nitrite [16-19] over supported bimetallic catalysts. Dissociation of hydrogen is assumed to be the first step, followed by reaction with nitrate to form nitrite as the rate limiting step. Subsequently, adsorbed nitrite reduces to adsorbed NO, which undergoes further reduction to nitrogen and hydrogenation to ammonia. In addition, some of the nitrite desorbs from the surface and was detected in the solution. Experimental evidence for the presence of the proposed intermediates and products in the solution is limited so

far to NO_2^-, N_2 and NH_4^+ [9,10,14,17,18]. Moreover, the proposed adsorbed species were never directly observed.

In electrochemical research, electro-catalytic reaction of inorganic nitrogen compounds on transition metals is a classical topic. The electrochemical reduction of nitrate was shown to be more complex than the catalytic hydrogenation. The electrochemical reduction has been mainly investigated on platinum electrodes, which points to the presence of a variety of intermediates such as NO_2, HNO_2, NO, N_2O, N_2, H_2NO, HNO, NH_2OH and NH_3, depending on reaction conditions [20-34]. However, only limited infrared data is available on surface intermediates in these systems during electrochemical reaction. The formation of specific products depends on applied potential, electrolyte, acidity, and nitrate concentration. In addition, it was shown that the presence of adsorbed hydrogen inhibits nitrate reduction by blocking the adsorption sites for NO_3^- ions. The rate-determining step is the reduction of nitrate to nitrite, which in turn yields adsorbed NO [25-34]. Several papers report on the experimental evidence of adsorbed NO as an intermediate during electro reduction of nitrate and nitrite [20,22-26]. The subsequent electro-reduction of adsorbed NO mainly yielded ammonia, while also traces of N_2O were detected. In addition, N_2O was demonstrated to be an intermediate for the production of nitrogen [28,35].

Unfortunately, the insights obtained from electrochemical studies with FT-IR spectroscopy cannot be compared directly to catalytic studies because of two reasons. First, FTIR spectra can only be obtained operating with very thin liquid layers, inducing mass transfer problems during experiments. Second, these studies are confined to dense conducting electrodes, often single crystals, which are definitely different from practical catalysts containing nano-particles on porous (non-conducting) support materials. Moreover, because it is difficult to study heterogeneous catalysts *in-situ* if the reaction is carried out in water, detailed mechanistic studies of the heterogeneous catalytic hydrogenation of both nitrate and nitrite over supported noble metal catalysts is lacking.

Recently, we have demonstrated the benefit of Attenuated Total Reflection Infrared Spectroscopy (ATR-IR) to study *in-situ* the development of adsorbates on supported noble metal catalysts when performing liquid phase reactions in water [36]. ATR-IR is ideally suited for studying molecular vibrations at the solid-liquid interface because the evanescent wave is restricted to the region near the interface, thereby minimising the contribution from the liquid [37]. ATR-IR spectroscopic studies at the metal-liquid-interface have only recently started to receive attention [38-43]. For example, the

adsorption and oxidation of CO, and dissociation of small molecules such as formaldehyde over Pt/Al_2O_3 catalysts was reported [42]. In addition, ATR-spectroscopic studies of the water-gas shift reaction and methanol reforming over Pt/Al_2O_3 was combined with kinetic studies [40]. In addition, we showed for CO oxidation in water over Pt/Al_2O_3 that the properties of the adsorbed intermediate species are significantly altered by the presence of liquid water compared to gas phase or electro-chemical CO oxidation [36].

Presently, we work in our laboratory on resolving the reaction mechanisms of nitrite and nitrate reduction over supported metal catalysts by identifying adsorbed reaction intermediates on the catalyst surface using ATR-IR spectroscopy. It is the objective of this chapter to investigate the spectral properties of adsorbed $N_xO_yH_z$ species on Pt/Al_2O_3 and Pd/Al_2O_3 produced by adsorption of model compounds. In the following chapters (Chapter 7 and 8), the hydrogenation of nitrite will be reported.

6.2 Experimental

The experimental procedure, materials and catalyst preparation are described in details in the experimental section (Chapter 2). All spectra presented in the following section are corrected for the water background as published by our group. The integrated peak areas are calculated using curve fitting of the spectra following the procedure described in the experimental section (Chapter 2).

The characteristics of the 5 wt% Pd/Al_2O_3 (dispersion 45%), and 5 wt% Pt/Al_2O_3 (dispersion 75%) catalyst examined in the present study are described in details in the experimental section (Chapter 2). In both cases 6 mg of catalyst was deposited on the IRE, resulting in 1.3 10^{-6} mol accessible surface palladium atoms, whereas the accessible surface platinum atoms are 1.2 10^{-6} mol surface platinum deposited on the IRE. The thickness of the catalyst layer was measured to be 5.0 ± 0.5 μm for the Pd/Al_2O_3 catalyst layer, whereas the thickness of the Pt/Al_2O_3 layer was 3.50 ± 0.25 μm.

After assembling the ATR-IR cell, with a coated IRE, the catalyst was flushed with Ar/H_2O. Subsequently the Al_2O_3, Pt/Al_2O_3 or Pd/Al_2O_3 catalyst was exposed to nitrite, ammonia or hydroxylamine.

6.3 Results

6.3.1 $NO_2^-{}_{(aq)}$ adsorption

Figure 6.1A shows the ATR-IR spectra obtained after 15 minutes flowing with a solution of $NO_2^-{}_{(aq)}$ on either a clean ZnSe IRE, and layers of Al_2O_3, Pd/Al_2O_3 or Pt/Al_2O_3. For both ZnSe and Al_2O_3, one distinct peak is observed at 1235 cm^{-1}, while on Pt/Al_2O_3 and Pd/Al_2O_3 additional peaks are found at 1390 and 1305 cm^{-1} (Pt/Al_2O_3) and 1405 and 1325 cm^{-1} (Pd/Al_2O_3). In addition, small shoulders at 1460 cm^{-1} (Pt/Al_2O_3) and 1475 cm^{-1} (Pd/Al_2O_3) can be observed on the noble metal catalysts.

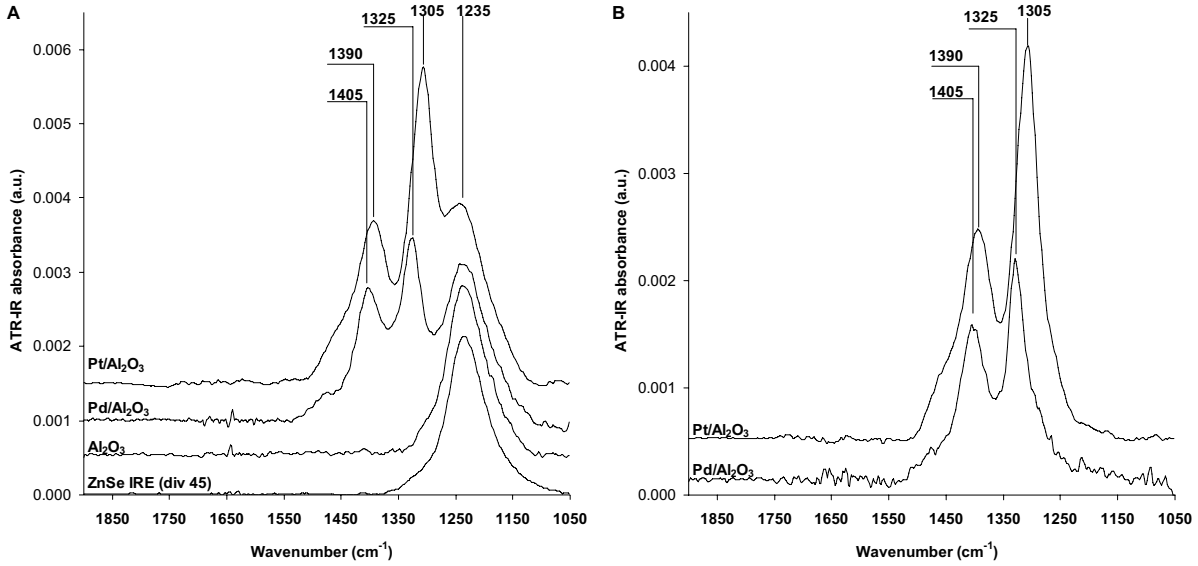

Figure 6.1. A: Water corrected ATR-IR spectrum from 1900 to 1050 cm^{-1} while a solution of $NO_2^-{}_{(aq)}$ at pH 7 was flown over a clean ZnSe IRE, (2.5 10^{-2} mol/L $NO_2^-{}_{(aq)}$ intensity scaled) or a solution of 4.3 10^{-4} mol/L $NO_2^-{}_{(aq)}$ at pH 7 was flown over Pt/Al_2O_3, Pd/Al_2O_3 and Al_2O_3 and B: after subsequent flow of Ar/Q2-water over Pd/Al_2O_3 and Pt/Al_2O_3.

Subsequent flow with Ar/H_2O removed the species giving rise to the peak at 1235 cm^{-1} for all samples within 90 sec (which is the time resolution of the spectrometer). The resulting spectra for Pt/Al_2O_3 and Pd/Al_2O_3 are shown in Figure 6.1B. For Pd/Al_2O_3 the integrated intensity of the peaks at 1405 and 1325 cm^{-1} remained constant during flushing. However, on Pt/Al_2O_3 a decrease in intensity for the peaks at 1390 and 1305 cm^{-1} was observed.

Figure 6.2 shows the evolution of the peaks observed on Pt/Al_2O_3 when flowing $NO_2^-{}_{(aq)}$ (0 – 16.5 min.) and subsequent Ar/H_2O (16.5 – 30 min.). During nitrite adsorption a stabilisation period of about 10 minutes is observed. This is due to a

chromatographic effect, because of the low flow rate (1 mL.min^{-1}) and the low concentration of nitrite in the solution. As an illustration, at least 3 minutes are needed to introduce sufficient NO_2^- to the catalysts to obtain a NO_2^-/Pt ratio of 1. However, longer flow times will be required if nitrite adsorbs also on the support. The delay is clearly not due to slow diffusion into the catalyst layer, since the peak at 1235 cm^{-1} disappears instantaneously (that means within 90 seconds which is the time resolution of the experiment) when flowing Ar/H_2O.

In addition, for Pt/Al_2O_3 a very slow decrease in integrated intensity of the peak at 1390 cm^{-1} was detected, while the intensity of the 1305 cm^{-1} peak decreased much more rapidly with about 30% in 14 minutes.

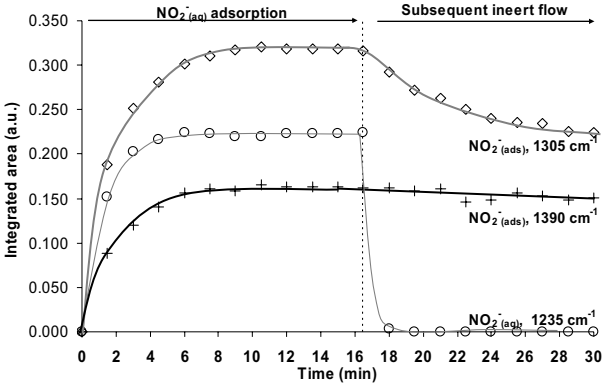

Figure 6.2. Integrated peak areas during adsorption of $NO_2^-_{(aq)}$ and during subsequent inert flow over Pt/Al_2O_3.

6.3.2 $NH_4^+_{(aq)}$ adsorption

Figure 6.3 shows the ATR-IR spectra obtained after flowing a solution of $NH_4^+_{(aq)}$ during 15 minutes on either a clean ZnSe IRE, and layers of Al_2O_3, Pd/Al_2O_3 or Pt/Al_2O_3. In all spectra, one evident peak with similar peak width (60 – 70 cm^{-1}) was found at 1455 cm^{-1} (ZnSe, Al_2O_3 and Pt/Al_2O_3) or 1450 cm^{-1} (Pd/Al_2O_3). During subsequent Ar/H_2O flow, the peak instantaneously disappeared from the ZnSe and Al_2O_3 spectra. The peaks appeared much more stable on Pt/Al_2O_3 and Pd/Al_2O_3 ; the integrated intensity decreased with only 5% and 15% respectively in 90 seconds, whereas peak positions did not change at all. Interestingly, a subsequent flow of H_2/H_2O completely removed the peaks at 1450 cm^{-1} on Pd/Al_2O_3 and 1455 cm^{-1} on Pt/Al_2O_3 within 90 seconds.

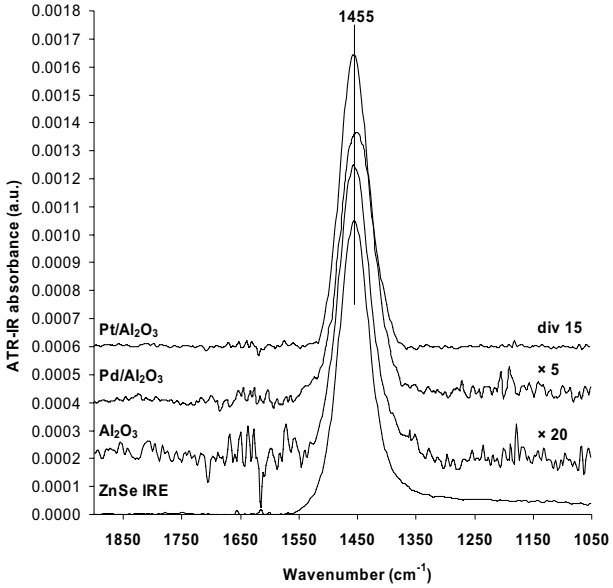

Figure 6.3. Water corrected ATR-IR spectra while a solution of 4.3 10^{-4} mol/L NH_4^+ was flown over Pt/Al_2O_3, Pd/Al_2O_3 and Al_2O_3 and while a solution of 2.5 10^{-2} mol/L NH_4^+ was flown over a clean ZnSe IRE

6.3.3 $NH_2OH_{(aq)}$ adsorption

$NH_2OH_{(aq)}$ (hydroxylamine) can disproportionate to ammonia, nitrous oxide and nitrogen [44,45]. As a typical example, Figure 6.4 shows the spectrum of Pt/Al_2O_3 after flowing a hydroxylamine solution at pH 7. Mainly one single peak is observed at 1455 cm^{-1}, similar to the peak observed after adsorption of ammonia (Figure 6.4), together with a small shoulder at 1550 cm^{-1}. In addition, a clear peak at 2231 cm^{-1} was found, which can be attributed to N_2O, since bulk N_2O is recognised be the N-N stretching vibration at 2224 cm^{-1} [46], and peaks around 2230 cm^{-1} are generally assigned to N_2O [26,35,47,48].

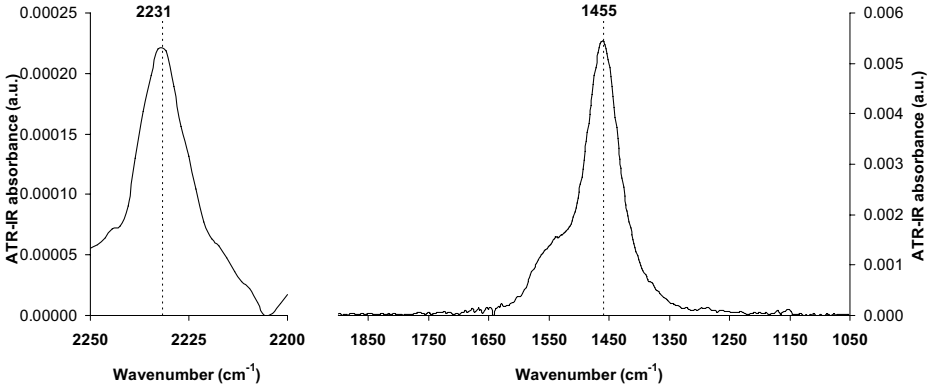

Figure 6.4. Water corrected ATR-IR spectra while a solution of 4.3 10^{-4} mol/L NH_2OH was flown over Pt/Al_2O_3 at pH 7.

The rate of the disproportionation reaction is known to decrease with decreasing pH. As the ZnSe crystal will start to corrode at pH 4, additional experiments were performed at pH 5, attempting to suppress the disproportionation of hydroxylamine.

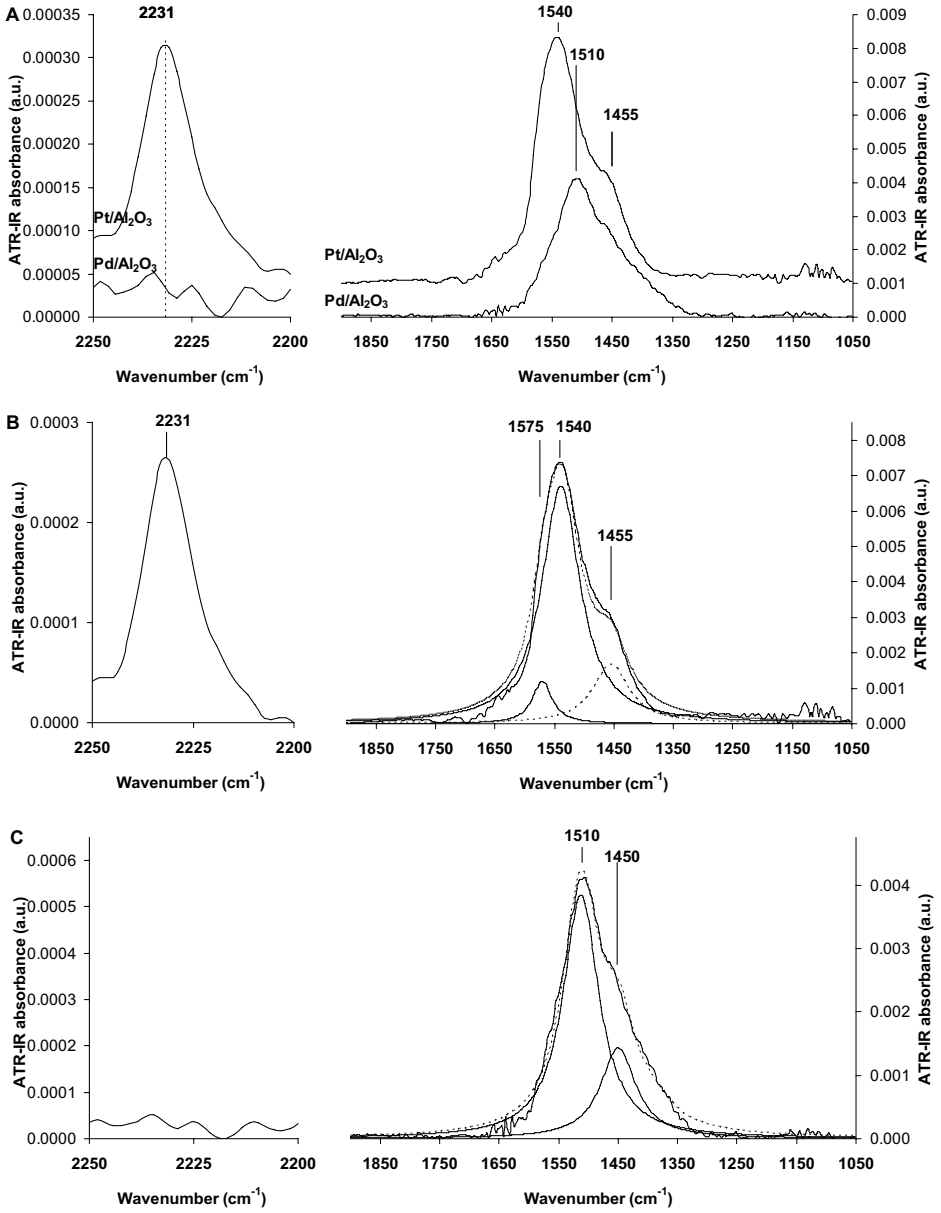

Figure 6.5. Water corrected ATR-IR spectra during adsorption of $NH_2OH_{(aq)}$ at pH 5 on a: Pt/Al_2O_3 and Pd/Al_2O_3 and the fitted peaks after adsorption on b: Pt/Al_2O_3 and c: Pd/Al_2O_3.

Figure 6.5 shows ATR-IR spectra after flowing $NH_2OH_{(aq)}$ at pH 5 over Pd/Al_2O_3 and Pt/Al_2O_3. Clearly, both catalysts show signals of adsorbed species but at different frequencies. No adsorption bands were observed during adsorption of $NH_2OH_{(aq)}$ on both Al_2O_3 as well as clean ZnSe. On Pd/Al_2O_3 a broad asymmetric peak was observed at 1510 cm^{-1}, which could be fitted into two peaks, positioned at 1510 cm^{-1}

and 1450 cm^{-1} (Figure 6.5C). The peak intensities and positions remained constant during both subsequent Ar/H_2O flow and subsequent O_2/H_2O flow.

For Pt/Al_2O_3, a broad peak at 1540 cm^{-1} with a shoulder on each side was detected. This overall signal was composed out of three specific peaks at respectively 1575 cm^{-1}, 1540 cm^{-1} and 1455 cm^{-1} (Figure 6.5B). Moreover, for Pt/Al_2O_3 also a peak at 2231 cm^{-1} was found, which was absent for Pd/Al_2O_3. Contrary to the stable signals on Pd/Al_2O_3, for Pt/Al_2O_3 the spectra significantly changed during Ar/H_2O flow after hydroxylamine adsorption as shown in Figure 6.6. The peak at 2231 cm^{-1} disappeared quickly within 90 sec. during Ar/H_2O flow, while the peak at 1540 cm^{-1} seemed to shift to 1580 cm^{-1}. Peak fitting of the signal, however, again revealed the presence of two peaks at 1540 and 1575 cm^{-1}, the latter shifting to 1580 cm^{-1} with increasing time. The evolution of the intensities of these two peaks with time is shown in Figure 6.6B.

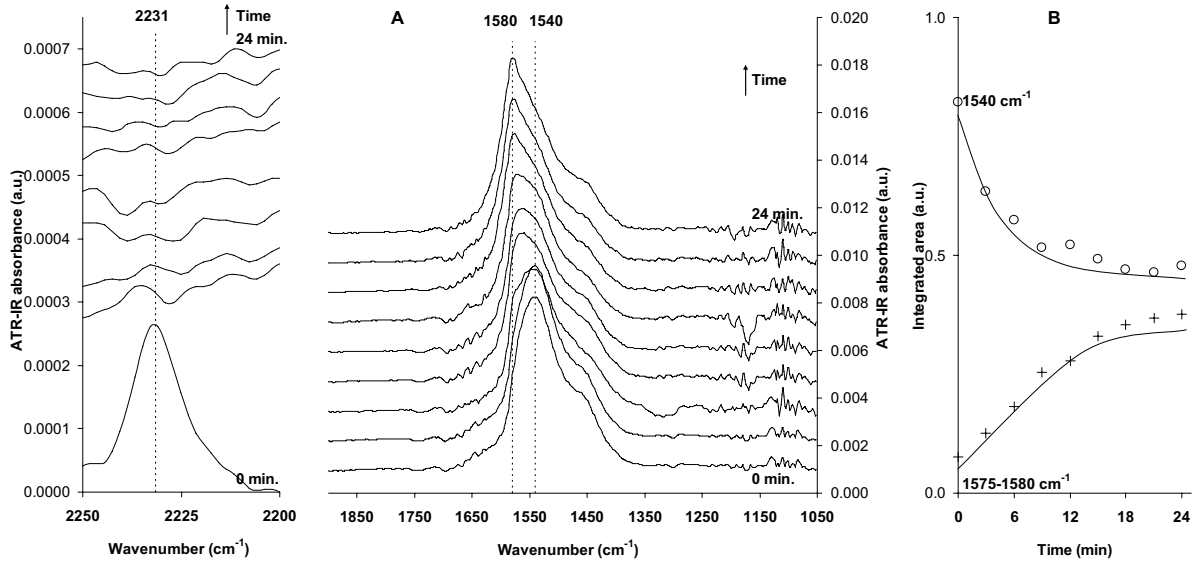

Figure 6.6. A: Water corrected ATR-IR spectra during flow of Ar/H_2O after adsorbing $NH_2OH_{(aq)}$ on Pt/Al_2O_3 and B: Corresponding integrated peak areas.

Figure 6.6B clearly shows that the decrease in intensity of the peak at 1540 cm^{-1} is accompanied by a simultaneously increase of the peak at 1575 - 1580 cm^{-1}. Both signals stabilise after approximately 20 minutes of Ar/H_2O flow.

To examine the stability of the species at 1540 cm^{-1} towards oxygen, NH_2OH was adsorbed on Pt/Al_2O_3 and subsequently O_2/H_2O was introduced to the cell while ATR-IR spectra were recorded (Figure 6.7). Similar to the experiment with Ar/H_2O flow, the peak at 2231 cm^{-1} disappeared instantaneously. However, the signal at 1540 cm^{-1} diminished in about 15 minutes and a new peak at 1305 cm^{-1} appeared

concurrently. A similar peak at 1305 cm^{-1} was also observed during NO_2^- adsorption on Pt/Al_2O_3, although with much higher intensity (see Figure 6.1).

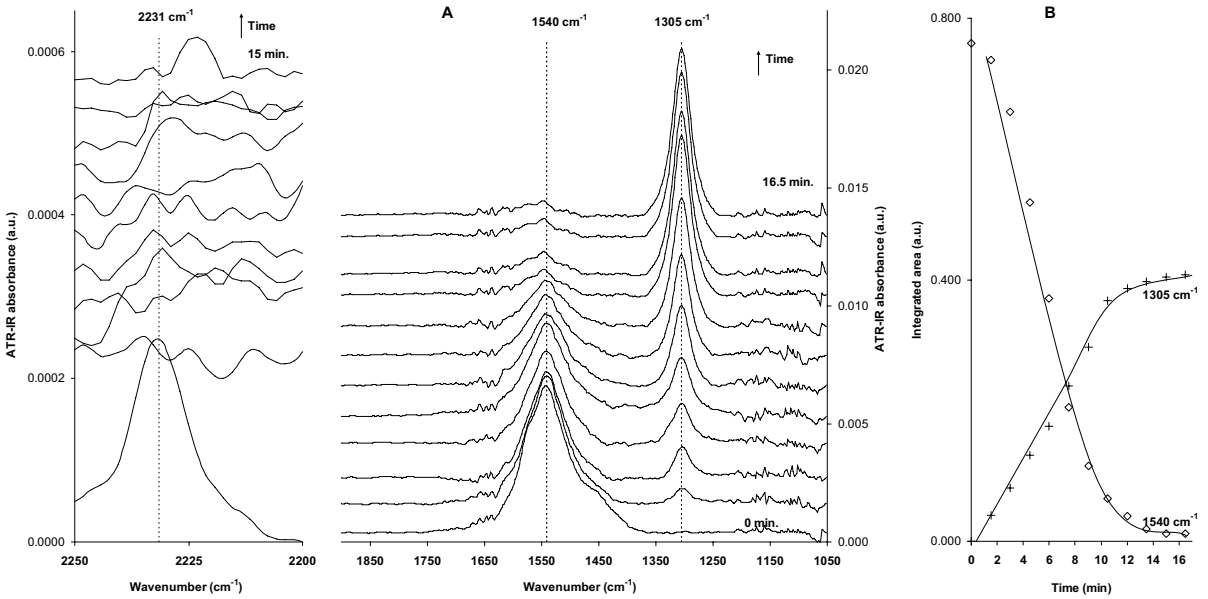

Figure 6.7. A: Water corrected ATR-IR spectra during flow of O_2/H_2O after adsorbing $NH_2OH_{(aq)}$ on Pt/Al_2O_3 and B: Corresponding integrated peak areas.

6.4 Discussion

The final goal of our work is to study the surface intermediates during the heterogeneous catalytic hydrogenation of nitrite over supported noble metal catalysts [49,50]. As a first step, this study reports on the spectral properties of adsorbed $N_xO_yH_z$ species on Pt/Al_2O_3 and Pd/Al_2O_3 produced by adsorption of model compounds. In the following the catalyst characterisation and the assignments of the peaks will be discussed.

6.4.1 $NO_2^-{}_{(aq)}$ adsorption

In literature, several peak positions for the ν_{as} of the free nitrite ion have been reported, varying between 1235 and 1286 cm^{-1}[51,52]. When flowing a solution of $NO_2^-{}_{(aq)}$ over a clean ZnSe IRE or an Al_2O_3 layer, in both cases a single peak at 1235 cm^{-1} with identical peak width was observed, which rapidly disappeared during inert Ar/H_2O flow (Figure 6.1). Consequently, the peak at 1235 cm^{-1} is assigned to free, dissolved NO_2^-. In addition, it can be concluded that NO_2^- does not adsorb strongly on Al_2O_3 under the applied experimental conditions.

Nitrite adsorption on Pd/Al_2O_3 or Pt/Al_2O_3 also showed the presence of free NO_2^- as indicated by the peak at 1235 cm^{-1}, which quickly disappeared during Ar/H_2O flow (Figure 6.1). In addition, peaks at higher wave number were found at 1405 and 1325 cm^{-1} (Pd/Al_2O_3) and 1390 and 1305 cm^{-1} (Pt/Al_2O_3), together with a small shoulder at 1460 cm^{-1} (Pt/Al_2O_3) and 1475 cm^{-1} (Pd/Al_2O_3) (Figure 6.1). Clearly, these peaks must be associated with species adsorbed on the metal particles, because the bands are not observed on either ZnSe or Al_2O_3. In addition, the peak shift of about 20 cm^{-1} to higher wave number observed for Pd/Al_2O_3 compared to Pt/Al_2O_3 strongly suggests that the adsorbed species are similar in nature for Pd/Al_2O_3 and Pt/Al_2O_3. In general, for a given adsorbed species, observed frequencies on palladium are at higher wave number than on platinum. For example, CO on palladium absorbs approximately 20 cm^{-1} higher than CO on platinum [53-58]. Similarly, NO on Pt(111) in water is characterised by a peak at 1660 – 1680 cm^{-1} [20,24], whereas linear adsorbed NO on Pd(111) is located at 1720 – 1748 cm^{-1} [59].

Figure 6.2 shows that during inert flow the ratio of integrated intensities of the two peaks on Pt/Al_2O_3 changed. On the other hand, on Pd/Al_2O_3, the intensity remained constant (not shown) indicating a stronger adsorption of nitrite on palladium compared to on platinum. Furthermore, the integrated intensity ratio of the two peaks on each sample varied with pH (not shown). Therefore, the two peaks must be assigned to two different adsorbed species.

It is well-known that nitrite can adsorb in different geometries, which can be divided into two main categories: nitro (coordinated via the nitrogen atom) and nitrito (coordinated by one or two of the oxygen atoms). All of these species have N-O stretch frequencies reported between 1500 and 1200 cm^{-1}; there is significant disagreements in literature concerning the exact assignment [51]. Moreover, infrared frequencies for nitrate species have been reported in the same range. Since the experiments were performed on catalyst surfaces that were passivated during transport through the air, the formation of nitrates cannot be excluded at this point. Furthermore, the high dispersion of the metal particles indicates that many different crystal planes, steps and kinks will be present, which provide a variety of metal adsorption sites. From single crystal studies it is well-known that each type of adsorption site gives rise to unique metal-adsorbate vibrational properties.

In conclusion, the peaks at 1405 and 1325 cm^{-1} (Pd/Al_2O_3) and 1390 and 1305 cm^{-1} (Pt/Al_2O_3), and the accompanying shoulders at 1460 cm^{-1} (Pt/Al_2O_3) and 1475 cm^{-1} (Pd/Al_2O_3) are assigned to NO_x^- (x = 2,3) species adsorbed on respectively palladium and platinum, without further precision.

6.4.2 $NH_4^+{}_{(aq)}$ adsorption

A peak at 1455 cm^{-1}, with a peak width of peak width 61 cm^{-1}, was observed when flowing a solution of $NH_4^+{}_{(aq)}$ over a clean ZnSe IRE or an Al_2O_3 layer, which rapidly disappeared during inert Ar/H_2O flow (Figure 6.3) The band at 1455 cm^{-1} can be assigned to the symmetric bending mode of NH_4^+ [60-62]. Its frequency is approximately 30 to 60 cm^{-1} lower than in typical ammonium salts, suggesting that NH_4^+ forms strong hydrogen bonds with the surrounding water molecules [62]. Clearly, NH_4^+ does not adsorb strongly on either ZnSe or Al_2O_3 under the applied experimental conditions, since the band rapidly disappears when flushing with Ar/H_2O.

Adsorption of $NH_4^+{}_{(aq)}$ on Pd/Al_2O_3 or Pt/Al_2O_3 showed similar bands, at respectively 1450 and 1455 cm^{-1}, which decreased with respectively 5% and 15% in intensity within 90 seconds during flushing with Ar/H_2O. The small red shift for Pd/Al_2O_3 compared to Pt/Al_2O_3 and the relative high stability of the signals during inert flow indicates that NH_4^+ is interacting with the metal particles. The similarity in peak position, width and shape between NH_4^+ detected on respectively Al_2O_3 and the catalysts, however, suggests that NH_4^+ is not chemisorbed, but is interacting electrostatically as hydrated ions with the noble metal catalysts. Chemisorption would induce a significant change in the vibrational spectrum of the ion, since then H^+ would need to dissociate, resulting in an adsorbed NH_3 fragment. $NH_{3(ads)}$ would show an umbrella mode between 1300 and 1250 cm^{-1}, which was not observed in our experiments [62]. Moreover, introduction of hydrogen (H_2/H_2O) resulted in instantaneous disappearance of the ammonium signal, most likely caused by the complete reduction of metal particles. As indicated earlier, the catalysts are passivated in air, before mounted in the ATR cell. As a result, the surface of the metal particles is oxidised. This surface oxidation introduces charge separation, and the oxygen-atoms on the surface are slightly negatively charged. Obviously, NH_4^+ can be stabilised on this oxide layer electro-statically. As soon as hydrogen is introduced, the oxygen is removed and the metal particles are covered by chemisorbed hydrogen, leaving no adsorption sites for electrostatic interaction with ammonium ions. This explanation is supported by electrochemical experiments that show that NH_4^+ cannot adsorb on a clean metal surface, but only adsorbs when negatively charged ions are stabilised on the electrode surface [62].

6.4.3 $NH_2OH_{(aq)}$ adsorption

Remarkably, a hydroxylamine solution flown over either ZnSe or Al_2O_3 did not result in any observable infrared bands. In literature, only infrared spectra of solid hydroxylamine have been reported so far [63].The fact that no signals are observed from the solution might be due to a low extinction coefficient of dissolved hydroxylamine in water. Also, it demonstrates that no disproportionation whatsoever takes place in the absence of palladium and platinum.

When a hydroxylamine solution at pH 7 is flown over Pt/Al_2O_3, mainly adsorbed NH_4^+ (1455 cm^{-1}) is observed (Figure 6.4), but also nitrous oxide (2231 cm^{-1}) was observed together with an increased infrared intensity at 1570 cm^{-1} and 1540 cm^{-1}, which will be discussed below. It has been reported that hydroxylamine undergoes a disproportionation reaction which is accelerated by the presence of metals like platinum or palladium. In acidic and neutral media the disproportionation results in ammonia and nitrous oxide according to the overall reaction [45]:

$$4NH_3^+OH \rightarrow NH_4^+ + N_2O + 2\,H^+ + 3\,H_2O \qquad (6.1)$$

When the spectra of Pt/Al_2O_3 and Pd/Al_2O_3 during flow of hydroxylamine at pH 5 are compared (Figure 6.5), clear differences can be seen. On Pd/Al_2O_3 a broad asymmetric peak was observed, which could be fitted with two bands at respectively 1510 and 1450 cm^{-1} (Figure 6.5C). The band at 1450 cm^{-1} corresponds to the vibration of NH_4^+ (*vide ante*), indicating that at pH 5 still some disproportionation occurred on Pd/Al_2O_3, although no N_2O was detected. The observed peak at 1510 cm^{-1} is close to what has been reported for the NH_2 scissors mode in solid NH_2OH at 1515 cm^{-1} [63]. Moreover, the NH_2 scissor mode in inorganic complexes such as such as $Me(NH_2)_xCl_y$ is normally found between 1560 and 1500 cm^{-1} [52]. Further, the band is about 200 cm^{-1} too low to be assigned to NO species on palladium [59]. For solid hydroxylamine, also a band at 1191 cm^{-1} was reported, suggested to arise from the N-OH bending vibration in NH_2OH [63]. Further, the N-O stretch frequency in NH_3^+OH in vacuum was calculated to be at 1196 cm^{-1} [48]. In both cases a band around 1190 cm^{-1} is associated with oxygen in hydroxylamine. Clearly, in our data this band is completely absent (Figure 6.5A and C), from which we conclude that the species giving rise to the peak at 1510 cm^{-1} on Pd/Al_2O_3 does not contain oxygen. As a result, we assign the band at 1510 cm^{-1} to the scissor mode of $NH_{2(ads)}$ on palladium. Since this peak is completely stable during Ar/H_2O and O_2/H_2O flow, it can be concluded that it is strongly adsorbed on the palladium particle and cannot be

easily oxidised. In Chapter 7, it will be shown that this species is sensitive to hydrogen, and can be converted into ammonia [49].

During adsorption of $NH_2OH_{(aq)}$ at pH 5 on Pt/Al_2O_3, a peak was observed at 2231 cm^{-1} (Figure 6.5A and B). This band indicates the presence of N_2O, which is dissolved in the water in the pores and voids in the catalysts layer, since it immediately disappears when Ar/H_2O is introduced (Figure 6.6A and B). Nevertheless, weak adsorption on the catalyst cannot be ruled out. Therefore, N_2O is continuously being removed from the catalyst layer and must be continuously formed on Pt/Al_2O_3 during the presence of $NH_2OH_{(aq)}$. The fact that no N_2O could be detected on palladium indicates that the rate of formation of N_2O on palladium is much lower or even absent, which is in agreement with the fact that platinum is an order of magnitude more active then palladium for the disproportionation of hydroxylamine, as reported in literature [45].

For Pt/Al_2O_3, also a broad peak was observed centered at 1540 cm^{-1} with a shoulder on each side. Peak fitting indicated the presence of three bands: a shoulder at 1575 cm^{-1}, a main peak at 1540 cm^{-1} and a shoulder at 1455 cm^{-1} (Figure 6B). The latter peak can be assigned to NH_4^+ (*vide ante*). During subsequent Ar/H_2O flow, the band at 1540 cm^{-1} decreased in intensity, and the peak at 1575 cm^{-1} gained intensity and shifted gradually to 1580 cm^{-1} after 24 minutes of inert flow (Figure 6.6), while the band at 1455 cm^{-1} remained its position and intensity. From Figure 6.5 and Figure 6.6, it can be concluded that the peaks at 1540 and 1575 - 1580 cm^{-1} represent two different adsorbed species. The observed blue shift for the band at 1575 cm^{-1} with increasing intensity is characteristic for molecules with a dipole such as NO. With increasing coverage, dipole-dipole coupling would occur which causes a blue shift of the band [64,65]. The peak at 1575 cm^{-1} indicates thus the production of $NO_{(ads)}$ from the species giving rise to the band at 1540 cm^{-1}, since during Ar/H_2O flow no hydroxylamine was present (Figure 6.6). Obviously, we cannot rule out that other routes to form $NO_{(ads)}$ are open when hydroxylamine is present. This observation is in agreement with literature, reporting the reduction of platinum-ions by hydroxylamine as well as the dehydrogenation of hydroxylamine over metallic platinum, both resulting in the formation of $NO_{(ads)}$ [48], The remarkable stability of the band at 1455 cm^{-1} in Figure 6.6 indicates that the electrostatic interaction of hydrated NH_4^+ is rather strong; possibly the platinum surface is partly covered with O, inducing sufficient charge on the surface to bind ammonia ions.

NO adsorbed on platinum was reported at infrared frequencies ranging from 1430 to 1800 cm^{-1} depending on coverage, surface orientation, and experimental conditions

[20,22-27]. Characterisation of the water-metal interface during adsorption of NO has so far only been reported in electrochemical studies, where beside coverage and surface orientation also applied potential is influencing the infrared frequency [24]. Table 6.1 summarises the NO stretch frequencies reported on a variety of platinum surfaces in electrochemistry. Most importantly, on Pt(111) and Pt(110) bands below 1600 cm^{-1} (bridging NO) were only observed at low NO-coverage, and always combined with bands above 1650 cm^{-1} (Linear NO) [20,23,24]. $NO_{(ads)}$ on Pt(100) only yields one peak at 1590 shifting to 1625 cm^{-1} with increasing coverage and applied potential [22-24]. Finally, on polycrystalline platinum, adsorbed NO at low coverage is characterised by one single infrared frequency at 1580 cm^{-1} [25,26].

In conclusion, the band at 1575 - 1580 cm^{-1} observed on Pt/Al_2O_3 in the present study can be assigned to the stretch frequency of $NO_{(ads)}$ at low coverage. This assignment is also consistent with the observation that N_2O forms on Pt/Al_2O_3 during $NH_2OH_{(aq)}$ flow, since it was shown that N_2O is the product of the (electro)catalytic reaction between NO and hydroxylamine on supported platinum catalysts [45,66,67]. The low coverage of NO during hydroxylamine exposure is therefore consistent with its continuous conversion into N_2O. Only in the absence of hydroxylamine, the NO stays adsorbed on the platinum surface, and no N_2O is observed anymore. It was indeed published before that the rate of disproportionation of hydroxylamine increases when NO is added [45]. The presence of $NO_{(ads)}$ on Pt/Al_2O_3 and its absence on Pd/Al_2O_3 strongly suggests that the easy formation of NO from NH_2OH on platinum elegantly explains its high activity for hydroxylamine disproportionation, as compared to the low activity of Pd/Al_2O_3 on which no NO can be detected.

Table 6.1. Summary of vibrational frequency for adsorbed NO on platinum electrodes.

Electrode	Frequency (cm^{-1})		Comment	Reference
	Low coverage	High coverage		
Pt(111)	1440	1666→1680		[24]
	1430	1680		[20]
Pt(100)	1590→1620		Shift with applied potential	[22]
	1590→1625		Shift with increasing coverage or applied potential	[24]
	Between 1630 - 1610		No shift with increasing coverage	[20]
Pt(110)	1582	1770		[23]
	1590	1740		[20]
Pt(poly)	1580		Low coverage	[25,26]

Finally, the only remaining band to be assigned is the peak observed on Pt/Al_2O_3 at 1540 cm^{-1}. The simultaneous decrease of the peak at 1540 cm^{-1} and increase of the 1575 cm^{-1} band in Figure 6.6 indicates that species giving rise to a vibration at 1540 cm^{-1} is converted into $NO_{(ads)}$ during inert flow after hydroxylamine adsorption. According to the literature cited in Table 6.1, the species detected at 1540 cm^{-1} cannot be $NO_{(ads)}$ on platinum. The frequency is, on the other hand, located in the region of the scissor mode of coordinated NH_2 groups in inorganic complexes such as $Me(NH_2)_xCl_y$, which is found between 1560-1500 cm^{-1}[52,68]. However, it is 25 cm^{-1} higher than reported for the NH_2 scissors mode of solid NH_2OH [63]. In addition, it is 30 cm^{-1} blue shifted compared to a similar band on palladium which was assigned above to an $NH_{2(ads)}$ species, which would not be expected if it would be an identical adsorbate. As mentioned above, generally, adsorbed species on platinumexhibit lower vibrational frequencies compared to the same species adsorbed on palladium [53,55-58,69]. Another relevant example is the NH_2 scissor mode in $Pt(NH_3)_4Cl_2$ at 1563 cm^{-1}, whereas the NH_2 scissor mode in $Pd(NH_3)_4Cl_2$ was reported at 1601 cm^{-1} [70]. Finally, theoretical studies have shown that NH_2 fragments are not stable on Pt(111), which would be the most common crystal facets in our metal particles [70]. From all this we conclude that the 1540 cm^{-1} band also cannot be due to an NH_2 fragment adsorbed on platinum.

Clearly, the species characterised at 1540 cm^{-1} is reactive towards oxygen (Figure 6.7) in contrast to $NH_{2(ads)}$ on palladium. The species is converted into a product with an absorption band at 1305 cm^{-1}. This band is identical to the peak observed during nitrite adsorption on Pt/Al_2O_3 and was assigned to NO_x^-(x = 2,3). So, it is clear that the species at 1540 cm^{-1} is formed from NH_2OH and still contains nitrogen. NO and NH_2 can be excluded based on the reasons given above. Also H_2NO can be

excluded, since this would give rise to an NH_2 scissor vibration as well as an N-O stretch frequency, but only one band is detected. The only remaining possibilities are HNO, NOH or HNOH. It has been shown previously by theoretical calculations that HNO is the more stable fragment in vacuum [70,71]. Since the 1540 cm^{-1} species on platinum can be easily converted into NO, it is most likely $HNO_{(ads)}$ because only a single dehydrogenation step would be required. However, the other two options can certainly not be ruled out at this stage. Theoretical calculation of the IR absorbance of these species, taking into account the influence of the surrounding water, would be necessary answer this question. In the rest of this discussion this specie will be denoted "HNO"$_{(ads)}$. The oxidation of "HNO"$_{(ads)}$ with O_2/H_2O results in the production of $NO_x^-{}_{(ads)}$ without a notable presence of Pt-NO, since no peak was found at 1575 cm^{-1} during oxidation. This indicates that either production of $NO_x^-{}_{(ads)}$ occurs *via* the formation of $HNO_{2(ads)}$, or the oxidation of $NO_{(ads)}$ is much faster than the oxidation of "HNO"$_{(ads)}$.

In summary we can conclude that Pd/Al_2O_3 and Pt/Al_2O_3 show similar adsorption behaviour towards $NO_2^-{}_{(aq)}$ and $NH_4^+{}_{(aq)}$, while during the adsorption of hydroxylamine at pH 5 significant differences were observed. Table 6.2 summarises the assignments for the species observed in this chapter. These assignments will be used in our future work on the hydrogenation of nitrate and nitrite.

Clearly, on Pd/Al_2O_3 hydroxylamine is converted into a stable $NH_{2(ads)}$ species, while on Pt/Al_2O_3, first "HNO"$_{(ads)}$ is observed, which decomposes into NO. These observations also explain why on Pd/Al_2O_3 no nitrous oxide is observed. Normally, N_2O is thought to be produced from either dimerization of NO, or dimerization of speculated "HNO"$_{(ads)}$ fragments or a reaction between NO and adsorbed HNO [26,28,48,72-80]. Since neither $NO_{(ads)}$ nor "HNO"$_{(ads)}$ is observed on Pd/Al_2O_3, the formation of N_2O was not expected, which is in agreement with our experimental findings. This also agrees well with the fact that palladium is less active for disproportionation of hydroxylamine.

Table 6.2. Peak assignment during adsorption of $NO_2^-{}_{(aq)}$, $NH_2OH_{(aq)}$ and $NH_4^+{}_{(aq)}$ on Pd/Al_2O_3 and Pt/Al_2O_3.

Infrared frequency	Assignment
1235 cm^{-1}	$NO_2^-{}_{(aq)}$
1455 cm^{-1}	$NH_4^+{}_{(aq)}$
Pd/Al_2O_3	
1510 cm^{-1}	$Pd\text{-}NH_{2(ads)}$
1450 cm^{-1}	$NH_4^+{}_{(ads)}$ on PdO
1405 cm^{-1}	$Pd\text{-}NO_x^-{}_{(ads)}$ (x = 2,3)
1325 cm^{-1}	$Pd\text{-}NO_x^-{}_{(ads)}$ (x = 2,3)
Pt/Al_2O_3	
2231 cm^{-1}	N_2O
1575 - 1580 cm^{-1}	$Pt\text{-}NO_{(ads)}$ (low coverage)
1540 cm^{-1}	Pt-"HNO"$_{(ads)}$
1455 cm^{-1}	$NH_4^+{}_{(ads)}$ on PtO
1390 cm^{-1}	$Pt\text{-}NO_x^-{}_{(ads)}$ (x = 2,3)
1305 cm^{-1}	$Pt\text{-}NO_x^-{}_{(ads)}$ (x = 2,3)

6.5 Conclusion

The surface intermediates during heterogeneous catalytic hydrogenation of nitrite over supported noble metal catalysts were so far not investigated spectroscopically. This study convincingly shows, for the first time, the potential of *in-situ* ATR-IR spectroscopy to detect and identify inorganic nitrogen compounds, i.e. $NO_{2,3}^-$, NH_2, NH_4^+, NO and HNO, adsorbed on supported metal catalysts in water.

Pd/Al_2O_3 and Pt/Al_2O_3 show similar adsorption behaviour towards $NO_2^-{}_{(aq)}$ and $NH_4^+{}_{(aq)}$. Adsorption of NO_2^- leads to comparable adsorbed NO_x^- species on the metal particles for both catalysts, which could not be further identified. Adsorption of ammonia suggests that NH_4^+ is not chemisorbed but interacting as hydrated ions via an electrostatic interaction on oxygen containing surfaces.

On the other hand, major differences were found when adsorbing $NH_2OH_{(aq)}$ on Pd/Al_2O_3 and Pt/Al_2O_3. On Pd/Al_2O_3, hydroxylamine is converted into a stable $NH_{2(ads)}$ fragment, which is even not reactive to oxygen, while on Pt/Al_2O_3 hydroxylamine is

converted into NO via a intermediate, which is probably $HNO_{(ads)}$ or possible $NOH_{(ads)}$ or $HNOH_{(ads)}$. This intermediate is reactive to oxygen, forming $NO_x^-{}_{(ads)}$. These observations can explain why platinum is much more active than palladium for disproportionation of hydroxylamine.

The observations on the adsorption behaviour will be used in Chapter 7 and 8, in which the hydrogenation of nitrite on respectively Pd/Al_2O_3 and Pt/Al_2O_3 will be described.

6.6 References

[1] World Health Organization, Water and health in Europe, WHO, Regional Office for Europe, Copenhagen, 2002.
[2] A. Pintar, Catal.Today 77 (2003) 451.
[3] World Health Organization, Nitrate and nitrite in Drinking-water, WHO, Regional Office for Europe, Copenhagen, 2003.
[4] C.S. Bruning-Fann, J.B. Kaneene, Vet.Hum.Toxicol. 35 (1993) 521.
[5] K.D. Vorlop, T. Tacke, Chem.Ing.Tech. 61 (1989) 836.
[6] N. Barrabes, J. Just, A. Dafinov, F. Medina, J.L.G. Fierro, J.E. Sueiras, P. Salagre, Y. Cesteros, Appl.Catal.B 62 (2006) 77.
[7] K.J. Reddy, J.P. Lin, Wat.Res. 34 (2000) 995.
[8] A. Kapoor, T. Viraraghavan, J.Environ.Eng. 123 (1997) 371.
[9] J. Wärnå, I. Turunen, T. Salmi, T. Maunula, Chem.Eng.Sci. 49 (1994) 5763.
[10] K.D. Vorlop, U. Prusse, Environmental catalysis (1999) 195
[11] U. Prüsse, J. Daum, C. Bock, K.D. Vorlop, Stud.Surf.Sci.Catal. 130 (2000) 2237.
[12] A. Pintar, J. Batista, J. Levec, Water.Sci.Technol. 37 (1998) 177.
[13] S. Hörold, K.D. Vorlop, T. Tacke, M. Sell, Catal.Today 17 (1993) 21.
[14] S. Hörold, T. Tacke, K.D. Vorlop, Environ.Technol. 14 (1993) 931.
[15] M. Hahnlein, U. Prusse, J. Daum, V. Morawsky, M. Koger, M. Schroder, M. Schnabel ,K.D. Vorlop, Preparation of catalysts VII (1998) 99
[16] K. Daub, G. Emig, M.J. Chollier, M. Callant, R. Dittmeyer, Chem.Eng.Sci. 54 (1999) 1577.
[17] J. Daum, K.D. Vorlop, Chem.Eng.Tech. 22 (1999) 199.
[18] A. Pintar, J. Batista, J. Levec, T. Kijiuchi, Appl.Catal.B 11 (1996) 81.
[19] U. Prüsse, M. Hahnlein, J. Daum, K.D. Vorlop, Catal.Today 55 (2000) 79.
[20] R. Gomez, A. Rodes, J.M. Orts, J.M. Feliu, J.M. Perez, Surf.Sci. 342 (1995) L1104.
[21] A. Rodes, R. Gomez, J.M. Orts, J.M. Feliu, A. Aldaz, J.Electroanal.Chem. 359 (1993) 315.
[22] V. Rosca, M.T.M. Koper, J.Phys.Chem.B. 109 (2005) 16750.
[23] V. Rosca, G.L. Beltramo, M.T.M. Koper, Langmuir 21 (2005) 1448.
[24] Weaver M.J., S.Z. Zou, C. Tang, J.Chem.Phys. 111 (1999) 368.
[25] M.C.P.M. da Cunha, M. Weber, F.C. Nart, J.Electroanal.Chem. 414 (1996) 163.
[26] M.C.P.M. da Cunha, J.P.I. De Souza, F.C. Nart, Langmuir 16 (2000) 771.
[27] M.T. de Groot, M.T.M. Koper, J.Electroanal.Chem. 562 (2004) 81.

[28] A.C.A. de Vooys, Koper M.T.M., R.A. van Santen, J.A.R. van Veen, Electrochim.Acta 46 (2001) 923.
[29] G.E. Dima, A.C.A. de Vooys, Koper M.T.M., J.Electroanal.Chem. 554-555 (2003) 15.
[30] H.N. Heckner, J.Electroanal.Chem. 44 (1973) 9.
[31] K. Nishimura, K. Machida, M. Enyo, Electrochim.Acta 36 (1991) 877.
[32] O.A. Petrii, T.A. Safonova, J.Electroanal.Chem. 331 (1992) 897.
[33] S. Silva, M.J. Sottomayor, A. Martins, Electrochim.Acta 39 (1994) 491.
[34] J.F. van der Plas, E. Barendrecht, Electrochim.Acta 25 (1980) 1463.
[35] I.T. Bae, R.L. Barbour, D.A. Scherson, Analytical Chemistry 69 (1997) 249.
[36] S.D. Ebbesen, B.L. Mojet, L. Lefferts, J.Catal. Submitted (2006)
[37] N.J. Harrick, Internal Reflection Spectroscopy, Interscience Publishing, New York, 1967.
[38] T. Bürgi, A. Baiker, J.Phys.Chem.B. 106 (2002) 10649.
[39] S.D. Ebbesen, B.L. Mojet, L. Lefferts, (Chapter 3 in this thesis), Langmuir 22 (2006) 1079.
[40] R. He, R.R. Davda, J.A. Dumesic, J.Phys.Chem.B. 109 (2005) 2810.
[41] N. Kizhakevariam, X. Jiang, M.J. Weaver, J.Chem.Phys. 100 (1994) 6750.
[42] I. Ortiz-Hernandez, C.T. Williams, Langmuir 19 (2003) 2956.
[43] N.C. Yee, G.S. Chottiner, D.A. Scherson, J.Phys.Chem.B. 109 (2005) 7610.
[44] P.C. Moews, L.F. Audrieth, J.Inorg.Nucl.Chem. 11 (1959) 242.
[45] C.G.M. van de Moesdijk, The Catalytic Reduction of Nitrate and Nitric Oxide to Hydroxylamine: Kinetics and Mechanism, Doctoral Thesis, Technische Hogeschool , Eindhoven, 1979.
[46] G.M. Begun, W.H. Fletcher, J.Chem.Phys. 28 (1958) 414.
[47] A. Rodes, R. Gomez, J.M. Orts, J.M. Feliu, J.M. Perez, A. Aldaz, Langmuir 11 (1995) 3549.
[48] V. Rosca, G.L. Beltramo, M.T.M. Koper, J.Electroanal.Chem. 566 (2004) 53.
[49] S.D. Ebbesen, B.L. Mojet, L. Lefferts, (Chapter 7 in this thesis) To be submitted (2006)
[50] S.D. Ebbesen, B.L. Mojet, L. Lefferts, (Chapter 8 in this thesis) To be submitted (2006)
[51] K.I. Hadjiivanov, Catal.Rev.-Sci.Eng. 42 (2000) 71.
[52] K. Nakamoto, Infrared Spectra of Inorganic and Coordination Compounds, Wiley-Interscience publication, New York, 1970.
[53] R.S. Monteiro, L.C. Dieguez, M. Schmal, Catal.Today 65 (2001) 77.
[54] R. Barth, R. Pitchai, R.L. Anderson, X. Verykios, J.Catal. 116 (1989) 61.
[55] O. Dulaurent, K. Chandes, C. Bouly, D. Bianchi, J.Catal. 188 (1999) 237.
[56] A. Bourane, O. Dulaurent, D. Bianchi, J.Catal. 196 (2000) 115.

[57] M. Skotak, Z. Karpinski, W. Juszczyk, J. Pielaszek, L. Kepinski, D.V. Kazachkin, V.I. Kovalchuk, J.L. d'Itri, J.Catal. 227 (2004) 11.
[58] A. Bourane, O. Dulaurent, D. Bianchi, Langmuir 17 (2001) 5496.
[59] S. Zou, R. Gomez, Weaver M.J., J.Electroanal.Chem. 474 (1999) 155.
[60] R.A. Nyquist, R.O. Kagel, Infrared Spectra of Inorganic Compounds, Academic Press, New York, 1971.
[61] N.E. Schumaker, C.W. Garland, J.Chem.Phys. 53 (1970) 392.
[62] W. Zhou, T. Fukushima, M. Ito, Sci.Technol.Adv.Mater 7 (2006) 216.
[63] R.E. Nightingale, E.L. Wagner, J.Chem.Phys. 22 (1954) 203.
[64] D.S. Dunn, M.W. Severson, J.L. Hylden, J. Overend, J.Catal. 78 (1982) 225.
[65] B.E. Hayden, Surf.Sci. 131 (1983) 419.
[66] V. Rosca, G.L. Beltramo, Koper M.T.M., J.Phys.Chem.B. 108 (2004) 8294.
[67] B. Piela, P.K. Wrona, J.Electrochem.Soc. 151 (2004) 69.
[68] G. Socrates, Infrared and raman characteristic group frequencies, John Wiley & Sons Ltd, West Susses, England, 2001.
[69] R. Barth, R. Pitchai, R.L. Anderson, X. Verykios, J.Catal. 116 (1989) 61.
[70] G. Novell-Leruth, A. Valcarcel, A. Clotet, J.M. Ricart, J. Perez-Ramirez, J.Phys.Chem.B. 109 (2005) 18061.
[71] G.L. Beltramo, M.T.M. Koper, Langmuir 19 (2003) 8907.
[72] L.J.J. Janssen, M.M.J. Pieterse, E. Barendrecht, Electrochim.Acta 22 (1977) 27.
[73] I. Paseka, J. Vonkova, Electrochim.Acta 25 (1980) 1251.
[74] I. Paseka, A. Hodinar, Electrochim.Acta 27 (1982) 1461.
[75] J.A. Colucci, M.J. Foral, S.H. Langer, Electrochim.Acta 30 (1985) 521.
[76] A.C.A. de Vooys, G.L. Beltramo, B. van Riet, J.A.R. van Veen, M.T.M. Koper, Electrochim.Acta 49 (2004) 1307.
[77] J.H. MacNeil, P.A. Berseth, G. Westwood, W.C. Trogler, Environ,Sci.Technol. 32 (1998) 876.
[78] S. Kuwabata, S. Uezumi, K. Tanaka, T. Tanaka, Inorg.Chem. 25 (1986) 3018.
[79] A.C.A. de Vooys, Koper M.T.M., R.A. van Santen, J.A.R. van Veen, J.Catal. 202 (2001) 387.
[80] D.D. De, J.D. Englehardt, E.E. Kalu, J.Electrochem.Soc. 147 (2000) 4573.

CHAPTER 7

Hydrogenation of nitrite over Pd/Al_2O_3

Abstract

The mechanism of nitrite hydrogenation over a Pd/Al_2O_3 catalyst layer deposited on a ZnSe Internal Reflection Element was investigated in aqueous phase using Attenuated Total Reflection Infrared Spectroscopy. Nitrite hydrogenates to $NO_{(ads)}$, $NH_{2(ads)}$ and NH_4^+ on the palladium surface. Hydrogenation of adsorbed NO on palladium results in the formation of a reaction product that is not infrared active, most likely nitrogen, whereas no ammonia is formed. Ammonia is formed solely from hydrogenation of the $NH_{2(ads)}$ intermediate. The present study clearly shows that formation of nitrogen and ammonia proceeds via two separate pathways, which calls for a revised reaction scheme as presented in this study.

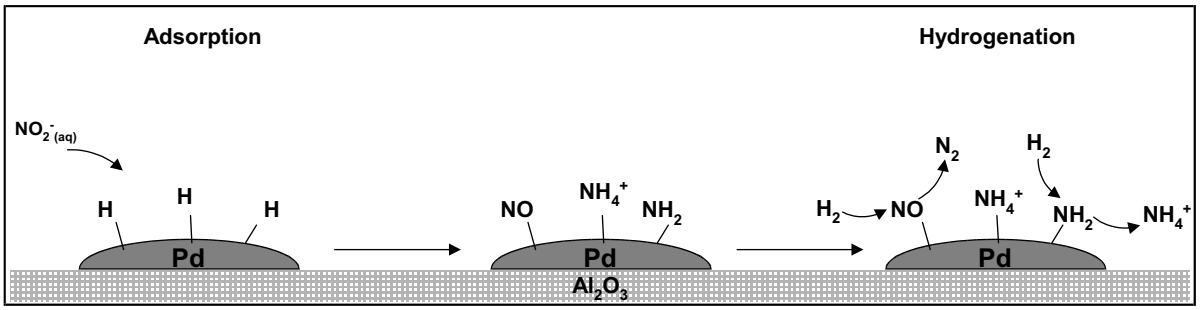

7.1 Introduction

Much attention has been focused on technologies for the treatment of ground water for nitrite and nitrate due to increasing nitrite and nitrate concentration of ground water and increasingly strict regulation of drinking water quality [1]. Both biological and catalytic denitrification processes have potential for water purification [2]. The biological processes has a slow reaction rate, making these processes insufficient for ground water treatment [2]. The catalytic hydrogenation of nitrate and nitrite over noble metal catalysts, which was described for the first time in 1989 [3], is the most promising technique for nitrate and nitrite removal. To date, the catalytic hydrogenation of nitrite and nitrate for use in water purification has been examined extensively in order to develop efficient catalysts [3-14]. However the mechanism of the nitrite hydrogenation over supported noble metal catalysts has not yet been resolved. Based on kinetic studies, adsorbed NO was suggested as an intermediate [10]. Several authors have proposed a reaction scheme including adsorbed NO as the key intermediate for the catalytic hydrogenation of nitrate and nitrite [11-14], although this was never supported by experimental evidence. We have recently examined adsorption of nitrite, hydroxylamine and ammonia on Pd/Al_2O_3 and Pt/Al_2O_3 by ATR-IR spectroscopy, in order to determine the adsorbed reactants and possible intermediates during hydrogenation of nitrite [15]. Nitrite and ammonia adsorb on Pd/Al_2O_3, whereas hydroxylamine decomposes on the palladium surface to form $NH_{2(ads)}$. The objective of this study is to gain insight in the mechanism of the heterogeneous hydrogenation of nitrite over Pd/Al_2O_3 in aqueous phase by examination of the surface intermediates during steady state as well as transient (stepwise adsorption followed by hydrogenation) hydrogenation of nitrite over the Pd/Al_2O_3 catalyst using ATR-IR spectroscopy.

7.2 Experimental

The experimental procedure, materials and catalyst preparation are described in details in the experimental section (Chapter 2). All spectra presented in the following section are corrected for the water background. The integrated peak areas are calculated using curve fitting of the spectra following the procedure described in the experimental section (Chapter 2).

The characteristics of the 5 wt% Pd/Al_2O_3 (dispersion 45%) catalyst examined in the present study are also described in details in the experimental section (Chapter 2). 6 mg of catalyst was deposited on the Internal reflection Element (IRE), resulting in

$1.3 \cdot 10^{-6}$ mol accessible surface palladium atoms deposited on the IRE. The thickness of the catalyst layer was measured to be 5.0 ± 0.5 μm.

After assembling the ATR-IR cell, with a coated IRE, the catalyst was reduced *in-situ* by introducing H_2/H_2O ($4.1 \cdot 10^{-4}$ mol/L H_2; saturation at 0.5 bar). This catalyst is denoted $H\text{-}Pd/Al_2O_3$, because the Pd/Al_2O_3 catalyst contains hydrogen. Even though the concentration is lower in aqueous phase, the chemical potential of hydrogen is assumed to be equal in gas and aqueous phase, if the same concentration is used for saturation. In gas phase, formation of β-palladium-hydride occurs at hydrogen pressures above 0.025 bar [16]. Saturation of the aqueous phase with a hydrogen pressures above 0.025 bar will therefore result in formation of β-palladium-hydride during reduction in aqueous phase. The $H\text{-}Pd/Al_2O_3$ catalyst used in this study therefore consists of β-palladium-hydride ($PdH_{0.7}$) after reduction in aqueous phase. Reduction using lower hydrogen concentration ($8.2 \cdot 10^{-6}$ mol/L H_2; saturation at 0.01 bar) results in surface hydrogen and α-Pd-hydride only ($PdH_{0.05}$). The results obtained after reduction at low concentration are qualitatively identical with experiments after reduction at high pressure (not presented in this study).

7.3 Results and discussion

7.3.1 Adsorption of $NO_2^-{}_{(aq)}$ on $H\text{-}Pd/Al_2O_3$

Adsorption of $NO_2^-{}_{(aq)}$ ($4.3 \cdot 10^{-4}$ mol/L) was performed at pH 7 on $H\text{-}Pd/Al_2O_3$ and infrared peaks evolved as shown in Figure 7.1A. The integrated peak areas during adsorption are shown in Figure 7.1B.

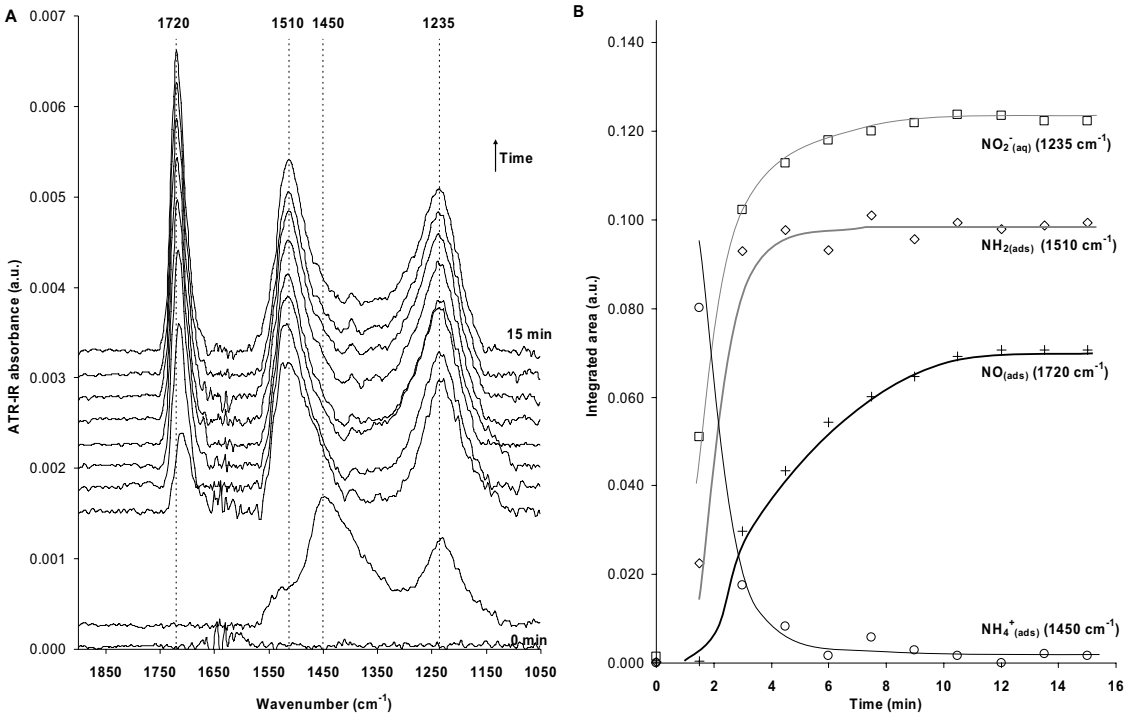

Figure 7.1. A: Water corrected ATR-IR spectra while flowing a solution of $NO_2^-_{(aq)}$ ($4.3 \cdot 10^{-4}$ mol/L) over H-Pd/Al_2O_3 at pH 7; B: Integrated peak areas of observed species during $NO_2^-_{(aq)}$. Flow.

Initially, i.e. the first two minutes, infrared peaks evolved at 1450 (width of 62 cm^{-1}) and 1235 cm^{-1}. Subsequently, two other bands developed at 1510 cm^{-1} and 1705 cm^{-1}, the latter shifting to 1720 cm^{-1} with increasing time, as can be seen in Figure 7.1A.

$NO_2^-_{(aq)}$ was detected at 1235 cm^{-1}, with a peak width of 78 cm^{-1}, which is identical to the peak for $NO_2^-_{(aq)}$ during blank experiments, recently published by our group [15]. During adsorption on H-Pd/Al_2O_3 the intensity of the peak for $NO_2^-_{(aq)}$ continued to increase with time slightly, which can be due to conversion of NO_2^- during the first minutes and the concentration of $NO_2^-_{(aq)}$ is thereby for some time lower than offered in the feed. No clear peaks for $NO_x^-_{(ads)}$ (x = 2,3) on palladium were detected (expected at 1405 and 1325 cm^{-1}) as compared to adsorption of $NO_2^-_{(aq)}$ on Pd/Al_2O_3, without pre-adsorbed hydrogen (passivated in air) [15]. However, the presence of a small amount of $NO_x^-_{(ads)}$ cannot be excluded because of the increased intensity between 1300 and 1450 cm^{-1}. Nevertheless, the intensity of a possible broad band at that position would be at least one order of magnitude lower as compared to $NO_x^-_{(ads)}$ on a passivated Pd/Al_2O_3 catalyst [15].

According to previous blank experiments with NH_4^+, the band developing initially at 1450 cm^{-1} can be assigned to NH_4^+ [15]. The band at 1510 cm^{-1} was observed during

decomposition of hydroxylamine on Pd/Al_2O_3 and was assigned to $NH_{2(ads)}$ [15]. Ammonia is either adsorbed on palladium or present in the liquid; no distinction is possible based on the infrared spectrum [15].

The only new signal is observed at 1705 cm^{-1}, shifting to 1720 cm^{-1} with increasing time. The observed blue shift is characteristic for molecules with a dipole such as NO. To the best of our knowledge, only one paper reported on NO adsorption on palladium in presence of water examined by IR spectroscopy [17]. Adsorbed NO on a Pd(111) electrode, held at a potential of 0.4 V, was detected by a single peak that blue shifted from 1720 to 1748 cm^{-1} with increasing coverage [17]. The formation of adsorbed NO during heterogeneous hydrogenation of nitrite over supported noble metal catalysts was proposed in literature, but was never supported with experimental evidence [5,6,10,11]. In electrochemistry, on the other hand, NO adlayers were prepared from nitrite and nitrate solutions on platinum electrodes [18-20], thereby showing formation of adsorbed NO as an intermediate during electrochemical reduction of nitrite on platinum electrodes. Based on the literature and the observed blue shift, we assign the infrared peak at 1705 – 1720 cm^{-1} to NO adsorbed on palladium.

Initially the peak for ammonia dominates the spectrum; in addition to ammonia, a small shoulder indicating the formation of $NH_{2(ads)}$ can already be seen in the first spectrum (after 90 seconds of adsorption) in Figure 7.1A. Formation of ammonia on the palladium surface during the initial adsorption of $NO_2^-{}_{(aq)}$ can occur via reaction with hydrogen on the $H\text{-}Pd/Al_2O_3$ catalyst. Formation of ammonia at high hydrogen concentrations is in good agreement with reports on heterogeneous hydrogenation of NO_2^- in batch reactors over palladium catalysts. The selectivity to ammonia was found to increase with increasing hydrogen concentrations [4,8,21,22]. Figure 7.1B clearly shows that the ammonia signal is initially high, subsequently, the ammonia signal decreases while both $NH_{2(ads)}$ and $NO_2^-{}_{(aq)}$ gain intensity during respectively the following 4 to 6 minutes. Clearly, the signal of $NH_{2(ads)}$ stabilises earlier than that of $NO_2^-{}_{(aq)}$. Moreover, the formation of $NO_{(ads)}$ is delayed and stabilises not earlier than after 12 minutes, along with the $NO_2^-{}_{(aq)}$ signal. Since no hydrogen is added during the adsorption of nitrite, NH_4^+ and $NH_{2(ads)}$ species must have been formed from hydrogen on the catalyst. Assuming an $H/Pd_{surface}$ ratio of unity, an H/Pd ration of 0.7 in β-palladium-hydride and assuming complete conversion of nitrite, it can be estimated that just two and a half minute of nitrite flow would be required to convert all hydrogen present in/on the catalyst into ammonia. This is in reasonable agreement with the fact that the initial intensity of ammonia is high where after it drops close to zero after four minutes. Subsequently, NO is formed which seems to

originate from NO_2^- similarly to preparation of NO adlayer on platinum electrodes in electrochemistry [18-20].

7.3.2 Hydrogenation of $NO_{(ads)}$ and $NH_{2(ads)}$ on H-Pd/Al_2O_3

After adsorption of $NO_2^-{}_{(aq)}$ on H-Pd/Al_2O_3 as shown in Figure 7.1 and described above, the cell was flushed with Ar/H_2O. During flushing all adsorbed species appeared stable, whereas $NO_2^-{}_{(aq)}$ (1235 cm^{-1}) was flushed out of the cell, resulting in the spectrum in Figure 7.2. Subsequently H_2/H_2O ($4.1 \cdot 10^{-6}$ mol/L H_2) was introduced into the cell and infrared peaks evolved as shown in Figure 7.2. Experiments were performed at very low hydrogen concentration in order to slow down reaction rates ($4.1 \cdot 10^{-6}$ mol/L H_2, saturated at 0.001 bar H_2).

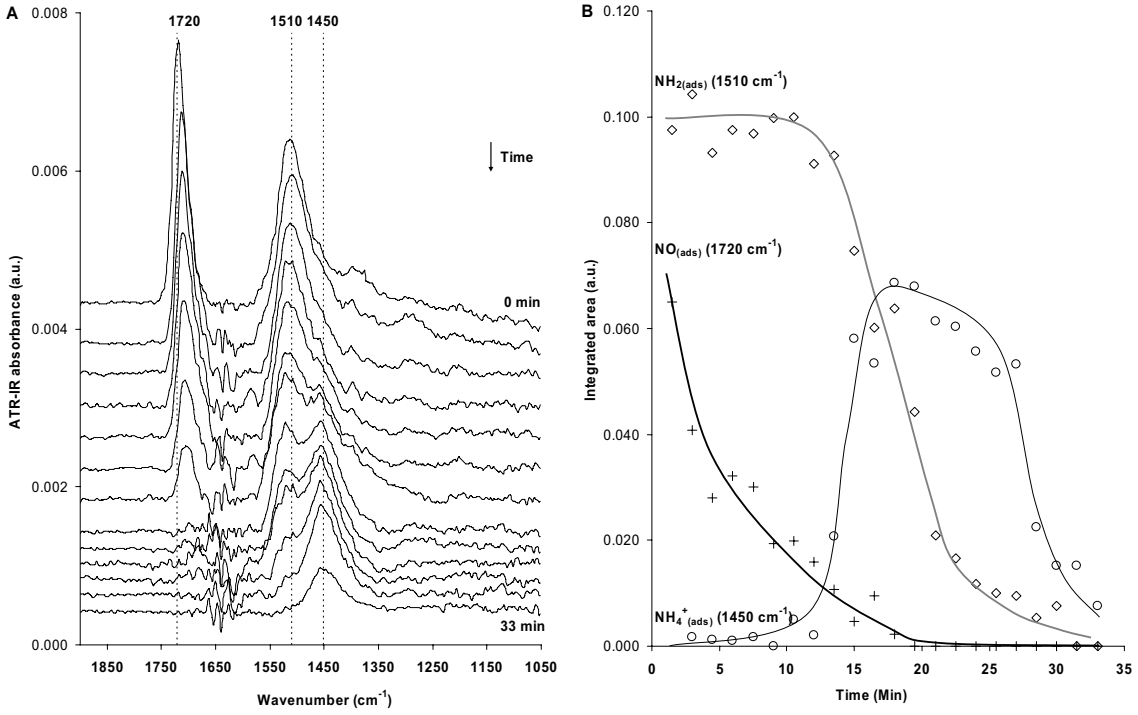

Figure 7.2. A: Water corrected ATR-IR spectra while H_2/H_2O ($4.1 \cdot 10^{-6}$ mol/L H_2) was flown over Pd/Al_2O_3 with $NO_{(ads)}$ and $NH_{2(ads)}$, previously formed during adsorption of $NO_2^-{}_{(aq)}$ on H-Pd/Al_2O_3 (Figure 7.1); B: integrated peak areas during flow of H_2/H_2O.

First, the peak at 1720 cm^{-1} ($NO_{(ads)}$) decreased in intensity during exposure to hydrogen while simultaneously shifting to 1705 cm^{-1}. Initially no changes in intensity of the peaks at 1510 cm^{-1} ($NH_{2(ads)}$) and 1450 cm^{-1} (NH_4^+) were observed (Figure 7.2A and B). After approximately 12 min (Figure 7.2B), the peak for $NH_{2(ads)}$ at 1510 cm^{-1} started to decrease and simultaneously a band for NH_4^+ at 1450 cm^{-1} appeared. The ammonia band reached a maximum after 20 minutes and subsequently decreased to almost zero.

During the initial hydrogenation of adsorbed NO and NH_2 (Figure 7.2), a decrease in peak intensity was observed for $NO_{(ads)}$, whereas initially no change in $NH_{2(ads)}$ or $NH_4^+{}_{(ads)}$ was detected. Clearly the hydrogenation product of $NO_{(ads)}$ can neither be $NH_{2(ads)}$ nor NH_4^+. $NO_{(ads)}$ must be either desorbed or converted into a product that could not be detected by ATR-IR. So far, NO was never detected in the gas phase or aqueous phase during hydrogenation of nitrite [5,8]. Because NO adsorbs stronger on palladium than hydrogen, similar to CO, we suggest that in the present experiment $NO_{(ads)}$ is hydrogenated to N_2, which, obviously can not be observed with infrared spectroscopy. We are currently developing a method for detection of extremely small amounts of dissolved gases in aqueous solutions, to unambiguously determine the hydrogenation product of $NO_{(ads)}$.

The fact that $NH_{2(ads)}$ decreases simultaneously with the increasing ammonia signal, strongly points to a hydrogenation of $NH_{2(ads)}$ into NH_4^+ in the presence of hydrogen. Initially, the rate of formation of ammonia from $NH_{2(ads)}$ is high, since a lot of $NH_{2(ads)}$ is available. After some time the surface becomes depleted in $NH_{2(ads)}$ and NH_4^+ is flushed out of the cell, decreasing the intensity of the band for NH_4^+.

During the first 12 minutes of hydrogenation of adsorbed NO and NH_2 (Figure 7.2) only $NO_{(ads)}$ is converted and later on $NH_{2(ads)}$ is converted. The maximal initial surface coverage of $NO_{(ads)}$ and $NH_{2(ads)}$ can be estimated, assuming complete consumption of hydrogen. Based on the equations of both surface reactions ($2\,NO_{(ads)} + 2\,H_2 \rightarrow N_2 + 2\,H_2O$ and $2\,NH_{2(ads)} + H_2 + 2\,H_2O \rightarrow 2\,NH_4^+ + 2\,OH^-$), it follows that maximal $4.9 \cdot 10^{-8}$ mol $NO_{(ads)}$ is converted within the first 12 min, corresponding to an initial NO coverage of 4% max. In the following 20 min, $NH_{2(ads)}$ is converted into NH_4^+, corresponding to a maximal initial NH_2 coverage of 6%. Although the final NO coverage is as low as 4% (Figure 7.1), a clear blue shift, due to dipole-dipole coupling, was observed with increasing NO coverage during adsorption of nitrite on $H\text{-}Pd/Al_2O_3$. Blue shifts for NO were indeed reported at NO coverage's as low as 2% [23], demonstrating consistency of the experimental observations in this study on the blue shift of the peak for $NO_{(ads)}$ with increasing NO coverage.

Interestingly, after adsorption of nitrite on $H\text{-}Pd/Al_2O_3$ (Figure 7.1), no adsorbed nitrite was detected. With a coverage of NO and NH_2 of only 10% max, sites for nitrite adsorption should be available. The absence of $NO_x^-{}_{(ads)}$ indicates that adsorption of nitrite do not fully cover the palladium surface and that the adsorption can be structure sensitive, which is well known for electrochemical reduction of nitrite and nitrate over platinum electrodes [24-26].

The result in Figure 7.2 demonstrates that $NO_{(ads)}$ is much more reactive towards hydrogen than $NH_{2(ads)}$, since hydrogenation of $NH_{2(ads)}$ only occurs after almost all $NO_{(ads)}$ has disappeared. Fast hydrogenation of NO also explains the delayed detection of $NO_{(ads)}$ during adsorption of $NO_2^-{}_{(aq)}$ on H-Pd/Al_2O_3 (Figure 7.1). Initially $NO_{(ads)}$ is rapidly hydrogenated to nitrogen, so that $NO_{(ads)}$ is not detected. As the hydrogen concentration on the catalyst surface decreases, the hydrogenation is slowed down and $NO_{(ads)}$ is detected. A maximum of 20% of the initial hydrogen is consumed, in order to form 4% coverage of $NO_{(ads)}$ and 6% of $NH_{2(ads)}$, during adsorption of $NO_2^-{}_{(aq)}$ on H-Pd/Al_2O_3 (Figure 7.1). The remaining 80% hydrogen has to be consumed during the initial formation of ammonia, explaining the high initial peak intensity for ammonia observed during adsorption of nitrite on H-Pd/Al_2O_3 (Figure 7.1).

7.3.3 Continuous hydrogenation of $NO_2^-{}_{(aq)}$ over H-Pd/Al_2O_3

For the *in-situ* nitrite hydrogenation, an aqueous solution of $4.3 \cdot 10^{-4}$ mol/L $NO_2^-{}_{(aq)}$ and $4.1 \cdot 10^{-4}$ mol/L H_2 was introduced to the cell with a pre-reduced H-Pd/Al_2O_3 catalyst layer (Figure 7.3).

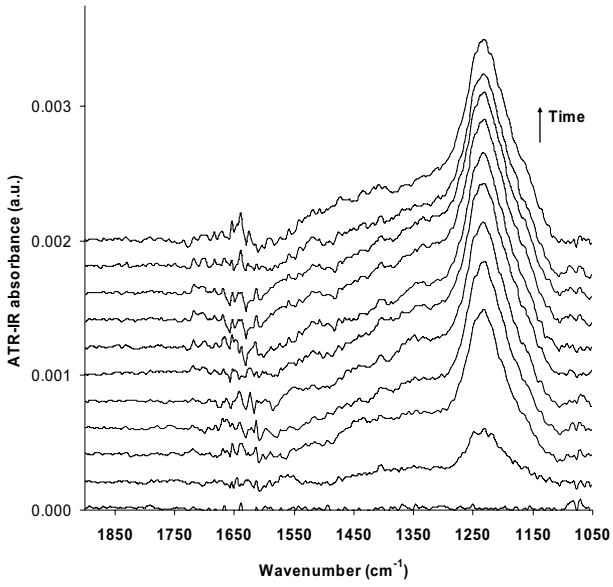

Figure 7.3. Water corrected ATR-IR spectra during hydrogenation of $NO_2^-{}_{(aq)}$ over H-Pd/Al_2O_3 ($4.3 \cdot 10^{-4}$ mol/L $NO_2^-{}_{(aq)}$ and $4.1 \cdot 10^{-4}$ mol/L H_2) (the time between spectra was 1.5 minutes).

One clear peak at 1235 cm^{-1} with a width of 79 cm^{-1} was detected, which is assigned to $NO_2^-{}_{(aq)}$ [15]. In addition, an increase in intensity was observed between 1550 and 1300 cm^{-1}, indicating the presence of adsorbed species at low coverage. However, the low intensity did not allow identification of adsorbed species.

The low surface coverage of the hydrogenation intermediates is most likely due to fast subsequent hydrogenation of the surface intermediates. Conversion of $NO_2^-{}_{(aq)}$ is estimated to be less than one percent, based on nitrite conversion rates during kinetic studies in a batch reactor published in literature [27].

Since no adsorbed species were detected during continuous hydrogenation using a ratio of H_2/NO_2^- of 1, solutions with lower concentrations of H_2 were used. This will slow down the reaction rates and increase the ability to detect reaction intermediates *in-situ*. Hydrogenation intermediates and products were only observed at hydrogen concentrations of $2.1 \cdot 10^{-5}$ mol/L and below. *In-situ* ATR-IR spectra during hydrogenation of $4.3 \cdot 10^{-4}$ mol/L $NO_2^-{}_{(aq)}$ using different hydrogen concentrations are shown in Figure 7.4A, 4C and 4E along with the integrated peak areas shown in Figure 7.4B, 4D and 4F.

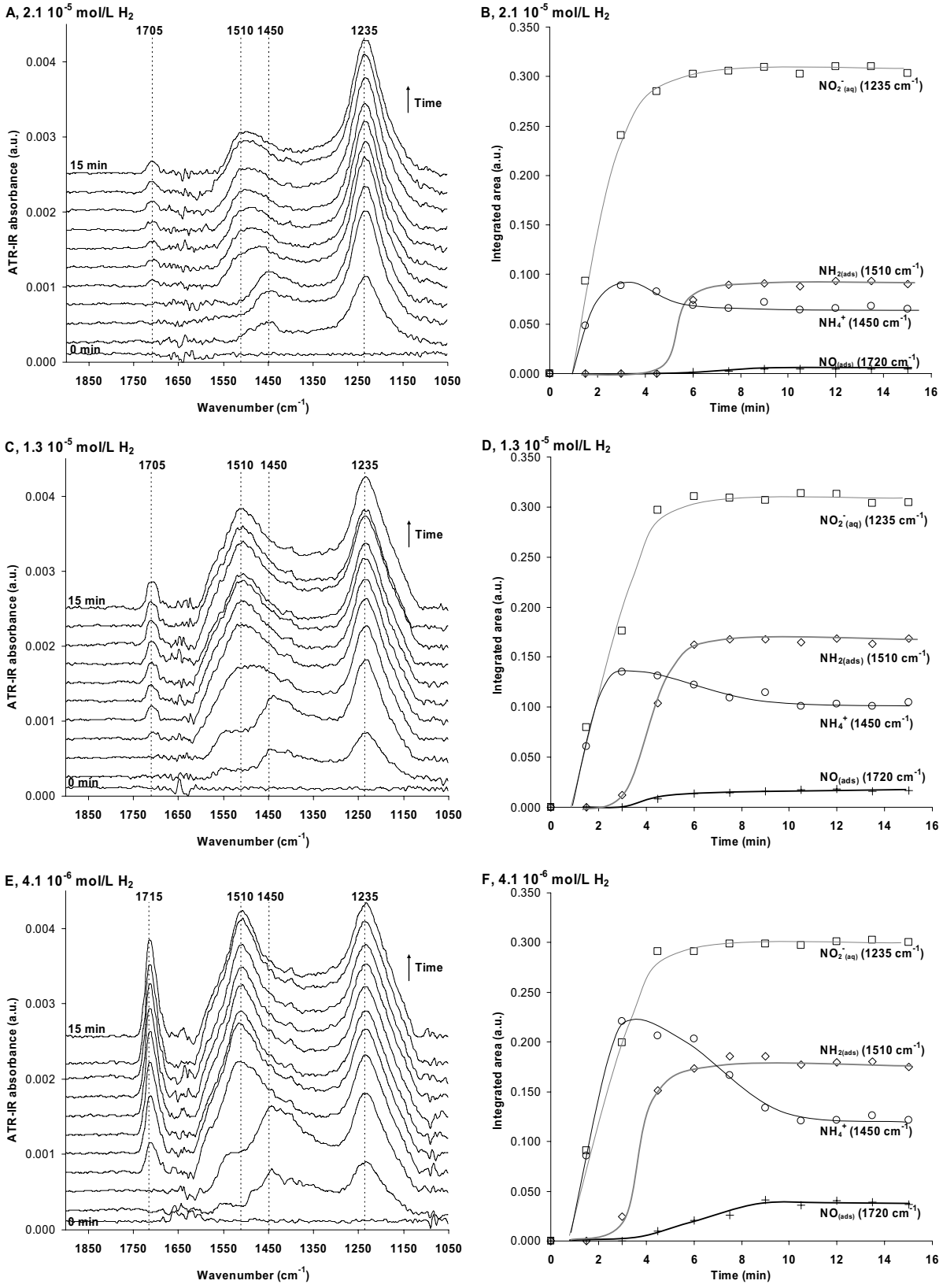

Figure 7.4. A, C, E: Water corrected ATR-IR spectra during hydrogenation of $NO_{2\,(aq)}^-$ ($4.3 \cdot 10^{-4}$ mol/L) over H-Pd/Al_2O_3 and B, D, E: integrated peak areas during hydrogenation ($A, B: 2.1 \cdot 10^{-5}$ mol/L H_2, $C, D: 1.3 \cdot 10^{-5}$ mol/L H_2, $E, F: 4.1 \cdot 10^{-6}$ mol/L H_2)

Figure 7.4 shows that surface intermediates from reaction between nitrite and hydrogen could be observed at the three hydrogen concentrations applied. Within 15 minutes, clear infrared peaks evolved at 1705 – 1715, 1510, 1450 and 1235 cm^{-1}; which are assigned to $NO_{(ads)}$, $NH_{2(ads)}$, NH_4^+ and $NO_2^-{}_{(aq)}$ respectively. In addition, a shoulder around 1575 – 1550 cm^{-1} appeared which has not been assigned yet. The nature of this specie is at present unknown. Since bridged adsorbed NO is normally detected at lower frequency than linear adsorbed NO, it could be speculated that the shoulder represents NO adsorbed on palladium in bridged geometry.

No significant amount of adsorbed NO_2^- on palladium was detected (1405 and 1325 cm^{-1}), whereas $NO_2^-{}_{(aq)}$ was observed at 1235 cm^{-1}. Moreover, at the investigated hydrogen concentrations, no difference in intensity of the peak for $NO_2^-{}_{(aq)}$ was observed, which is in agreement with the estimated low conversion of $NO_2^-{}_{(aq)}$. In fact, the $NO_2^-{}_{(aq)}$ intensities in Figure 7.4 and Figure 7.3 were similar. Moreover, based on nitrite conversion rates during kinetic studies [27], the hydrogen conversion is estimated to be between one and six percent, thus the catalyst is not exhausted in hydrogen during the hydrogenation.

The development of the other bands with time (Figure 7.4B, D and F) illustrates that in all cases initially NH_4^+ was formed on the palladium surface while, as for the titration experiments, simultaneously $NO_2^-{}_{(aq)}$ was observed (Figure 7.1). The bands resulting from $NO_{(ads)}$ and $NH_{2(ads)}$ increased in intensity after approximately three minutes, when the ammonia signal started to decrease in intensity. This delay is similar to the one observed when only nitrite was flown over $H\text{-}Pd/Al_2O_3$ (Figure 7.1) and can be explained by the time required to introduce a sufficient amount of nitrite to convert the excess of $H_{(ads)}$ on the pre-reduced $H\text{-}Pd/Al_2O_3$ catalyst (*vide ante*). The first 10 minutes of all experiments presented in Figure 7.4, thereby, represent the same transient response as shown in Figure 7.1. After 10 minutes, when stable levels are observed, steady state hydrogenation is achieved.

Further, it is evident that larger amounts of the surface intermediates $NO_{(ads)}$, $NH_{2(ads)}$ and NH_4^+ are observed at lower hydrogen concentrations. Clearly, lower H_2/NO_2^- ratios slow down hydrogenation reactions of the intermediates and the concentrations of the intermediates therefore increase. Moreover, different ratios of the amounts of the respective surface intermediates as a function of hydrogen concentration are observed, which is clearly illustrated in Figure 7.5.

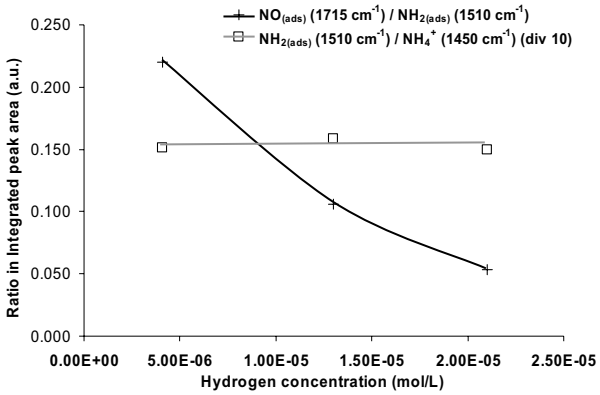

Figure 7.5. Ratio between the peak intensity of $NO_{(ads)}$ and $NH_{2(ads)}$ and between $NH_{2(ads)}$ and NH_4^+ at steady state during continuous hydrogenation at hydrogen concentration varying from $4.1 \cdot 10^{-6}$ to $2.1 \cdot 10^{-5}$ mol/L H_2.

The ratio between the integrated peak intensities of $NO_{(ads)}$ and $NH_{2(ads)}$ at steady state (at 15 minutes time on stream) decreases with increasing hydrogen concentration. Moreover, the $NH_{2(ads)}$ / NH_4^+ ratio is constant in all cases. Assuming that $NO_{(ads)}$ is converted to N_2 and $NH_{2(ads)}$ is converted to NH_4^+, as discussed in the previous section, the decrease of $NO_{(ads)}$ / $NH_{2(ads)}$ ratio with increasing hydrogen concentration indicate a higher selectivity to ammonia, explaining the increase in selectivity to ammonia with increasing hydrogen pressure, as normally found for hydrogenation of nitrite in batch reactors [4,9,21,22].

7.3.4 Nitrite hydrogenation mechanism

This paper reports a detailed insight in the surface intermediates and accordingly the mechanism of the heterogeneous catalytic hydrogenation of nitrite in water over Pd/Al_2O_3 as obtained by *in-situ* ATR-IR spectroscopy.

Adsorption of $NO_2^-{}_{(aq)}$ on H-Pd/Al_2O_3 yields $NO_{(ads)}$, $NH_{2(ads)}$ and NH_4^+. These species originate from reaction with hydrogen on the palladium surface (Figure 7.1 and Figure 7.4). Moreover, subsequent hydrogenation showed that $NO_{(ads)}$ is most likely converted to N_2 while the hydrogenation of $NH_{2(ads)}$ solely yield NH_4^+. Interestingly, the production of NH_4^+ only occurs after most of the $NO_{(ads)}$ has disappeared (Figure 7.2). This study clearly shows that ammonia and nitrogen are formed via two parallel stepwise hydrogenation processes as shown in Scheme 7.1. Moreover, these two reactions pathways are independent. The observation that $NH_{2(ads)}$ cannot be converted to N_2 is rather obvious. The fact that $NO_{(ads)}$ cannot be converted to $NH_{2(ads)}$ or NH_4^+ is certainly less obvious; this is indicated with the interrupted arrows in Scheme 7.1.

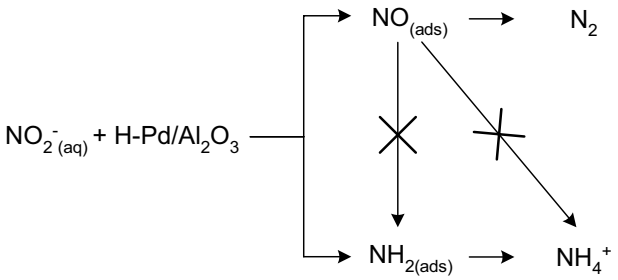

Scheme 7.1. Reaction scheme of the catalytic hydrogenation of nitrite over Pd/Al_2O_3 based on the reactions observed in the present study.

The order in $H_{(ads)}$ for formation of $NH_{2(ads)}$ is apparently lower than the order for hydrogenation of $NH_{2(ads)}$ to ammonia, since hydrogenation of $NH_{2(ads)}$ to NH_4^+ becomes rate limiting at low hydrogen concentration (Figure 7.1). The order in $H_{(ads)}$ for hydrogenation of $NO_{(ads)}$ to N_2, on the other hand, is lower than for hydrogenation of $NH_{2(ads)}$ since $NO_{(ads)}$ converts faster than $NH_{2(ads)}$ at low hydrogen concentrations (Figure 7.2). This results in increasing selectivity to ammonia with increasing hydrogen concentration.

The reaction scheme shown in Scheme 7.1, contains the species observed in the present study and the reaction steps are clearly not elementary reaction steps. It is clear that hydrogenation to $NH_{2(ads)}$ must be a sequence of elementary reaction steps. Since $NO_{(ads)}$ is evidently not an intermediate for ammonia formation (Figure 7.2), there must be a reaction pathway from NO_2^- to NH_4^+, excluding $NO_{(ads)}$ as an intermediate species. The only possible reaction path is addition of hydrogen to nitrite as the first step, to form HNO_2, which undergoes further stepwise hydrogenation to $NH_{2(ads)}$. Formation of HNO_2^- as an intermediate for electrochemical reduction of nitrite over platinum was indeed suggested in literature [25,28-30]. Dissociation of hydrogen is assumed to be the first step, followed by reaction with nitrite [11-14]. NH_2OH is regarded as a possible intermediate for formation of ammonia, since we have recently shown that formation of the $NH_{2(ads)}$ intermediate can arise from decomposition / reaction of NH_2OH on Pd/Al_2O_3. Accordingly, the heterogeneously catalytic hydrogenation of nitrite to ammonia may be described as:

$$NO_2^-{}_{(aq)} + H_{(ads)} \xrightarrow{Pd/Al_2O_3} HNO_2^-{}_{(ads)} \quad (7.1)$$

$$HNO_2^-{}_{(ads)} + H_{(ads)} \xrightarrow{Pd/Al_2O_3} HNO_{(ads)} + OH^- \quad (7.2)$$

$$HNO_{(ads)} + H_{(ads)} \xrightarrow{Pd/Al_2O_3} H_2NO_{(ads)} \quad (7.3)$$

$$H_2NO_{(ads)} + H_{(ads)} \xrightarrow{Pd/Al_2O_3} NH_2OH_{(ads)} \quad (7.4)$$

$$NH_2OH_{(ads)} + H_{(ads)} \xrightarrow{Pd/Al_2O_3} NH_{2(ads)} + H_2O \quad (7.5)$$

$$NH_{2(ads)} + H_{(ads)} \xrightarrow{Pd/Al_2O_3} NH_{3(ads)} \quad (7.6)$$

$$NH_{3(ads)} + H_2O \xrightarrow{Pd/Al_2O_3} NH_4^+ + OH^- \quad (7.7)$$

The formation of ammonia via hydrogenation of $HNO_2^-{}_{(ads)}$ is supported by the reaction mechanisms proposed from electrochemical reduction of nitrate and nitrite over platinum electrodes [24,28-31]. Furthermore it was suggested that the reaction pathway for the heterogeneous catalytic hydrogenation and electrochemical reduction of nitrite are the same for both platinum and palladium catalysts [11,12,32].

Since $NH_{2(ads)}$ was observed only during adsorption of $NO_2^-{}_{(aq)}$ on H-Pd/Al_2O_3 (Figure 7.1), either (i) the entire stepwise hydrogenation process proceeds too fast to detect the intermediates and $NH_{2(ads)}$ is observed exclusively after exhaustion of hydrogen as mentioned above or (ii) the steps from NO_2^- to $NH_{2(ads)}$, step (7.1) to (7.5), are fast compared to the further hydrogenation of $NH_{2(ads)}$, step (7.6) and (7.7). No intermediates were observed during continuous hydrogenation using a NO_2^-/H_2 ratio of 1, indicating that the hydrogenation reactions of the intermediates to both N_2 and NH_4^+ are indeed fast. We have recently shown that NH_2OH decomposes to $NH_{2(ads)}$ on palladium [15], indicating that step (7.5), proceeds fast. Accordingly all reactions up to $NH_{2(ads)}$ proceed fast, in agreement with the experimental evidence shown in Figure 7.1.

The formation of nitrogen on the other hand has to proceed via $NO_{(ads)}$ as an intermediate. In the present study it is clear that $NO_{(ads)}$ is formed on the palladium surface during hydrogenation of nitrite, which is in agreement with proposed mechanisms based on kinetic studies [5,6,10,11]. At present, in literature, the mechanism for formation N_2 is unclear, but the most frequently suggested mechanism involves dimerisation of $NO_{(ads)}$ [31-41] with N_2O as an intermediate, which however was not observed here. This might be explained by fast reduction of N_2O to N_2 reported for palladium catalysts [32].

This scheme with two parallel reaction pathways for ammonia and nitrogen, contradicts proposed reaction schemes of the heterogeneous hydrogenation of nitrite over supported noble metal catalysts in literature. In literature adsorbed NO was proposed to be an intermediate in the formation of both nitrogen and ammonia [5,6,10,11]. Based on literature and the results presented in the present study, we suggest an improved reaction scheme for the hydrogenation of NO_2^- over Pd/Al_2O_3 in water (Scheme 7.2). In this new reaction scheme, adsorbed NO is still an intermediate which, however, hydrogenates to N_2 (⑨ and ⑩) while $NH_{2(ads)}$ is converted to NH_4^+ (⑥ and ⑦) via $HNO_2^-{}_{(ads)}$ as an intermediate. Moreover, the rates of formation of $NO_{(ads)}$ and $NH_{2(ads)}$ are influenced by the hydrogen concentration; at high hydrogen concentration the rate to yield $NH_{2(ads)}$ (①) increases compared to $NO_{(ads)}$ (⑧), as indicated in Scheme 7.2. This results in increased selectivity to ammonia with increasing hydrogen concentration.

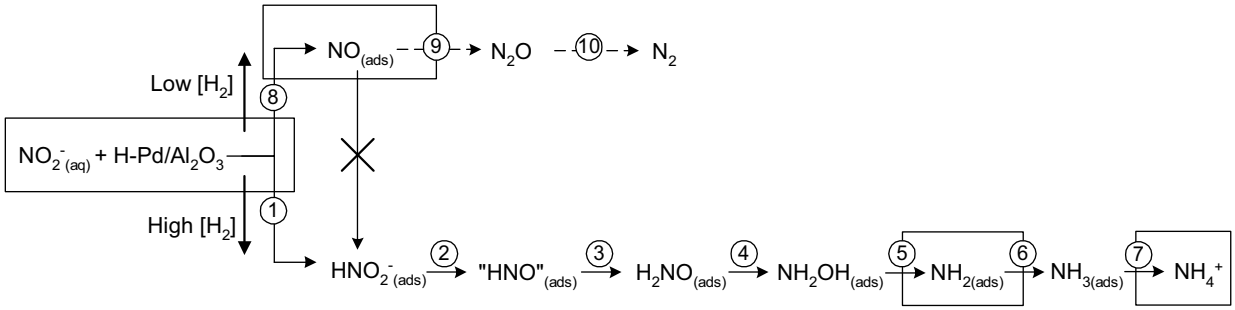

Scheme 7.2. Improved reaction scheme of the catalytic hydrogenation of nitrite over Pd/Al2O3. The reactions in the boxes are based on the findings in the present paper. The other reactions in the scheme have been discussed before in literature [42]. The dotted lines represent possible reaction pathways for N_2O and N_2 formation, although at present there is no evidence for these pathways. The numbers corresponds the reaction sequence described in the text.

7.4 Conclusion

The surface intermediates during the catalytic hydrogenation of NO_2^- over Pd/Al_2O_3 in aqueous phase have been examined. Adsorbed NO, NH_2 and NH_4^+ are formed as surface intermediates on the palladium surface during reaction of $NO_2^-{}_{(aq)}$ with surface hydrogen. $NO_{(ads)}$ is more reactive to hydrogen than $NH_{2(ads)}$. Hydrogenation of adsorbed NO on palladium results in the formation of a reaction product that is not infrared active, most likely nitrogen, whereas no ammonia is formed. Ammonia on the other hand is formed solely from hydrogenation of the $NH_{2(ads)}$ intermediate. The rate of formation of $NO_{(ads)}$ and $NH_{2(ads)}$, is influenced by the hydrogen concentration; at high hydrogen concentration the formation of $NH_{2(ads)}$ is favoured over $NO_{(ads)}$. This results in increased selectivity to ammonia with increasing hydrogen concentration and provides a mechanistic explanation for the well known fact that that the

selectivity to ammonia for palladium catalysts increases with the hydrogen concentration. The present study clearly shows that formation of nitrogen and ammonia proceeds via two independent pathways, which calls for a revised reaction scheme.

7.5 References

[1] World Health Organization, Water and health in Europe, WHO, Regional Office for Europe, Copenhagen, 2002.

[2] A. Kapoor, T. Viraraghavan, J.Environ.Eng. 123 (1997) 371.

[3] K.D. Vorlop, T. Tacke, Chem.Ing.Tech. 61 (1989) 836.

[4] S. Hörold, K.D. Vorlop, T. Tacke, M. Sell, Catal.Today 17 (1993) 21.

[5] S. Hörold, T. Tacke, K.D. Vorlop, Environ.Technol. 14 (1993) 931.

[6] K.D. Vorlop, U. Prusse, Environmental catalysis (1999) 195

[7] M. Hahnlein, U. Prusse, J. Daum, V. Morawsky, M. Koger, M. Schroder, M. Schnabel ,K.D. Vorlop, Preparation of catalysts VII (1998) 99

[8] U. Prüsse, J. Daum, C. Bock, K.D. Vorlop, Stud.Surf.Sci.Catal. 130 (2000) 2237.

[9] A. Pintar, J. Batista, J. Levec, Water.Sci.Technol. 37 (1998) 177.

[10] J. Wärnå, I. Turunen, T. Salmi, T. Maunula, Chem.Eng.Sci. 49 (1994) 5763.

[11] A. Pintar, J. Batista, J. Levec, T. Kijiuchi, Appl.Catal.B 11 (1996) 81.

[12] U. Prüsse, M. Hahnlein, J. Daum, K.D. Vorlop, Catal.Today 55 (2000) 79.

[13] K. Daub, G. Emig, M.J. Chollier, M. Callant, R. Dittmeyer, Chem.Eng.Sci. 54 (1999) 1577.

[14] J. Daum, K.D. Vorlop, Chem.Eng.Tech. 22 (1999) 199.

[15] S.D. Ebbesen, B.L. Mojet, L. Lefferts, (Ads) To be submitted (2006)

[16] F.A. Lewis, The Palladium Hydrogen System, Academic Press, New York, 1967.

[17] S. Zou, R. Gomez, Weaver M.J., J.Electroanal.Chem. 474 (1999) 155.

[18] A. Rodes, R. Gomez, J.M. Perez, J.M. Feliu, A. Aldaz, Electrochim.Acta 41 (1996) 729.

[19] V. Rosca, G.L. Beltramo, M.T.M. Koper, Langmuir 21 (2005) 1448.

[20] E. Casero, C. Alonso, J.A. Martin-Gago, F. Borgatti, R. Felici, F. Renner, T.L. Lee, J. Zegenhagen, Surf.Sci. 507-510 (2002) 688.

[21] Y. Matatov-Meytal, V. Barelko, I. Yuranov, M. Sheintuch, Appl.Catal.B 27 (2000) 127.

[22] Y. Matatov-Meytal, Y. Shindler, M. Sheintuch, Appl.Catal.B 45 (2003) 127.

[23] B.E. Hayden, Surf.Sci. 131 (1983) 419.

[24] G.E. Dima, G.L. Beltramo, M.T.M. Koper, Electrochim.Acta 50 (2005) 4318.

[25] S. Ye, H. Kita, J.Electroanal.Chem. 346 (1993) 489.

[26] J.F.E. Gootzen, R.M. van Hardeveld, W. Visscher, R.A. van Santen, J.A.R. van Veen, Recl.Trav.Chim.Pays-Bas 115 (1996) 480.

[27] A. Pintar, G. Bercic, AIChE J. 44 (1998) 2280.

[28] K. Nishimura, K. Machida, M. Enyo, Electrochim.Acta 36 (1991) 877.

[29] F. Balbaud, G. Sanchez, G. Santarini, G. Picard, Eur.J.Inorg.Chem. 4 (2000) 665.
[30] A. Rodes, R. Gomez, J.M. Orts, J.M. Feliu, A. Aldaz, J.Electroanal.Chem. 359 (1993) 315.
[31] M.C.P.M. da Cunha, J.P.I. De Souza, F.C. Nart, Langmuir 16 (2000) 771.
[32] A.C.A. de Vooys, Koper M.T.M., R.A. van Santen, J.A.R. van Veen, J.Catal. 202 (2001) 387.
[33] L.J.J. Janssen, M.M.J. Pieterse, E. Barendrecht, Electrochim.Acta 22 (1977) 27.
[34] I. Paseka, J. Vonkova, Electrochim.Acta 25 (1980) 1251.
[35] I. Paseka, A. Hodinar, Electrochim.Acta 27 (1982) 1461.
[36] J.A. Colucci, M.J. Foral, S.H. Langer, Electrochim.Acta 30 (1985) 521.
[37] A.C.A. de Vooys, Koper M.T.M., R.A. van Santen, J.A.R. van Veen, Electrochim.Acta 46 (2001) 923.
[38] A.C.A. de Vooys, G.L. Beltramo, B. van Riet, J.A.R. van Veen, M.T.M. Koper, Electrochim.Acta 49 (2004) 1307.
[39] R.R. Gadde, S. Bruckenstein, J.Electroanal.Chem. 50 (1974) 163.
[40] V. Rosca, G.L. Beltramo, M.T.M. Koper, J.Electroanal.Chem. 566 (2004) 53.
[41] D.D. De, J.D. Englehardt, E.E. Kalu, J.Electrochem.Soc. 147 (2000) 4573.
[42] V. Rosca, Koper M.T.M., Surf.Sci. 584 (2005) 258.

CHAPTER 8

Hydrogenation of nitrite over Pt/Al_2O_3

Abstract

The mechanism of the heterogeneous hydrogenation of nitrite over a Pt/Al_2O_3 catalyst layer deposited on a ZnSe Internal Reflection Element was investigated in aqueous phase using Attenuated Total Reflection Infrared Spectroscopy. In addition to adsorbed nitrite, the hydrogenation intermediates $NO_{(ads)}$, "HNO"$_{(ads)}$, $HNO_2^-{}_{(ads)}$ are formed on the platinum surface. Hydrogenation of all surface intermediates results in the formation of NH_4^+ mainly, but traces of N_2O are observed as well, which is believed to be an intermediate in the formation of nitrogen. "HNO"$_{(ads)}$ is the most prominent surface species during steady state operation and is therefore involved in the rate detemining step. Some $NO_{(ads)}$ accumulates at steps in titration experiments, showing a very low reactivity. The results indicate that the reaction pathway of nitrite hydrogenation on platinum and palladium is rather similar, but the rate determining steps on both metals are definitely different.

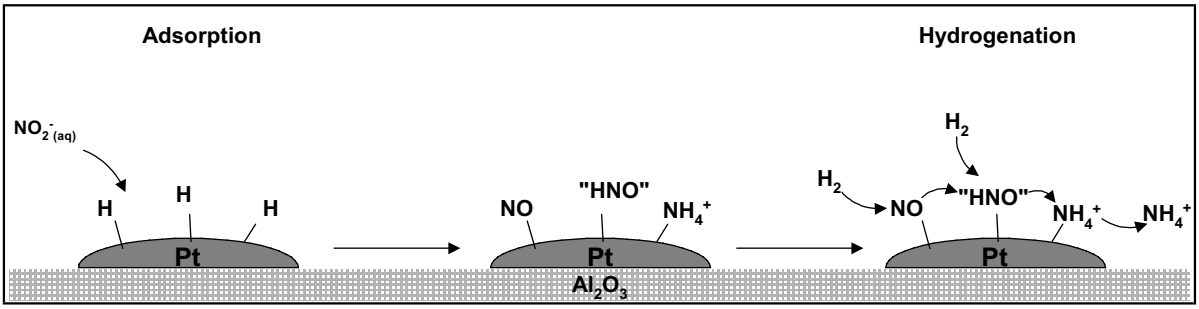

8.1 Introduction

Groundwater pollution by nitrate and nitrite is a widespread problem and is a potential risk to human health worldwide. High concentrations of nitrate and nitrite in drinking water can be fatal for infants, as nitrate and nitrite can cause blue baby syndrome [1]. Furthermore, nitrate can be converted into nitrosamine, which can cause cancer and hypertension [1]. In recent years, nitrate and nitrite concentrations in groundwater have increased at many locations throughout the world [2], and consequently wells have to be shut down [2,3]. As a result, there is a renewed interest in processes for removal of nitrite and nitrate from groundwater. Most promising is the heterogeneous hydrogenation over palladium and platinum catalysts, which have been studied extensively [4-11]. In general, it is accepted that the same reaction mechanism holds for both palladium and platinum catalysts; nitrite is hydrogenated to nitrogen and ammonia with adsorbed NO as an intermediate [5,6,12-16]. Palladium catalysts show higher selectivity to nitrogen than platinum catalysts [4,7,17]. We have recently applied ATR-IR spectroscopy to study the adsorption behaviour of nitrite, hydroxylamine (NH_2OH) and ammonia on both Pd/Al_2O_3 and Pt/Al_2O_3 [18]. In addition, we have studied the reaction mechanism of nitrite hydrogenation over Pd/Al_2O_3 [15]. Nitrite and ammonia adsorb on both Pd/Al_2O_3 and Pt/Al_2O_3, while hydroxylamine decomposes on the metal surfaces. On Pt/Al_2O_3, decomposition of NH_2OH forms a specie, which is most likely adsorbed HNO, that decomposes to adsorbed NO. On Pd/Al_2O_3, on the other hand, NH_2OH decomposes to form a stable NH_2 fragment. The NH_2 fragment was also observed during hydrogenation of nitrite over Pd/Al_2O_3, along with NO and NH_4^+ adsorbed on the palladium surface [15]. Formation of ammonia was found to proceed solely *via* hydrogenation of adsorbed NH_2, whereas the hydrogenation product of adsorbed NO could not be detected. N_2, which is not infrared active, was regarded as the most likely hydrogenation product of NO [15]. Based on these findings a reaction mechanism involving two parallel hydrogenation reactions on palladium (i.e. hydrogenation of NO to N_2 and hydrogenation of NH_2 to NH_4^+) was suggested [15].

In contrast to the parallel hydrogenation reactions suggested for Pd/Al_2O_3, a single stepwise hydrogenation process of nitrite was proposed for the electrochemical reduction of nitrite over platinum electrodes [19]. Several papers report on the experimental evidence of adsorbed NO as an intermediate during electrochemical reduction of nitrate and nitrite [20-25]. The subsequent electrochemical reduction of adsorbed NO mainly yields ammonia, although traces of N_2O were also detected. In addition, N_2O was demonstrated to be an intermediate in the formation of nitrogen [26,27].

Catalytic studies cannot be compared directly to electrochemical studies. Electrochemical studies are confined to dense conducting electrodes, often single crystals, instead of practical catalysts containing supported metal nano-particles on porous support materials. It is well known that the large difference in the structure of the metal surface causes large differences in the chemical and catalytic properties.

It is the objective of this study to examine the surface intermediates during hydrogenation of nitrite over Pt/Al_2O_3 by ATR-IR spectroscopy, to give an insight in the mechanism of the heterogeneous hydrogenation of nitrite over Pt/Al_2O_3. Also, similarities and differences between hydrogenation of nitrite over Pt/Al_2O_3 and Pd/Al_2O_3 will be discussed.

8.2 Experimental

The experimental procedure and materials are described in detail in the Experimental Section (Chapter 2). All spectra presented in the following sections are corrected for the water background. The integrated peak areas are calculated using curve fitting of the spectra following the procedure described in the Experimental Section (Chapter 2).

The catalyst preparation and characteristics of the 5 wt% Pt/Al_2O_3 (dispersion 75%) catalysts examined in the present study are also described in detail in the Experimental Section (Chapter 2). 6 mg of catalyst was deposited on the Internal Reflection Element (IRE), resulting in $1.2 \cdot 10^{-6}$ mol accessible surface atoms for the Pt/Al_2O_3 catalyst. The thickness of the Pt/Al_2O_3 catalyst layer was measured to be 3.50 ± 0.25 μm.

After assembling the ATR-IR cell, with an IRE coated with a Pt/Al_2O_3 catalyst layer, the catalyst was reduced *in-situ* by introducing H_2/H_2O ($4.1 \cdot 10^{-4}$ mol/L H_2; saturation at 0.5 bar). The catalyst is denoted $H\text{-}Pt/Al_2O_3$, because of the hydrogen covered platinum surface.

8.3 Results and discussion

8.3.1 Adsorption of $NO_2^-_{(aq)}$ on H-Pt/Al_2O_3

In order to follow the surface reaction between nitrite and pre-adsorbed hydrogen, the H-Pt/Al_2O_3 catalyst was exposed to $NO_2^-_{(aq)}$ ($4.3 \cdot 10^{-4}$ mol/L) at pH 7 and infrared peaks evolved as shown in Figure 8.1A. The integrated peak areas obtained by curve fitting are shown in Figure 8.1B and C.

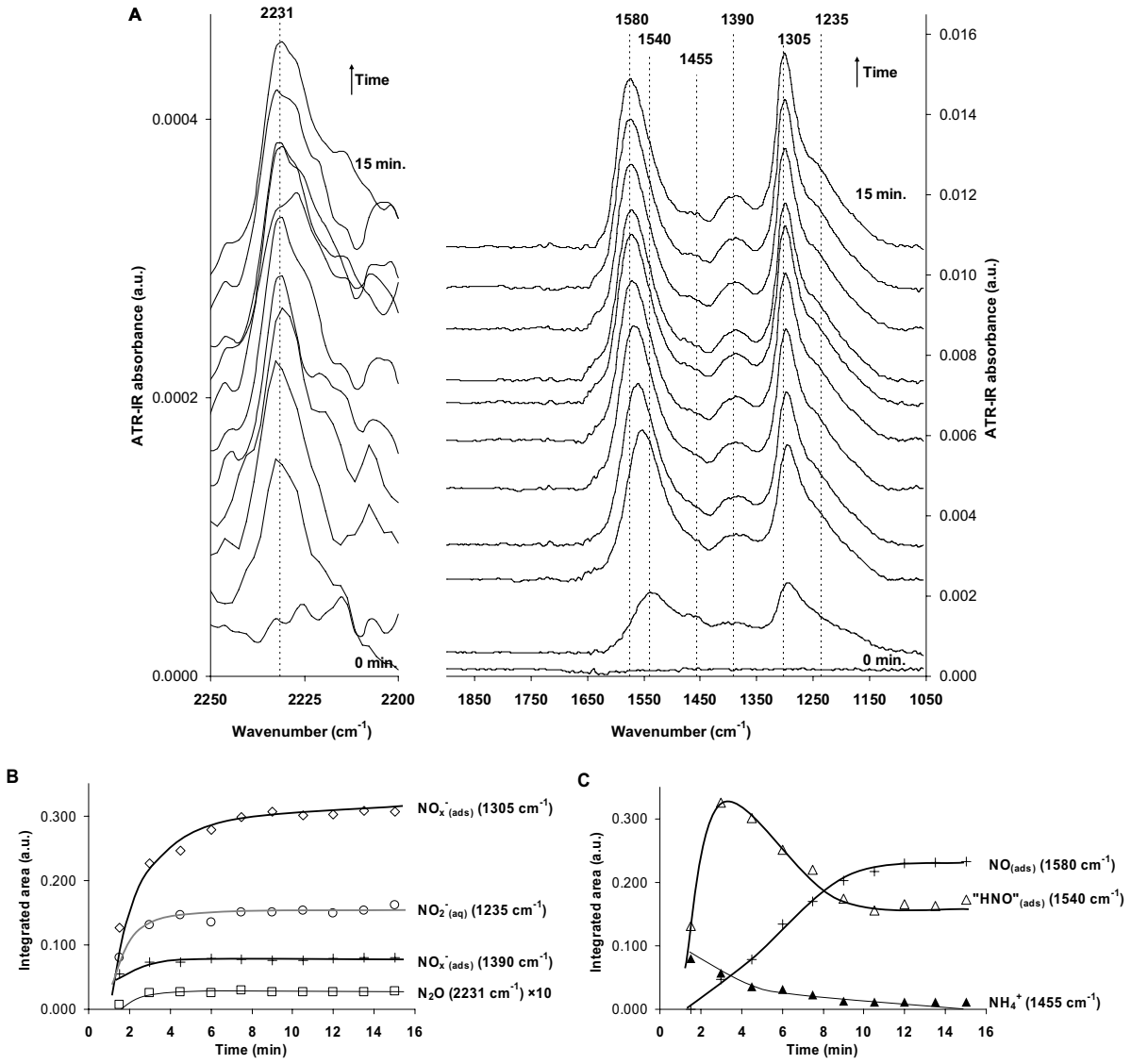

Figure 8.1. A: Water corrected ATR-IR spectra during adsorption of NO_2^- on H-Pt/Al_2O_3; B and C: Integrated peak areas during adsorption.

Initially peaks developed at 2231, 1540, 1455, 1390 and 1305 cm^{-1}. Further a shoulder was observed at 1235 cm^{-1}. During continuous flow of $NO_2^-_{(aq)}$, the band at

1455 cm^{-1} disappeared in approximately 10 minutes. At the same time, gradually a new peak appeared at 1570 cm^{-1}, which shifted to 1580 cm^{-1} with increasing intensity. Simultaneously the peak at 1540 cm^{-1} reached a maximum after 3 minutes, subsequently decreased, and stabilised after 10 minutes.

Based on blank experiments, the peak at 1235 cm^{-1} can be assigned to $NO_{2\,(aq)}^-$ as shown in Chapter 6. The intensity of $NO_{2\,(aq)}^-$ needs a few minutes to stabilise. Since this is much longer than the residence time of the liquid in the cell of 7.2 seconds, the time needed for stabilisation is probably due to conversion of nitrite by adsorbed hydrogen. According to previous adsorption experiments (Chapter 6), the band initially present at 1455 cm^{-1} can be assigned to NH_4^+. As discussed in Chapter 6, the specie characterised by the peak at 1540 cm^{-1} is most likely $HNO_{(ads)}$ but due to the uncertainty in the assignment (NOH and HNOH can not be excluded), this specie will be denoted "HNO"$_{(ads)}$. The peak at 2231 cm^{-1} is assigned to N_2O [18,21,26,28-30], which is dissolved or weakly adsorbed at the catalyst surface. The peaks at 1390 and 1305 cm^{-1} arise from NO_x^- (x = 2,3) species adsorbed on the platinum surface as previously discussed (Chapter 6). For clarity, these two NO_x^- species will be denoted as $NO_{x\,(ads)}^{-\ 1305\ cm^{-1}}$ and $NO_{x\,(ads)}^{-\ 1390\ cm^{-1}}$ in the following. Finally, the band at 1570 cm^{-1}, shifting to 1580 cm^{-1}, originates from bridged adsorbed NO at low coverage on the platinum surface [18,20,21]. This NO specie will be denoted $NO_{(ads)}^{1580\ cm^{-1}}$.

Figure 8.1 clearly shows a variety of products formed when H-Pt/Al_2O_3 is exposed to $NO_{2\,(aq)}^-$. In addition to adsorbed NO_x^- species (1390 and 1305 cm^{-1}) that were found previously on Pt/Al_2O_3 without hydrogen [18], hydrogenation products like $NO_{(ads)}^{1580\ cm^{-1}}$, "HNO"$_{(ads)}$, NH_4^+ and N_2O were observed. Initially, when the surface coverage of hydrogen is high, formation of "HNO"$_{(ads)}$ and NH_4^+ occurs, whereas $NO_{(ads)}^{1580\ cm^{-1}}$ starts to appear from 3 minutes on.

Production of ammonia during catalytic hydrogenation of nitrite is well documented, moreover platinum catalysts are known to be selective towards ammonia [4,7,17]. The initial formation of ammonia, when the hydrogen coverage is still high, is in agreement with the observation that selectivity to NH_4^+ increases with increasing hydrogen concentration in batch operated experiments reported in literature [4,5,11,31,32].

After approximately 10 minutes the surface seems to become exhausted in adsorbed hydrogen; the formation rate of NH_4^+ is close to zero and the concentrations of

$NO_{(ads)}^{1580\ cm^{-1}}$ and "HNO"$_{(ads)}$ seem to stabilise, presumably because there is no hydrogen available for further hydrogenation. In other words $NO_{(ads)}^{1580\ cm^{-1}}$ and "HNO"$_{(ads)}$ are trapped at the platinum surface. This seems to resemble the preparation of NO adlayers on platinum electrodes by electrochemical reduction of nitrite [19,23,24,33,34].

8.3.2 Hydrogenation of $NO_{(ads)}^{1580\ cm^{-1}}$, "HNO"$_{(ads)}$ and $NO_x^-{}_{(ads)}$ on H-Pt/Al_2O_3

After 15 minutes adsorption of $NO_2^-{}_{(aq)}$ on H-Pt/Al_2O_3 (see Figure 8.1), the cell was flushed with Ar/H_2O for 5 minutes to remove $NO_2^-{}_{(aq)}$ (not shown). When flowing with Ar/H_2O, $NO_2^-{}_{(aq)}$ (1235 cm^{-1}) was completely flushed out of the cell. In addition, a slight increase in the peak for $NO_{(ads)}^{1580\ cm^{-1}}$ was observed (+7%), along with a decrease in the peaks for "HNO"$_{(ads)}$ (-5%) and $NO_x^-{}_{(ads)}$ (1305 cm^{-1}) (-10%). These changes are in good agreement with our previous study, where we showed that "HNO"$_{(ads)}$ decomposes into $NO_{(ads)}^{1580\ cm^{-1}}$ during inert flow [18]. The resulting spectrum of the catalyst surface is shown in Figure 8.2, bottom spectrum (t = 0 min). Remarkably, even after inert water flow, N_2O is still detectable, although with very low intensity, indicating continuous production of N_2O. Most likely, N_2O is produced from either dimerisation of $NO_{(ads)}$ or "HNO"$_{(ads)}$ or a reaction between $NO_{(ads)}$ and adsorbed "HNO"$_{(ads)}$, as we have previously discussed in Chapter 6. However, the fact that the total amount of $NO_{(ads)}^{1580\ cm^{-1}}$ and "HNO"$_{(ads)}$ hardly changes indicates that the rate of formation must be very low. Nevertheless, N_2O is detected demonstrating the high sensitivity of ATR-IR for N_2O.

Subsequently, H_2/H_2O ($4.1 \cdot 10^{-6}$ mol/L H_2) was introduced into the cell to study the reactivity of the adsorbed species towards hydrogen. During H_2/H_2O flow, infrared peaks evolved as shown in Figure 8.2A: the integrated peak areas are shown in Figure 8.2B and C.

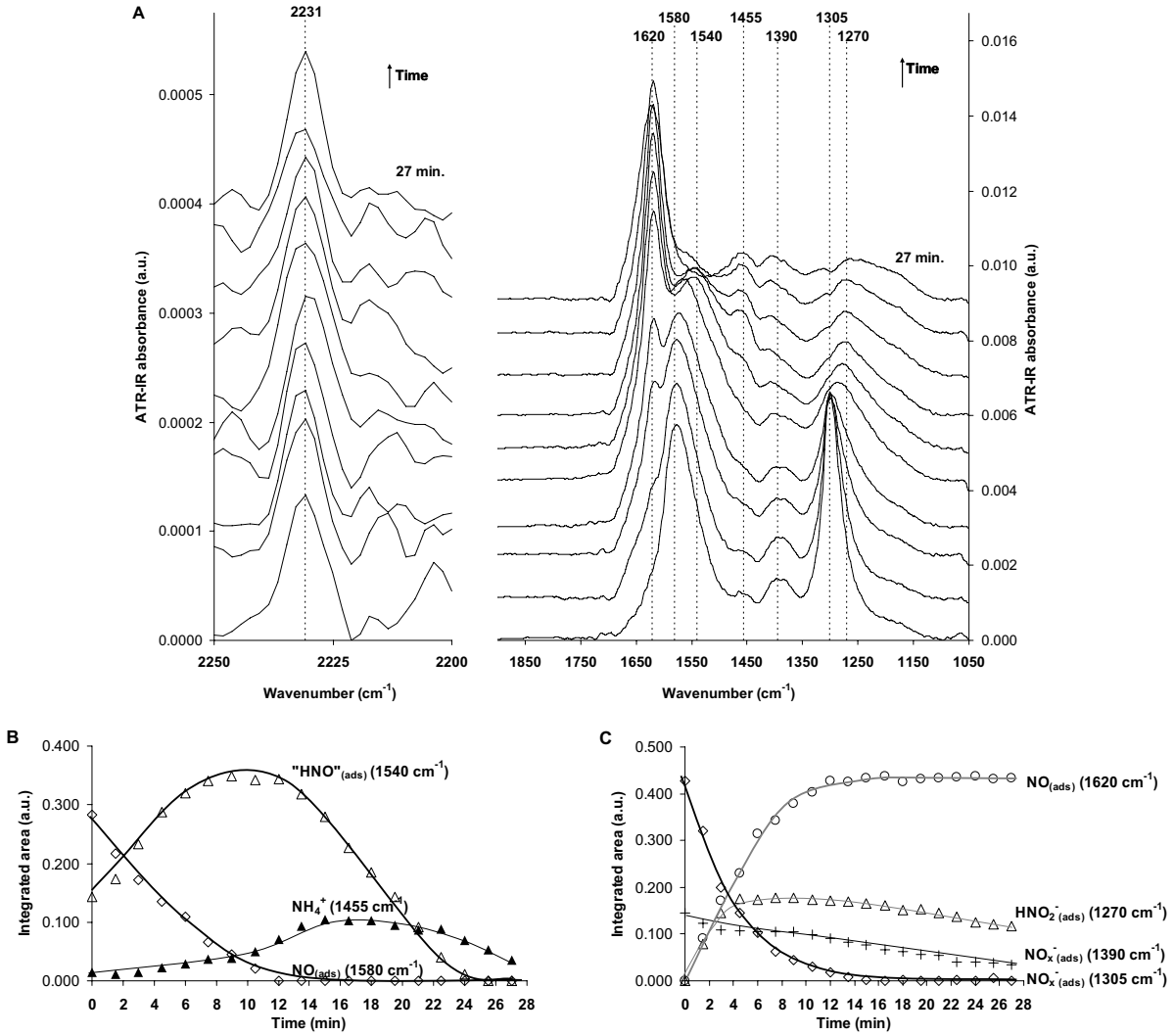

Figure 8.2. A: Selected water corrected ATR-IR spectra (time between spectra is 3 min) during hydrogenation (flow of $4.1 \cdot 10^{-6}$ mol/L H_2/H_2O) of N_2O, $NO^{1580\ cm^{-1}}_{(ads)}$, "HNO"$_{(ads)}$ and $NO_x^-{}_{(ads)}$ on Pt/Al_2O_3, formed on the catalyst surface during adsorption of $NO_2^-{}_{(aq)}$ on H-Pt/Al_2O_3 (Figure 8.1); B and C: integrated peak areas during flow of H_2/H_2O.

Right from the start of the hydrogenation experiment, the peak for $NO^{1580\ cm^{-1}}_{(ads)}$ started to decrease in intensity, while simultaneously the peak for "HNO"$_{(ads)}$ (1540 cm^{-1}) increased. NH_4^+ (1455 cm^{-1}) was first observed after 5 minutes and steadily increased, while the band of "HNO"$_{(ads)}$ reached a maximum after 10 minutes. Subsequently, the peak for "HNO"$_{(ads)}$ decreased with a simultaneous increase in the peak for NH_4^+ up to 18 minutes, after which it started to decrease slowly. These observations clearly show that $NO^{1580\ cm^{-1}}_{(ads)}$ under hydrogenation conditions is converted to "HNO"$_{(ads)}$ and subsequently to NH_4^+, being the final hydrogenation product.

Figure 8.2C shows that the peaks for adsorbed nitrite (1390 and 1305 cm^{-1}) also decreased in intensity during exposure to hydrogen. The peak for $NO_{x\ (ads)}^{-\ 1390\ cm^{-1}}$ decreases significantly slower than the peak for $NO_{x\ (ads)}^{-\ 1305\ cm^{-1}}$, clearly demonstrating that these two peaks represent two different adsorbed NO_x^- species, as discussed in Chapter 6. At present, further precision of the assignment is not possible.

In addition, a new peak at 1620 cm^{-1} appeared along with the disappearance of the band for $NO_{x\ (ads)}^{-\ 1305\ cm^{-1}}$, which seems to stabilise after 12 minutes. Furthermore, also an asymmetric peak at 1270 cm^{-1} appeared, which decreased with time only slowly.

The band at 1270 cm^{-1} was reported before, in electrochemistry studies on nitrate hydrogenation on platinum electrodes, and was assigned to $HNO_{2\ (ads)}^-$ [21]. Since hydrogenation of NO_2^- to $HNO_{2\ (ads)}^-$ is a reasonable proposition and no other assignments were found in literature, the peak at 1270 cm^{-1} is assigned to $HNO_{2\ (ads)}^-$. The intensity of this specie is low and it can only be observed in absence of species with much stronger absorption bands, such as $NO_{x\ (ads)}^{-\ 1305\ cm^{-1}}$ and $NO_{2\ (aq)}^-$. For this reason, the presence of $HNO_{2\ (ads)}^-$ in the nitrite titration experiment (Figure 8.1) cannot be excluded.

In literature, the band at 1620 cm^{-1} has been attributed to $NO_{(ads)}$ on a stepped Pt(100) surface [22]. Its frequency is too low to originate from linearly adsorbed NO on Pt(111), which is reported at 1680 cm^{-1} [18,22,25]. In addition, a characteristic of NO adsorbed on steps is that the molecules are separated from each other, preventing dipole-dipole coupling with increasing coverage. This is in agreement with our experimental evidence (Figure 8.2), revealing no shift of the peak position. Consequently, the band at 1620 cm^{-1} is speculatively assigned to NO adsorbed on steps, and will be denoted $NO_{(steps)}^{1620\ cm^{-1}}$ in the following. In any case, this peak is definitely different from the peak at 1570-1580 cm^{-1}, assigned to bridged NO. The concentration of $NO_{(steps)}^{1620\ cm^{-1}}$ decreased very slowly when flowing of H_2/H_2O. The fact that $NO_{(steps)}^{1620\ cm^{-1}}$ is not reactive to hydrogen, in contrast to all other species, can not be explained at this time, since NO dissociation is normally favoured on stepped surfaces [35-37]. On the other hand, it is well known that the electrochemical reduction of both nitrite and NO adlayers is structure sensitive [38-40]; NO was suggested to accumulate at steps during electrochemical reduction of nitrate over platinum electrodes [38].

At this point, it is not clear from which species the $NO^{1620\ cm^{-1}}_{(steps)}$ adsorbate originates. During decomposition of hydroxylamine on Pt/Al_2O_3, both "HNO"$_{(ads)}$ and $NO^{1580\ cm^{-1}}_{(ads)}$ were found, while no $NO^{1620\ cm^{-1}}_{(steps)}$ was observed (Chapter 6). That result suggests that the production of $NO^{1620\ cm^{-1}}_{(steps)}$ possibly occurs *via* direct hydrogenation of NO_x^- and/or *via* $HNO_2^-{}_{(ads)}$.

The peak at 1580 cm^{-1} (Figure 8.1 and Figure 8.2) is assigned to bridged adsorbed NO on the polycrystalline platinum surface at low coverage [20,21]. From Figure 8.2B it can be seen that it takes 24 minutes to hydrogenate adsorbed $NO^{1580\ cm^{-1}}_{(ads)}$ and "HNO"$_{(ads)}$. The coverage of $NO^{1580\ cm^{-1}}_{(ads)}$ and "HNO"$_{(ads)}$ can thus be estimated based on the amount of hydrogen supplied, assuming complete hydrogen consumption and complete hydrogenation of $NO^{1580\ cm^{-1}}_{(ads)}$ and "HNO"$_{(ads)}$ to NH_4^+, compared to the number of platinum surface atoms present. It follows that the maximal initial coverage of $NO_{(ads)}$ is as low as 3.5%. Indeed the low coverage estimated corresponds to the observed peak position at 1580 cm^{-1} assigned bridged adsorbed NO on the polycrystalline platinum surface at low coverage [20,21] (Figure 8.1 and Figure 8.2). This low coverage illustrates the extreme sensitivity of ATR-IR for adsorbed species, enabling the detection of adsorbed species at very low surface coverage. Finally Figure 8.2 reveals, like Figure 8.1, continuous formation of N_2O, as discussed earlier.

8.3.3 Continuous hydrogenation of $NO_2^-{}_{(aq)}$ on H-Pt/Al_2O_3

In order to follow the continuous hydrogenation of nitrite *in-situ*, a solution containing both $4.3 \cdot 10^{-4}$ mol/L $NO_2^-{}_{(aq)}$ and $4.1 \cdot 10^{-4}$ mol/L H_2 was introduced into the cell with a freshly-prepared pre-reduced catalyst (H-Pt/Al_2O_3) (*vide ante*). Water corrected ATR-IR spectra during the continuous hydrogenation of nitrite are shown in Figure 8.3A. The integrated peak areas are shown in Figure 8.3B.

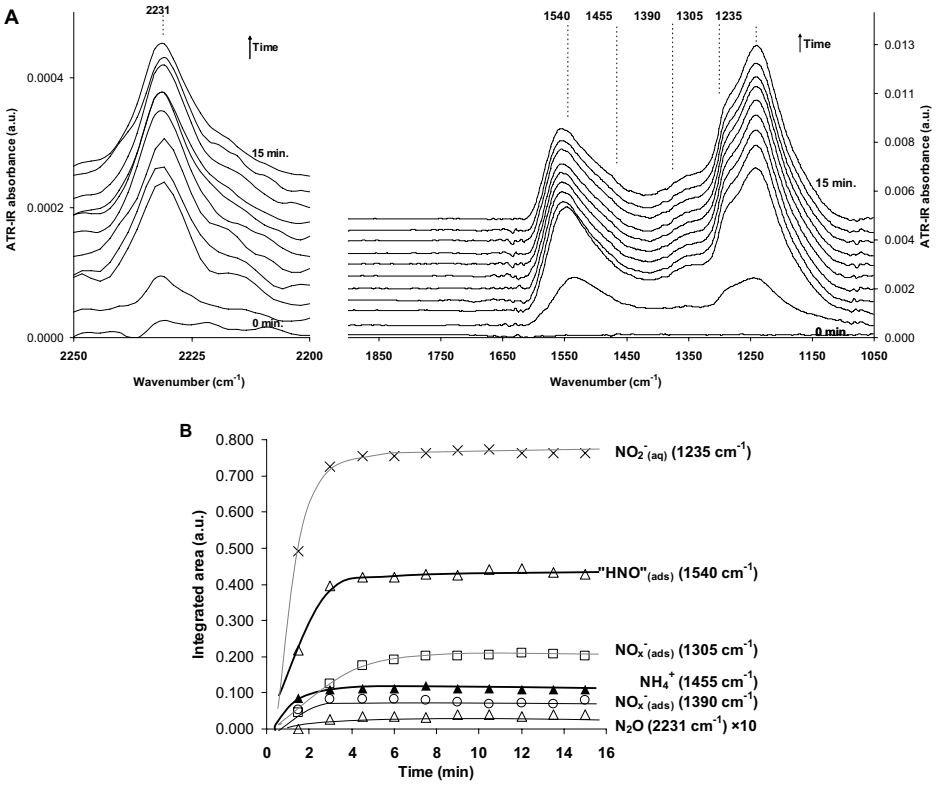

Figure 8.3. A: Water corrected ATR-IR spectra during continuous hydrogenation of nitrite over H-Pt/Al_2O_3; B: Integrated peak areas during continuous hydrogenation.

Figure 8.3 shows that surface intermediates resulting from reaction between nitrite and hydrogen could be observed under the conditions applied. Within 5 minutes, clear infrared peaks evolved at 2231 cm^{-1} (N_2O), 1540 cm^{-1} ("HNO"$_{(ads)}$), 1455 cm^{-1} (NH_4^+), 1390 cm^{-1} ($NO_{x\ (ads)}^{-\ 1390\ cm^{-1}}$), 1305 cm^{-1} ($NO_{x\ (ads)}^{-\ 1305\ cm^{-1}}$) and 1235 cm^{-1} ($NO_2^-{}_{(aq)}$). The development of the other bands with time (Figure 8.3B) illustrates that initially N_2O, "HNO"$_{(ads)}$, NH_4^+ and NO_x^- were formed on the platinum surface while, as for the titration experiments, simultaneously $NO_2^-{}_{(aq)}$ was observed (Figure 8.3). The formation of $HNO_2^-{}_{(ads)}$ can not be excluded because of the presence of $NO_2^-{}_{(aq)}$ which has a very strong absorption band, as discussed above (Figure 8.2).

The first 5 minutes of the experiment presented in Figure 8.3, represent a similar transient response as shown in Figure 8.1. After 5 minutes, when stable levels are observed, steady state hydrogenation is achieved.

To the best of our knowledge no kinetic studies of the hydrogenation of nitrite have been performed on Pt/Al_2O_3. However, platinum catalysts are reported to be comparable in activity to palladium catalysts for the hydrogenation of nitrite [17], Conversion of $NO_2^-{}_{(aq)}$ over a similar layer of Pd/Al_2O_3 catalyst is estimated to be

around four percent under identical conditions (with a hydrogen conversion of 11% assuming selectivity to ammonia), based on nitrite conversion rates based on kinetic studies in a batch reactor [41]. Therefore, the experiments in this study are close to differential conditions.

During continuous hydrogenation on H-Pt/Al_2O_3, no adsorbed NO was detected at either 1620 or 1580 cm^{-1}, in contrast to the step change experiments, introducing either $NO_2^-{}_{(aq)}$ to a hydrogen-covered catalyst or dissolved hydrogen to a catalyst surface partly covered with (H)NO species (Figure 8.1 and Figure 8.2). Apparently, titration experiments reveal surface species ($NO_{(ads)}$ that are rapidly converted under steady-state conditions. Moreover, comparison with Figure 8.1 clearly shows that the ratio of adsorbed species and free nitrite is opposite; during the stepwise adsorption (Figure 8.1), adsorbed nitrite ($NO_{x\ (ads)}^{-\ 1305\ cm^{-1}}$) is dominant, whereas the opposite is observed during continuous hydrogenation, where $NO_2^-{}_{(aq)}$ is dominant. Although direct comparison of the intensities of free $NO_2^-{}_{(aq)}$ is not allowed because the catalyst layers were not identical, it can be concluded that the surface coverages of the intermediates species is even lower than the already low coverages achieved in the step-wise experiments. Nevertheless, "HNO"$_{(ads)}$ is the dominant surface specie (Figure 8.3), indicating that hydrogenation of $NO_{(ads)}^{1580\ cm^{-1}}$ to "HNO"$_{(ads)}$ is fast and the consecutive hydrogenation of "HNO"$_{(ads)}$ to NH_4^+ relatively slow. Thus the rate determining step is the hydrogenation of "HNO"$_{(ads)}$, as suggested from electrochemical reduction of NO adlayers over platinum electrodes [42]. The fact that the surface coverage is nevertheless low, is suggesting that only part of the platinum surface contributes, or that the adsorption of nitrite is also rate limiting.

During continuous hydrogenation of nitrite, "HNO"$_{(ads)}$ is the main partially hydrogenated product found on the catalyst surface. As discussed above, hydrogenation of "HNO"$_{(ads)}$ produces ammonia, which is in agreement with literature describing electrochemical reduction of nitrite/NO adlayers over platinum [21,38,43-45]. Figure 8.3 reveals, like Figure 8.1 and Figure 8.2 continuous formation of N_2O, indicating that nitrogen is also formed, as N_2O was proven to reduce to nitrogen [26,27].

8.3.4 Nitrite hydrogenation mechanism

The experiments presented in this paper, show that a variety of species can be formed from nitrite over the Pt/Al_2O_3 catalyst, depending on the amounts of nitrite and hydrogen present during the experiment.

Adsorption of $NO_2^-{}_{(aq)}$ on H-Pt/Al_2O_3 yields, beside adsorbed nitrite, the hydrogenation products $NO_{(ads)}^{1580\ cm^{-1}}$ (reaction 8.1) "HNO"$_{(ads)}$ (reaction 8.2) and NH_4^+, as also shown by reaction ① and ② in Scheme 8.1, respectively.

These species originate from reaction with hydrogen on the platinum surface (Figure 8.1 and Figure 8.3). The first step to $NO_{(ads)}^{1580\ cm^{-1}}$ resembles the preparation of NO adlayers on platinum electrodes by electrochemical reduction of nitrite [19,23,24,33,34]. This study (Figure 8.2) shows that $NO_{(ads)}^{1580\ cm^{-1}}$ on the platinum surface undergoes a stepwise hydrogenation process first to "HNO"$_{(ads)}$ and subsequently to NH_4^+ the final hydrogenation product, as shown in Scheme 8.1 (reaction ② to ⑦ in Scheme 8.1). Under continuous hydrogenation conditions (Figure 8.3) "HNO"$_{(ads)}$ is the dominant intermediate, indicating that hydrogenation of "HNO"$_{(ads)}$ to NH_4^+ is, at least partly, rate determining.

$$NO_2^- + H_{(ads)} \xrightarrow{Pt/Al_2O_3} NO_{(ads)} + OH^- \qquad (8.1)$$

$$NO_{(ads)} + H_{(ads)} \rightleftharpoons \text{"HNO"}_{(ads)} \qquad (8.2)$$

The exact nature of the specie characterised by the peak at 1540 cm^{-1} is uncertain; most likely it can be assigned to $HNO_{(ads)}$, but $NOH_{(ads)}$ and $HNOH_{(ads)}$ can not be excluded, as discussed in Chapter 6. Nevertheless, since each one of these species are intuitively intermediate species, the overall reaction scheme is reliable; the exact nature of the relatively stable in intermediate can still be debated.

In the present study, $NO_{(ads)}^{1580\ cm^{-1}}$ is hydrogenated to "HNO"$_{(ads)}$, which subsequently hydrogenates to NH_4^+ (Figure 8.2). In Chapter 6 we showed that during inert flow, the reverse reaction, where "HNO"$_{(ads)}$ is converted to $NO_{(ads)}^{1580\ cm^{-1}}$, also occurs. Reaction 8.2 (reaction ② Scheme 8.1) is apparently reversible, as also suggested from electrochemical reduction of NO adlayers over platinum electrodes [42], where

$NO_{(ads)}^{1580\ cm^{-1}}$ is converted to "HNO"$_{(ads)}$ in the presence of hydrogen, while the reversed reaction occurs in the absence of hydrogen. However, we have also shown that "HNO"$_{(ads)}$ can be oxidised to $NO_{x\ (ads)}^{-\ 1305\ cm^{-1}}$, supporting the hypothesis that under hydrogenation conditions $NO_{x\ (ads)}^{-\ 1305\ cm^{-1}}$ is an intermediate in the formation of "HNO"$_{(ads)}$. $HNO_2^-{}_{(ads)}$ was also detected during hydrogenation of nitrite, although only in the absence $NO_{x\ (ads)}^{-\ 1305\ cm^{-1}}$ and $NO_2^-{}_{(aq)}$. Because of the much stronger absorption bands of $NO_{x\ (ads)}^{-\ 1305\ cm^{-1}}$ and $NO_2^-{}_{(aq)}$ (Figure 8.2) the formation of "HNO"$_{(ads)}$ *via* $HNO_2^-{}_{(ads)}$ can not be excluded. Formation of HNO_2^- as an intermediate for electrochemical reduction of nitrite over platinum was indeed suggested in literature [39,44-46].

Hydrogenation of "HNO"$_{(ads)}$ results in the formation of NH_4^+ (Figure 8.2). It is clear that hydrogenation of nitrite *via* "HNO"$_{(ads)}$ to NH_4^+ must be a sequence of elementary reaction steps in which oxygen is removed and hydrogen is attached to the nitrogen atom. We have recently shown that formation of $NO_{(ads)}^{1580\ cm^{-1}}$ and "HNO"$_{(ads)}$ can arise from decomposition/reaction of NH_2OH on Pt/Al_2O_3 (Chapter 6). Therefore NH_2OH is regarded as a possible intermediate for the hydrogenation of $NO_{(ads)}$. Accordingly, the elementary reaction steps for the hydrogenation of "HNO"$_{(ads)}$ to NH_4^+ are postulated as:

$$\text{"HNO"}_{(ads)} + H_{(ads)} \xrightarrow{Pt/Al_2O_3} H_2NO_{(ads)} \quad (8.3)$$

$$H_2NO_{(ads)} + H_{(ads)} \xrightarrow{Pt/Al_2O_3} NH_2OH_{(ads)} \quad (8.4)$$

$$NH_2OH_{(ads)} + H_{(ads)} \xrightarrow{Pt/Al_2O_3} NH_{2(ads)} + H_2O \quad (8.5)$$

$$NH_{2(ads)} + H_{(ads)} \xrightarrow{Pt/Al_2O_3} NH_{3(ads)} \quad (8.6)$$

$$NH_{3(ads)} + H_2O \xrightarrow{Pt/Al_2O_3} NH_4^+ + OH^- \quad (8.7)$$

The proposed reaction sequence of ammonia formation *via* hydrogenation of $NO_{(ads)}$ and "HNO"$_{(ads)}$ (reaction 8.2 to 8.7 and ② to ⑦ in Scheme 8.1) is similar to the proposed formation of NO adlayers from nitrite and nitrate solutions on platinum electrodes described in literature [23,44]. Furthermore, electrochemical reduction of NO adlayers was proposed to proceed *via* an $HNO_{(ads)}$ intermediate, with ammonia as the final product [21,38,43-45].

N_2O was detected during all hydrogenation experiments presented in this study. From the present results, the mechanism for formation of N_2O is not clear yet. The formation of N_2O can be formed either *via* dimerisation of $NO_{(ads)}$ and / or "HNO"$_{(ads)}$ or *via* dissociation of NO on steps as proposed in literature [16,21,27,29,40,47-54], as indicated in Scheme 8.1. In addition, N_2O was demonstrated to be an intermediate in the formation of nitrogen [26,27]. This shows the possibility for nitrogen formation, although no nitrogen was detected in the present study, since it is not infrared active.

The reaction scheme of the heterogeneous hydrogenation of nitrite shown in Scheme 8.1 is similar to the schemes proposed for both heterogeneous hydrogenation of nitrite over supported noble metal catalysts [5,7,8,13] and electrochemical reduction of nitrite (and NO adlayers) on platinum electrodes [19,24,33,34], showing the similarities between the heterogeneous hydrogenation and the electrochemical reduction of nitrite. For the first time, this study provides experimental evidence for some of the surface intermediates during the heterogeneous hydrogenation of nitrite over a supported platinum catalyst.

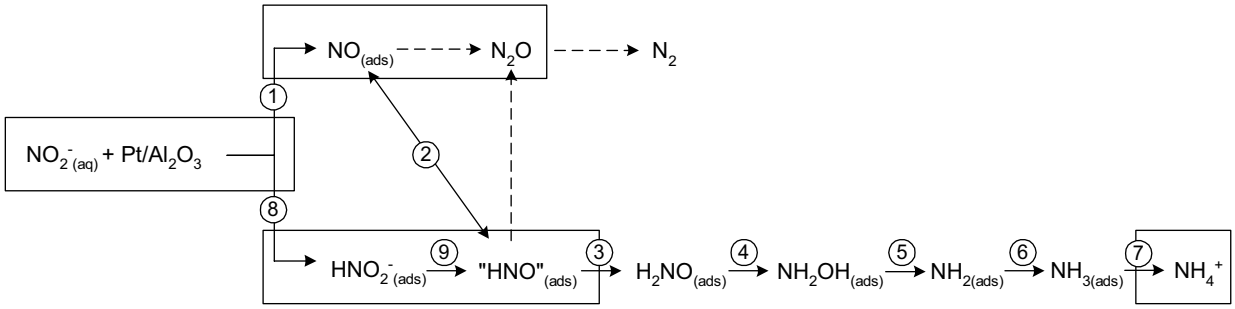

Scheme 8.1. Suggested reaction scheme of the catalytic hydrogenation of nitrite over Pt/Al_2O_3. The reactions in the boxes are based on the findings in the present study. The other reactions in the scheme have been discussed before in literature [19]. The dotted lines represent possible reaction pathways for N_2O and N_2 formation, although at present there is no evidence for these pathways. The numbers correspond to the reaction sequence described in the text.

In literature, it was suggested that the reaction pathway for the heterogeneous catalytic hydrogenation of nitrite as well as for the electrochemical reduction of NO adlayers are the same for both platinum and palladium catalysts [13,14,16]. As described above, nitric oxide adsorbed on Pt/Al_2O_3 hydrogenates at least partly to ammonia, with "HNO"$_{(ads)}$ as an intermediate, On Pd/Al_2O_3, on the other hand, we recently showed that hydrogenation of nitric oxide does not result in ammonia, as ammonia is formed exclusively *via* a pathway including hydrogenation of $NH_{2(ads)}$ and excluding adsorbed NO[15].

As discussed above, $NO_x^-{}_{(ads)}$ was observed when adsorbing nitrite on H-Pt/Al_2O_3 (Figure 8.1), while it was not on H-Pd/Al_2O_3 (as shown in Chapter 7). As discussed it might be that only part of the platinum surface contributes in the hydrogenation, as a consequence more adsorption sites for nitrite adsorption can be available after adsorption of nitrite on H-Pt/Al_2O_3, although this only applies if different sites are involved in the hydrogenation and the adsorption of nitrite. That only a part of the platinum surface contributes in the hydrogenation might also explain why $NO_{(steps)}^{1620\ cm^{-1}}$ is observed on platinum. At steps, the rate of dissociation of hydrogen is lower, therefore it can be speculated this leads to a lower hydrogenation rate of $NO_{(steps)}^{1620\ cm^{-1}}$. However, the fact that $NO_{(steps)}^{1620\ cm^{-1}}$ is not reactive to hydrogen, in contrast to all other species, can not be fully explained at present.

The main goal of this study and the study described in Chapter 7 was to evaluate/verify the mechanism for hydrogenation of nitrite over Pd/Al_2O_3 and Pt/Al_2O_3 proposed in literature [5,7,8,13], by identifying the absorbed intermediates. The same surface intermediates are involved on both metals, as shown in Scheme 8.1, which lead, however, to different products. It was previously suggested that nitric oxide, formed on both noble metal catalysts, hydrogenates to both ammonia and nitrogen. Our spectroscopic evidence clearly shows that adsorbed nitric oxide on palladium does not hydrogenate to ammonia (as shown in Chapter 7), whereas on platinum ammonia is found as a product for hydrogenation of nitric oxide, as shown in Scheme 8.1 and proposed in literature [5,7,8,13,19,24,33,34].

As discussed above, "HNO"$_{(ads)}$ is observed during the continuous hydrogenation of nitrite (Figure 8.3). On Pd/Al_2O_3, on the other hand, $NO_{(ads)}$ and $NH_{2(ads)}$ is observed during the continuous hydrogenation, where $NO_{(ads)}$ hydrogenated to nitrogen and $NH_{2(ads)}$ hydrogenates to ammonia. These observations indicate that, different steps in the formation of ammonia are rate limiting over platinum and palladium; hydrogenation of "HNO"$_{(ads)}$ is rate limiting for Pt/Al_2O_3, whereas the hydrogenation of $NH_{2(ads)}$ is rate limiting over Pd/Al_2O_3. This explains why "HNO"$_{(ads)}$ is observed on Pt/Al_2O_3 only.

The hydrogen concentration, at which hydrogenation intermediates were observed during the continuous hydrogenation of nitrite over H-Pt/Al_2O_3 (Figure 8.3) is approximately ten times higher compared to for continuous hydrogenation of nitrite over H-Pd/Al_2O_3, as shown in Chapter 7. This means that under identical conditions more surface species are observed on the platinum surface (this study) compared to on palladium (Chapter 7). This observation implies that the rate determining step,

hydrogenation of "HNO"$_{(ads)}$, is slower on platinum compared to hydrogenation of $NH_{2(ads)}$ on palladium, which is rate determining on palladium.

The reversible reaction between $NO_{(ads)}^{1580\ cm^{-1}}$ and "HNO"$_{(ads)}$ (as discussed in Chapter 6 and above) shows that on platinum insertion of a hydrogen atom to nitric oxide is possible without breaking the NO bond. This is in contrast to palladium, where $NO_{(ads)}$ is converted to N_2 exclusively. It can be speculated that the higher NO bond strength and dissociation temperature on platinum [55] cause the insertion of a hydrogen atom before breaking the NO bond as the rate limiting step (reaction ③ in Scheme 8.1). Thus NO adsorbed on platinum can hydrogenate to NH_4^+. On palladium on the other hand, the NO bond is easily broken, possibly *via* dimerisation, leading to the formation of nitrogen.

8.4 Conclusion

The surface intermediates during the heterogeneous hydrogenation of nitrite over Pt/Al_2O_3 were investigated in aqueous phase by ATR-IR spectroscopy. In addition to adsorbed nitrite, $NO_{(ads)}$, "HNO"$_{(ads)}$, $HNO_2^-{}_{(ads)}$ and NH_4^+ are formed on the platinum surface. Hydrogenation of nitrite yields ammonia *via* a stepwise hydrogenation process *via* $NO_{(ads)}$ and "HNO"$_{(ads)}$ as intermediates, wherein hydrogenation of "HNO"$_{(ads)}$ is the rate determining step. Very slow conversion of $NO_{(ads)}$ to N_2O was also detected. A non-reactive $NO_{(ads)}$ species was detected in titration experiments, but not during steady state operation. The results indicate that the reaction pathway of nitrite hydrogenation on platinum and palladium is rather similar, but the rate determining steps on both metals are definitely different.

8.5 References

[1] C.S. Bruning-Fann, J.B. Kaneene, Vet.Hum.Toxicol. 35 (1993) 521.

[2] World Health Organization, Water and health in Europe, WHO, Regional Office for Europe, Copenhagen, 2002.

[3] World Health Organization, Nitrate and nitrite in Drinking-water, WHO, Regional Office for Europe, Copenhagen, 2003.

[4] S. Hörold, K.D. Vorlop, T. Tacke, M. Sell, Catal.Today 17 (1993) 21.

[5] J. Wärnå, I. Turunen, T. Salmi, T. Maunula, Chem.Eng.Sci. 49 (1994) 5763.

[6] J. Daum, K.D. Vorlop, Chem.Eng.Tech. 22 (1999) 199.

[7] S. Hörold, T. Tacke, K.D. Vorlop, Environ.Technol. 14 (1993) 931.

[8] K.D. Vorlop, U. Prusse, Environmental catalysis (1999) 195

[9] M. Hahnlein, U. Prusse, J. Daum, V. Morawsky, M. Koger, M. Schroder, M. Schnabel ,K.D. Vorlop, Preparation of catalysts VII (1998) 99

[10] U. Prüsse, J. Daum, C. Bock, K.D. Vorlop, Stud.Surf.Sci.Catal. 130 (2000) 2237.

[11] A. Pintar, J. Batista, J. Levec, Water.Sci.Technol. 37 (1998) 177.

[12] K. Daub, G. Emig, M.J. Chollier, M. Callant, R. Dittmeyer, Chem.Eng.Sci. 54 (1999) 1577.

[13] A. Pintar, J. Batista, J. Levec, T. Kijiuchi, Appl.Catal.B 11 (1996) 81.

[14] U. Prüsse, M. Hahnlein, J. Daum, K.D. Vorlop, Catal.Today 55 (2000) 79.

[15] S.D. Ebbesen, B.L. Mojet, L. Lefferts, (Chapter 7 in this thesis) To be submitted (2006)

[16] A.C.A. de Vooys, Koper M.T.M., R.A. van Santen, J.A.R. van Veen, J.Catal. 202 (2001) 387.

[17] M. D'Arino, F. Pinna, G. Strukul, Appl.Catal.B 53 (2004) 161.

[18] S.D. Ebbesen, B.L. Mojet, L. Lefferts, (Chapter 6 in this thesis) To be submitted (2006)

[19] V. Rosca, Koper M.T.M., Surf.Sci. 584 (2005) 258.

[20] M.C.P.M. da Cunha, M. Weber, F.C. Nart, J.Electroanal.Chem. 414 (1996) 163.

[21] M.C.P.M. da Cunha, J.P.I. De Souza, F.C. Nart, Langmuir 16 (2000) 771.

[22] R. Gomez, A. Rodes, J.M. Orts, J.M. Feliu, J.M. Perez, Surf.Sci. 342 (1995) L1104.

[23] V. Rosca, M.T.M. Koper, J.Phys.Chem.B. 109 (2005) 16750.

[24] V. Rosca, G.L. Beltramo, M.T.M. Koper, Langmuir 21 (2005) 1448.

[25] Weaver M.J., S.Z. Zou, C. Tang, J.Chem.Phys. 111 (1999) 368.

[26] I.T. Bae, R.L. Barbour, D.A. Scherson, Analytical Chemistry 69 (1997) 249.

[27] A.C.A. de Vooys, Koper M.T.M., R.A. van Santen, J.A.R. van Veen, Electrochim.Acta 46 (2001) 923.
[28] G.M. Begun, W.H. Fletcher, J.Chem.Phys. 28 (1958) 414.
[29] V. Rosca, G.L. Beltramo, M.T.M. Koper, J.Electroanal.Chem. 566 (2004) 53.
[30] A. Rodes, R. Gomez, J.M. Orts, J.M. Feliu, J.M. Perez, A. Aldaz, Langmuir 11 (1995) 3549.
[31] Y. Matatov-Meytal, V. Barelko, I. Yuranov, M. Sheintuch, Appl.Catal.B 27 (2000) 127.
[32] Y. Matatov-Meytal, Y. Shindler, M. Sheintuch, Appl.Catal.B 45 (2003) 127.
[33] A. Rodes, R. Gomez, J.M. Perez, J.M. Feliu, A. Aldaz, Electrochim.Acta 41 (1996) 729.
[34] E. Casero, C. Alonso, J.A. Martin-Gago, F. Borgatti, R. Felici, F. Renner, T.L. Lee, J. Zegenhagen, Surf.Sci. 507-510 (2002) 688.
[35] Y.O. Park, W.F. Banholzer, R.I. Masel, Appl.Surf.Sci. 19 (1984) 145.
[36] J.M. Gohndrone, Y.O. Park, R.I. Masel, J.Catal. 95 (1985) 244.
[37] R.J. Gorte, L.D. Schmidt, J.L. Gland, Surf.Sci. 109 (1981) 367.
[38] G.E. Dima, G.L. Beltramo, M.T.M. Koper, Electrochim.Acta 50 (2005) 4318.
[39] S. Ye, H. Kita, J.Electroanal.Chem. 346 (1993) 489.
[40] J.F.E. Gootzen, R.M. van Hardeveld, W. Visscher, R.A. van Santen, J.A.R. van Veen, Recl.Trav.Chim.Pays-Bas 115 (1996) 480.
[41] A. Pintar, G. Bercic, AIChE J. 44 (1998) 2280.
[42] G.L. Beltramo, M.T.M. Koper, Langmuir 19 (2003) 8907.
[43] F. Balbaud, G. Sanchez, G. Santarini, G. Picard, Eur.J.Inorg.Chem. 2000) 665.
[44] A. Rodes, R. Gomez, J.M. Orts, J.M. Feliu, A. Aldaz, J.Electroanal.Chem. 359 (1993) 315.
[45] K. Nishimura, K. Machida, M. Enyo, Electrochim.Acta 36 (1991) 877.
[46] F. Balbaud, G. Sanchez, G. Santarini, G. Picard, Eur.J.Inorg.Chem. 4 (2000) 665.
[47] L.J.J. Janssen, M.M.J. Pieterse, E. Barendrecht, Electrochim.Acta 22 (1977) 27.
[48] I. Paseka, J. Vonkova, Electrochim.Acta 25 (1980) 1251.
[49] I. Paseka, A. Hodinar, Electrochim.Acta 27 (1982) 1461.
[50] J.A. Colucci, M.J. Foral, S.H. Langer, Electrochim.Acta 30 (1985) 521.
[51] A.C.A. de Vooys, G.L. Beltramo, B. van Riet, J.A.R. van Veen, M.T.M. Koper, Electrochim.Acta 49 (2004) 1307.
[52] J.H. MacNeil, P.A. Berseth, G. Westwood, W.C. Trogler, Environ,Sci.Technol. 32 (1998) 876.

[53] S. Kuwabata, S. Uezumi, K. Tanaka, T. Tanaka, Inorg.Chem. 25 (1986) 3018.

[54] D.D. De, J.D. Englehardt, E.E. Kalu, J.Electrochem.Soc. 147 (2000) 4573.

[55] W.A. Brown, D.A. King, J.Phys.Chem.B. 104 (2000) 2578.

CHAPTER 9

Concluding remarks and recommendations

The understanding of chemistry on surfaces is a challenging but critical step in catalytic research. Understanding of surface chemistry in the presence of liquid solvents is lacking because it is difficult to study heterogeneous catalysis *in-situ* when the reactions are carried out in liquid solvents, water in particular.

The work presented in this thesis aims to develop ATR-IR spectroscopy to study adsorption and catalytic reactions on metal surfaces during heterogeneous catalytic reactions in aqueous phase. Properties of the technique and the influence of water on the supported metal catalysts were demonstrated using two reactions (i) CO oxidation and (ii) nitrite hydrogenation. The work described in this thesis clearly demonstrates the application of ATR-IR spectroscopy to study adsorption and catalytic reactions in water. By coating an Internal Reflection Element (IRE) with a thin (in the order of a few microns), stable catalyst layer, adsorption and reaction at the solid-aqueous interface were studied successfully.

9.1 Adsorption and oxidation of carbon monoxide

Adsorption and oxidation of carbon monoxide was performed in both gas and aqueous phase over Pt/ZnSe, Pt/Al_2O_3 and Pd/Al_2O_3, investigating the influence of water on both CO and the noble metals. Adsorption of CO from gas and aqueous phase on the supported catalysts (Pt/Al_2O_3 and Pd/Al_2O_3) revealed significant spectral changes. Co-adsorption of water on the noble metals and a direct interaction of water with the adsorbed CO molecule cause a clear red shift of the CO stretch frequency and a decreased linear to bridged (L/B) ratio of adsorbed CO in aqueous phase. Moreover, the infrared absorbance increased when adsorbing CO from aqueous phase, compared to gas phase adsorption.

The red shift and changed L/B ratio, is caused by the direct effect of water on the CO molecule or by an indirect effect *via* modification of the metal particle potential, inducing an increased π-back-donation from the metal to CO, or a combination of

both phenomena. Remarkably, the CO intensity increased drastically when adsorbed in aqueous phase compared to adsorption in gas phase, for all three catalysts. This can be caused by a polarisation of the CO molecule, for example *via* hydrogen bonding, which directly influences its extinction coefficient by increasing the transition dipole moment. In aqueous phase, the stretch frequency of adsorbed CO shifts down with increasing pH, which is attributed to increasing π-back-donation from the supported metal to adsorbed CO, caused by decreasing potential of the supported metal particles.

The oxidation rate of pre-adsorbed CO increases significantly in aqueous phase compared to in gas phase. In addition, an increase in pH significantly enhances the CO oxidation rate. Over Pt/Al_2O_3, the stretch frequency of adsorbed CO is linearly related to the CO oxidation rate, which suggests an effect of the metal particle potential on the rate determining step of CO oxidation in aqueous phase. The increased π-back donation weakens the CO bond by supplying electrons in the anti-bonding orbital; therefore CO is more reactive towards the p-electrons of adsorbed oxygen atoms. As a result, the CO molecule is more easily oxidised in aqueous phase and with increasing pH. Furthermore, palladium particles are more easily oxidised in water and with increasing pH, further increasing the oxidation rate of adsorbed CO over Pd/Al_2O_3. Scheme 9.1 summarises the influence of the presence of water and the pH value on both the CO stretch frequency and the CO oxidation rate.

Preliminary calculations show that the effect of co-adsorption of water has a more distinct effect on the CO peak position than the formation of hydrogen bonds. However, to explain the influence of water on the CO adsorption on supported noble metal in detail, theoretical calculations are necessary and can be subject of further investigation.

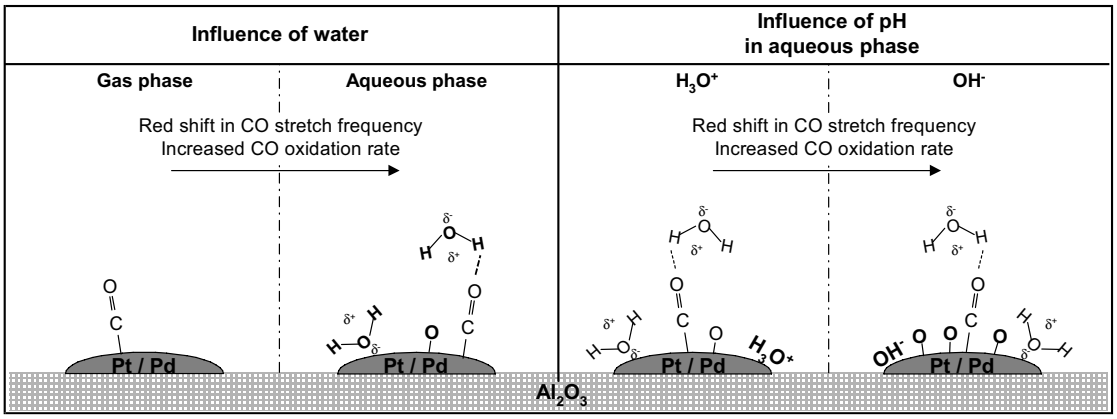

Scheme 9.1 Schematic presentation of the influence of water and pH on the CO stretch frequency and CO oxidation rate.

9.2 Nitrite hydrogenation

In relation to the heterogeneous hydrogenation of nitrite, adsorption of nitrite (NO_2^-), ammonia (NH_4^+) and hydroxylamine (NH_2OH) from aqueous phase was first examined on Pd/Al_2O_3, Pt/Al_2O_3 and Al_2O_3. Hydrogenation was thereafter performed by adsorbing nitrite on a pre-reduced Pd/Al_2O_3 or Pt/Al_2O_3 catalyst (denoted H-Pd/Al_2O_3 or H-Pt/Al_2O_3), where $NO_2^-{}_{(aq)}$ can react with adsorbed hydrogen.

Adsorption of $NO_2^-{}_{(aq)}$ and $NH_4^+{}_{(aq)}$ show similar adsorption characteristics on both Pd/Al_2O_3 and Pt/Al_2O_3. The vibrational spectrum of the nitrite ion changes substantially upon adsorption; clearly, nitrite chemisorbs onto the noble metal catalysts. Contrary, adsorption of NH_4^+ does not lead to significant changes in the vibrational spectrum of the ion, indicating that NH_4^+ does not chemisorb on the noble metal. Instead, NH_4^+ is stabilised via electrostatic interaction given the fact that NH_4^+ is not rapidly flushed out. Adsorption of $NH_2OH_{(aq)}$ on Pd/Al_2O_3 and Pt/Al_2O_3 however, leads to different adsorbed species on the two metals. On Pd/Al_2O_3, hydroxylamine is converted into a stable $NH_{2(ads)}$ fragment, whereas on Pt/Al_2O_3 hydroxylamine is converted into NO, possibly via $HNO_{(ads)}$ (denoted "HNO"$_{(ads)}$ because of uncertainty in the assignment; NOH and HNOH can not be excluded) as an intermediate .

Hydrogenation of nitrite leads to similar species as formed during adsorption and decomposition of NH_2OH on the catalyst surface. Adsorption of NO_2^- on H-Pd/Al_2O_3 results in formation of the intermediates $NO_{(ads)}$ and $NH_{2(ads)}$. During subsequent hydrogenation, $NO_{(ads)}$ is most likely converted to N_2, while the hydrogenation of $NH_{2(ads)}$ produces solely NH_4^+. Interestingly, NH_4^+ is only produced after almost all $NO_{(ads)}$ has disappeared, demonstrating that $NO_{(ads)}$ is more reactive towards

hydrogen than $NH_{2(ads)}$. As for palladium, nitrite adsorption on H-Pt/Al_2O_3, leads to the intermediate $NO_{(ads)}$. However, in contrast to palladium, further hydrogenation of $NO_{(ads)}$ on platinum results in the formation of "HNO"$_{(ads)}$, which is subsequently hydrogenated to ammonia. In the stepwise hydrogenation of $NO_{(ads)}$ to ammonia, hydrogenation of "HNO"$_{(ads)}$ is the rate determining step.

A small amount of N_2O is formed during all hydrogenation experiments over Pt/Al_2O_3. Nitrogen is believed to be formed from reduction of N_2O over platinum, thus the presence of N_2O indicates the formation of nitrogen, and the main species on Pt/Al_2O_3 are $NO_{(ads)}$ and "HNO"$_{(ads)}$ which hydrogenate to NH_4^+. On Pd/Al_2O_3, on the other hand, hydrogenation of $NO_{(ads)}$, which was formed at relatively high amounts compared to NH_2, is assumed to lead to nitrogen solely, explaining why palladium is more selective to nitrogen than platinum.

This study is the first to show the surface intermediates during heterogeneous hydrogenation of nitrite over supported palladium and platinum catalysts. In literature, it was suggested that the reaction pathways for heterogeneous catalytic hydrogenation of nitrite and for electrochemical reduction of NO adlayers (produced from nitrite solutions) are similar for both platinum and palladium catalysts. It was suggested that nitric oxide, formed on both noble metal catalysts, hydrogenates to ammonia and nitrogen. From this study, it is clear that nitric oxide adsorbed on Pt/Al_2O_3 hydrogenates to both N_2O and ammonia. The formation of ammonia proceeds *via* "HNO"$_{(ads)}$ as an intermediate; in other words, the reaction mechanism proposed in literature holds for platinum catalysts. However, on Pd/Al_2O_3, nitric oxide is not an intermediate in the formation of ammonia; instead, ammonia is formed *via* hydrogenation of $NH_{2(ads)}$ only.

The main difference between the mechanisms for hydrogenation of nitrite on Pt/Al_2O_3 and Pd/Al_2O_3 proposed here and the mechanism previously suggested in literature involves identification of the key adsorbed intermediate. The same surface intermediates are involved on both metals as shown in Scheme 9.2, but the species observed which are involved in the rate determining step(s) are quite different: $NO_{(ads)}$ and $NH_{2(ads)}$ on palladium versus "HNO"$_{(ads)}$ on platinum. On top of that, the reaction pathways are different; conversion of $NO_{(ads)}$ to ammonia is possible on platinum but not on palladium.

However, to explain the mechanism for nitrite hydrogenation in more detail, experimental information on the formation of dissolved gaseous products, such as nitrous oxide and nitrogen, would be required. Our group is currently working on the

development of a method for detection of extremely small amounts of dissolved gases in aqueous solutions, to unambiguously determine the hydrogenation products of $NO_{(ads)}$ and N_2O. It is well known that the pH value of the solution influences the hydrogenation activity and the selectivity towards nitrogen and ammonia, which is also subject for further investigation. Another issue for hydrogenation of nitrite over palladium catalysts is the stability of β-palladium-hydride in aqueous phase. Experiments performed in the present study, surprisingly show that the β-palladium-hydride is stable during aqueous flow, but further investigation is necessary.

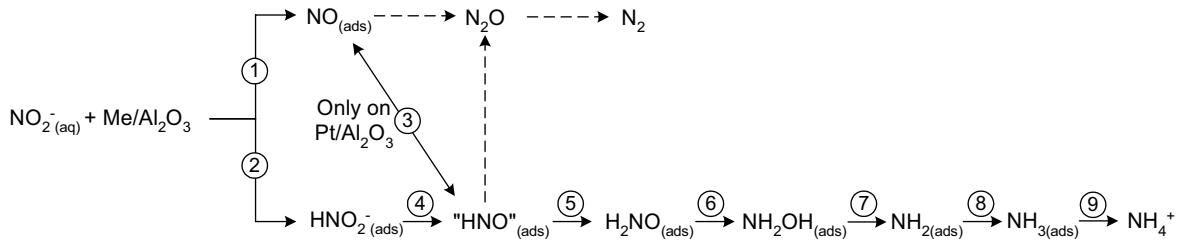

Scheme 9.2. Reaction scheme of the catalytic hydrogenation of nitrite over Pd/Al_2O_3 and Pt/Al_2O_3. The dotted lines represent possible reaction pathways for N_2O and N_2 formation, although at present there is no evidence for these pathways. Step ③ applies for Pt/Al_2O_3 only. All other steps apply for both catalysts.

9.3 ATR-IR spectroscopy

This study convincingly shows that ATR-IR spectroscopy can be applied to study adsorption and reaction on supported catalysts in dry and wet gas as well as in aqueous phase. As such, ATR-IR spectroscopy allows direct comparison between adsorption and reactions in gas and liquid phase. In conclusion, water interacts both directly with the adsorbed species and indirectly by influencing the metal potential of the supported metal catalysts. The metal potential is further influenced by the pH of the solution, affecting reaction rates.

Acknowledgements

Now it is finally time to look back over the last four years plus I have spent in the Netherlands. I have had the opportunity to meet people from all over the world; there are many people who have provided me help and support, to make my stay pleasant and meaningful. Here, I would like to take this opportunity to express my sincere acknowledgements.

First of all, my special thanks to Prof. Dr. Ir. Leon Lefferts for having offered me a PhD position in the group of Catalytic Processes and Materials. These four years has made me stronger and smarter in many ways. Dr. Barbara Mojet, my assistant promoter, and most of all, my supervisor; we are two very different persons, I know you are not an engineer, and we are sometimes speaking two different languages, but working with you has been a great experience. I know that it was sometimes difficult for those directly involved in my research activities. However, I am glad that finally everyone has profited from the collaboration and survived the time with me!

I would like to thank all the committee members for the careful reading of this thesis.

The work presented in this thesis could not have been performed without the financial support by DSM Research B.V., Geleen, The Netherlands, for which I am grateful. Moreover I would like to thank Henk Oevering (DSM Research), it was always pleasant having meetings with you. You had nice comments on my work, when no one else could find and/or give positive feedback. Your comments always gave me an extra boost, thanks.

Dr. Jan Van Ommen, we always started our discussion with the project, and ended with something else … mostly diving, always a good experience; Thanks. Dr K. Seshan; thanks for the nice time we spend during the conference in Tokyo.

During the past four years plus, I have met many nice colleagues. I will especially like to thank all my co-workers; you have made my life in Twente a great experience. Most likely because my life in Twente mostly consisted of a life as a lab rate.

A special thanks to all of my colleagues, you have been more than friends to me, you have also been a great help through my life as a PhD:

Bert: If you ever need a beer, a swim or anything I'll be there, I am deeply in debt to you, thanks for your technical flair, also when I used "too much water" during Infrared Experiments …

Berta: I love you too, thanks for everything. You also stood by me this time, being my paranimf; Thanks.

Cristiano: Where to start … I can not thank you enough, your Roman spirit lifts the mood in even the most difficult situations. Also you are prepared to go on stage with me as a paranimf; Thanks.

Davide: One more nice Italian spirit … If you ever need "pleasure", you know where to find me. It has been a pleasure meeting you and I am sure that there will be more "pleasure" to come.

Dejan: Thanks for sharing the lab with me during our late nights. If you are up for a "snaps", you know where to find me.

Francesca: You know, thanks for everything, especially; thanks for the nice time we had during our coffee breaks. Always nice to blow off some steam. I miss our "lonely" coffee breaks at the university.

Gacia: Thanks for being among us, always lifting the mood. Also thanks for making my "escape" from the Netherlands smooth by taking over.

Hans: You had the nice habit of meeting early in the morning, which made me never feel alone in the building; thanks a lot.

Igor: Without you, this would never have been possible; Thanks.

Iris: I am very grateful to you, even we have only known each other shortly, we have spend much time together, mostly this meant hard work for you, I am deeply in depth, thanks.

Jeroen: You are one of the easiest people to provoke to a laugh, and believe me it is all good. Thanks for your cheerful mood.

Jiang: Always up for a good story, we shared a lot of good memories about China, thanks. I hope that I will get much more of those experiences hands on.

Karin: Thanks for your enthusiasm, teaching me what is and most of all what is not allowed lab; I know I was not always listening as I should, sorry for that, but experiments have to be done …

Kazu(hiro): I already miss your samurai spirit; Cheers.

Khalid: You love your home country, which gave me a lot of opportunities to experience that long tale of your country, which were always pleasant, thanks. I hope, that in the future I can experience it hand on.

Kumar: My Indian friend, thanks for showing me the great heritage of India, and your cheerful mood, always a good time, thanks.

Lianne: Since you entered the dragons den it has never been the same; Thanks.

Louise: Always good for a chat, thanks, and thanks for all the XRF and BET measurements you have performed.

Patrick: My officemate; thanks for standing sharing the office with me these last few years.

Vijay: Another Indian friend, another great cheerful mood, thanks for everything.

Outside work I would like to express my deep gratitude for my swimming mates, Frederic, Michel and Jolanda, you were the best escape from the university anyone could ever have had, Thanks.

Publications

Articles

CO adsorption and oxidation at the catalyst - water interface — An investigation by Attenuated Total Reflection Infrared Spectroscopy
Sune D Ebbesen, Barbara L. Mojet and Leon Lefferts
Langmuir 2006, 22, 1079-1085.

***In-Situ* ATR-IR study of CO adsorption and oxidation over Pt/Al_2O_3 in gas and aqueous phase — Promotion effects by water and pH**
Sune D Ebbesen, Barbara L. Mojet and Leon Lefferts
Journal of Catalysis, 2007, 246, 66-73.

CO adsorption and oxidation over Pd/Al_2O_3 in gas and aqueous phase
Sune D Ebbesen, Barbara L. Mojet and Leon Lefferts
To be submitted

***In-Situ* ATR-IR study of adsorption of NO_2^-, NH_2OH and NH_4^+ on Pd/Al_2O_3 and Pt/Al_2O_3**
Sune D Ebbesen, Barbara L. Mojet and Leon Lefferts
To be submitted

***In-Situ* ATR-IR spectroscopic study of the heterogeneous catalytic hydrogenation of nitrite Pd/Al_2O_3**
Sune D Ebbesen, Barbara L. Mojet and Leon Lefferts
To be submitted

***In-Situ* ATR-IR spectroscopic study of the heterogeneous catalytic hydrogenation of nitrite Pt/Al_2O_3**
Sune D Ebbesen, Barbara L. Mojet and Leon Lefferts
To be submitted

***In-Situ* ATR-IR spectroscopic study of the heterogeneous catalytic hydrogenation of nitrite in aqueous solution over Pd/Al_2O_3 and Pt/Al_2O_3 at pH 5.1 – 9.1**
Sune D Ebbesen, Barbara L. Mojet and Leon Lefferts
In preparation

***In-Situ* ATR-IR spectroscopic study of hydrogenation of nitrate in aqueous solution over Pt/Al_2O_3**
Sune D Ebbesen, Barbara L. Mojet and Leon Lefferts
In preparation

Oral presentations

***In-Situ* ATR-IR spectroscopic study of the heterogeneous catalytic hydrogenation of nitrite in aqueous solution over Pd/Al_2O_3**
Sune D Ebbesen, Barbara L. Mojet and Leon Lefferts
July 2006, 5th Tokyo Conference on Advanced Catalytic Science and Technology (TOCAT 5)

***In-Situ* ATR-IR study of CO oxidation on Pt/Al_2O_3 in aqueous solution. Mimicking support effect by pH variation**
Sune D Ebbesen, Barbara L. Mojet and Leon Lefferts
April 2006, 2nd International Congress on Operando Spectroscopy

***In-Situ* ATR-IR spectroscopic study of nitrite hydrogenation in aqueous solution over Pt/Al_2O_3**
Sune D Ebbesen, Barbara L. Mojet and Leon Lefferts
March 2006, 7th Netherlands' Catalysis and Chemistry Conference (NCCC 7)

Attenuated Total Reflection Infrared Spectroscopy – at the solid-liquid interface
Sune D Ebbesen, Barbara L. Mojet and Leon Lefferts
March 2004, 5th Netherlands' Catalysis and Chemistry Conference (NCCC 5)

Poster presentations

Probing adsorption on supported noble metal catalysts during aqueous phase reactions
Sune D Ebbesen, Igor V. Babich, Barbara L. Mojet and Leon Lefferts
March 2005, 6th Netherlands' Catalysis and Chemistry Conference (NCCC 6)

Microkinetic modelling of the selective oxidation of propene to acrolein – Preparation of bismuth-molybdateoxide
Sune D Ebbesen, Jacob B Larsen, Charlotte V Ovesen and Per Stoltze
June 2002, 10th Nordic Symposium on Catalysis.

Preparation and Modification of the BiMoO-system
Sune D Ebbesen and Per Stoltze
December 2001, Annual Meeting of Interdisciplinary Research Centre for Catalysis (ICAT).

ISBN 978-90-365-2467-4